597

GL04463

Contrib. Mineral. Petrol. 67, 289–295 (1978)

FC
597

Contributions to Mineralogy and Petrology
© by Springer-Verlag 1978

UNIVERSITY OF UTAH
RESEARCH INSTITUTE
EARTH SCIENCE LAB.

Trace-Element Distribution and Ore Formation in Vein-Metasomatised Peridotite at Kalskaret, Near Tafjord, South Norway

R. Kanaris-Sotiriou, F.G.F. Gibb, D.A. Carswell, and C.D. Curtis

Department of Geology, The University of Sheffield, S1 3JD, Great Britain

Abstract. The concentration profiles of the trace elements S, Ti, V, Cr, Mn, Co, Ni, Cu, Zn, Sr, and Y have been determined across a metasomatic vein in peridotite. The introduced elements Ti, V, Sr, and Y show specific enrichment in particular silicate phases in accordance with the availability of suitable lattice sites. In contrast, the other introduced trace elements (Cu and S) behave more like the redistributed elements, Cr, Ni, Mn, and Co which do not show concentration 'fronts' that can be simply related to the silicate minerals. Concentration of pentlandite, chalcopyrite, and Cr-magnetite near the boundary between the enstatite and anthophyllite zones gives rise to maxima in the Ni, Cu, S, and Cr distributions, while in the chlorite zone significant concentrations of Cr and Ni occur in the chlorite itself. Control of the distribution of Ni, Cu, and Cr is ascribed to the oxidation/reduction reactions involved in the formation of pentlandite, chalcopyrite and Cr-magnetite, together with the critical role of Al in limiting chlorite formation during metasomatism.

Introduction

The mineralogy and major-element geochemistry of a complex assemblage of silicates in a vein cross-cutting a peridotite body at Kalskaret, Norway, have previously been reported in some detail (Carswell et al., 1974). The symmetrically zoned sequence of vein minerals on either side of a fracture in the peridotite was concluded to have developed by the reaction of the peridotite with supercritical hydrous fluids that originated from the acid gneiss country rocks. Each half of the sequence is around 10 cm thick with a common central zone of chlorite occupying the position of the fracture and zones of tremolite, anthophyllite and enstatite between this and the peridotite on either side (Fig. 1).

The sequence is believed to have formed at temperatures of about 700° C and at a P_{total} of greater than 6 kb. A later reaction episode was thought to account for the presence on a small scale of lower temperature phases (talc and serpentine) which occur to a limited extent throughout the ultrabasic bodies and in the metasomatic vein assemblage. Ultramafic fracture assemblages from Almklovdalen, further west in the Norwegian Basal Gneiss Complex, have been tentatively dated as having formed in the late Caledonian (c. 400 m.y.) by Brueckner (1975), although it was recognised that the metamorphic histories of the ultramafic bodies may extend as far back as the Svecofennian (1600–1800 m.y.).

It was suggested (Carswell et al., 1974) that each mineral zone represented a local attainment of equilibrium, although overall the reaction was incomplete. The outer boundary (towards the peridotite) of each zone was thought to represent the limit of penetration of the particular chemical species from the fluid controlling the growth of the mineral phase forming that zone. In this way, the zone 'front' for chlorite was determined by Al^{3+}, tremolite by Ca^{2+}, anthophyllite by H_2O and enstatite possibly by $Si(OH)^0_4$. With progressive influx of fluids all zones simultaneously expanded towards the peridotite.

The study is here extended to the trace elements of the same sequence, with a view to establishing the ways in which the distribution of these elements may be controlled in metasomatic systems of this type. Detailed elemental distributions for other examples of similar complexity to the Kalskaret vein sequence do not appear to have been recorded although work illustrating the mobility of Ni in altered ultramafic rocks has been reported (e.g., Rucklidge (1972), Eckstrand (1975), and Groves et al. (1974)). Curtis and Brown (1971) discussed trace-element behaviour in the zoned metasomatic bodies of Unst, Shetland but, in case, the complete zonal sequence is rarely seen.

0010-7999/78/0067/0289/$01.40

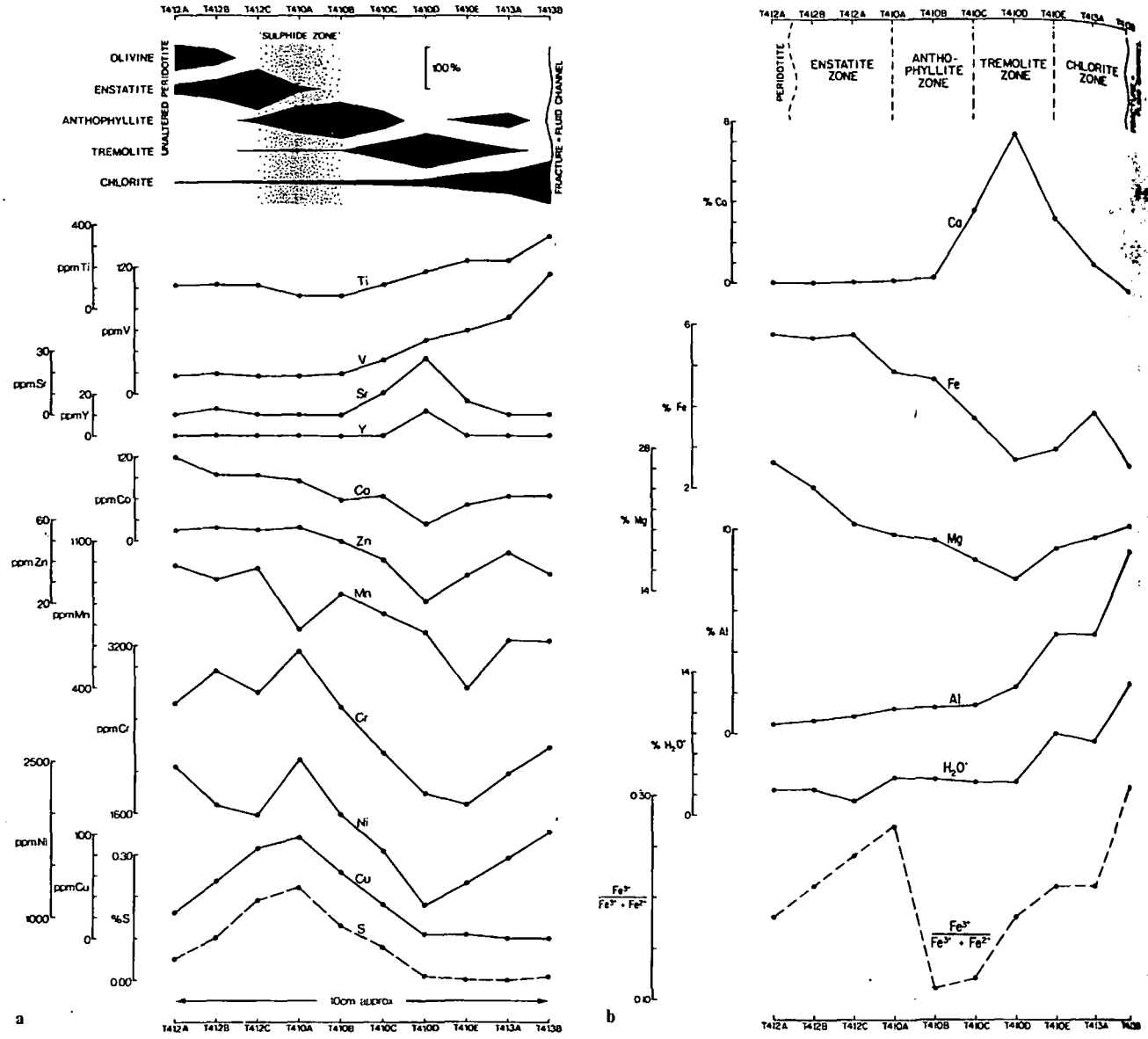

Fig. 1a and b. Chemical and mineralogical variations across the Kalskaret metasomatic vein. (a) shows (top) the variation in major silicate mineral contents and the position of the sulphide concentration which accounts for up to 0.5% by volume of the rock. Plotted below are the distributions of the various trace elements. (b) shows the corresponding critical variations in major element geochemistry

The same bulk samples from the Kalskaret vein that were previously analysed for major elements were used for the determination of trace elements by X-ray Fluorescence Spectrometry using pressed-powder specimens. The elements determined were Zr, Y, Sr, Rb, Zn, Cu, Mn, V, Ni, Cr, Co, Ba, and Pb, but of these Zr, Rb, Ba, and Pb were close to the limit of detection (about 2 ppm) and showed little variation. The remaining trace-element contents are plotted in Figure 1a together with values for Ti and S determined by XRFS using a fusion sample preparation technique. A schematic representation of the mineralogy of the sequence as determined by a combination of X-ray diffraction modal analysis and normative calculations is given in Figure 1a.

Sources of the Trace-Elements

The following assumptions have been made in attempting to establish the sources of the various elements:

(a) The trace elements contained in the zonal sequence were derived either from the original peridotite *or* were introduced with the incoming fluids.

(b) The original trace elements within the peridotite were uniformly distributed on the scale of a hand specimen.

(c) Any volume changes as a result of the metasomatism were relatively small and/or uniformly distributed over the region of the peridotite affected.

Table 1. Electron microprobe partial analyses of Kalskaret silicate and oxide phases

Zone	Mineral	wt % Cr[a]	wt % Ni[a]	wt % FeO[a]	wt % Al_2O_3[a]
	Oxide	33.29	0.13	45.84	3.91
	Enstatite	0.02	0.11	n.d.	n.d.
	Anthophyllite	0.04	0.12	n.d.	n.d.
Enstatite	Chlorite A	2.16	n.d.	n.d.	n.d.
	Chlorite B	1.96	n.d.	n.d.	n.d.
	Chlorite C	1.64	0.23	3.25	15.35
	Oxide	34.38	0.11	36.85	7.21
	Anthophyllite	0.03	0.11	n.d.	n.d.
Anthophyllite	Chlorite	1.55	0.20	3.37	15.40
	Tremolite	0.03	0.10	n.d.	n.d.
	Talc	0.03	0.18	n.d.	n.d.
	Oxide	29.15	0.32	45.40	7.18
	Anthophyllite	0.03	0.11	n.d.	n.d.
Tremolite	Chlorite A	0.60	0.22	3.25	17.29
	Chlorite B	0.72	0.18	n.d.	n.d.
	Tremolite	0.01	0.13	n.d.	n.d.
Chlorite	Chlorite	0.17	0.25	3.37	16.76

n.d. = not determined

[a] ZAF correction factors derived from mineral compositions calculated from bulk analyses except for oxide for which a spinel composition of similar Fe, Cr, and Al content was used

Table 2. Electron microprobe analyses of Kalskaret sulphide minerals

(a) Pentlandite

Sample/ Analysis No.	T410/0/A	T410/0/B	T412/0/B	T412/1/B	T412/1/C	P
wt %						
S	33.1	33.3	32.7	32.7	35.0	32.81
Cu	0.0	0.0	0.14	0.0	0.0	
Ni	32.6	34.5	32.7	33.1	28.6	35.12
Fe	33.6	32.7	34.8	33.0	34.3	29.48
Co	n.d.	n.d.	n.d.	0.57	0.55	2.20
Total	99.30	100.50	100.34	99.37	98.45	99.61

[a] Average of twenty pentlandite analyses from pentlandite-pyrrhotite assemblages after Harris and Nickel (1972)

(b) Chalcopyrite

Sample/ Analysis No.	T412/1/A	T412/2/A	C[b]
wt %			
S	34.4	34.8	34.95
Cu	34.5	34.6	34.20
Ni	0.13	0.22	
Fe	29.8	29.8	30.65
Co	0.04	0.05	
Total	98.87	99.47	99.80

[b] Average of three chalcopyrite analyses from Dana's System of Mineralogy, Vol. 1, (Palance, Berman and Frondel, 1958) p. 221, analyses 1, 2, and 6

If these conditions are accepted it seems clear that elements occurring in much greater quantities overall in the zonal sequence than in the relatively unaltered peridotite must have been introduced by the metasomatizing fluids. Components of this type are Ti, V, Sr, Y, Cu, and S, all of which occur in virtually negligible quantities in the peridotite and yet show a significant build-up in various parts of the vein sequence (see Fig. 1). By contrast, Co, Mn, Cr, and Ni all occur in adequate quantities in the peridotite to account for the amounts of these elements present in the zones.

A sample of peridotite, T156 (90% olivine, 7% chlorite and 3% opaque minerals), from an adjacent body unaffected by vein metasomatism has whole-rock contents of 0.30 wt % Ni and 0.25 wt % Cr (Carswell, 1968) which are close to the values found for the least-altered zone of the present example (T412A) which has 0.25 wt % Ni and 0.26 wt % Cr.

Trace-Element Contents of the Minerals

It is evident from Figure 1 that there is only a limited correlation between the distribution of the various trace elements and the silicate phases forming the bulk of the metasomatic sequence. For example, peaks in the Cr, Ni, and Cu distributions are located near the *junction* between the enstatite and anthophyllite zones. These particular trace elements do, however, show a strong correlation with the sulphur content, indicating that they may be in part associated with phases other than the silicates. The mineralogical distribution of these trace elements has been ascertained by electron microprobe analyses of both silicate and opaque phases. Sulphides and oxides are common constituents of the samples and both are relatively concentrated in the region of the boundary between the enstatite and anthophyllite zones. The sulphide phase is mainly pentlandite with minor chalcopyrite intergrowths. The microprobe analyses of these sulphides are similar to previously reported compositions (see Table 2). The oxide phases are identified as Cr-rich magnetite (see Table 1), with lesser amounts of Cr-free magnetite. The Cr-rich magnetite may be classified as a 'ferritchromit' (Spangenberg, 1943) the occurrence of which may be of some genetic significance (see later). Original (i.e., peridotite derived) chromite is not found in the Kalskaret vein sequence, but evidence from nearby peridotite bodies suggests that chromite was almost certainly the source of Cr. Sample T156 (unaltered peridotite from an adjacent body) contains chromite with approximately 40 wt % Cr and olivine with 0.3 wt % Ni.

It is evident from Table 1 that, with the exception of chlorite, the contents of the quantitatively important trace elements, Cr and Ni, in the silicate phases show remarkably little variation both between different grains of the same phase and between different phases. Average values for these silicates are:

enstatite	0.02 wt % Cr	0.11 wt % Ni
anthophyllite	0.03 wt % Cr	0.11 wt % Ni
tremolite	0.02 wt % Cr	0.12 wt % Ni

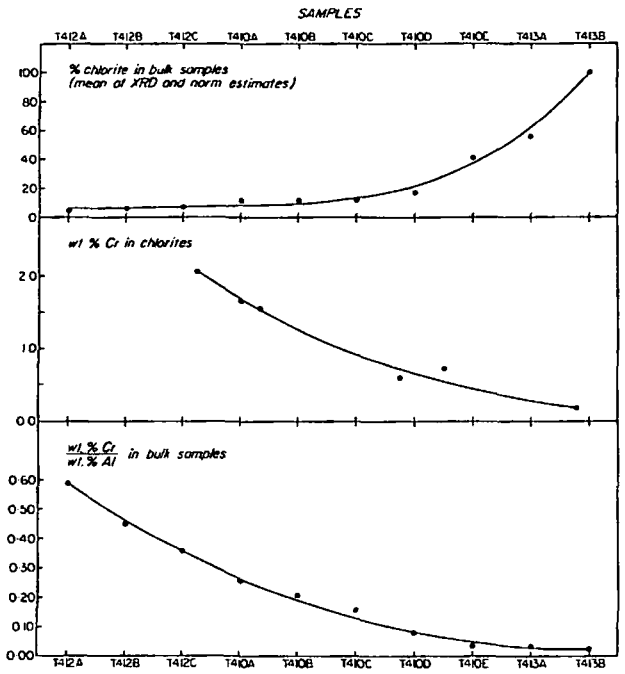

Fig. 2. Variations in modal % chlorite (top), Cr content of chlorite (determined by EMP analysis) (centre) and Cr: Al ratio (bottom) across the vein

In contrast to the Ni content of the chlorite which shows a comparatively small variation (0.18–0.25 wt % Ni) the Cr content exhibits a wide range (0.17–2.16 wt % Cr) and varies systematically across the zonal sequence. The lowest values for Cr content occur in the chlorite zone itself (see Fig. 2), the Cr content decreasing with increasing chlorite concentration in the zonal sequence.

Zonal Trace-Element Distributions

As previously noted, only limited correlation exists between the distribution of the various trace elements and the silicate phases and this is due to the incorporation of significant quantities of some elements into the opaque phases.

The exact coincidence of the distributions of Cu and S throughout the sequence and the identification of chalcopyrite as one of the opaque phases indicates that Cu occurs almost entirely in the chalcopyrite and, like the S, has clearly been introduced during the metasomatism.

The distribution pattern of Ni is irregular, rising to a peak between the enstatite and anthophyllite zones and then decreasing into the tremolite zone before increasing again in the chlorite zone. In the part of the sequence (around sample T410A) where the sulphides are concentrated (about 0.5% by volume) Ni in the pentlandite (about 33 wt % Ni) accounts for a large proportion of the Ni in the bulk sample. Towards the fluid channel it is obvious that chlorite becomes the most important host for Ni, with the whole-rock Ni content of 0.18 wt % being in reasonable agreement with the microprobe value of 0.25 wt % Ni for chlorite in the chlorite zone. Apart from the obvious peak corresponding to the concentration of pentlandite, the Ni distribution pattern closely follows that of Mg (Fig. 1a and b).

This is not unexpected as Mg and Ni vary sympathetically in almost all rocks. It is clear that there has been an overall loss of Mg, Ni and Fe from the metasomatic sequence rather than any influx.

The Co and Mn contents also show a gradual decrease towards the fluid channel with only minor irregularities.

The distribution pattern of Cr, like Ni, is very irregular. Cr rises to a peak in sample T410A in which it is located in chrome-magnetite (about 33 wt % Cr), chlorite (about 2 wt % Cr) and anthophyllite (about 0.04 wt % Cr). The Cr content then drops steadily outwards from the enstatite/anthophyllite boundary to the tremolite zone, but then increases again in samples T413A and T413B. This increase is due to the progressively larger amounts of Cr-bearing chlorite in this part of the vein (see Fig. 2) even though the chlorite itself has a considerably lower Cr content (about 0.17 wt % Cr) in comparison with the chlorite in sample T410A.

Brady (1977), from a theoretical standpoint, offered a completely novel geological explanation for the Kalskaret vein sequence, namely, that it was initially a granitic dyke. The justification for this was that it is difficult to envisage movement of an 'immobile' species such as Al (the critical element in chlorite formation). Because of this, Brady suggested that the initial wall-rock/'fluid' channel boundary in metasomatically zoned systems of the Kalskaret type may be identified by discontinuities in the weight ratios of two components such as Al and Cr. In the present example the Al: Cr ratio decreases steadily from the peridotite to the centre of the chlorite zone (see Fig. 2) without any such discontinuity. There is therefore no evidence, using Brady's own criterion, to support his implication that the chlorite zone does not represent part of the altered peridotite. His alternative model, that the fracture may have been originally occupied by granitic material, is consequently untenable and in any case does not fit the observed field relationships.

Of the undoubtedly introduced elements, V and Ti have distributions that show a direct correlation with chlorite content. Both elements apparently substitute for Al^{3+} in the chlorite. In contrast, the striking restrictions of Sr and Y to the tremolite zone indicate that these elements have predictably substi-

tuted for Ca^{2+} and are preferentially incorporated into the tremolite lattice.

The various introduced trace elements therefore tend to show quite specific concentration in particular mineral species in accordance with the availability of suitable lattice sites for their incorporation. This behaviour contrasts markedly with that of the re-distributed trace elements, notably Ni and Cr, which do not show such simple concentration 'fronts' probably because these elements were originally present throughout the region of the peridotite that has undergone reaction.

Origins of the Trace-Element Distributions

The distributions of Ti, V, Sr, and Y are compatible with the previously proposed mechanism for the origin of the zoning (Carswell et al., 1974), each of these incoming elements being preferentially incorporated where lattice sites are favourable. The behaviour of the Cr and Ni derived from the peridotite and the Cu introduced via the incoming fluids is less easily understood. Several possibilities exist, based on the following observations:

(a) The Cr, Ni, and Cu distributions show coincident maxima at the junctionof the enstatite and anthophyllite zones. This position also marks the transition from anhydrous to OH-bearing phases in the zonal sequence.

(b) A concentration of talc and magnetite occurs at the same position.

(c) At the position of maximum concentrations of Ni and Cu, i.e., in the 'sulphide zone', these elements occur mainly in pentlandite and chalcopyrite respectively.

(d) In the chlorite zone most of the Ni occurs in the chlorite itself, pentlandite being absent.

(e) The Cr is mainly located in chlorite in which the concentration of Cr varies systematically across the sequence, and in chromiferous magnetite which exhibits a maximum concentration in the 'sulphide zone'.

(f) The Cr and Ni contents of the zonal sequence were derived from the original peridotite where the Cr was located in the chromite and the Ni in the olivine. Cu and S were introduced via the incoming fluids.

It was previously suggested (Carswell et al., 1974) that the talc and serpentine were low temperature reaction products formed after the main zonal sequence was established. In view of the correlation between the 'sulphide zone' and the talc-oxide concentration it is appropriate to consider here whether the location of the Cr, Ni and Cu was related to either the high or low temperature reaction episodes or to both.

The occurrence in the zonal sequence of a chromiferous magnetite may reveal something about the way the original chromite has been broken down and the chromium relocated in other phases. Bliss and McLean (1975), cite numerous reported instances where the breakdown of chromite to form ferritchromit ± chlorite has occurred in serpentinites, although this reaction has been variously ascribed to the serpentinisation process itself, to the subsequent metamorphism of the serpentinite or to alteration prior to serpentinisation. Although ferritchromit (Spangenberg, 1943) does not represent a specific composition of chromiferous magnetite, the characteristic features of the reaction seem to have some uniformity, with the ferritchromit being relatively depleted in Mg and Al (and sometimes in Cr) and enriched in Fe relative to the parent chromite. Beeson and Jackson (1969), for example, describe the chemistry of altered primary chromites from the Stillwater complex where one chromite (47.1 wt % Cr_2O_3, 18.6 wt % Al_2O_3, 2.1 wt % Fe_2O_3, 19.7 wt % FeO, 10.0 wt % MgO) shows alteration to ferritchromit (42.0 wt % Cr_2O_3, 3.1 wt % Al_2O_3, 22.4 wt % Fe_2O_3, 30.1 wt % FeO, 2.1 wt % MgO) and chlorite (1.5 wt % Cr_2O_3, 21.0 wt % Al_2O_3, 6.6 wt % FeO, 29.4 wt % MgO). This is obviously similar to the situation in the Kalskaret vein, where, although the original chromite is not seen, the Cr-Fe oxide (approx. 47 wt % Cr_2O_3, 6 wt % Al_2O_3, 43 wt % total iron oxide as FeO) seems to be of the ferritchromit type and occurs in a part of the sequence where the small amounts of the chlorite present contain up to 2 wt % Cr_2O_3.

It is clear that the decomposition of primary chromite in the Kalskaret vein sequence must have taken place during the high-temperature reaction episode since Cr derived from the chromite (the major source of Cr) has been partially incorporated in silicates (notably chlorite) formed as a direct result of this reaction episode. This implies that the re-distribution of Cr may have been a stepwise process partially dependent upon redox potential (chromite ⇌ ferritchromit) and partially on the availability of Al to form chlorite. There is a strong tendency for Cr to be incorporated in chlorite. Where the availability of Al limits the quantity of chlorite formed, this results in chlorite with a high (c. 2 wt %) Cr content (see Fig. 2).

It is suggested that in the Kalskaret vein the distribution of Cr was controlled by two sequential reactions. Firstly, the original primary chromite was completely broken down to form ferritchromit plus small amounts of Cr-rich chlorite, this part of the

process being seen in the inner part of the zonal sequence (in the 'sulphide zone') where little or no introduced Al was present. Secondly, as the development of the zone sequence progressed, more Al became available via diffusion from the fluid channel, thus enabling the formation of more chlorite which incorporated the Cr released by the further breakdown of the ferritchromit, as seen in the outer parts of the sequence where no oxide phase remains and virtually all the Cr is located in chlorite.

It is interesting to note that Trommsdorff and Evans (1974) have observed the exact reverse of these reactions in metamorphosed serpentinised peridotite and associated the progressive reaction chlorite→ ferritchromit→chromite with increasing grade of metamorphism.

The occurrence of pentlandite (often with chalcopyrite) as ores associated with serpentinites is well known (Ramdohr, 1967) although the pentlandite may be primary (i.e., magmatic) (Groves et al., 1974) or derived from Ni originally contained in silicates (Eckstrand, 1975). In the Kalskaret sequence the Ni in the pentlandite is clearly derived from the original olivine of the peridotite.

Eckstrand (op. cit.) described a model for the development of the nickel-bearing opaque mineral assemblages of the Dumont serpentinite controlled by redox mechanisms that may be relevant here. He indicated that serpentinisation reactions involving the production of magnetite resulted in strongly reducing environments that ultimately control the formation of nickel sulphides. It therefore seems probable that the pentlandite in the Kalskaret vein resulted from such a reducing reaction with the S being introduced by the fluids as SO_4^{2-}. Complimentary oxidations may be involved in the formation of either the ferritchromit or the magnetite.

The overall reaction may be expressed as:

$$SO_4^{2-} + 8FeO \rightleftharpoons S^{2-} + 4Fe_2O_3$$

However, although the formation of the ferritchromit may be convincingly assigned to the high-temperature reaction episode, the formation of the magnetite could have resulted from the low-temperature reactions in which talc and antigorite were formed. The essential part of the equation for this reaction would be:

$$3\,FeO' + H_2O \rightleftharpoons Fe_3O_4 + H_2$$

(In olivine or enstatite) (Magnetite)

Oxidation reactions compensating for the reduction by which pentlandite formed may therefore be ascribed to either the high or low-temperature reaction episodes. Because the original Ni site (in the olivine) must have been destroyed as a result of the high-temperature reaction episode and because the Ni contents of the high-temperature reaction silicates are inadequate to account for the released Ni, it seems most likely that during the high-temperature reaction episode a significant proportion of the Ni was relocated in pentlandite where the conditions were favourable, i.e., in the 'sulphide zone'.

Experimental data from non-silicate systems suggest an upper stability limit for pentlandite of about 600° C (Kullerud, 1963) but evidence from Mg-rich silicate systems (e.g., Rajamani, 1976) indicates that it is possible for pentlandite to exist at much higher temperatures (c. 900° C). Thus experimental data do not preclude the possibility of pentlandite formation in the Kalskaret vein during the high-temperature reaction episode. However, this requires that with the continued expansion of the zonal sequence, pentlandite breaks down to provide Ni for incorporation in the chlorite which is the sole Ni-bearing mineral in the outer part of the sequence. Alternatively, Ni could have been temporarily located in another host (now destroyed) during the high-temperature reaction episode and relocated in pentlandite as a result of the low-temperature reactions.

On the balance of the evidence available, we favour the development of the pentlandite during the high-temperature reaction episode, but in either event, it seems clear that the distribution of Cr and Ni has been controlled by a complex interplay of oxidation-reduction mechanisms coupled with the availability of Al as the critical factor in chlorite formation.

References

Beeson, M.H., Jackson, E.D.: Chemical composition of altered chromites from the Stillwater complex. Montana. Am. Mineral. 54, 1084–1100 (1969)

Bliss, N.W., MacLean, W.H.: The paragenesis of zoned chromite from Central Manitoba. Geochim. Cosmochim. Acta 39, 973–990 (1975)

Brady, J.B.: Metasomatic zones in metamorphic rocks. Geochim. Cosmochim. Acta 41, 113–125 (1977)

Brueckner, H.K.: Contact and fracture ultramafic assemblages from Norway: Rb-Sr evidence for crustal contamination. Contrib. Mineral. Petrol. 49, 39–48 (1975)

Carswell, D.A., Curtis, C.D., Kanaris-Sotiriou, R.: Vein metasomatism in peridotite at Kalskaret, near Tafjord, South Norway. Contrib. Mineral. Petrol. 19, 97–124 (1968)

Carswell, D.A., Curtis, G.D., Kanaris-Sotirou, R.: Vein metasomatism in peridotite at Kalskaret, near Tefjord, South Norway. J. Petrol. 15, 383–402 (1974)

Curtis, C.D., Brown, P.E.: Trace element behaviour in the zoned ultrabasic bodies of Unst, Shetland. Contrib. Mineral. Petrol. 31, 87–93 (1971)

Eckstrand, O.R.: The Dumont Serpentinite: a model for control of nickeliferous opaque mineral assemblages by alteration reactions in ultramafic rocks. Econ. Geol. 70, 183–201 (1975)

Groves, D.I., Hudson, D.R., Hack, J.B.C.: Modification of iron-nickel sulphides during serpentinisation and talc-carbonate alteration at Black Swan, Western Australia. Econ. Geol. 69, 1265–1281 (1974)

Harris, D.C., Nickel, E.H.: Pentlandite compositions and associations in some mineral deposits. Can. Mineral. 11, 861–878 (1972)

Kullerud, G.: Thermal stability of pentlandite. Can. Mineral. 7, 353–366 (1963)

Palache, C., Berman, H., Frondel, C.: Dana's system of mineralogy, Vol. I, 7th Ed. New York: John Wiley & Sons 1978

Rajamani, V.: Distribution of iron, cobalt and nickel between synthetic sulphide and orthopyroxene at 900° C. Econ. Geol. 71, 795–802 (1976)

Ramdohr, P.: A widespread mineral association, connected with serpentinisation. N. Jb. Mineral. Abh. 107, 241–265 (1967)

Rucklidge, J.C.: A study of the redistribution of nickel in the serpentinisation of olivine. Proc. 6th Inter. Conf. X-ray Optics and Microanalysis, Tokyo (1972)

Spangenberg, K.: Die chromitlagenstätte von Tampadel in Zobten. Z. Prakt. Geol. 51, 13–35 (1943)

Trommsdorf, V., Evans, B.W.: Alpine metamorphism of peridotitic rocks. Schweiz. Mineral Petrol. Mitt. 54, 333–352 (1974)

Received April 19, 1978 / Accepted June 21, 1978

UNIVERSITY OF UTAH
RESEARCH INSTITUTE
EARTH SCIENCE LAB.

[AMERICAN JOURNAL OF SCIENCE, VOL. 275, DECEMBER, 1975, P. 1133-1163]

HIGH GRADE REGIONAL METAMORPHISM OF SOME CARBONATE BODIES: SIGNIFICANCE FOR THE ORTHOPYROXENE ISOGRAD*

WILLIAM E. GLASSLEY**

Mineralogisk-Geologisk Museum, Sars Gate 1, Oslo 5, Norway

ABSTRACT. Amphibolite facies to granulite facies metamorphism of carbonate bodies in the Lofoten-Vesterålen region of northern Norway has resulted in the development of a variety of mineral assemblages within each carbonate body and a mantle zone of metasomatically derived pyroxenite surrounding each body. The mineral assemblages in the core of the carbonate bodies and the sequence of assemblages encountered outward from the carbonate cores suggest that three different mineralogical sequences can be recognized. All bodies in the eastern and northeastern part of the study area (eastern province) have amphibole + diopside + dolomite ± calcite as an assemblage in the core of the carbonate bodies and forsterite + calcite in the outer part of the bodies. Just to the west (central province) the core assemblage becomes diopside + spinel + calcite + dolomite; the assemblage in the outer parts of the body includes forsterite + calcite. In the western part of the study area (western province) diopside and dolomite do not coexist and are superseded by the compositionally equivalent mineral pair forsterite + calcite in the carbonate cores. Mineral compositions and the phase equilibria suggest that mineralogical zoning of the carbonate bodies results from variation in the vapor composition in which μCO_2 and the ratio H_2O/HF decrease outward from the carbonate core. Variation in the sodium and potassium content of the vapor phase is also possible but is not required by the phase equilibria. The phase equilibria and vapor composition variation are interpreted as indicating that the gradient in vapor composition is inherited, although the absolute vapor composition must reflect modification of the inherited vapor composition through buffering reactions. Variation in mineral composition, which could be attributed to changes in metamorphic grade, were not observed. The province boundaries strongly diverge from the orthopyroxene isograd and suggest that the thermal structure of the deep crust was complex.

INTRODUCTION

The purpose of the research reported in this paper is to examine and model the phase relationships in silicate-bearing calcite–dolomite marbles in a high grade metamorphic terrain. Of specific interest are the following questions:

1. What phase relationships develop in siliceous marbles metamorphosed under granulite facies conditions?

2. Are there variations in mineral composition that can be related to metamorphic grade?

3. Can the phase relationships in the carbonates be used to define the thermal structure of the lower crust and to evaluate the role of mixed volatiles in the development of high grade metamorphic rocks?

Recent advances in studies of phase equilibria in mixed volatile systems relevant to parageneses in marbles (Korzhinskii, 1957; Greenwood, 1967; Vidale, 1969; Ryzhenko and Volkov, 1971; Skippen, 1971, 1974; Vidale and Hewitt, 1973) allow critical evaluation of the role of pressure, temperature, and vapor composition in the metamorphic process. It was anticipated that the role of mixed volatiles in the development of the solid phase assemblages in the marbles could be determined by

* Norwegian Geotraverse Project Contribution 106.

** Present address: Department of Oceanography, University of Washington, Seattle, Washington 98195

examining the mineral compositions and phase equilibria in the marbles. The results demonstrate that the vapor composition during metamorphism was a complex mixture of the components CO_2, H_2O, Na_2O, K_2O, and F, and that variations in the ratios of three of the components are adequate to describe most of the changes in phase equilibria exhibited at any given site.

Concerning the third question, it was anticipated that once the phase relationships in the marbles were modelled, it would be possible to evaluate the influence of vapor composition on the development of granulite facies gneisses. Of specific interest was the relative magnitude of the fugacity of H_2O (f_{H_2O}) during metamorphism of quartzo-feldspathic gneisses in the region. Progressive changes in phase equilibria and phase chemistry argue effectively that the development of granulite facies rocks is initiated through dehydration reactions involving biotite and hornblende (Binns, 1964, 1965; Buddington, 1939, 1963; Engel and Engel, 1960, 1962a, b; de Waard, 1965, 1967). Such reactions are a function of pressure, temperature, and f_{H_2O}; independent variation in these three parameters is sufficient to reconcile the range of estimated conditions for the orthopyroxene isograd (see Buddington, 1963; Buddington and Lindsley, 1964; Touret, 1971a, b; Turner, 1968). However, in only two published reports (Buddington, 1963; Touret, 1971b) have investigators documented the effect of variable f_{H_2O} on mineral parageneses at the amphibolite facies to granulite facies transition. The results of the research reported in this paper are consistent with several different interpretations. However, on the basis of supporting geological evidence, the most reasonable interpretation appears to be that, unlike the Adirondack terrain and the Precambrian region of southern Norway, variation in the fugacity of water was not of sufficient magnitude to cause the trend of the orthopyroxene isograd to deviate significantly from the trend of isothermal surfaces during metamorphism, even though the thermal structure, based on the regional trend of several isograds, appears to have been complex.

GENERAL GEOLOGY

The Lofoten-Vesterålen province is composed of intrusive rocks and amphibolite facies and granulite facies gneisses of Precambrian age which have experienced a complex, polymetamorphic history (Devaraju, ms; Heier, 1960; Griffin and Heier, 1969; Green and Jorde, 1971; Heier and Thoresen, 1971; Griffin, personal commun., 1973; P. Taylor, personal commun., 1973). The oldest petrographically recognizable event is a major synkinematic amphibolite facies to granulite facies metamorphism of 1850 m.y. (Rb–Sr whole rock age; P. Taylor, personal commun., 1973). This event appears to have affected the entire province, and evidence of it is well preserved. The amphibolite facies rocks consist mainly of well foliated, compositionally banded gneisses and migmatites, with alternating layers of mafic and felsic material. The felsic bands are composed of plagioclase, microcline, and quartz in a granoblastic fabric; biotite and hornblende in a lepidoblastic fabric are the dominant minerals in the

and phase equilibria in the marbles
vapor composition during metamor-
components CO_2, H_2O, Na_2O, K_2O,
ıtios of three of the components are
nges in phase equilibria exhibited at

t was anticipated that once the phase
delled, it would be possible to evalu-
on on the development of granulite
was the relative magnitude of the
tamorphism of quartzo-feldspathic
anges in phase equilibria and phase
evelopment of granulite facies rocks
ıctions involving biotite and horn-
ton, 1939, 1963; Engel and Engel,
). Such reactions are a function of
ependent variation in these three
ıe range of estimated conditions for
ddington, 1963; Buddington and
rner, 1968). However, in only two
Touret, 1971b) have investigators
$_2$o on mineral parageneses at the
transition. The results of the re-
tent with several different interpre-
pporting geological evidence, the
to be that, unlike the Adirondack
southern Norway, variation in the
agnitude to cause the trend of the
nificantly from the trend of iso-
n, even though the thermal struc-
eral isograds, appears to have been

OLOGY

s composed of intrusive rocks and
gneisses of Precambrian age which
amorphic history (Devaraju, ms;
reen and Jorde, 1971; Heier and
mun., 1973; P. Taylor, personal
cally recognizable event is a major
anulite facies metamorphism of
Taylor, personal commun., 1973).
entire province, and evidence of
ıcies rocks consist mainly of well
and migmatites, with alternating
ıe felsic bands are composed of
granoblastic fabric; biotite and
e the dominant minerals in the

mafic bands. The amphibolite facies rocks grade into the granulite facies rocks along strike.

The transition from the amphibolite facies rocks into the granulite facies rocks in the northern half of the island of Langöy (fig. 1) is characterized by several mineralogical changes. The most prominent change is the development of orthopyroxene at the expense of hornblende, biotite, and quartz (Heier, 1960). Other mineralogical changes described by Heier (1960) are (1) a continuous increase in the anorthite content of the plagioclase, (2) an increase in the optic axial angle of the hornblende and a change in color from green to brown (both variations correlating with apparent increases in tetrahedrally coordinated aluminum and octahedrally coordinated titanium), and (3) a change in the potassium feldspar symmetry expressed by the progression from microcline in the amphibolite facies rocks through orthoclase with undulose extinction in the charnockite border series (see below) to orthoclase in the banded series rocks (see below). For optical and X-ray data pertaining to the change in potassium feldspar symmetry consult Heier (1960).

The granulite facies rocks in the northern part of the island of Langöy are subdivided into the "charnockite border series" and the "banded series" (Heier, 1960). The charnockite border series is a distinctly banded unit in which mafic and felsic layers can be readily distinguished. Toward the west the bands become less distinct as the quartz and plagioclase in the felsic bands become darker. The change in color marks the transition to the banded series rocks. Because this transition is gradual, the boundary between these two units is only approximate (fig. 1). The granulite facies gneisses on Gimsöy and Austvagöy are similar to the banded series rocks on Langöy.

In the southern part of the island of Langöy, the transition from amphibolite facies to granulite facies is less well defined. Field and petrographic data appear to indicate that the metamorphic transition is defined by the mineralogical changes described above. However, the metamorphic transition also coincides with the transition from dioritic border series gneiss to red augen gneiss rich in potassium feldspar and is thus complicated by whole rock compositional contrasts. Details of the metamorphic transition in this region have yet to be understood.

A second metamorphic event (1100 m.y.; Rb–Sr whole rock age; P. Taylor, personal commun., 1973) resulted in local isoclinal folding and retrogression of granulite facies rocks to amphibolite facies parageneses. The retrogression is accompanied by color changes that allow rocks affected by this late event to be distinguished in the field from rocks affected solely by the older metamorphic episode.

A complex sequence of intrusive events involving granitic and mangeritic magmas occurred between 1450 and 1850 m.y. (P. Taylor, personal commun., 1973). These intrusive episodes appear not to be genetically related to the metamorphic events whose ages bracket them.

The carbonate bodies studied in this investigation occur throughout the Lofoten-Vesterålen province (fig. 1) as pods and lenses, with dimen-

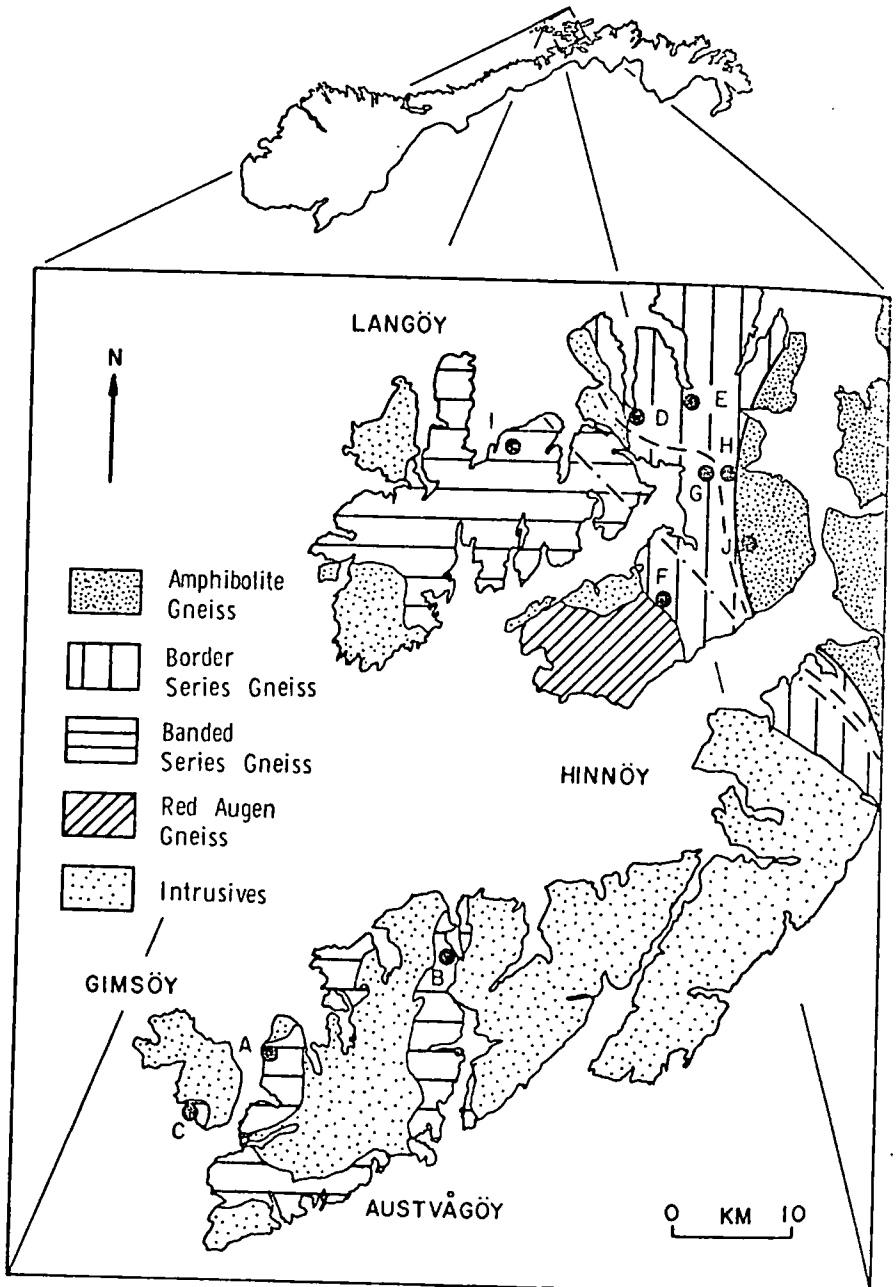

Fig. 1. General geology and the locations of the carbonate bodies in the study area. The heavy solid line is the orthopyroxene isograd: granulite facies rocks occur to the west of this line, and amphibolite facies rocks are restricted to the areas east of this line. The dashed line is the western limit of the eastern province, and the dash-dot line is the eastern limit of the western province. The central province is restricted to the area between the two broken lines. The trends of the province boundaries on the island of Hinnoy are based on data supplied by E. Tveten (personal commun., 1974).

carbonate bodie

sions of a few tens o
marbles in which app
made up of carbonat
of silicates and spinel
out the body or in ba

Development of
synchronous with the
sults from the followi
of non-carbonate min
result of solid state
phosis, tend to parall
(fig. 2), and (2) mine
(phlogopite) form ex
dimension parallel to

Immediately adj
clinopyroxenite. The
zones which vary in t
with the carbonate
phibole–phlogopite–
quartzo–feldspathic
by the amphibole–p
hibited by the enclosi
zones and the gneissi
metamorphosis.

The zones mant
eralized sequence, fr
a massive, granular
regime of phlogopit

Fig. 2. Generalized
are enclosed in gneiss (
cally altered zone of p
Layering in the carbo
When possible, sample
the layering in the carb

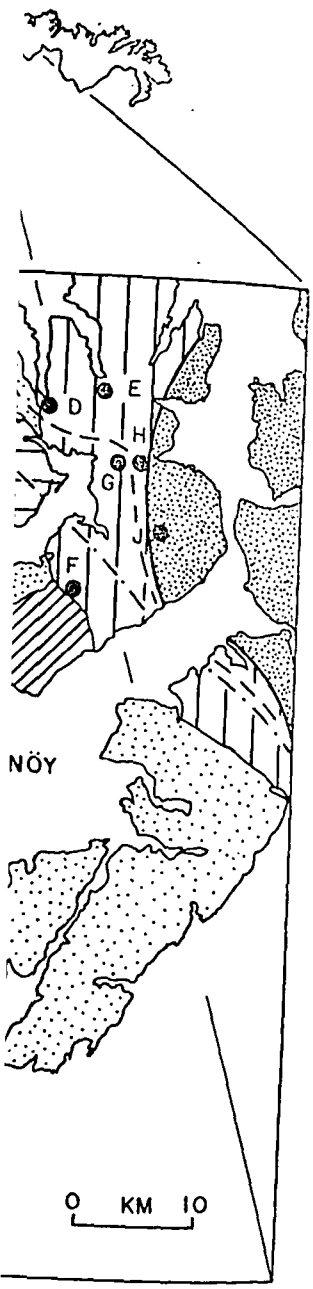

onate bodies in the study
nulite facies rocks occur to
ed to the areas east of this
province, and the dash-dot
al province is restricted to
rovince boundaries on the
personal commun., 1974).

sions of a few tens of meters. These bodies are impure calcite-dolomite marbles in which approximately 80 to 90 percent of the rock volume is made up of carbonate material. The remainder of the body is made up of silicates and spinel which occur as discrete grains disseminated throughout the body or in bands and knots a few centimeters wide.

Development of the metamorphic minerals in the carbonates was synchronous with the 1850 m.y. metamorphic event. This conclusion results from the following characteristics of the carbonate bodies: (1) bands of non-carbonate minerals, although somewhat folded and disrupted as a result of solid state "flow" of the carbonate during kinematic metamorphosis, tend to parallel banding and foliation in the country rock gneiss (fig. 2), and (2) minerals that occur in elongate (amphibole) or tabular (phlogopite) form exhibit a strong preference to have the longest crystal dimension parallel to the banding in the carbonates.

Immediately adjacent to all the carbonate bodies are mantles of clinopyroxenite. These monomineralic mantles are massive, dark green zones which vary in thickness from 50 to 200 cm. Away from the contact with the carbonate bodies the mantles grade into strongly foliated amphibole–phlogopite–clinopyroxene rocks which, in turn, grade into quartzo–feldspathic country rock gneisses (fig. 2). The foliation exhibited by the amphibole–phlogopite–clinopyroxene rock is parallel to that exhibited by the enclosing country rocks, strongly suggesting that the mantle zones and the gneissic country rocks developed during the same kinematic metamorphosis.

PETROLOGY OF THE MANTLE ZONES

The zones mantling the carbonate bodies exhibit the following generalized sequence, from the margin of the carbonate bodies outward: (1) a massive, granular inner regime of green clinopyroxene; (2) a banded regime of phlogopite + clinopyroxene ± amphibole in which lepido-

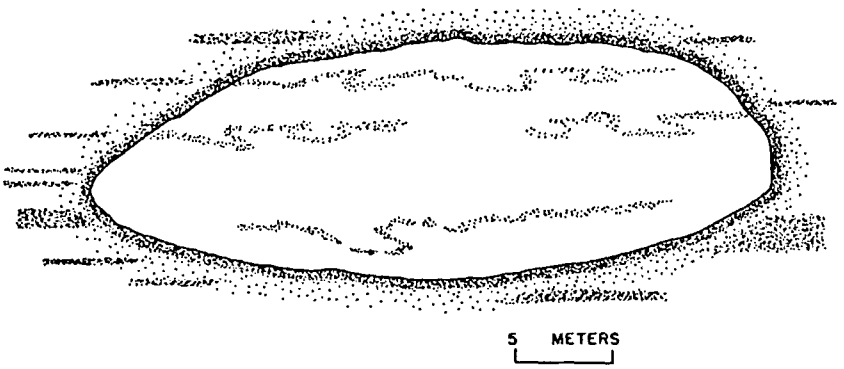

Fig. 2. Generalized diagram of the field aspect of the carbonate bodies. The bodies are enclosed in gneiss (banded zone around the body) and are mantled by a metasomatically altered zone of pyroxenite (heavy stipple) which grades into the enclosing gneiss. Layering in the carbonate bodies (lightly stippled bands) is contorted and disrupted. When possible, samples were collected along traverses parallel and perpendicular to the layering in the carbonate bodies.

TABLE 1

Chemical analyses of mantle zone minerals in carbonate free assemblages

	Phlogopites					Amphiboles				Clinoproxenes			
	D-6	D-7	F-2	H-9	J-10	D-4	D-6	H-9	J-10	D-4	D-6	D-7	F-2
SiO_2	39.4	40.6	40.6	41.3	40.9	40.0	41.9	43.9	42.2	47.2	52.3	53.5	49.2
TiO_2	0.63	1.26	0.87	0.91	0.43	1.55	0.60	n.d.	1.10	0.93	0.20	0.27	0.38
Al_2O_3	17.8	17.6	17.9	18.4	16.9	16.7	15.1	16.7	15.4	11.5	5.23	4.69	5.76
FeO*	3.76	6.18	2.72	5.32	1.00	12.8	7.04	6.16	4.89	7.65	3.71	4.19	3.10
MnO	0.08	n.d.	n.d.	n.d.	0.03	0.11	0.12	n.d.	0.05	0.10	0.12	0.19	0.19
MgO	24.5	21.9	24.9	23.8	26.9	12.1	16.4	16.2	18.5	10.8	15.4	14.8	15.2
CaO	n.d.	n.d.	n.d.	n.d.	n.d.	12.8	13.1	12.9	13.5	22.3	23.9	22.0	25.6
Na_2O	0.27	0.10	0.26	0.32	0.54	2.09	1.91	2.56	2.93	**	**	**	**
K_2O	9.50	9.89	9.67	8.69	9.26	1.11	1.32	0.40	0.39	n.d.	n.d.	n.d.	n.d.
F	1.45	1.09	1.31	1.02	2.06	n.d.	n.d.	n.d.	n.d.	n.d.	n.d.	n.d.	n.d.
Total***	96.78	98.16	97.68	99.33	97.15	99.26	97.49	98.82	98.96	100.48	100.86	99.64	99.43

* FeO = total iron. ** Na_2O is less than 0.03. *** Totals corrected for fluorine, if F is in the analysis.

n.d. = not determined. Sample letter designation refers to location in figure 1; sample number refers to a specific sample from a given site. Analyses were conducted on an ARL-EMX SM 3 channel electron microprobe which was operated at 15 Kv and a sample current of 0.05 μamps. Analyses are corrected for instrument deadtime and drift and for background, absorption, fluoresence, and mean atomic number effects.

blastic textures domin
(3) a regime transition
ions of clinopyroxene
hornblende, and sphe
the gneisses increases,
sphene. The width of

The field relatio
strongly suggest that
interchange across the
and the banded pyro
altered carbonate an
volumes of both rock
positions (table 1) an
(Heier, 1960), it is evi
have occurred (fig. 3).

The sequence of
experimentally produ
differences in bulk co
the experimental sys
differences in the ass
the experimental res
so, the sequence of a
experimental system
zones. By analogy to
migration of Si^{++}, A
Ca^{++} and Mg^{++} a
reasonably be attrib

Fig. 3. Approximat
through the mantle zo
deduced from mineral
basis) on the left hand
part of the figure rep
after (lower half of bo

blastic textures dominate (the banding in this regime is 1-10 mm wide); (3) a regime transitional to the country rock gneiss, with variable proportions of clinopyroxene, phlogopite, plagioclase, orthoclase, quartz, biotite, hornblende, and sphene. Away from the mantle zone the grain size in the gneisses increases, and opaque minerals appear at the expense of sphene. The width of each of the above regimes varies from site to site.

The field relationships and the sequence of mineral assemblages strongly suggest that the mantles developed as a result of metasomatic interchange across the carbonate-gneiss contact. If the massive pyroxenite and the banded pyroxenite correspond, respectively, to metasomatically altered carbonate and gneiss, the field relationships imply that large volumes of both rock types have been altered. Based on the mineral compositions (table 1) and the average composition of the banded granulites (Heier, 1960), it is evident that gross changes in initial bulk composition have occurred (fig. 3).

The sequence of assemblages in the mantle zones is similar to the experimentally produced "calc-silicate" bands of Vidale (1969). However, differences in bulk composition and pressure-temperature history between the experimental system and the natural system have resulted in some differences in the assemblages that have developed. Direct application of the experimental results to this natural system is thus not justified. Even so, the sequence of assemblages suggests that behavior of cations in the experimental system approximates the behavior of cations in the mantle zones. By analogy to the experimental system, the metasomatism involved migration of Si^{4+}, Al^{3+}, K^{+} (?), and Fe^{++} (?) toward the carbonate and Ca^{++} and Mg^{++} away from the carbonate. The element migration can reasonably be attributed to chemical potential gradients that developed

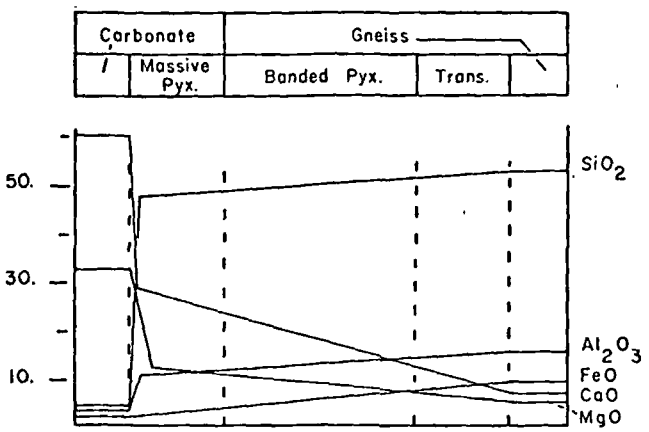

Fig. 3. Approximate changes in whole rock composition from the carbonate bodies, through the mantle zones, and into the enclosing gneiss. Whole rock compositions are deduced from mineral compositions and modes. The weight percent scale (CO_2-free basis) on the left hand side of the figure is approximate. The boxed area in the upper part of the figure represents the lithologic contrasts before (upper half of box) and after (lower half of box) metamorphism.

al metamorphism of some

* FeO = total iron. ** Na_2O is less than 0.03. *** Totals corrected for fluorine, if F is in the analysis.
n.d. = not determined. Sample letter designation refers to location in figure 1; sample number refers to a specific sample from a given site. Analyses were conducted on an ARL-EMX SM 3 channel electron microprobe which was operated at 15 Kv and a sample current of 0.05 μamps. Analyses are corrected for instrument deadtime and drift and for background, absorption, fluorescence, and mean atomic number effects.

as a result of compositional contrasts between the carbonate bodies and the quartzo-feldspathic gneisses.

PETROGRAPHY OF THE CARBONATE ROCKS

Each carbonate body exhibits a variety of mineral assemblages arranged in a regular manner from the interior of the carbonate outward. The assemblages are limited to various four-, five-, and six-mineral combinations of the phases calcite, dolomite, diopside, forsterite, pargasitic hornblende, phlogopite, and spinel.

Primary textures and mineralogies are well preserved; retrograde reactions have affected less than 10 percent of the samples examined. Primary assemblages are characterized by granoblastic or lepidoblastic textures and a complete absence of reaction textures. The ubiquitous development of equilibrium textures, even in assemblages that contain all minerals of a reaction assemblage (reactions discussed below), probably results from rapid approach of the carbonate assemblages to chemical and textural equilibrium, relative to the rate of change of the parameters controlling the metamorphism.

All the carbonate bodies, with the exception of site B, are mineralogically zoned. At any given site, the sequence of assemblages encountered outward from the core of the carbonate body is restricted to one of three types. Each sequence type is characterized by the mineral assemblage that occurs in the core of the carbonate. On the basis of the geographical distribution of the three sequence types, three provinces can be delineated in the study area. All bodies in the eastern province contain the core assemblage pargasitic hornblende + calcite + dolomite, all bodies in the central province contain the assemblage diopside + spinel + dolomite in the carbonate core, and all bodies in the western province contain the core assemblage forsterite + calcite ± spinel. The systematic changes in core mineralogy correspond to reaction relationships involving compositionally similar assemblages (mineral compositions used in the reactions are listed in table 4; justification for the mineral compositions used is presented in the section dealing with mineral chemistry):

$$\text{pargasite} + \text{calcite} + \text{dolomite} = \text{diopside} + \text{spinel} + \text{vapor} \quad (14)$$

$$\text{diopside} + \text{dolomite} = \text{forsterite} + \text{calcite} + CO_2. \quad (16)$$

The boundaries in figure 1 that define the limits of each province represent the apparent trace of the P–T–X surfaces to which reactions (14) and (16) would correspond. These reactions, and the provinces associated with them, are discussed in the following sections. All reaction numbers refer to the reactions tabulated in table 4.

Diopside–spinel reaction (reaction 14).—At locations D, E, H, and J mineral assemblages in the core of the carbonate bodies contain pargasitic hornblende + calcite + dolomite, but the same assemblage is totally lacking at sites A, B, C, F, G, and I (fig. 1). The compositionally equivalent mineral pair diopside + spinel occurs at all of the latter sites but is never found at sites D, E, H, and J.

Complete absence of
one boundary, if either c
presence of calcite and th
small modal proportion o
the practical consequence
This reaction evolves a v
percent of the component
reaction will take place is
exists with the amphibole
action.

Mineral assemblages
bodies in the eastern pro
containing amphibole +
Outward from the core of
occurs (table 2). At sites H
be written that relate so
each other:

Sites H and J	diopside
phlogopi
Site J	phlogopi
forsterite
	phlogopi
forsterite
	phlogopi
spinel +

For site J the reactions a
carbonate interior. The
table 4.

Assemblages that ca
treated as compositionall
coexisted with the assem
ponents indicated in the
tionally equivalent assem
tionally appropriate vap
not be assumed, howeve
rocks that contain assem
rock composition will b
all) minerals of the reac
compositional equivalen
of the reactant assembla
present in adjacent assem

Assemblages that c
action represent miner
from the adjacent assem

Complete absence of amphibole is not required beyond the eastern zone boundary, if either calcite or dolomite is absent. But the ubiquitous presence of calcite and the common presence of dolomite, as well as the small modal proportion of amphibole (always less than 2 percent), have the practical consequence of forcing complete reaction of the amphibole. This reaction evolves a vapor phase that contains more than 80 mole percent of the components CO_2 and H_2O. The temperature at which this reaction will take place is dependent on the vapor composition that coexists with the amphibole + calcite + dolomite assemblage prior to reaction.

Mineral assemblages within the eastern province.—All the carbonate bodies in the eastern province (D, E, H, and J) have core assemblages containing amphibole + diopside + dolomite ± calcite ± phlogopite. Outward from the core of the bodies a systematic sequence of assemblages occurs (table 2). At sites H and J (fig. 1) balanced chemical reactions can be written that relate some of the assemblages immediately adjacent to each other:

Sites H and J	diopside + dolomite + amphibole + $vapor_1$ = phlogopite + calcite + $vapor_2$	(12)
Site J	phlogopite + calcite + dolomite + $vapor_1$ = forsterite + amphibole + $vapor_2$	(9)
	phlogopite + dolomite + $vapor_1$ = forsterite + amphibole + spinel + $vapor_2$	(10)
	phlogopite + dolomite = forsterite + calcite + spinel + vapor.	(7)

For site J the reactions are listed in order of increasing distance from the carbonate interior. The precise vapor component ratios are given in table 4.

Assemblages that can be related by the reactions in table 4 can be treated as compositionally equivalent, if it is assumed that a vapor phase coexisted with the assemblages, and that the vapor contained the components indicated in the reactions. In subsequent discussions of compositionally equivalent assemblages, the assumption is made that a compositionally appropriate vapor phase coexisted with the assemblages. It need not be assumed, however, that bulk rock compositions are the same for rocks that contain assemblages related by a reaction; variation in bulk rock composition will be expressed by the persistence of some (but not all) minerals of the reactant assemblage in the product assemblage. The compositional equivalence discussed here only requires that all minerals of the reactant assemblage and all minerals of the product assemblage be present in adjacent assemblages.

Assemblages that cannot be related to adjacent assemblages by reaction represent mineral combinations that are compositionally distinct from the adjacent assemblages. Such assemblages are forsterite + spinel

TABLE 2

Mineral assemblages within carbonate bodies of the eastern province

Location	Core of carbonate			Margin of carbonate
D	Am–Di–Cc–Do	Am–Di–Fo–Phl–Cc–Do (Invariant point 1)		Fo–Phl–Cc–Do
E	Am–Di–Phl–Cc–Do (Reaction 12)			Di–Fo–Phl–Cc–Do (Reaction 16)
H	Am–Di–Phl–Do $\xleftrightarrow{(12)}$	Am–Di–Phl–Cc	Fo–Sp–Cc–Do	Di–Fo–Phl–Cc
J	Am–Di–Cc–Do $\xleftrightarrow{(12)}$	Di–Phl–Cc–Do	Am–Di–Fo–Phl–Cc–Do (Invariant point 1)	Am–Fo–Phl–Cc–Do (Reaction 9)
	Am–Fo–Phl–Sp–Cc–Do (Invariant point 2)		Fo–Phl–Sp–Cc–Do (Reaction 7)	Am–Fo–Phl–Sp–Do (Reaction 10)

Double ended arrows indicate assemblages related by the noted reaction. Assemblages that are univariant or invariant in the model system (see text) are indicated by the reaction or invariant point number to which they correspond (table 4). The abbreviations are defined in table 4.

Fig. 4. Solid phase
Phlogopite (PHL), fors
the tetrahedron; diopsi
tetrahedron (open circ
locations when projecte
ic diagrams used in t
dolomite–spinel–amphi
sequent diagrams per
CO_2–H_2O–Na_2O–K_2O–F

+ calcite + dolomi
site H. Composition
original compositic

At all sites w
mineral pair diopsi
+ calcite-bearing
tional equivalents.
bodies probably c
outer portion of t
that the temperat
morphism. The c
blage changes in t

[1] Chemographic r
4. Calcite and a CO_2
picted in the chemog
the phase equilibria
vided evidence for t
There are insufficient
solid phases as a fun
chemographic relatio

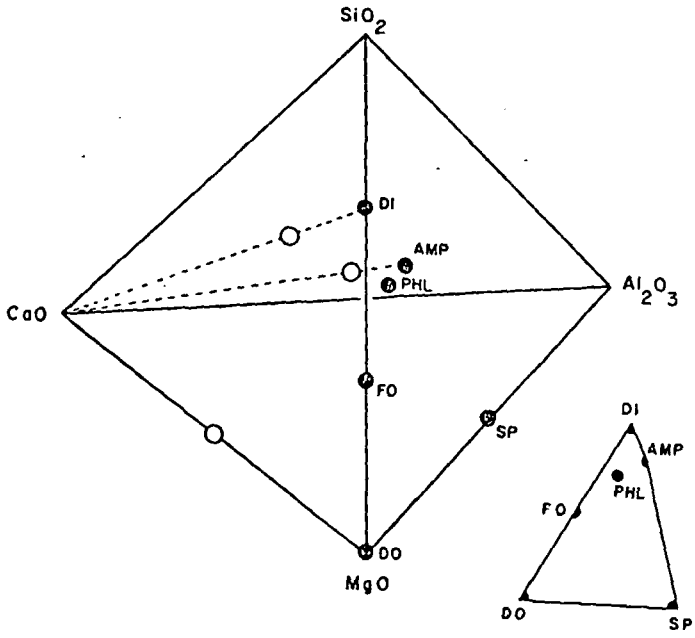

Fig. 4. Solid phase composition relations in the $CaO–MgO–SiO_2–Al_2O_3$ tetrahedron. Phlogopite (PHL), forsterite (FO), and spinel (SP) plot on the $SiO_2–MgO–Al_2O_3$ face of the tetrahedron; diopside (DI), amphibole (AM), and dolomite (DO) fall within the tetrahedron (open circles). Calcite lies at the CaO apex. The solid dots are the phase locations when projected from calcite onto the $SiO_2–MgO–Al_2O_3$ face. The chemographic diagrams used in this paper utilize that portion of the projection bounded by dolomite–spinel–amphibole–diopside. The chemographic relationships depicted in subsequent diagrams pertain only to calcite-bearing assemblages which coexist with a $CO_2–H_2O–Na_2O–K_2O–F$ vapor.

+ calcite + dolomite and diopside + forsterite + phlogopite + calcite at site H. Compositional differences such as these are probably the result of original compositional contrasts within the carbonate bodies.

At all sites within the province, the core assemblage contains the mineral pair diopside + dolomite; away from the carbonate core forsterite + calcite-bearing assemblages occur. These mineral pairs are compositional equivalents, and they demonstrate that the core of the carbonate bodies probably coexisted with a more CO_2-rich vapor phase than the outer portion of the carbonate bodies (Skippen, 1971, 1974), assuming that the temperature was uniform throughout each body during metamorphism. The chemographic relationships[1] that represent the assemblage changes in the carbonate bodies are shown in figures 7 through 11.

[1] Chemographic relationships presented later are based on the projection in figure 4. Calcite and a $CO_2–H_2O–K_2O–Na_2O–F$ vapor are present in all the assemblages depicted in the chemographic diagrams. The chemographic diagrams are developed from the phase equilibria; electron microprobe analyses and visual estimates of modes provided evidence for the compositional equivalence of contrasting mineral assemblages. There are insufficient data available to demonstrate any compositional variation in the solid phases as a function of P–T–X. Therefore, only single tie lines are used in the chemographic relationships.

tetamorphism of some

(Reaction 10)

(Reaction 7)

(Invariant point 2)

Double ended arrows indicate assemblages related by the noted reaction. Assemblages that are univariant or invariant in the model system (see text) are indicated by the reaction or invariant point number to which they correspond (table 4). The abbreviations are defined in table 4.

Mineral assemblages within the central province.—At site G the stable coexistence of diopside + spinel + dolomite and the absence of amphibole + calcite + dolomite (table 3) indicate that the core assemblage corresponds to the product assemblage of reaction (14). Therefore the boundary between the eastern and central provinces must lie to the east of this site. The assemblage that occurs in the outer portion of the body cannot be related to the core assemblage by any reaction. Hence, the two assemblages are compositionally distinct. However, as in the eastern province, the core assemblage contains the mineral pair diopside + dolomite, whereas the outer assemblage contains the mineral pair forsterite + calcite. Thus, during metamorphism the core of the carbonate body coexisted with a more CO_2-rich vapor phase than did the outer portion of the body. Variation in vapor composition at this site was, therefore, similar to that at sites in the eastern province.

Mineral assemblages in the western province.—At sites A, B, C, F, and I diopside + dolomite never occur as a mineral pair, although each mineral persists in assemblages in which the other mineral is absent. Instead, forsterite + calcite becomes the mineral pair in the core assemblages for compositions equivalent to diopside + dolomite. Hence, unlike the eastern and central provinces, forsterite + calcite is not restricted to the outer portion of the carbonate bodies in this province.

Although reactions that relate mineral assemblages at sites C and F (table 3) can be written, the majority of assemblages at the sites within this province are compositionally distinct from immediately adjacent assemblages. As in the eastern and central provinces, these compositional contrasts are believed to represent initial variations in the chemical characteristics of the carbonates. The reactions that relate compositionally equivalent but mineralogically distinct assemblages involve a mixed volatile phase, thus suggesting that, as in the eastern and central provinces, the phase equilibria developed in response to vapor compositions that were variable within a given carbonate body.

Summary.—Within each carbonate body specific mineral sequences occur outward from the carbonate core. Although compositionally distinct assemblages can be recognized in the carbonate bodies, reactions can be written between a number of contrasting assemblages, thus demonstrating compositional equivalence. These reactions involve mixed volatile phases and imply that the vapor composition systematically varied within each carbonate body. The distribution of the mineral pairs diopside + dolomite and forsterite + calcite within the carbonate bodies demonstrates that the variation in vapor composition was, at least in part, a decrease in CO_2 partial pressure outward from the carbonate core.

MINERAL CHEMISTRY

Electron microprobe analyses of minerals in selected samples (tables 5-8) demonstrate that only high magnesium, low iron compositions occur. The analyses also demonstrate that there is no recognizable systematic variation in mineral composition regionally; compositional contrasts at a

TABLE 3

Mineral assemblages within carbonate bodies of the central and western provinces

Location	Core of carbonate	Margin of carbonate
	Central province	
G	Di–Fo–Cc–Do–Sp (Reaction 16)	Fo–Phl–Cc–Do
	Western province	
A	Di–Fo–Phl–Cc	Fo–Phl–Cc–Sp — Phl–Cc
B		Fo–Phl–Cc–Do (7)
C	Fo–Sp–Cc–Do ←	→ Fo–Phl–Cc–Do
F	Di–Fo–Phl–Sp–Cc (Reaction 2)	Fo–Cc–Do–Sp — Di–Fo–Phl–Sp
I	Di–Fo–Phl–Cc	Fo–Cc–Sp — Di–Phl–Cc–Sp

See table 2 for explanation.

TABLE 4
Reactions in the model system

Phases absent	Reaction number	Reaction
Do, Cc	1	2 Phl + 4 Di + 2 Sp + 1 Na_2O = 2 Am + 2 Fo + 1 K_2O
Do, Am	2	6 Phl + 7 Cc = 7 Di + 4 Fo + 3 Sp + 7 CO_2 + 3 H_2O + 3 K_2O + 6 F
Do, Fo	3	2 Phl + 4 Am + 7 Cc = 15 Di + 7 Sp + 7 CO_2 + 3 H_2O + 1 K_2O + 6 F + 2 Na_2O
Do, Sp	4	18 Phl + 14 Cc + 3 Na_2O = 6 Am + 2 Di + 14 Fo + 14 CO_2 + 6 H_2O + 9 K_2O + 12F
Do, Phl	5	2 Fo + 6 Am + 7 Cc = 19 Di + 9 Sp + 7 CO_2 + 3 H_2O + 6 F + 3 Na_2O
Do, Di	6	38 Phl + 2 Sp + 28 Cc + 7 Na_2O = 30 Fo + 14 Am + 28 CO_2 + 12 H_2O + 19 K_2O + 24 F
Di, Am	7	2 Phl + 7 Do = 6 Fo + 7 Cc + 1 Sp + 7 CO_2 + 1 H_2O + 1 K_2O + 2 F
Di, Fo	8	4 Phl + 1 Sp + 9 Cc + 1 CO_2 + 1 Na_2O = 2 Am + 5 Do + 1 H_2O + 2 K_2O + 2 F
Di, Sp	9	6 Phl + 2 Do + 2 Cc + 1 Na_2O = 2 Am + 6 Fo + 6 CO_2 + 2 H_2O + 3 K_2O + 4 F
Di, Cc	10	46 Phl + 28 Do + 7 Na_2O = 54 Fo + 14 Am + 2 Sp + 56 CO_2 + 16 H_2O + 23 K_2O + 32 F
Di, Phl	11	2 Am + 19 Do = 12 Fo + 3 Sp + 23 Cc + 15 CO_2 + 1 H_2O + 2 F + 1 Na_2O
Sp, Fo	12	6 Phl + 14 Cc + 1 Na_2O = 2 Am + 3 Di + 7 Do + 2 H_2O + 3 K_2O + 4 F
Sp, Cc	13	12 Phl + 1 Di + 7 Do + 2 Na_2O = 4 Am + 14 Fo + 14 CO_2 + 4 H_2O + 6 K_2O + 8 F
Phl, Fo	14	2 Am + 1 Do + 1 Cc = 6 Di + 3 Sp + 3 CO_2 + 1 H_2O + 2 F + 1 Na_2O
Phl, Cc	15	8 Am + 7 Do = 23 Di + 2 Fo + 12 Sp + 14 CO_2 + 4 H_2O + 8 F + 4 Na_2O
Phl, Am, Sp	16	1 Di + 3 Do = 2 Fo + 4 Cc + 2 CO_2
Cc, Fo	17	10 Am + 7 Do + 1 K_2O = 2 Phl + 27 Di + 14 Sp + 14 CO_2 + 4 H_2O + 8 F + 5 Na_2O
Cc, Am	18	8 Phl + 7 Do = 7 Di + 4 Sp + 10 Fo + 14 CO_2 + 4 H_2O + 4 K_2O + 8 F
Am, Fo	19	2 Phl + 5 Cc = 3 Di + 2 Do + 1 Sp + 1 CO_2 + 1 H_2O + 1 K_2O + 2 F

Phase abbreviations and compositions: Cc = calcite ($CaCO_3$), Do = dolomite ($CaMg(CO_3)_2$), Di = diopside ($CaMgSi_2O_6$), Fo = forsterite (Mg_2SiO_4), Phl = phlogopite ($KMg_3Si_3AlO_{10}(OHF)_2$), Sp = spinel ($MgAl_2O_4$), Am = amphibole ($NaCa_2Mg_4Al(Si_6Al_2)O_{22}(OHF)_2$).

carbonate bodies: sign

given site (compare amphi
those exhibited between si
in mineral composition th
morphic grade.

Systematic variations
tions in the fluorine and h
ratio for phlogopites at si
carbonate-gneiss contact (s
the core of the carbonate
variation is suggested in t
variation suggests that the
cally decreased away from

Partitioning of magn
and forsterite–phlogopite
Mg between these phases
in chemical equilibrium.
amphibole exhibits greate
pairs. Figure 6, however,
tween phlogopite and am
to Mg + Fe in the amp
coefficient strongly sugges
librium; the regular distri
supports this suggestion.

Fig. 5. Mg-distribution
and phlogopite–forsterite
$Al^{[VI]}$) atoms.

given site (compare amphibole analyses from site J, for example) exceed those exhibited between sites. It is thus not possible to recognize changes in mineral composition that could be attributed to variations in metamorphic grade.

Systematic variations in vapor composition are suggested by variations in the fluorine and hydroxyl content of hydrous phases. The OH/F ratio for phlogopites at sites A and J is lower for phlogopites near the carbonate-gneiss contact (samples A-3, J-14, and J-17) than for samples in the core of the carbonate bodies (samples A-1, J-6, and J-9). A similar variation is suggested in the F content of the amphiboles. This chemical variation suggests that the ratio of H_2O to F in the vapor phase systematically decreased away from the core of the carbonate bodies.

Partitioning of magnesium between coexisting diopside–phlogopite and forsterite–phlogopite (fig. 5) demonstrates that the distribution of Mg between these phases is regular, thus suggesting that these phases are in chemical equilibrium. Partitioning of Mg between phlogopite and amphibole exhibits greater variation than that for the above two mineral pairs. Figure 6, however, demonstrates that the distribution of Mg between phlogopite and amphibole is a function of the atomic ratio of Ca to Mg + Fe in the amphibole. The regular change in the distribution coefficient strongly suggests that these two phases are in chemical equilibrium; the regular distribution of F between phlogopite and amphibole supports this suggestion.

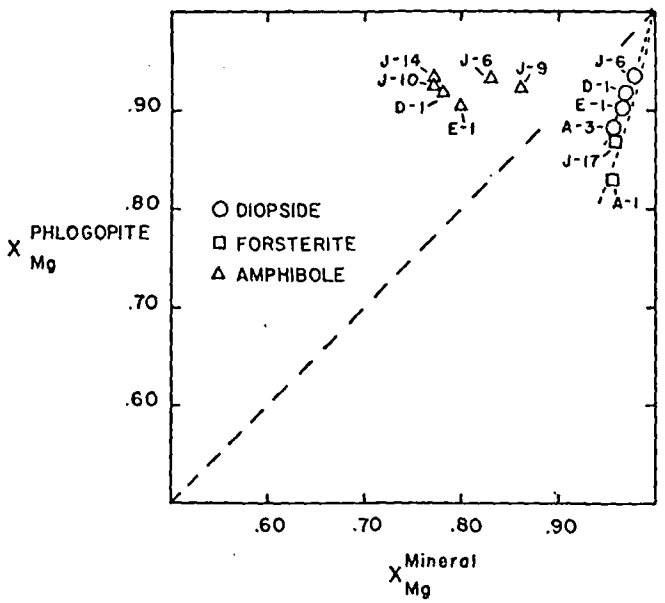

Fig. 5. Mg-distribution diagram for phlogopite–amphibole, phlogopite–diopside, and phlogopite–forsterite mineral pairs. X_{Mg} = (Mg atoms)/(Mg + Ti + Mn + Fe + Al^{VI}) atoms.

Am, Fo 19 2 Phl + 5 Cc = 3 Di + 2 Do + 1 Sp + 1 H_2O + 1 K_2O + 2 F

Phase abbreviations and compositions: Cc = calcite ($CaCO_3$), Do = dolomite ($CaMg(CO_3)_2$), Di = diopside ($CaMgSi_2O_6$), Fo = forsterite (Mg_2SiO_4), Phl = phlogopite ($KMg_3Si_3AlO_{10}(OH,F)_2$), Sp = spinel ($MgAl_2O_4$), Am = amphibole ($NaCa_2Mg_4Al(Si_6Al_2)O_{22}(OH)_2$).

The chemical formulas of minerals used in the model system (see table 4) are based on the compositional data in tables 5 through 8. Because the mole fraction of the Mg-end member in the pyroxenes, olivines, and spinels exceeds 0.85 and exhibits little variation from site to site, the pure Mg-end member formulas (that is, $CaMgSi_2O_6$, Mg_2SiO_4, $MgAl_2O_4$) were used in the reactions. The amphiboles analyzed exhibit significant compositional variability, but they consistently contain a high proportion of Na, Mg, Al, and F. Compositionally, fluorine-bearing pargasite ($NaCa_2Mg_4Al(Si_6Al_2)O_{22}(OHF)$) provides a reasonably close approximation to the amphibole in the natural system. The phlogopite analyses demonstrate that, although the micas approach pure Mg compositions, they deviate significantly from pure hydroxyl phlogopite compositions because they contain a relatively large amount of fluorine. The mica in the model system is therefore allocated one hydroxyl and one fluorine ($KMg_3Si_3AlO_{10}(OHF)_2$), in order to approximate the natural phlogopites.

ANALYSIS OF THE PHASE EQUILIBRIA

The changes in assemblages in each carbonate body that are attributable to reaction relationships must reflect variations in vapor composition or total vapor pressure; it is unreasonable to expect temperature or solid pressure gradients in bodies with dimensions of a few tens of meters in high grade, regionally metamorphosed terrains. The distribution of the mineral pairs diopside + dolomite and forsterite + calcite in bodies in the eastern and central provinces suggests that f_{CO_2} was higher in the cores of the bodies than in the rims. A similar variation in f_{CO_2} for bodies in the western province can be assumed. Variations in the ratio f_{H_2O}/f_{HF} in the vapor phase are suggested by compositions of phlogopites from bodies in the eastern and central provinces. The changes in phlogopite composi-

TABLE 5

Electron microprobe analyses of phlogopites from carbonate assemblages*

	A-1	A-3	D-1	E-1	J-6	J-9	J-10	J-14	J-17
SiO_2	40.9	43.4	42.3	41.0	41.4	41.1	40.9	40.9	40.9
TiO_2	1.02	0.70	0.17	0.43	0.48	0.38	0.43	0.57	0.44
Al_2O_3	18.2	15.4	14.7	16.6	15.4	16.6	16.9	15.6	16.9
FeO	1.70	1.84	2.32	1.51	1.14	1.44	1.00	1.30	1.91
MnO	n.d.	n.d.	0.04	0.00	0.02	0.01	0.03	0.03	n.d.
MgO	24.6	26.7	26.7	26.3	26.5	26.6	26.9	26.4	26.1
Na_2O	0.46	0.28	0.47	0.44	0.37	0.50	0.54	0.51	0.49
K_2O	9.03	9.37	9.42	9.63	9.68	9.45	9.26	9.51	9.59
F	1.04	1.99	1.74	1.49	2.19	2.17	2.06	2.17	2.41
Total	96.51	98.84	97.11	96.77	96.26	97.34	97.15	96.08	97.72
X_{Mg}	0.830	0.883	0.918	0.903	0.937	0.922	0.925	0.935	0.870
$\log (f_{H_2O}/f_{HF})$**	4.8	4.5	4.6	4.7	4.4	4.4	4.5	4.2	4.3

* See explanation for table 1.

** The fugacity ratio values are calculated assuming T = 600°C, and unit activities for the Mg-phlogopite component (Munoz and Ludington, 1974).

TABLE 6

Electron microprobe analyses of amphiboles from carbonate assemblages*

	D-1	E-1	J-6	J-9	J-7	J-10	J-14
SiO_2	44.5	44.5	44.5	46.5	47.5	42.2	43.6
TiO_2	0.40	0.69	0.80	0.70	0.59	1.10	0.60
Al_2O_3	13.3	14.5	13.4	10.5	10.0	15.4	14.0
FeO	4.90	2.90	4.05	3.69	3.85	4.89	5.16
MnO	n.d.	0.06	n.d.	0.04	0.05	0.05	n.d.
MgO	18.5	19.4	18.5	20.7	20.4	18.5	18.6
CaO	13.2	13.7	13.0	13.7	13.5	13.5	13.7
Na_2O	2.78	2.53	2.40	2.89	2.33	2.93	2.75
K_2O	0.43	0.72	0.71	0.37	0.38	0.39	0.49
F	1.39	1.04	1.53	1.51	n.d.	n.d.	1.52
Total	98.81	99.60	98.24	99.83	98.60	98.96	99.78
X_{Mg}	0.78	0.80	0.78	0.86	0.83	0.77	0.77

* See explanation for table 1.

TABLE 7

Electron microprobe analyses of clinopyroxenes from carbonate assemblages

	A-3	D-1	E-1	G-2	H-2	J-6
SiO_2	55.6	56.2	54.8	54.4	55.5	56.2
TiO_2	0.05	0.03	0.14	0.06	0.08	0.05
Al_2O_3	0.30	0.13	2.09	1.73	0.94	0.21
FeO*	0.97	0.98	1.11	0.61	0.95	0.50
MnO	0.13	0.05	0.03	0.06	0.06	0.00
MgO	17.6	18.4	17.7	18.6	17.5	18.6
CaO	25.3	24.3	23.9	25.3	25.3	25.3
Na_2O	**	**	**	**	**	**
Total	99.95	100.09	99.77	100.76	100.33	100.86
X_{Mg}	0.954	0.968	0.965	0.913	0.929	0.979

*, ** See explanation for table 1.

TABLE 8

Electron microprobe analyses of olivines and spinels from carbonate and mantle zone assemblages

	Olivines					Spinels		
	A-1	F-2†	G-2	J-12	J-17	A-1	F-2†	G-2
SiO_2	41.9	41.8	42.2	42.0	41.2	0.01	0.01	0.04
TiO_2	b.d.	b.d.	b.d.	b.d.	b.d.	0.02	0.03	0.07
Al_2O_3	b.d.	b.d.	b.d.	b.d.	b.d.	69.2	67.5	71.2
FeO*	4.16	7.67	3.64	0.89	3.97	6.62	11.2	4.46
MnO	0.25	0.52	0.13	0.03	0.07	0.25	0.37	0.09
MgO	54.2	51.5	54.5	57.0	54.0	23.0	21.6	24.6
CaO	b.d.	n.d.	n.d.	0.11	0.16	0.04	0.02	0.12
Na_2O	b.d.	b.d.	b.d.	n.d.	n.d.	0.05	b.d.	0.01
Total	100.51	101.49	100.47	100.03	99.40	99.19	100.73	100.59
X_{Mg}	0.956	0.918	0.963	0.991	0.960	0.856	0.769	0.906

b.d. = below detection limit. † from mantle zone assemblages.
*, ** See explanation for table 1.

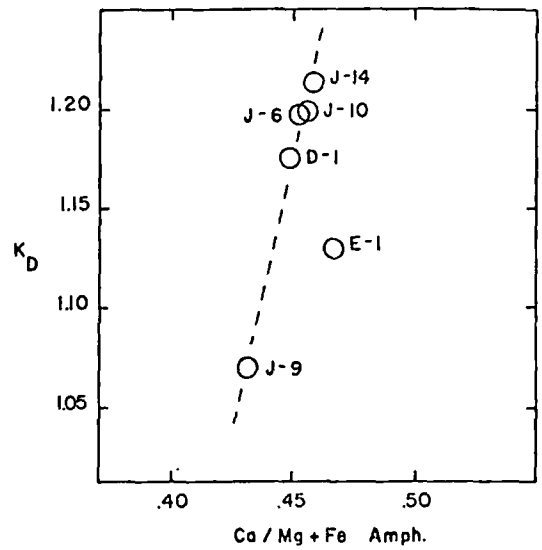

Fig. 6. Distribution coefficients (K_D) versus the atomic ratio of Ca to Mg + Fe in the amphiboles of coexisting phlogopite-amphibole pairs. $K_D = X_{Mg}^{Phl}/X_{Mg}^{Am}$.

tions reflect an increase in the fugacity of HF by a factor of about 2 (Munoz and Ludington, 1974) outward from the carbonate core (table 4). Even so, the absolute amount of HF in the vapor phase is exceedingly small. If the vapor phase was a pure mixture of the components H_2O and F, the phlogopite compositions imply that it contained less than 0.1 mole percent HF (Munoz and Eugster, 1969); if significant CO_2 were present the mole percent of HF would be even less (a constant temperature of 600°C is assumed, simply for illustration).

A model for the observed changes in the mineral assemblages and vapor compositions within the carbonate bodies can be described by the components CaO–MgO–Al_2O_3–SiO_2–Na_2O–K_2O–H_2O–CO_2–F. These components are chosen on the basis of the mineral compositions. Reactions in which pargasite is a reactant result in the liberation of Na_2O. Since no other solid phase has an appreciable sodium content, it is assumed that sodium was evolved into the vapor phase as a result of amphibole reaction. Similarly, since phlogopite is the only potassium-bearing phase among the solid phases, it is assumed that K_2O was a vapor phase component in reactions involving phlogopite. Of the other components in this nine component system, four will be treated as inert (CaO, MgO, Al_2O_3, and SiO_2); the remainder (F, H_2O, and CO_2) will be discussed below.

The nine component system contains seven solid phases (calcite, diopside, dolomite, forsterite, pargasite, phlogopite, and spinel). The reactions for phlogopite- and amphibole-bearing assemblages possess five degrees of freedom, and phlogopite or amphibole absent reactions possess four degrees of freedom, if the equilibrium parameters are pressure, tem-

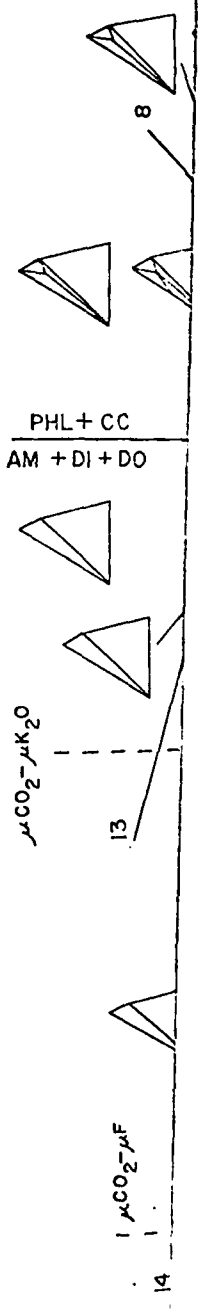

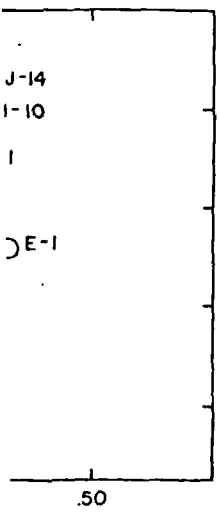

e atomic ratio of Ca to Mg + Fe in
: pairs. $K_D = X_{Mg}^{Phl}/X_{Mg}^{Am}$.

of HF by a factor of about 2
m the carbonate core (table 4).
he vapor phase is exceedingly
re of the components H_2O and
it contained less than 0.1 mole
f significant CO_2 were present
ss (a constant temperature of

the mineral assemblages and
odies can be described by the
K_2O–H_2O–CO_2–F. These com-
neral compositions. Reactions
e liberation of Na_2O. Since no
m content, it is assumed that
as a result of amphibole reac-
nly potassium-bearing phase
K_2O was a vapor phase com-
Of the other components in
treated as inert (CaO, MgO,
, and CO_2) will be discussed

seven solid phases (calcite,
logopite, and spinel). The re-
ring assemblages possess five
ibole absent reactions posses
parameters are pressure, tem-

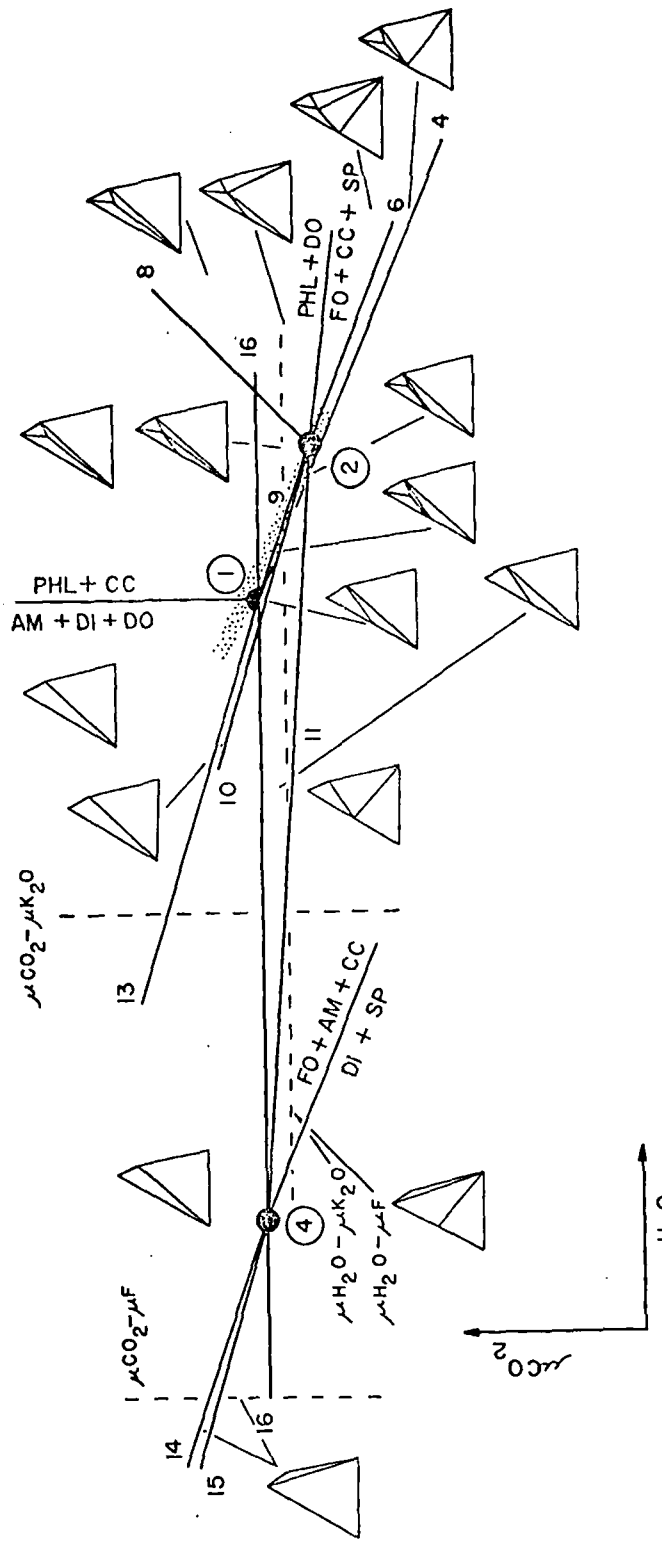

Fig. 7. μCO_2–μH_2O chemical potential diagram for the reactions tabulated in table 4. Dashed lines represent the locations of the indicated sections through this figure. Circled numbers refer to the intersection points and correspond to the lines in figure 12. The stippled area represents possible conditions for the eastern province.

perature, and the chemical potentials of all the components. Pressure and temperature can be assumed uniform for a given carbonate body. If it is also assumed that two of the vapor components are dependent equilibrium parameters, then all the reactions become univariant, and the phlogopite- and amphibole-absent reactions become compositionally degenerate, if spinel is absent. In the following treatment μNa_2O is assumed to be dependent; other vapor components will be discussed individually or in groups of two and three.

All the univariant reactions belonging to this system are listed in table 4. The topological relationships of these reactions are presented in μH_2O–μCO_2 (fig. 7), μCO_2–μF (fig. 8), μH_2O–μF (fig. 9), μH_2O–μK_2O (fig.

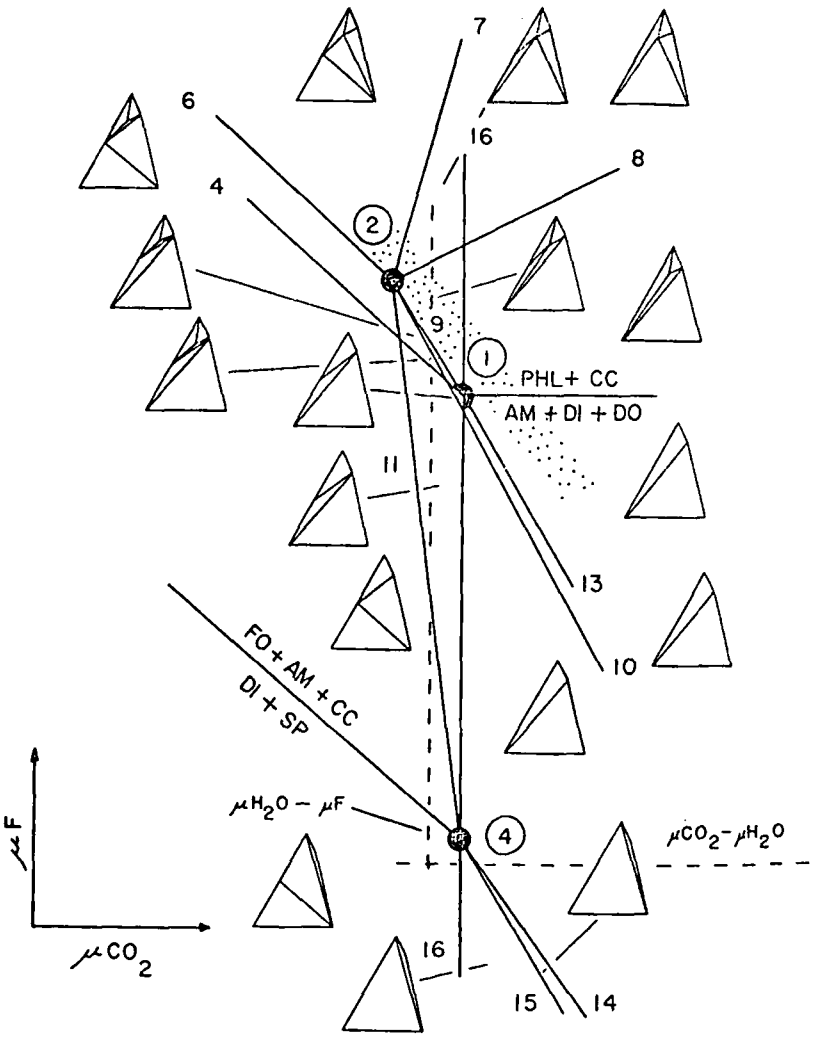

Fig. 8. μCO_2–μF chemical potential diagram. For explanation, see figure 7.

10), and μCO_2–μK_2O (fig. 11) diagrams (Korzhinskii, 1957). Only the stable intersections of the reactions are shown. The stability of these intersections (isobaric–isothermal invariant points, for the chemical potential conditions outlined above) is demonstrated by the existence of the assemblages amphibole–diopside–forsterite–phlogopite–calcite–dolomite (sites D and J, invariant point 1) and amphibole–forsterite–phlogopite–spinel–calcite–dolomite (site J, invariant point 2).

The topological relationships of the intersections of the reactions are diagrammed in figure 12. The dashed lines in figures 7 to 11 indicate the locations of the two-dimensional vapor component planes with respect to each other.

Changes in hydroxyl/fluorine ratios in hydrous minerals and the changes in phase equilibria within single carbonate bodies require that simultaneous variation in the chemical potentials occur for at least three of the vapor components. It is thus not possible to describe completely the changes in phase relationships in the two-dimensional μ–μ diagrams. For example, diopside–phlogopite–calcite–spinel assemblages that occur at sites F and I are not possible equilibrium assemblages in figures 8 and 9, although figure 11 allows such assemblages. Even so, the chemical potential diagrams individually and collectively demonstrate the necessary changes in the chemical potentials of the vapor components needed to describe the changes in phase equilibria.

The changes in phase relationships that occur in bodies within the eastern province can be completely described by an increase in $\mu F/\mu CO_2$ and a simultaneous decrease in $\mu CO_2/\mu H_2O$ (figs. 7-9) outward from the cores of the bodies. This conclusion is consistent with the independent observations that (1) the distribution of diopside + dolomite and forsterite + calcite pairs requires a decrease in P_{CO_2}/P_{H_2O} outward from the carbonate cores, and (2) the fluorine content of the hydrous phases suggests that P_{HF}/P_{H_2O} increases outward from the core of the bodies. Although variation in μK_2O is also possible, it is not required by the phase relationships; variation in μCO_2, μH_2O, and μF are completely sufficient to describe the phase relationships. Even though similar data are not available for the central and western provinces, it can reasonably be inferred that the changes in phase relationships within a given body in these provinces result from variations in vapor composition similar to the vapor composition variations in the eastern province.

It is clearly evident from figures 7 through 12, however, that although the relative core to rim changes in the chemical potential ratios may be similar for all bodies within the study area, the absolute values of the chemical potentials are strikingly different, from one province to another, for the reactions that bound the observed phase relationships. For example, the diopside + phlogopite + spinel-bearing assemblages that occur at sites F and I in the western province are restricted to the region between reactions (1) and (3) in figure 10. This region in figure 10 corresponds to a volume in figure 12 in which the lowest μK_2O values possible are defined by line 6. In contrast, sites D, E, H, and J in the eastern prov-

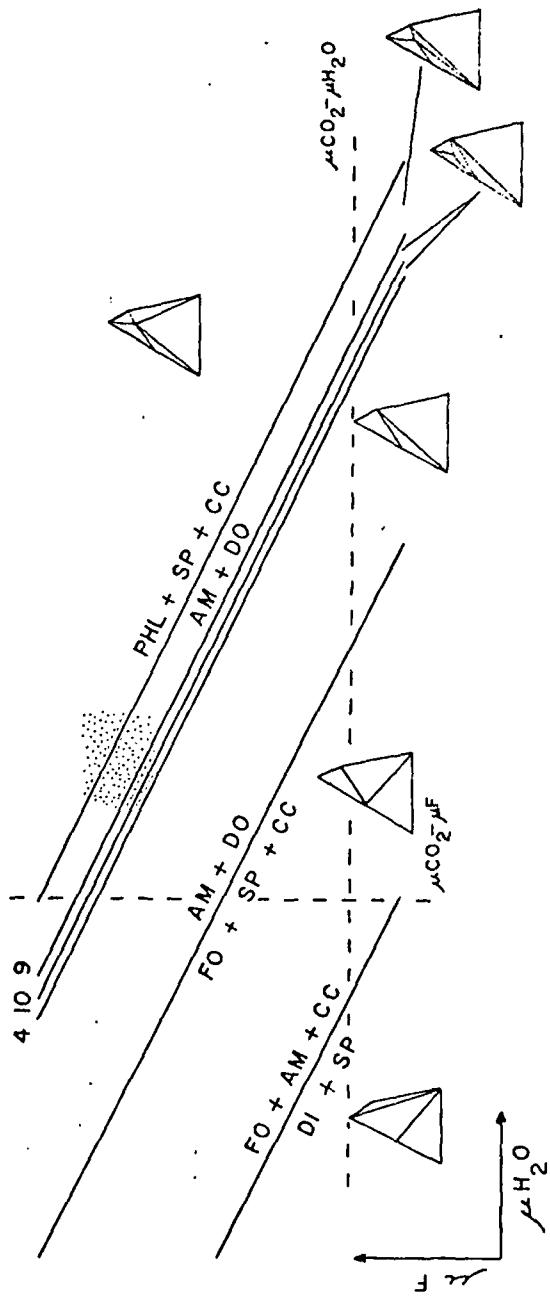

Fig. 9. μH_2O-μF chemical potential diagram. For explanation, see figure 7.

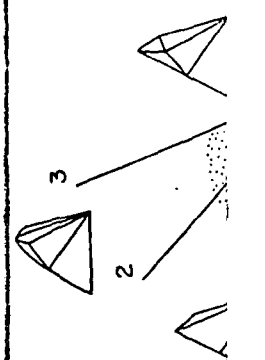

Fig. 9. μH_2O–μF chemical potential diagram. For explanation, see figure 7.

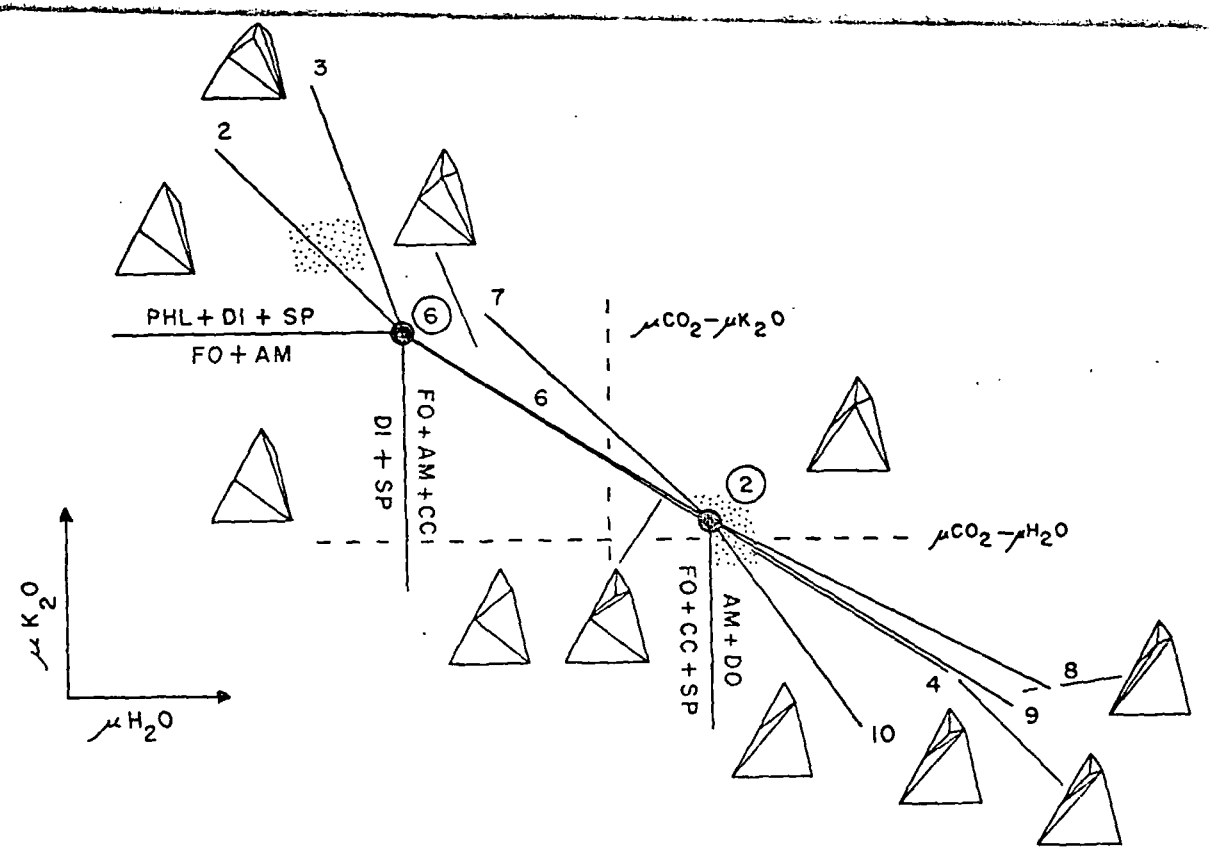

Fig. 10. μH_2O–μK_2O chemical potential diagram. Reaction and invariant point designations are the same as for figure 7. The stippled area around invariant point 2 represents possible conditions for the eastern province; the stippled area around reaction 2 represents possible conditions for the western province.

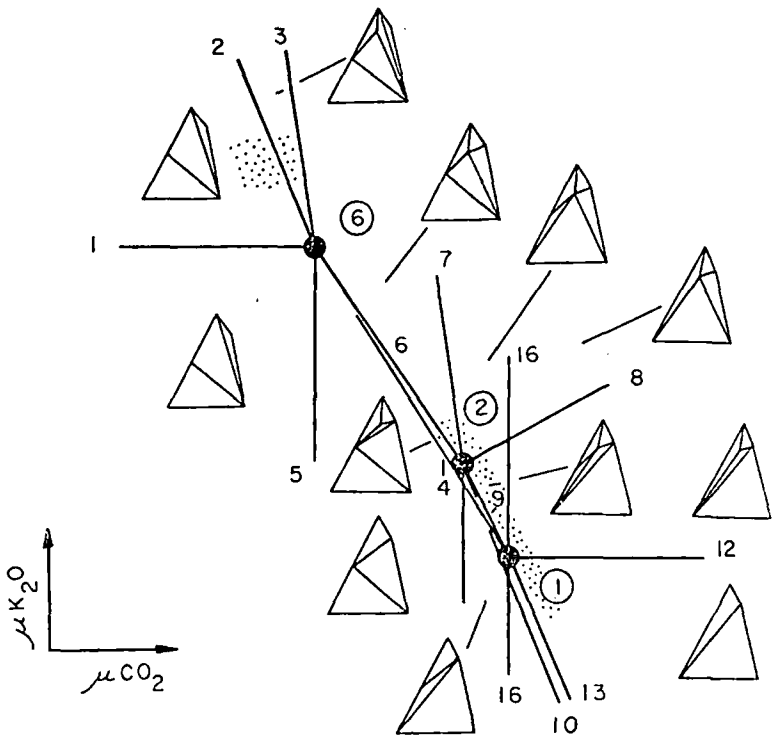

Fig. 11. μCO_2–μK_2O chemical potential diagram. For explanation, see figure 10.

ince contain amphibole-bearing assemblages that are restricted to μK_2O values below that of line 6 (fig. 12). Examples of such assemblages are amphibole + diopside + phlogopite + calcite + dolomite + forsterite (sites D and J) and amphibole + diopside + phlogopite + calcite + dolomite (sites E, H, and J).

The above contrasts in chemical potential conditions almost certainly developed as a result of the regional changes in pressure, temperature, and/or vapor composition that caused the progressive changes in mineral assemblages in the country rock gneiss; the chemical potentials of the vapor phase components and the chemical potential conditions for the reactions in the system are a function of pressure, temperature, and vapor composition and would therefore change as P, T, and X changed regionally. The possible changes in the vapor phase component chemical potentials and the chemical potential conditions for the reactions are shown schematically by the plane in figure 12. If the changes in vapor component chemical potentials were the dominant factors affecting the phase equilibria as P, T, and/or X changed, the change in chemical potential conditions would correspond to migration of the chemical potentials from the region where lines 1 and 2 pierce the plane (fig. 12) to the region where line 6 pierces the plane. If, on the other hand, the chemical potential conditions for the reactions changed more drastically than did

carbonate bodies:

1 DI AM PHL FO CC D
2 SP AM PHL FO CC D
3 DI SP PHL FO CC D
4 DI AM SP FO CC D
5 DI AM PHL FO SP D
6 DI AM PHL FO CC
7 DI AM PHL SP CC

Fig. 12. Three dimen
stable projections of lines
pierce the μCO_2–μH_2O pl
the μCO_2–μH_2O plane. Lir
of the stippled plane. Th
planes.

the chemical potentia
varied, the changes i
grated from the posit
province) to a positio
mately the same loca
net. In fact, a weigh
but the direction and

Although the s
possible representat
planar or nonplanar
termine the geometr

Single body T-
variations in phase
7 through 12. Thes
composition diagra
pressure remains c
pendently, (3) mine
which the vapor c
that all these constr

The temperat
assumption that, f
picted in figures 7
figure 12. Thus, fo

1 DI AM PHL FO CC DO
2 SP AM PHL FO CC DO
3 DI SP PHL FO CC DO
4 DI AM SP FO CC DO
5 DI AM PHL FO SP DO
6 DI AM PHL FO CC SP
7 DI AM PHL SP CC DO

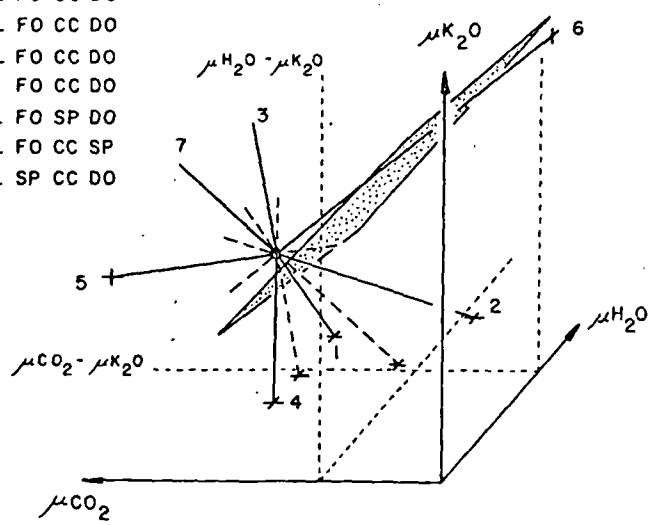

Fig. 12. Three dimensional representation of the μCO_2–μH_2O–μK_2O space. The stable projections of lines 1, 2, and 4 and the metastable projections of lines 3 and 7 pierce the μCO_2–μH_2O plane. Line 5 pierces the μCO_2–μK_2O plane and is parallel to the μCO_2–μH_2O plane. *Line 6 intersects the μH_2O–μK_2O plane. See text for explanation* of the stippled plane. The locations of the μ–μ sections are indicated by the labelled planes.

the chemical potentials of the vapor phase components, as P, T, and/or X varied, the changes in phase equilibria suggest that the net of curves migrated from the position shown in figure 12 (appropriate for the eastern province) to a position in which line 6 would pierce the plane in approximately the same location as did lines 1 and 2 before translation of the net. In fact, a weighted combination of both possibilities is most likely, but the direction and degree of weighting is unknown.

Although the surface in figure 12 is shown as planar (the simplest possible representation), the chemical potential surface can be either planar or nonplanar. The data available, however, are insufficient to determine the geometry of the surface.

Single body T–X variations.—The chemical potential changes and variations in phase equilibria within a single body are depicted in figures 7 through 12. These changes can be represented in a temperature-vapor composition diagram if the following constraints are satisfied: (1) vapor pressure remains constant, (2) only one vapor component varies independently, (3) mineral compositions are constant, and (4) the extent to which the vapor components behave ideally is known. If it is assumed that all these constraints are met, figure 13 results.

The temperature-vapor composition diagram is constructed on the assumption that, for a given body, the chemical potential variations depicted in figures 7 through 11 can be represented by a continuous line in figure 12. Thus, for a given $X^*_{CO_2}$, the mole fractions of the other vapor

species are specified ($X^*_{CO_2}$ is defined as the mole fraction of CO_2 in the vapor phase, divided by 0.75; see below).

Although the reactions diagrammed in figure 13 cannot be located precisely with respect to temperature and vapor composition, boundary conditions can be placed on the system. W. L. Griffin, E. Krogh, and D. Ormaasen (personal commun., 1974) have suggested that a pressure of 10 kb ± 3 kb was attained during metamorphism. Extrapolation of data presented in figure 14 to pressures of 10 kb suggests a maximum temperature of about 650°C for reaction (16). If the reactions in the system are important controls on the vapor composition, CO_2 would not make up more than 75 mole percent of the vapor for many of the reactions in the system. Although this percentage is approximate and is strictly applicable only to those reactions evolving vapor components in addition to CO_2, such a limiting approximation is necessary in order to construct a usable T–X diagram for reactions evolving several components. If $P_{solid} = P_{vapor}$, the maximum temperature possible for reaction (16) is about 640°C, for $P_{CO_2} = 0.75\ P_{vapor}$. The remaining curves in figure 13 are placed schematically, such that they are consistent with the topological constraints applicable to the phase equilibria in the chemical potential diagrams.

The mineralogical sequences at all sites except H and J can be duplicated in figure 13, if it is assumed that temperature was constant at any given site. The sequence of assemblages at sites H and J cannot be derived from figure 13 at a constant pressure, thus implying variations in vapor component ratios different from those appropriate for the other

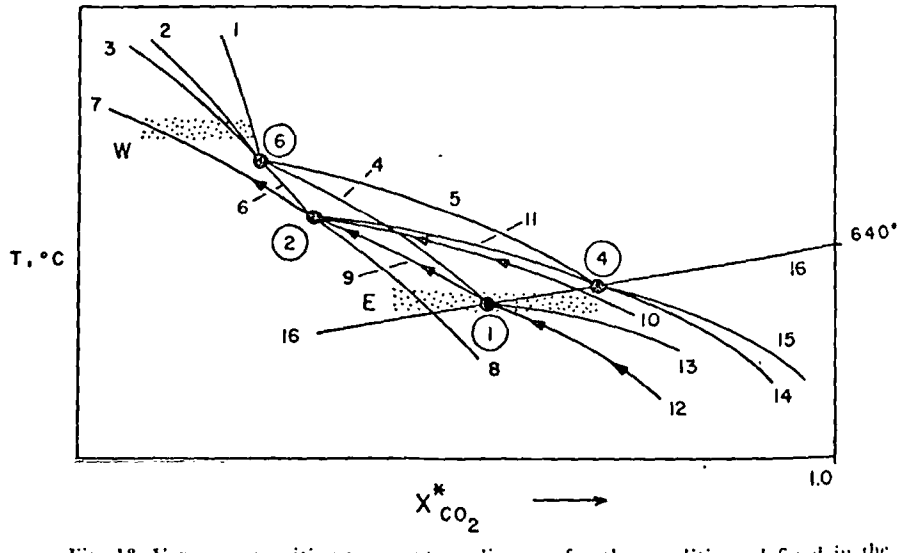

Fig. 13. Vapor composition-temperature diagram for the conditions defined in the text. The stippled area E encloses the approximate conditions for the eastern province; stippled area W encloses the approximate conditions for the western province. The arrows indicate buffering pathways at site J; arrows migrate toward carbonate rim.

carbonate bod

sites. The low f_{H_2O}/

this observation.

It is evident th

equilibria in figure

encountered, thus s

vapor component r

province. Although

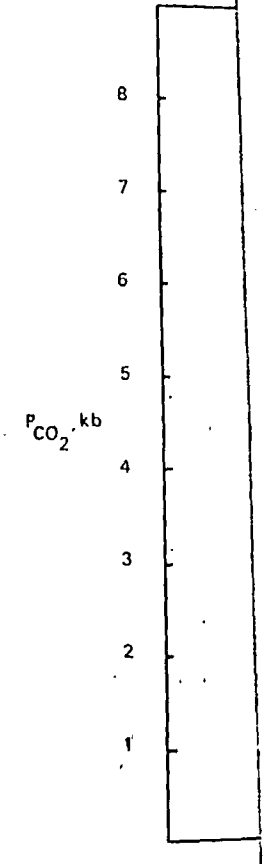

Fig. 14. The effect of
(16) ($P_{vapor} = P_{CO_2}$). The c
$\Delta G_{reaction}$ (T,P)

The free energies (ΔG) an
and Waldbaum (1968); d
Davis (1969); fugacity coef
and from 3 kb to 10 kb f
in the reaction. The there
experimental results of Sk
curve for the case $P_{vapor} =$
curve for the case $P_{vapor} <$

sites. The low f_{H_2O}/f_{HF} ratio at site J, relative to the other sites, confirms this observation.

It is evident that for eight of the ten carbonate bodies the phase equilibria in figure 13 represent adequately the sequence of assemblages encountered, thus supporting the suggestion made previously that the vapor component ratios varied similarly at most bodies throughout the province. Although figure 13 suggests that a significant temperature dif-

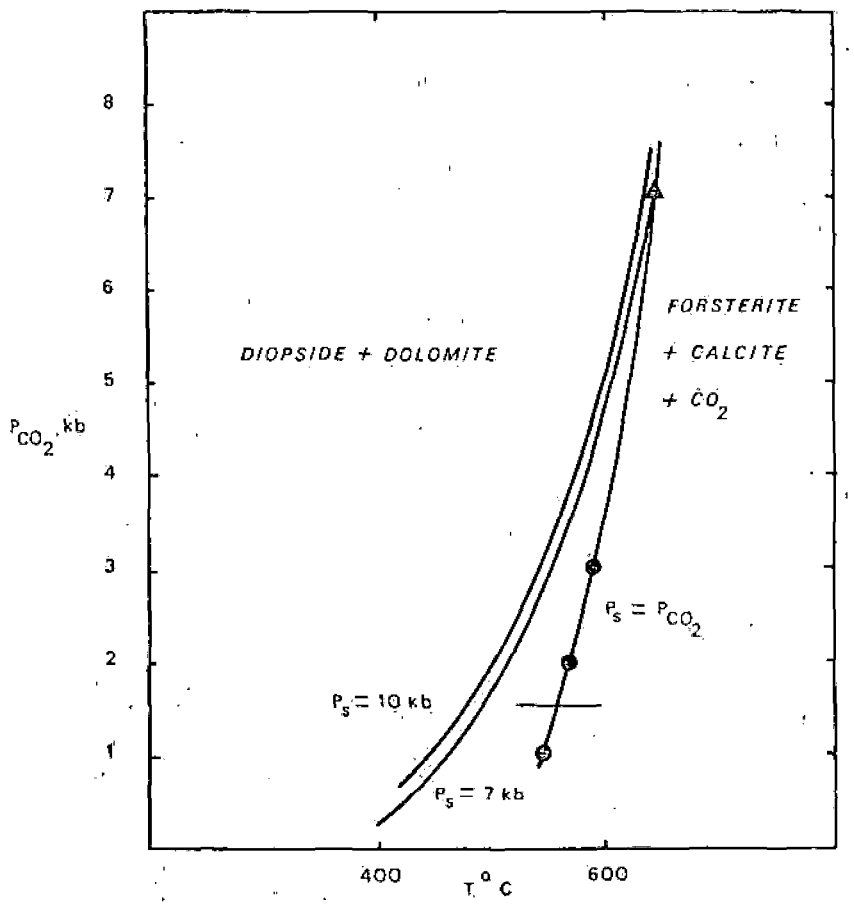

Fig. 14. The effect of variable vapor pressure, at a fixed solid pressure, on reaction (16) ($P^{\circ}_{vapor} = P_{CO_2}$). The calculation was based on the equation

$$\Delta G_{reaction}(T,P) = \Delta G_{reaction}(T, 1\ bar) + 0.024\ \Delta V_{solids} \cdot (P - 1.) + \lambda_{CO_2} RT \ln \gamma P_{CO_2}.$$

The free energies (ΔG) and molar volumes of the solid phases were taken from Robie and Waldbaum (1968); data for H_2O were obtained from Burnham, Holloway, and Davis (1969); fugacity coefficients for CO_2 to 3 kb were obtained from Skippen (1971) and from 3 kb to 10 kb from Ryzhenko and Volkov (1971); λ is the coefficient of CO_2 in the reaction. The thermodynamic calculations were adjusted to correspond to the experimental results of Skippen (1974). The results demonstrate that the equilibrium curve for the case $P_{vapor} = P_{solids}$ has a much greater dP/dT slope than the equilibrium curve for the case $P_{vapor} < P_{solids}$, P_{solids} = constant.

nal metamorphism of some

he mole fraction of CO_2 in the

in figure 13 cannot be located vapor composition, boundary V. L. Griffin, E. Krogh, and D. suggested that a pressure of orphism. Extrapolation of data suggests a maximum tempera- he reactions in the system are ion, CO_2 would not make up r many of the reactions in the imate and is strictly applicable nponents in addition to CO_2, in order to construct a usable components. If $P_{solid} = P_{vapor}$, ction (16) is about 640°C, for figure 13 are placed schemati- he topological constraints ap- nical potential diagrams.

ites except H and J can be t temperature was constant at s at sites H and J cannot be e, thus implying variations in se appropriate for the other

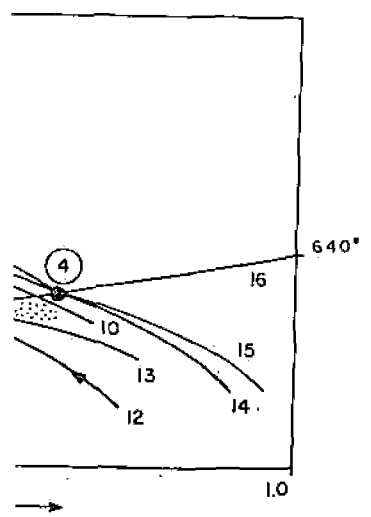

for the conditions defined in the nditions for the eastern province; s for the western province. The igrate toward carbonate rim.

ference between the eastern and western province is required by the phase equilibria, the absence of P_{solid} and P_{vapor} data do not allow quantification of the temperature contrasts.

The distribution of the assemblages within the carbonate bodies strongly suggests that the vapor composition was buffered during metamorphism. At site J, for example, reaction assemblages are systematically distributed throughout the body. Although such a variety of reaction assemblages is lacking at other sites, the common occurrence of univariant assemblages supports the contention that vapor composition was buffered at these sites as well.

However, the gradients in vapor composition that existed at all sites cannot be explained *solely* by buffering of the vapor composition by the mineral assemblages, since it is not possible for a closed system to develop vapor composition gradients if the initial mineral and vapor compositions were constant throughout the body. These gradients must reflect either compositional gradients imposed on the carbonates prior to metamorphism or slow diffusion of some vapor components into or out of the carbonate system. The gradients currently recorded in the rocks would necessarily represent modification of the imposed gradients by evolution of volatiles during metamorphism.

IMPLICATIONS FOR GRANULITE FACIES TERRAINS

The assemblages that have developed in the carbonate bodies demonstrate that the bulk compositions of the bodies are similar. Thus, the zone boundaries (fig. 1) are isograds. The most eastern isograd, the diopside–spinel isograd, marks the first appearance of the mineral pair diopside + spinel in the core assemblages. The western isograd, the forsterite isograd, marks the replacement of the mineral pair diopside + dolomite by the compositionally equivalent mineral pair forsterite + calcite, in the core assemblages.

The diopside–spinel and forsterite isograds radically diverge from the orthopyroxene isograd north of site G (fig. 1). Because the three isograds represent phase equilibria involving a mixed volatile phase, there are a number of possible explanations for the divergence of the isograds.

1. The isograds paralleled isotherms, thus implying radically diverging isothermal surfaces.

2. Total vapor pressure or CO_2 partial pressure was significantly higher at sites D, E, and I than at the other sites (assuming that the regional isotherms paralleled the orthopyroxene isograd).

3. The partial pressure of H_2O in the country rock gneiss was lower in the northern half of the island of Langoy than in the southern half (assuming the regional isotherms paralleled the diopside–spinel and forsterite isograds).

4. The trend of regional isotherms exhibits no necessary relationship to the isograds (a combination of 2 and 3).

5. Mineral compositions in either the gneisses or the carbonate systematically varied regionally.

The results presented in this paper and by Heier (1960) demonstrate adequately that bulk rock compositional contrasts cannot explain the isograd trends; point 5 can therefore be dismissed. Although points 1 through 4 cannot be evaluated individually, geological observations suggest that point 1 is the most probable. The transition from border series gneiss to banded series gneiss is delineated by a change in potassium feldspar symmetry (see Heier, 1960, for obliquity data), which is a function of temperature alone (pressure effects are negligible). This transition can be treated as the trace of an isothermal surface. The transition from amphibolite facies to granulite facies coincides with changes in potassium feldspar symmetry and parallels trend surfaces that trace changes in anorthite content in plagioclase and changes in the coordination of Al and Ti in amphibole. Although a variety of equilibrium parameters can explain these phase variations, temperature is the only equilibrium parameter all these changes have in common. It is reasonable to suggest, therefore, that the orthopyroxene isograd also traces an isothermal surface.

The isograds defined on the basis of the carbonate assemblages obliquely cross the banded series-border series transition in the northern part of the island of Langöy and parallel the orthopyroxene isograd in the southern half of the study area. This suggests that the carbonate derived isograds nearly paralleled the traces of isothermal surfaces. The parallelism may, in fact, be more pronounced than is apparent from figure 1, since the locations of all isograds and the border series-banded series transition are only located approximately.

CONCLUSIONS

Phase equilibria in the carbonate bodies.—The phase relationships in the carbonate bodies require the presence of a multicomponent vapor during metamorphism. Systematic variations in the ratios of three of the five vapor components are sufficient to describe most of the changes in phase equilibria exhibited at any given site. The mineral compositions and phase equilibria demonstrate that all the carbonate bodies experienced gradients in vapor composition outward from the carbonate cores; in all instances where data are available, a decrease in f_{CO_2} and in the ratio f_{H_2O}/f_{HF} can be documented. Changes in other vapor components are also possible. The gradients in vapor composition are probably relicts of an inherited vapor phase, the composition of which was modified by volatiles evolved during reaction. The reaction relationships strongly suggest that the carbonate bodies behaved as nearly closed systems except, perhaps, for those vapor phase components that were perfectly mobile and at the carbonate–gneiss contact where metasomatic processes dominated the development of the mineral assemblages.

The behavior of vapor components during metamorphism cannot be defined precisely, even though the general pattern of vapor composition variation can be recognized. For example, aluminum exchange between amphibole and spinel could be expected in response to changes in

P–T conditions. Such exchange could effect changes in the sodium content of the amphibole and, hence, would modify the sodium content of the vapor phase. However, because the spinel generally contained exsolution phases, adequate compositional data for coexisting amphibole–spinel could not be obtained. Therefore, controls on the sodium content of the vapor phase could not be examined.

Systematic changes in mineral composition that would correlate with apparent changes in P and T were not observed. This suggests that for the range of conditions encountered in the study area, minor variations in the bulk compositions of the carbonate bodies had a more profound effect on mineral composition than did P and T. However, because of a lack of data for mineral pairs that include spinel, evidence for compositional control by P and T on spinel-bearing assemblages is inconclusive.

Implications for high grade, regionally metamorphosed terrains.—If the three isograds discussed in this paper parallel the trend of isothermal surfaces that developed during metamorphism, a complex thermal structure for the deep crust is implied. Also, unlike other high grade metamorphic terrains (for example, southern Norway (Touret, 1971a, b) and the Adirondacks (Buddington, 1963)), there does not appear to have been a large regional variation in the fugacity of H_2O during metamorphism.

ACKNOWLEDGMENTS

This research was supported by the G. Unger Vetlesen Foundation, through a post-doctoral fellowship at the Mineralogisk-Geologisk Museum, Oslo. Sincere thanks are extended to the foundation and to Professor Knut S. Heier and Dr. William L. Griffin of the museum, for their support. B. W. Evans, W. L. Griffin, and J. K. Winter provided useful comments on an early draft of this manuscript. L. Milburn provided very able field support during the course of this work, and her assistance is gratefully acknowledged.

REFERENCES

Binns, R. A., 1964, Zones of progressive metamorphism in the Willyama complex, Broken Hill district, New South Wales: Geol. Soc. Australia, v. 11, p. 283-330.

———— 1965, The mineralogy of metamorphosed basic rocks from the Willyama complex, Broken Hill district, New South Wales: Mineralog. Mag., v. 35, p. 561-587.

Buddington, A. F., 1939, Adirondack igneous rocks and their metamorphism: Geol. Soc. America Mem. 7, 354 p.

———— 1963, Isograds and the role of H_2O in metamorphic facies of orthogneisses of the northwest Adirondack area, New York: Geol. Soc. America Bull., v. 74, p. 1155-1182.

Buddington, A. F., and Lindsley, D. H., 1964, Iron-titanium oxide minerals and synthetic equivalents: Jour. Petrology, v. 5, p. 310-357.

Burnham, C. W., Holloway, J. R., and Davis, N. F., 1969, Thermodynamic properties of water to 1000°C and 10,000 bars: Geol. Soc. America Spec. Paper 132, p. 1-96.

Devaraju, T. C., ms, 1971, Geology of north Langoy, Vesteralen: Oslo, Mineralog. Geol. Mus. Field Rept.

de Waard, Dirk, 1965, The occurrence of garnet in the granulite facies terrain of the Adirondack Highlands: Jour. Petrology, v. 6, p. 165-191.

———— 1967, The occurrence of garnet in the granulite facies terrain of the Adirondack Highlands and elsewhere, an amplification and a reply: Jour. Petrology, v. 8, p. 210-232.

Engel, A. E. J., and Engel, C. E., 1960, Progressive metamorphism and granitization of the major paragneiss, northwest Adirondack mountains, New York: Geol. Soc. America Bull., v. 71, p. 1-58.

———— 1962a, Progressive metamorphism of amphibolite, northwest Adirondack mountains, New York: Geol. Soc. America, Buddington v., p. 37-82.

———— 1962b, Hornblendes formed during progressive metamorphism of amphibolite, northwest Adirondack mountains, New York: Geol. Soc. America Bull., v. 73, p. 1499-1514.

Green, T. H., and Jorde, K., 1971, Geology of Moskenes, Lofoten, North Norway: Norges geol. undersöklse, v. 270, p. 47-76.

Greenwood, H. J., 1967, Mineral equilibria in the system MgO–SiO_2–H_2O–CO_2, *in* Abelson, P. H., ed., Researches in Geochemistry: New York, John Wiley & Sons, Inc., p. 542-567.

Griffin, W. L., and Heier, K. S., 1969, Parageneses of garnet in granulite facies rocks, Lofoten-Vesterålen, North Norway: Contr. Mineralogy and Petrology, v. 23, p. 89-116.

Heier, K. S., 1960, Petrology and geochemistry of high-grade metamorphic and igneous rocks on Langoy, northern Norway: Norges geol. undersökelse, v. 207, p. 1-246.

Heier, K. S., and Thoresen, K., 1971, Geochemistry of high-grade metamorphic rocks, Lofoten-Vesterålen, North Norway: Geochim. et Cosmochim. Acta, v. 35, p. 89-99.

Korzhinskii, D. S., 1957, Physiochemical Basis of the Analysis of the Paragenesis of Minerals: New York, Consultants Bur. Inc., 142 p.

Munoz, J. L., and Eugster, H. P., 1969, Experimental control of fluorine reactions in hydrothermal systems: Am. Mineralogist, v. 54, p. 943-959.

Munoz, J. L., and Ludington, S. D., 1974, Fluoride-hydroxyl exchange in biotite: Am. Jour. Sci., v. 274, p. 396-413.

Robie, R. A., and Waldbaum, D. R., 1968, Thermodynamic properties of minerals and related substances at 298.15°K (25.0°C) and one atmosphere (1.013 bars) pressure and at higher temperatures: U.S. Geol. Survey Bull. 1259, p. 1-256.

Ryzhenko, B. N., and Volkov, V. P., 1971, Fugacity coefficients of some gases in a broad range of temperatures and pressures: Geochem. Internat., v. 8, p. 468-481.

Skippen, G. B., 1971, Experimental data for reactions in siliceous dolomites: Jour. Geology, v. 79, p. 457-481.

———— 1974, An experimental model for low pressure metamorphism of siliceous dolomitic marble: Am. Jour. Sci., v. 274, p. 487-509.

Touret, Jacques, 1971a, Le faciès granulite en Norvège méridionale. I. Les associations minéralogiques: Lithos, v. 4, p. 239-249.

———— 1971b, Les faciès granulite en Norvège méridionale. II. Les inclusions fluides: Lithos, v. 4, p. 423-436.

Turner, F. J., 1968, Metamorphic Petrology: Mineralogical and Field Aspects: New York, McGraw-Hill Co., p. 328.

Vidale, Rosemary, 1969, Metasomatism and a chemical gradient and the formation of calc-silicate bands: Am. Jour. Sci., v. 267, p. 857-874.

Vidale, Rosemary, and Hewitt, D. A., 1973, "Mobile" components and the formation of calc-silicate bands: Am. Mineralogist, v. 58, p. 991-997.

FC
620

UNIVERSITY OF UTAH
RESEARCH INSTITUTE
EARTH SCIENCE LAB.

Micromineralogy and geochemistry of sphalerites from Sulitjelma mining district, Norway

KISHANLAL RAI

Rai, K. L.: Micromineralogy and geochemistry of sphalerites from Sulitjelma mining district, Norway. *Norsk Geologisk Tidsskrift*, Vol. 58, pp. 17–31. Oslo 1978. ISSN 0029-196X.

A wide range of zinc-rich to zinc-poor ore bodies characterizes the famous Caledonian pyritic copper-zinc ore deposit of Sulitjelma. It is, however, observed that, in general, the sphalerites from the two main assemblage types of ores in different ore bodies display remarkably analogous minor- and trace-element geochemistry marked with comparable concentrations of individual elements. The distribution of certain common minor elements between sphalerite and co-existing iron-sulphide minerals tends to be regular. On the crystal scale too, the sphalerites show no evidence of physical or chemical heterogeneity. The implications of the study in deciphering equilibration or re-equilibration of ores during regional metamorphism and the probable optimum geobarometric conditions have been considered.

K. L. Rai, Department of Applied Geology, Indian School of Mines, Dhanbad – 826004, Bihar, India.

The Sulitjelma mining district, located at ca. 67° N. lat. in northern Norway, constitutes a small yet important subprovince of the great Caledonian metallogenetic province of Scandinavia. It owes its economic significance to the occurrences of several pyritic copper-zinc ore bodies that have sustained a mining and smelting industry in this part of the country since the turn of this century. By 1975, the district had already produced more than 19 million tons of raw ore, the annual production in recent years having been about 360,000 tons of ore that yields about 20,000 tons of copper concentrates, 2000 tons of zinc concentrates and 80,000 tons of pyrite (1968 figures).

The present study on sphalerites from this important, and in many respects, representative deposit of its type in the Scandinavian Caledonides, was undertaken as a part of a larger project dealing with detailed mineralogical and geochemical studies of Sulitjelma ores. The primary objective of this study is to evaluate and assess the physical, mineralogical, and geochemical characteristics of sphalerites belonging to various types of ores and the ore bodies represented in this deposit. No such study seems to have been carried out so far. Limited information based on the analyses of a few sphalerite samples from this deposit has, of course, been available in certain earlier publications dealing with broad-scale studies on sphalerites from the Norwegian/Scandinavian sulphide deposits (Oftedal 1940, Kullerud, Padget & Vokes 1953).

The ore geology of the Sulitjelma district

The Sulitjelma deposit lies in the central section of the 1,500 km long Caledonian mountain belt within a sequence of eugeosynclinal volcanic-sedimentary rocks that constitute the 'western facies' of the Caledonian geosyncline. Tectonically, these rocks belong to the lower of the two nappe units that have been distinguished in Sulitjelma region. The rocks have, in general, undergone a complex tectonic, structural, and metamorphic history, principally during Caledonian orogeny. Exhaustive accounts of all these and various other aspects of regional geology and tectonics are already available in the published literature (Sjögren 1900, Vogt 1927, Kautsky 1953, Mason 1967, Nicholson & Rutland 1969, Henley 1970, Wilson 1973).

Sulphide mineralization in the region consists of a series of strata-bound, elongated lenticular ore bodies that often lie en-echelon with their longer axes running parallel to the preferred orientation of the minor fold axes and linear structures of the country rocks. These ore bodies occur well within a single structural unit of the area (Wilson 1973) at or near the lower junction of the Sulitjelma amphibolites with the underlying Furulund Group metasediments (Fig. 1). The exact nature of the geologic setting of sulphide mineralization has received varied interpretations from earlier workers (J. H. L. Vogt 1894, Th. Vogt 1927, Kautsky 1953, Wilson 1973).

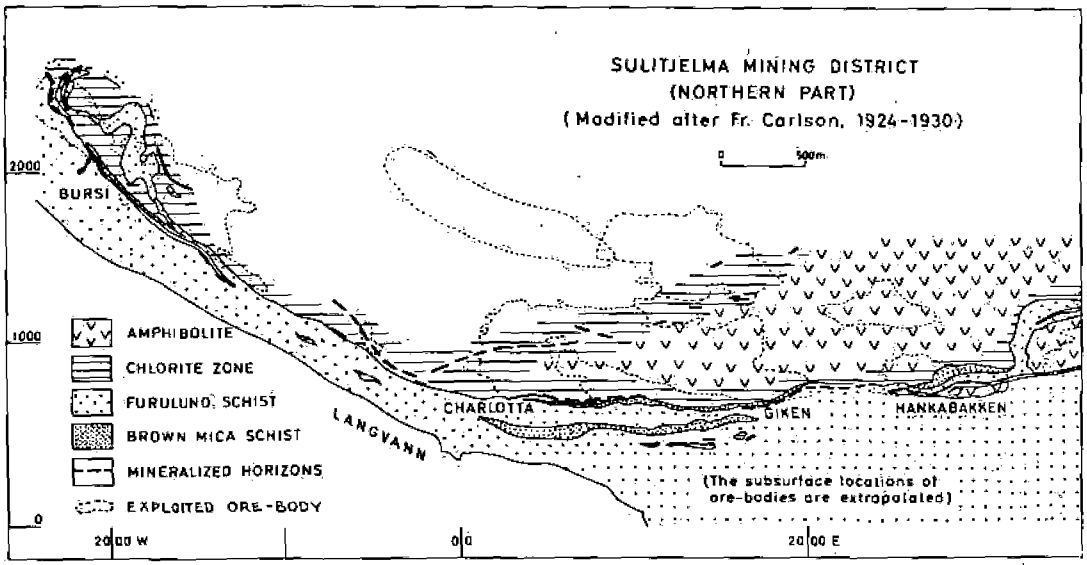

Fig. 1. Geological map of northern part of Sulitjelma mining district, Norway.

Two common paragenetical types of massive ores, namely pyritic and pyrrhotitic types, whose general occurrence in the massive sulphide deposits of Norwegian Caledonides has been highlighted by Vokes (1962), are also observed in the Sulitjelma deposit in close association and with widely variable proportions in its different ore bodies. The pyrrhotitic ores represent distinctly a younger mineralization as they clearly cut across the massive stratiform pyritic ores at several places.

Mineralogically, the ores comprise principally pyrite, pyrrhotite, chalcopyrite, and sphalerite that often constitute over 95% of the ore mass. Quantitative differences in the mineralogy of various ores relate largely to the two iron-sulphide minerals and to a lesser extent, to the two matrix base-metal sulphides. Other minerals occurring in minor- to trace amounts and rarely exceeding 2 or 3 percent of the ore mass include galena, arsenopyrite, tetrahedrite, molybdenite, machinawite, bournonite, and many other sulphosalts. The occurrence of a multitude of Cu-, Pb-, Ag-, As-, and Sb-sulphides and sulphosalts and silver, gold, and antimony as native metals was reported by Ramdohr (1938) from an antimony-rich paragenesis at Jakobsbakken mine, that had been abandoned about 30 years ago. The common gangue minerals observed in the ores are quartz, calcite, hornblende, kyanite, feldspar, and anhydrite. The observed textures and microstructures show that the ores have, in general, undergone varied effects of high-grade regional metamorphism.

Classification and micromineralogy of sphalerites

Sphalerite occurs as a common and important matrix sulphide next only to chalcopyrite in the Sulitjelma ores. Considerable variations, both of qualitative as well as quantitative nature, however, characterize its occurrence in the different ore types and ore bodies constituting the deposit.

Variations in quantitative proportion of sphalerite to other base-metal sulphides in different ores and ore bodies of the deposit seemingly find best expression in the average base-metal composition of the ores. Relevant data in this connection, assembled and depicted in triangular diagram in Fig. 2, shows that a wide range of zinc-rich to zinc-poor ore bodies is represented in the deposit. No systematic trend in the geographic distribution of such ore bodies, however, seems discernible. Abnormally high zinc content of Jakobsbakken ores, for example, prominently contrasts with the zinc-poor ores of Sagmo ore body which lies in an exactly similar

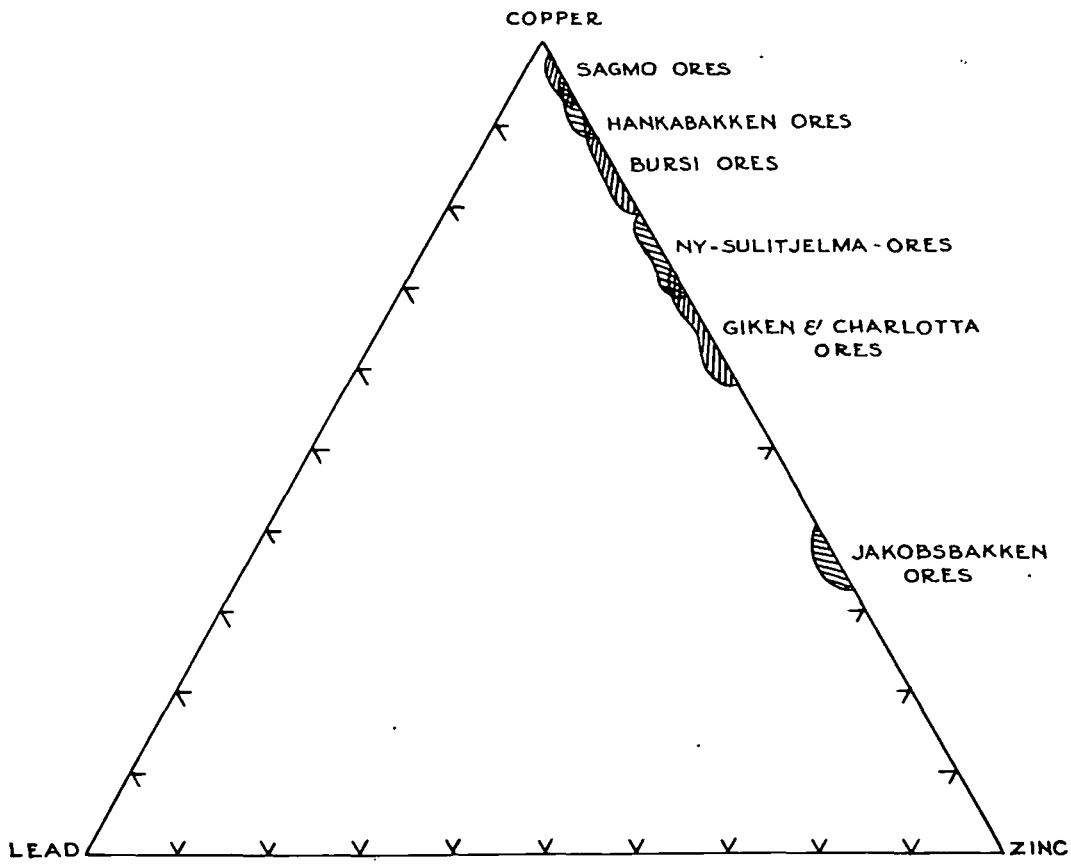

Fig. 2. Triangular diagram showing base-metal composition of ores from different ore bodies of Sulitjelma deposit.

geologic environment only about a kilometer north of Jakobsbakken Mine. On the scale of an individual ore body, however, the variability of the average base-metal composition of ores seems to be relatively much less, and often restricted between characteristically narrow limits.

In the light of the observations made as above, it was considered desirable to study the differences, if any, in the sphalerites belonging to different ore types and ore bodies of the deposit and subsequently evaluate their probable significance. With this in view, detailed studies were planned on about 120 samples of sphalerite-bearing ores collected according to definite sampling schemes, principally from four ore bodies of the deposit under active exploitation, namely Giken, Hankabakken, Charlotta, and Bursi. Detailed megascopic and microscopic studies of these samples helped to evolve the following classification on the basis of characteristic mineral assemblages:

Group A: Pyrite-sphalerite assemblage (with no visible pyrrhotite).

Group B: Pyrrhotite-sphalerite assemblage (with or without pyrite).

Group C: Sphalerite-galena assemblage.

Chalcopyrite occurs as a common constituent of all the assemblages mentioned above.

Group A and B assemblages represent the two most common types of sphalerite-bearing ores, although gradations between them are also present in the deposit. Typical megascopic and morphologic characteristics of these ores are depicted through representative specimen photographs in Figs. 3A and 3B. Studies on chalcopyrite-sphalerite ore show that it can be remobilized equivalent to one or the other of the two principal ore types. Such ore, found usually

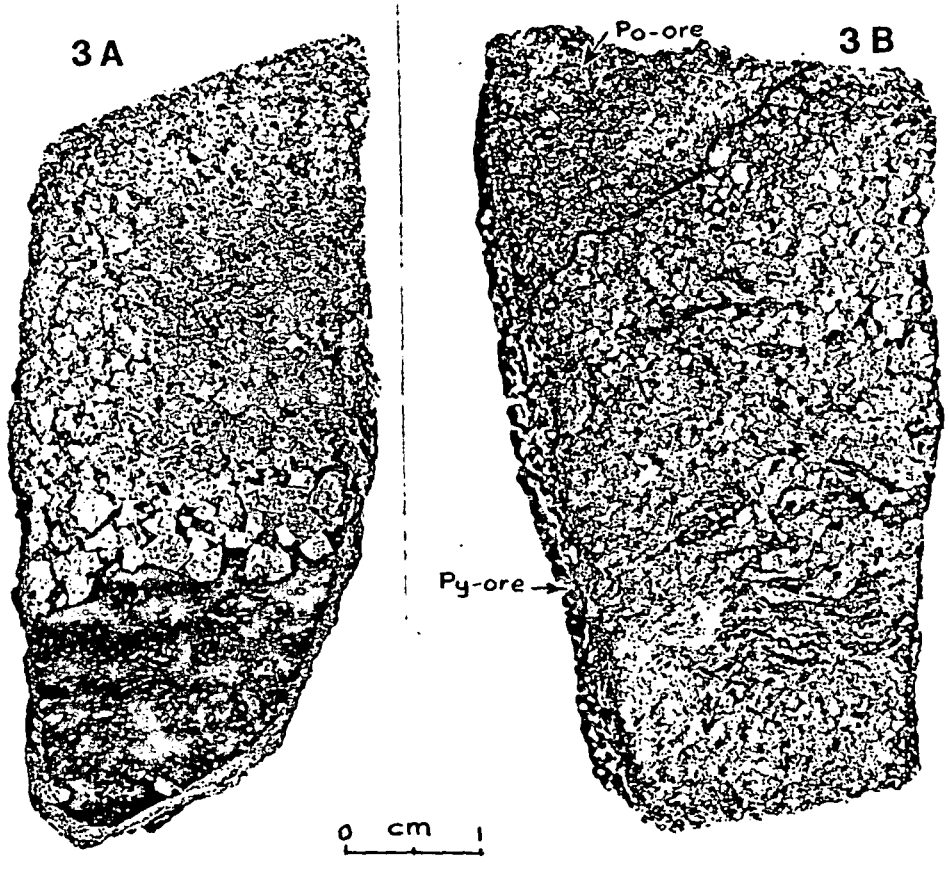

Fig. 3A. Representative specimen photograph of massive pyritic ore at its contact with the wall rock. Sphalerite may be seen infilling the interspaces of the pyrite crystal aggregates.
Fig. 3B. Specimen photograph displaying the contact of pyrrhotitic ore (Po-ore) with massive pyritic ore (Py ore).

in association with pyrrhotitic ore, however, seems to be of limited occurrence in the deposit.

Mineralogic and textural characteristics of different types of sphalerite-bearing ores and the essential aspects of the micromineralogy of their sphalerites are briefly described below.

Group A: Pyrite-sphalerite assemblage

Sphalerite in samples of this group occurs commonly as the principal matrix mineral occupying the interstitial spaces of the interlocked mosaic aggregates of pyrite crystals (Fig. 4A). It is often fine- to medium-grained, the diameter of grains commonly ranging from 0.05 mm to 2 mm or even more.

The mineral generally appears light grey in colour and sometimes shows a little birefringence, possibly due to strain effects. It commonly shows yellowish and reddish internal reflections. Lamellar twinning is exhibited by the mineral in some of the sections (Fig. 4B).

Sphalerite commonly shows mutual boundary relations with pyrite (Fig. 5A). Fracturing due to cataclasis, so commonly observed in the pyrite crystals of this paragenesis, is also noted sometimes in the interstitial sphalerite mass (Fig. 5B). Chalcopyrite, though most commonly associated with sphalerite of this group, is never seen exsolved or intergrown in it.

Fig. 4A (right). Sphalerite (Sp) occurring as the infilling of the interspaces of pyrite crystal aggregates in massive pyritic ore. Magnification ×50.
Fig. 4A (left). Sphalerite (Sp) showing lamellar twinning. Associated chalcopyrite (Cp) also exhibits similar twinning. Magnification ×100.

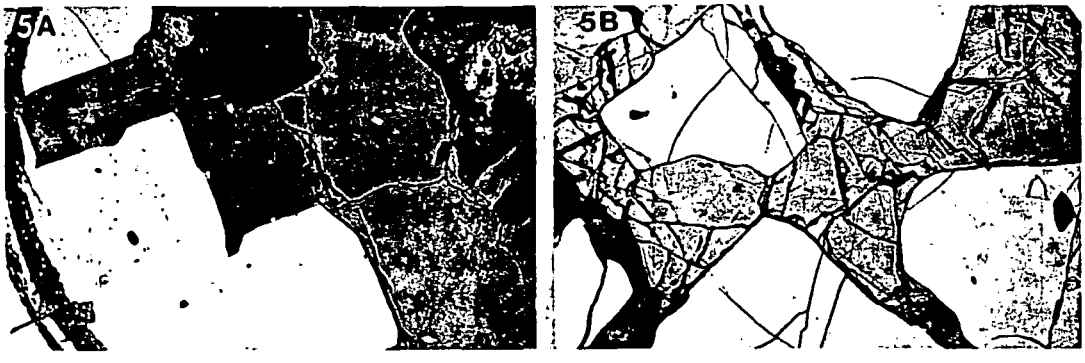

Fig. 5A. Photomicrograph displaying typical mutual boundary relations between sphalerite and pyrite of sphalerite-pyrite assemblage. Magnification × 100.
Fig. 5B. Photomicrograph exhibiting large-scale fracturing of groundmass sphalerite and to a lesser extent of pyrite, both belonging to sphalerite-pyrite assemblage. Magnification ×50.

Group B: Pyrrhotite-sphalerite assemblage

Sphalerite of this assemblage commonly occurs as aggregates, patches or crude bands within the pyrrhotite or chalcopyrite rich ore mass. It is also frequently seen infilling the fractures of the cataclastically-deformed pyrite porphyroblasts. Lamellar twinning possibly caused by shearing stresses during crystallization is more commonly seen in sphalerites of this paragenesis.

Under the microscope, the mineral appears grey to dark-grey in colour and shows deep-reddish or reddish-brown internal reflections. In some of the sections, it shows weak to distinct anisotropism. Under high magnification, some of the sphalerite grains are seen containing numerous blebs or shreds of chalcopyrite in random or vague orientation.

The mineral commonly replaces earlier generation (usually porphyroblastic) pyrite often along its fractures and cracks (Fig. 6A). The latter has to be distinguished from pyrite of sphalerite-pyrrhotite assemblage which is often characterized by perfect euhedral shape and freedom from effects of cataclasis (Fig. 6B). The textural relations between various minerals of this assemblage, by and large, indicate contemporaneity of their crystallization/recrystallisation (Figs. 7A and 7B).

Sphalerite belonging to remobilized-type chalcopyrite-sphalerite ore, which is occasionally found associated with pyrrhotitic ores, shows coarse unmixing of chalcopyrite (Fig. 8A). The unusual shape and distribution of chalcopyrite bodies in and around (particularly near the grain boundaries of) sphalerite of this ore, possibly

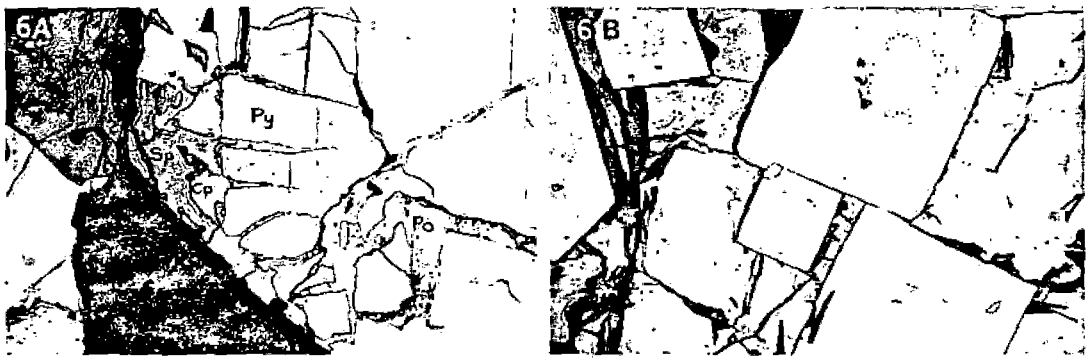

Fig. 6A. Sphalerite (Sp), chalcopyrite (Cp), and pyrrhotite (Po) replacing earlier generation porphyroblastic pyrite (Py) along its fractures and cracks. Magnification ×50.
Fig. 6B. Euhedral and undeformed crystals of pyrite belonging to sphalerite-pyrrhotite assemblage, floating in pyrrhotite groundmass. Magnification ×50.

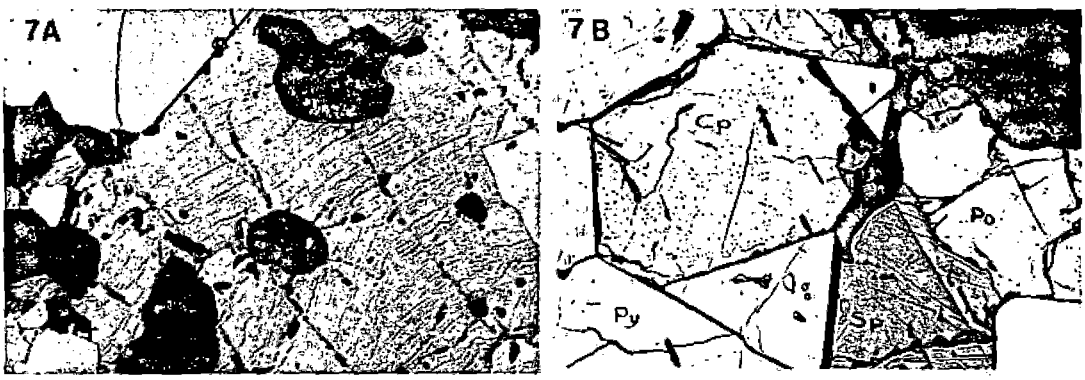

Fig. 7A. Photomicrograph exhibiting mutual boundary relationship of pyrrhotite and pyrite in sphalerite-pyrrhotite assemblage. Pyrrhotite contains exsolved lamellae of troilite. Magnification ×100.
Fig. 7B. Photomicrograph displaying common textural relations of sphalerite (Sp), pyrrhotite (Po), pyrite (Py) and chalcopyrite (Cp) in ores having sphalerite-pyrrhotite assemblage. Magnification ×50.

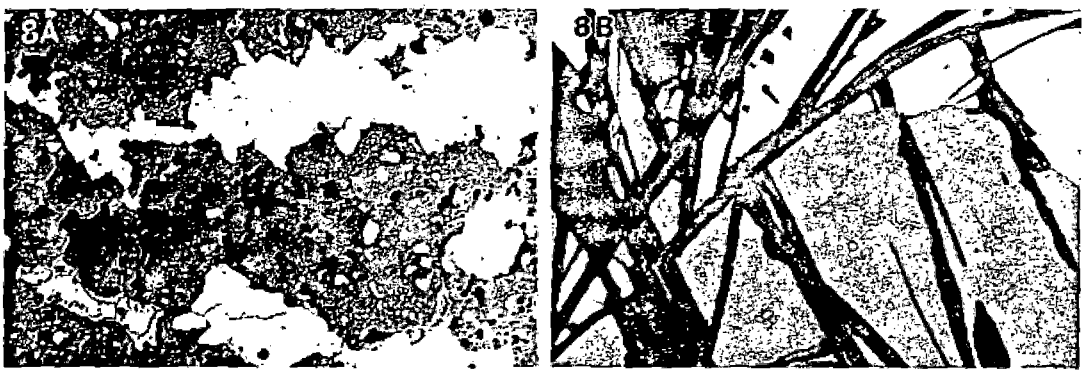

Fig. 8A. Sphalerite from remobilized-type chalcopyrite-sphalerite ore exhibiting coarse unmixing of chalcopyrite which occurs as minute blebs or spherical droplets of varying shape and size in sphalerite-bearing layers. The concentration of chalcopyrite droplets all along the grain-boundaries of sphalerite seems specifically notable. Magnification ×50.
Fig. 8B. Photomicrograph exhibiting cuspate intergrowth of silicates with ore minerals of sphalerite-chalcopyrite assemblage. Minute blebs and shreds of chalcopyrite exsolved randomly in sphalerite may be seen. Magnification ×100.

points to its complicated history. Ramdohr (1969) has noted that he has not observed chalcopyrite bodies of the type mentioned above in high-temperature sphalerites which, according to him, are best exemplified by sphalerites from the Boliden and Sulitjelma deposits. The present observation seems quite significant and may need consideration in this connection. The chalcopyrite-sphalerite ore of this type at times shows intimate intergrowth of lath-shaped hornblende crystals in sulphide ore mass displaying cuspate texture which is typical of the metamorphic nature of the ore (Fig. 8B). Thin bands of magnetite ore are sometimes found associated with massive sulphide ores of this type.

Group C: Sphalerite-galena assemblage

This assemblage seems to be of limited occurrence in the deposit. It has been observed along or near the contact of the main ore mass with the wall rocks, particularly in the Hankabakken and Giken ore bodies.

Sphalerite of this assemblage is characterized by its light-grey colour and yellowish to yellowish-brown internal reflections. It is further characterized by the occurrence of numerous minute inclusions as shreds or lamellae of chalcopyrite in crystallographic orientation along its dodecahedral cleavage planes, thus representing typical exsolution texture.

Sphalerite composition

Material studied

Field relationships of various ore types, megascopic studies of their hand specimens, and microscopic investigations on mineral associations, texture, inclusions, and paragenetic relations were integratedly considered in selecting 50 most representative samples of various types of sphalerite-bearing ores for detailed mineral-chemical investigations. These samples were subjected to a series of mineral-separating operations in order to obtain purest possible concentrates of sphalerites and associated iron-sulphide minerals. Final checks on the purity of concentrates were effected through the microscopic studies of their polished grain-mounts and chemical analyses of the final concentrates for copper and lead. All possible attempts were thus made to obtain up to about 98 % purity of the concentrates and the samples for which this could not be achieved, were simply rejected. Ultimately only 30 sphalerite concentrates belonging principally to the three main ore bodies – Giken, Charlotta, and Bursi – could be taken up for the desired analytical studies. A larger data base, although desirable, was not possible under the then existing constraints of time.

Analytical methods

Combinations of atomic absorption, electron probe and X-ray diffraction techniques were employed to determine the minor- and trace-element composition of sphalerites. About a dozen selected samples were analysed by all the three techniques for certain elements, and the analytical data so obtained have been assembled in Table 1 to facilitate comparative study of the results. The procedures and results of analytical work by the three methods have been as follows:

Atomic absorption spectrophotometric analyses. This method was employed for the quantitative determination of minor elements, namely Fe, Mn, Cd, Pb & Cu and some trace elements, e.g. Ga, Co and Ni in the sphalerite samples of this study. The analytical work was carried out in F. J. Langmyhr's atomic absorption spectrophotometric laboratory at Kjemisk institutt, Universitetet i Oslo.

Sphalerite concentrates were subjected to dissolution in acids by decomposition bomb technique. The detailed procedure described by Langmyhr & Paus (1968, 1970) was in general adopted for sample preparation and for analytical work that was carried out on Perkin Elmer AAS Model-303 in the laboratory of Kjemisk institutt, Oslo.

The results of analyses of sphalerites of the two principal groups are presented in Tables 2 and 3 respectively and are discussed in detail later on. The analysis of a sphalerite sample (sp.no. H/13) representing Group C, i.e. sphalerite-galena assemblage, has been included only in Table 1. It was extremely difficult to get adequately pure sphalerite concentrate from this ore; it was therefore considered futile to take up any more samples of this group for chemical analyses by this method.

Electron probe microanalyses. – Electron probe microanalyses of sphalerites from 12 selected samples of different ore types from different ore

Table 1. Comparison of atomic absorption spectrophotometric, electron microprobe, and X-ray diffraction data on selected sphalerites from Sulitjelma mining district, Norway.

Ore body	Specimen No.	Atomic absorption spectrophotometric Results (in mole percent)				Electron Microprobe Results (in Mole %)		X-ray diffraction results		
		FeS	MnS	CdS	Total	FeS	MnS	Measured cell edge (A)	Apparent mole % FeS	Calculated cell edge (A)
Giken	G/111	12.3	0.38	0.31	12.99	13.0	0.35	5.4180	16.4	5.4174
Giken	G/107	17.3	0.14	0.15	17.59	13.5	0.14	5.4164	14.1	5.4165
Giken	G/37	15.8	0.04	0.14	15.88	13.3	0.02	5.4170	15.6	5.4158
Giken	G/39	13.7	0.10	0.19	13.99	16.3	0.08	5.4165	14.3	5.4157
Giken	G/57	12.0	0.06	0.25	12.31	12.0	0.05	5.4165	14.3	5.4157
Giken	G/51	9.9	0.12	0.16	10.18	11.5	0.09	5.4160	13.5	5.4154
Giken	G/48	13.3	0.13	0.14	13.57	16.0	0.09	5.4175	16.3	5.4176
Charlotta	G/102	12.9	0.14	0.21	13.25	14.0	0.13	5.4172	15.8	5.4176
Charlotta	C/94	16.5	0.16	0.15	16.80	14.1	0.14	5.4170	15.6	5.4165
Bursi	B/7	16.2	0.12	0.17	16.49	13.9	0.17	5.4165	14.3	5.4167
Bursi	B/21	14.5	0.09	0.20	14.79	13.4	0.09	5.4176	16.5	5.4170
Hankabakken	H/13	3.6	0.10	0.51	4.21	1.9	0.09	5.4116	4.3	5.4126

bodies were carried out principally to detect and study the microchemical zoning, or the iron-rich patches in sphalerite, if present. The samples were also analysed for their iron- and manganese content as a measure of cross-check on the results of atomic absorption spectrophotometric analyses. In addition, zinc- and sulphur content of samples were also determined to provide a check on the correction procedure.

The analytical work was carried out at Sentralinstituttet for industriell forskning in Oslo, with the kind cooperation of Dr. W. L. Griffin, on an A. R. L. EMX-Model Electron probe microanalyser at 20 KV with an effective specimen current of 0.05 MA. Standards used were ZnO, natural pyrite, natural sphalerite and manganese sulphide of well-established composition kindly provided to the author by Dr. Otteman of the University in Heidelberg. Instrumental corrections for absorption (Philibert 1963), fluorescence (Read 1965), dead-time, and atomic number effect were calculated using the Springer Programme on the computer. Under the analytical conditions employed, detection limits were 0.02 % for iron and 0.01 % for manganese determination. In the iron-concentration range commonly encountered, analytical precision was usually better than ± 2 % of the amount present.

The results of analyses by this method have been presented in Tables 1 and 4.

Unit-cell measurements of sphalerite. – Cell dimensions of sphalerite from the above-mentioned 12 selected samples were determined by the X-ray diffractometric method of Smith (1955) as revised by Short & Steward (1959). Extrapolation of these measurements on the X-ray determinative curve of Barton & Toulmin (1965) was then adopted to estimate the iron content of the corresponding sphalerite samples. For purposes of comparison, these results expressed as apparent FeS content are incorporated in Table 1 side by side with the results of atomic absorption spectrophotometric and microprobe analyses.

Comparative study of the analytical results

Comparative study of analytical results on the 12 selected samples which were analysed by all the three methods mentioned above (Table 1) brings out a fairly good agreement of the electron-probe and atomic absorption spectrophotometric results for both the FeS and MnS content of the sphalerites. X-ray diffraction results on the mole percent FeS content of sphalerites, as obtained from the measured cell dimensions, on the other hand, appear to be generally on the high side as compared to the corresponding electron probe or AAS results. This is presumably attributable to the expansion of unit-cell dimensions of sphalerites by their manganese- and cadmium contents. In order to check this, the unit-cell dimensions of the sphalerite samples were calculated, using the atomic absorption spectrophoto-

Table 2. Composition of Group-A sphalerites associated with pyrite only (pyrrhotite being absent).

Ore body and mine level	Specimen No.	FeS mole %	MnS mole %	CdS mole %	Ga ppm	Co ppm	Ni ppm	Pb %
Giken(+100)	G/109	13.9	0.08	0.18	7	60	20	0.11
Giken(−106)	G/37	15.7	0.04	0.14	8	50	15	0.08
Giken(−142)	G/38	13.4	0.09	0.15	6	55	20	0.01
Giken(−233)	G/41	16.2	0.06	0.23	8	25	15	0.11
Giken(−233)	G/57	12.0	0.06	0.25	5	25	20	0.01
Giken(−233)	G/24	13.7	0.06	0.14	5	40	15	0.02
Giken(−256)	G/42	13.9	0.09	0.15	10	50	20	0.02
Giken(−283)	G/43	14.1	0.10	0.19	15	35	20	0.03
Giken(−351)	G/46	9.5	0.06	0.22	5	40	25	0.03
Charlotta(−233)	C/55	15.7	0.09	0.15	15	120	35	0.02
Hankabakken	H/20	11.2	0.06	0.23	10	25	20	0.20
Bursi	B/7	16.2	0.12	0.17	12	130	15	0.02
Average (of 12 samples)		13.8	0.08	0.18	9	54	20	0.05
Standard deviation		1.9	0.02	0.04	3	33	5	0.03

Table 3. Composition of Group-B sphalerites associated pyrrhotite (with or without pyrite).

Ore body and mine level	Specimen No.	FeS mole %	MnS mole %	CdS mole %	Ga ppm	Co ppm	Ni ppm	Pb %
Giken(+127)	G/110	13.4	0.06	0.17	10	70	22	0.15
Giken(+61)	G/108	12.9	0.09	0.16	6	50	20	0.03
Giken(+61)	G/107	17.3	0.14	0.15	15	75	30	0.05
Giken(−111)	G/39	13.7	0.10	0.19	7	40	25	0.10
Giken(−233)	G/51	9.9	0.11	0.17	5	75	25	0.01
Giken(−396)	G/74	14.5	0.16	0.15	12	60	12	0.01
Charlotta(+17)	G/102	12.9	0.14	0.21	10	110	15	0.01
Charlotta(−233)	C/94	16.5	0.16	0.15	8	75	30	0.01
Charlotta(−289)	C/74	14.6	0.19	0.15	18	95	30	0.01
Charlotta(−289)	C/9	17.1	0.08	0.19	10	65	20	0.01
Charlotta(−325)	C/78	19.9	0.06	0.13	15	200	40	0.01
Bursi(+80R)	B/3	14.5	0.10	0.17	10	75	20	0.14
Bursi(+60R)	B/4	18.2	0.06	0.20	10	120	12	0.01
Bursi(−5R)	B/13	12.4	0.06	0.20	10	120	12	0.01
Jakobsbakken	J/1	12.7	0.31	0.22	8	65	18	0.04
Jakobsbakken	J/2	15.7	0.21	0.19	15	70	15	0.05
Average (of 16 samples)		14.7	0.12	0.17	11	80	22	0.04
Standard deviation		2.4	0.06	0.02	4	38	7	0.04

metric results, from the following function after Barton & Skinner (1967):

$$a_o = 5.4093 + 0.000456\ x + 0.00424\ y + 0.00202\ z$$

were x, y, and z represent the mole percent FeS, CdS, and MnS respectively. The results so obtained from calculations are placed side by side with those of actual measurements in Table 1 for comparative observations. As may be seen, there is generally a good agreement between the measured and calculated cell dimensions, the differences (often ± 0.0003) being well within the limits of tolerable error in the measurement. The observed agreement confirms that the iron, manganese, and cadmium are the principal elements affecting the cell dimensions of sphalerite. It also confirms that the contents of these elements, as detected by atomic absorption technique, largely represent their amount fixed within the lattice of the respective sphalerites.

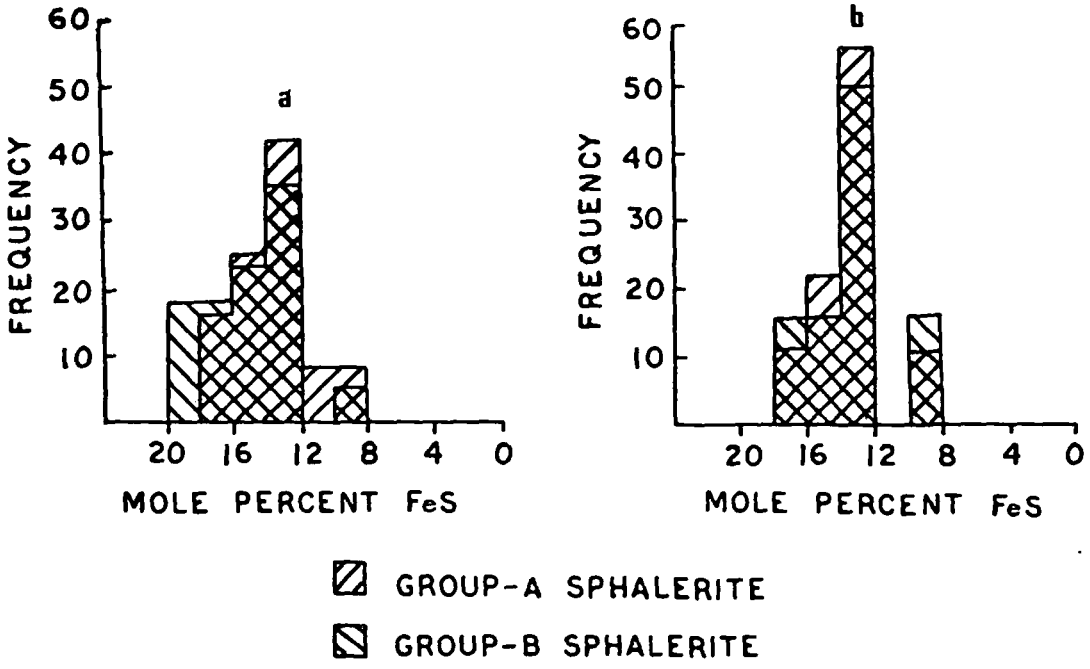

Fig. 9. Composite histograms showing the distribution of analyses of (a) Sulitjelma sphalerites and (b) Giken sphalerites.

Results

Iron content of sphalerites

The FeS-content of sphalerites belonging to two principal groups of ores in Sulitjelma deposit varies, in general, from 9.5 to 19.9 mole percent, the ranges of variation for the two groups overlapping each other for the major part of their spreads (Fig. 9a). The range from 12 to 17 mole % FeS covers nearly 90 % of Group-A and 75 % of Group-B sphalerites and, therefore, largely represents the composition of sphalerites of the deposit in general.

The pattern and trend of variation of iron content in sphalerites of the two groups of ores may be best studied on the scale of an individual ore body. Accordingly, a study of the analysed samples from Giken ore body, the biggest and most representative of the deposit (Fig. 9b), leads to the following interesting and significant observations.

Group-A sphalerites show a variation in mole % FeS from 9.5 to 16.2 with an average of 13.6 and a mode of 13.9 while those while those belonging to Group-B exhibit a range from 9.9 to 17.3 mole % FeS with an average of 13.6 and a mode of 12.2. Group-A sphalerites thus tend to show relatively higher FeS-content than their Group-B counterparts.

The pattern of distribution of iron analyses in either group is unimodal with pronounced mode in 12 to 14 mole % FeS range. In either group, over 65 % of the analysed samples have their iron analyses clustered closely within or around the mode.

The spread of analyses is comparatively larger for sphalerites of the pyrrhotitic assemblage.

Manganese content

The two paragenetical groups of sphalerites exhibit fairly distinctive and rather characteristic ranges of their manganese content. Group-A sphalerites seem to have generally low and relatively more consistent manganese content in the narrow range of 0.02 % to 0.07 %. Group-B sphalerites, on the other hand, exhibit higher manganese content in a wider range of 0.04 % to 0.22 %. Sphalerites from the Jakobsbakken ore body show abnormally high manganese content, usually exceeding 0.2 %.

The graphic evaluation of the iron-manganese

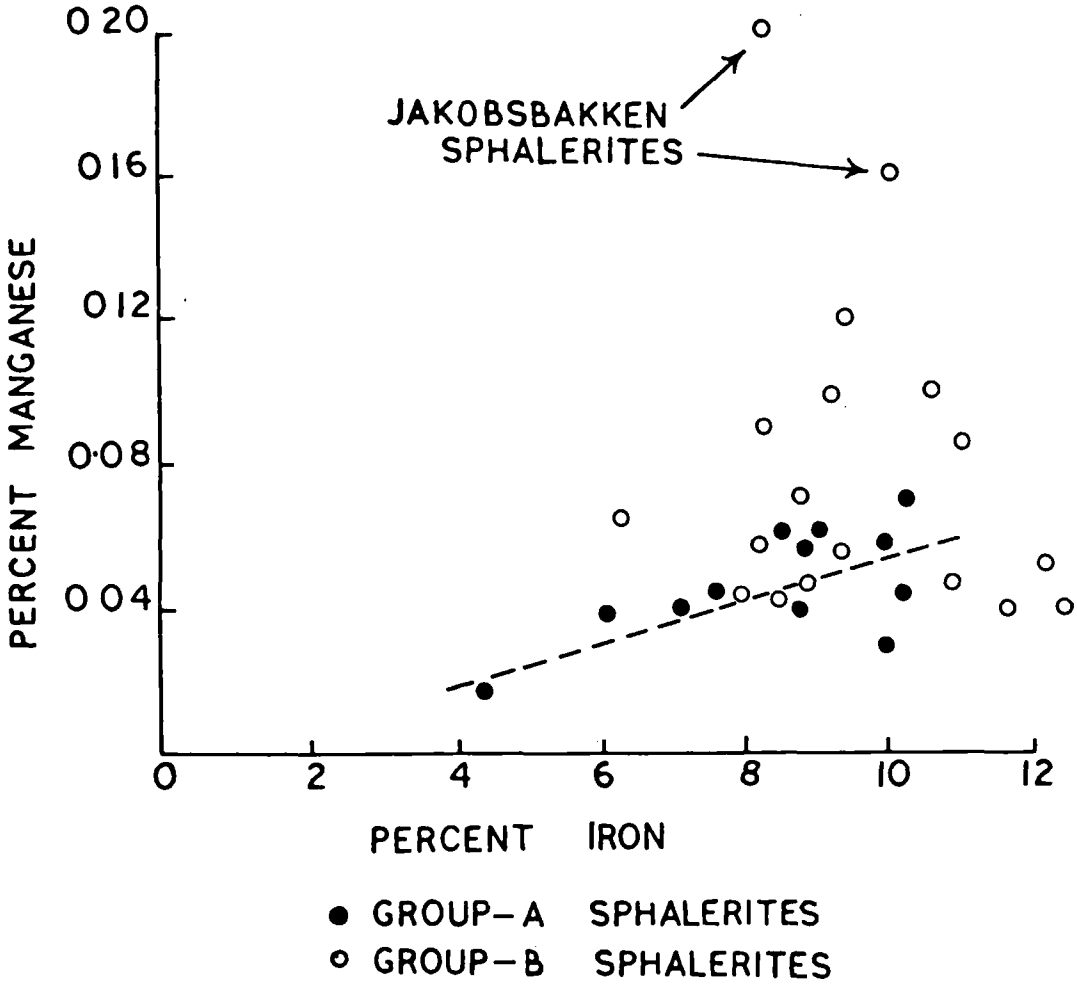

Fig. 10. Graph showing relationship of iron- and manganese-contents in Group-A and Group-B sphalerites.

relationship in Fig. 10 brings out clearly discernible sympathetic correlation between the iron and manganese content of Group-A sphalerites. No such relationship, however, is visible in Group-B sphalerites.

Cadmium content

The cadmium content of the two principal groups of sphalerites varies over a characteristically narrow range of 0.11 % to 0.19 % with a prominent modal concentration around 0.14 %. Ranges of cadmium content pertaining to the two principal groups of sphalerites appear to be overlapping for the large part of their spreads. The cadmium content of sphalerite from the sphalerite-galena assemblage, on the other hand, appears strikingly high, being about 0.37 % in its analysed sample.

There is no discernible linear nor logarithmic correlation between the iron- and cadmium content of Group-A or Group-B sphalerites of the deposit.

Other trace elements

Elements detected in trace amounts in almost all the sphalerite samples of this study include gallium, cobalt, nickel, silver, arsenic, and antimony. The abundances of the first three of them, determined quantitatively, appear in Tables 2 and 3. It is difficult to say how much of the

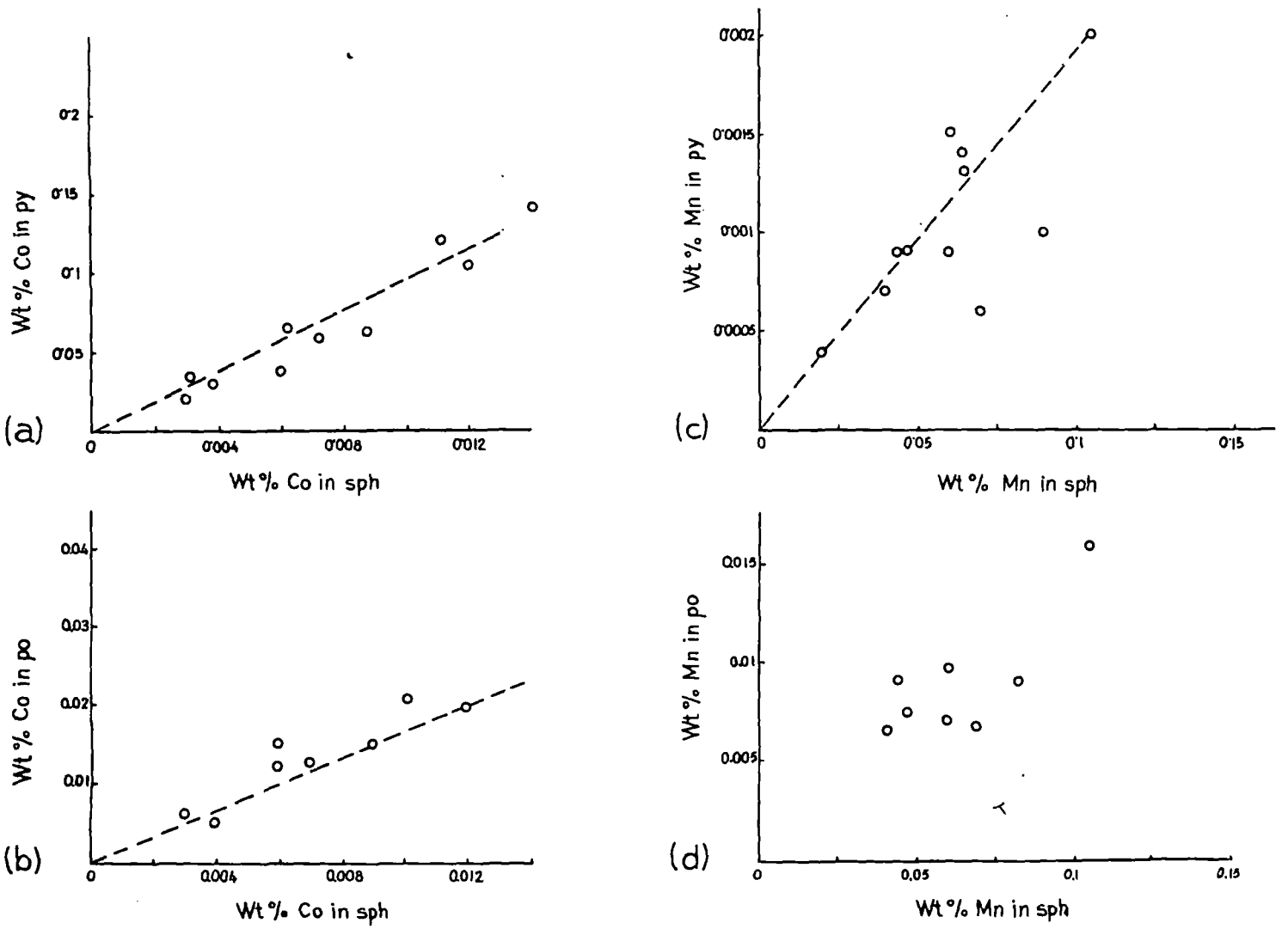

Fig. 11. (a) and (b): Roozeboom diagrams showing the distribution of cobalt between (a) pyrite and sphalerite, and (b) pyrrhotite and sphalerite in Sulitjelma ores.

Fig. 11. (c) and (d): Roozeboom diagram showing the distribution of manganese between (c) pyrite and sphalerite and (d) pyrrhotite and sphalerite in Sulitjelma ores.

Table 4. Chemical composition of different parts of selected sphalerite crystals.

Sample No.	Part of the crystal		Zn %	Fe %	Mn %	S %
G/107	Central part (core)	(1)	57.02	8.79	0.13	34.74
	Marginal part	(2)	56.14	8.37	0.11	35.18
		(1a)	0.86	0.16	0.00	1.00
		(2a)	0.85	0.15	0.00	1.00
G/57	Central part (core)	(1)	58.00	7.49	0.03	33.99
	Marginal part	(2)	58.15	7.77	0.03	34.22
		(1b)	0.87	0.13	0.00	1.00
		(2b)	0.88	0.14	0.00	1.00

1(a) and 2(a) and 1(b) and 2(b) represent no. of atoms calculated from the analyses 1 and 2 on the basis of 1(S).

observed abundances of these elements in the analysed sphalerite samples should be ascribed to the microcrystalline particles or grains of chalcopyrite, galena etc. that may be occurring as minute, invisible, and inseparable inclusions in sphalerite, or to the copper possibly present in solid solution with zinc. In this connection, two important facts have to be taken into account:

The analytical results show fairly low concentration of both copper and lead in the analysed sphalerite samples, thus indicating minimal contamination.

The abundances of the above-mentioned microelements in the analysed sphalerites, in general, fall within appreciably narrow ranges.

It is, therefore, surmised that the observed abundances of the trace elements by and large represent the amount fixed within the lattice of sphalerite itself, and the contributions of the impurities, if any, are almost negligible.

Unlike iron, manganese, and cadmium, none of the trace elements mentioned above exhibit any dependence upon the paragenetic grouping of sphalerites. The ranges of abundance of the various trace elements corresponding to the two paragenetic groups of sphalerites are found to be characteristically narrow and almost overlapping for the whole or the large part of their spreads.

Sphalerite composition on a crystal scale

Microprobe analyses of numerous spots representing central (core) and marginal (rim) portions of several sphalerite crystals in about a dozen selected samples of the two principal types of ores were carried out to examine the homogeneity/heterogeneity of sphalerite composition on the crystal scale. Representative results of this study referring to two typical samples, summarised in Table 4, exhibit nearly identical composition in the core and rim portions of the crystals thereby indicating total absence of zoning in them and almost homogeneous chemical constitution of the sphalerites.

Following suggestions of Scott & Barnes (1971), microprobe traverses across a few sphalerite grains in three polished sections of typical ores belonging to sphalerite-pyrrhotite assemblage were also undertaken in order to detect the presence of iron-rich patches, if any. No such patch, however, could be detected in the analysed sphalerites.

Element distribution between sphalerite and associated iron-sulphide minerals

The partitioning of some common minor elements, particularly manganese and cobalt between sphalerite and pyrite of pyritic ores on the one hand, and sphalerite and pyrrhotite of pyrrhotitic ores on the other, was studied on a limited scale. The results of this study are presented graphically as 'Roozeboom diagrams' in Fig. 11. As may be seen the study brings out fairly distinct and meaningful distribution patterns. The distribution of cobalt between sphalerite and pyrite, as well as between sphalerite and pyrrhotite, shows remarkably little scatter of points on the diagrams. The distribution of manganese in both the mineral pairs, on the other hand, exhibits less distinct, yet still delineable trend towards consistency of distributional relationship. The magnitude of deviations, of course, appears relatively more but is still within reasonable limit of error.

While it may be desirable to have many more analytical results to study partitioning of elements, the aforesaid study possibly succeeds within its limitations to focus upon the discernible trend towards regularity of element partitioning in the typomorphic mineral pairs representing the two ore-types.

Synthesis and discussion

The overall observations of the present study confirm the classification of sphalerite-bearing ores of Sulitjelma deposit into three typomorphic groups that have distinguishable modes of occurrence, mineral associations, and micromineralogic and geochemical characteristics of sphalerites. This fact is, in itself, suggestive of the polycyclic nature and complicated history of sulphide mineralization in the region.

The first two groups of sphalerite-bearing ores, represented by pyrite-chalcopyrite-sphalerite and pyrrhotite-chalcopyrite-sphalerite assemblages, constitute over 90 % of the ore mass in the deposit. They vary considerably not only in their own relative proportion in the average ore mass, but also in their average chemical composition from one ore body to another. A big range of zinc-rich to zinc-poor ore bodies having no definite pattern in their setting is consequently represented in the deposit. This observation has a significant bearing on the problem of ore genesis in the region (Rai 1972, 1977).

In contrast to the above-mentioned picture regarding their average chemical composition, the two groups of ores exhibit only minor differences, essentially of quantitative nature, in the minor- and trace-element geochemistry of their sphalerites. The ranges of variation in the content of an element in sphalerites of the two groups of ores are overlapping for the large part of their spreads in the case of minor elements like iron and manganese and cadmium and are generally quite narrow and indistinguishable for trace elements like gallium, cobalt, nickel, etc. Similarities in the pattern and trend of distribution of analytical results of iron in the two groups of sphalerites are also striking and significant. All these observations seem to be suggestive of final crystallization or recrystallization of the two groups of sphalerites and related ores under almost identical physico-chemical conditions corresponding possibly to the isofacial high-grade metamorphism of ores and the country rocks.

In the Giken ore body, the sphalerites of pyritic assemblage exhibit a tendency to be slightly richer in iron as compared to the sphalerites of the pyrrhotitic assemblage. While this significant observation needs to be strengthened with a larger data base covering the entire deposit, it may be mentioned that a similar pattern and trend of sphalerite composition has been observed recently in the massive lead-zinc deposit of Sullivan in British Columbia, Canada (Barton pers. comm. 1975). It is difficult to say if observations of this sort can be explained simply by high (total) pressures during crystallization or by the equilibration at low temperatures or even both. As suggested by Barton, a better explanation might well be multiple mineralization or limited re-equilibration wherein the pyrite was inert. The possibility of interactions between some phases while others remained inert or sluggish as temperatures and pressures fell has, accordingly, to be considered. The modifying role of lower temperature phenomena which are capable of clouding or even destroying the records of metastable stages also needs proper evaluation in this connection.

The present study on sphalerites also has an important bearing on the problem related to equilibrium control of ore formation in the deposit. The observed textural relations of sphalerite and associated iron-sulphide minerals in the two ore types indicate essentially the co-existing nature of the sulphide minerals concerned. The homogeneity of sphalerite composition on the crystal scale, as brought out by the microprobe studies, seems to be suggestive of effective equilibration even on the micro scale in the ore mass of the two ore-types. This is further substantiated by the observed regularity in the partitioning of certain minor elements, particularly manganese and cobalt, between sphalerite and associated iron-sulphide minerals in the two ore-types. The study on minor- and trace-element composition of sphalerites further brings out a close approach to compositional uniformity of sphalerites of each group on the scale of an ore body as well as the ore deposit in general. All these micro-, macro- and mega-scale observations suggest a good degree of equilibrium control of ore formation in the deposit under study.

As shown by Scott & Barnes (1971) and Scott (1973), sphalerite co-existing with pyrrhotite and pyrite may be used confidently as a geobarometer in most of the geologic environments. In

regionally metamorphosed sulphide deposits, according to them, this geobarometer is most likely to succeed because the duration and extent of the metamorphic event offers optimum conditions for equilibration and homogenization of mineral assemblages. Accordingly, in the Sulitjelma deposit, where the equilibration of mineral assemblages on all scales has already been surmised and is presumably an effect of the regional metamorphism, the sphalerite geobarometer seems to be best-suited for deciphering the pressure conditions of deposition and metamorphism of ores. Paucity of adequate data regarding the temperature conditions of ore formation, however, circumscribes the effective application of this geobarometer. Meanwhile, some provisional estimates regarding the pressure conditions may be made on the basis of the following available data:

Henley's (1970b) estimates regarding the upper limit of temperature of recrystallization of country rocks at 550°C–600°C, this being presumably applicable also to the ores in the light of isofacial nature of regional metamorphism of country rocks and the ore deposit.

The estimates of minimum temperatures in 375°–425°C range, as obtained from the application of pyrrhotite geothermometer.

The composition of sphalerites co-existing with pyrrhotite and pyrite commonly in the range of 12 to 17 mole % FeS, as observed in this study.

The extrapolation of the above data on the geobarometric curves of Scott & Barnes (1971) indicates the pressures of 4.0 ± 1 Kb in the deposit. While presenting this estimate tentatively, it may be emphasized that the existing composition of sphalerites in both the major paragenetical groups of ores represents at best the optimum conditions undergone by them during regional metamorphism and not necessarily the primary conditions of ore-formation in the deposit.

Acknowledgement. – The valuable guidance and encouragement received from Prof. J. A. W. Bugge are gratefully acknowledged. Dr. Paul B. Barton, Jr., was kind enough to go through the manuscript critically and make valuable suggestions. The author received considerable help and cooperation from dosent F. J. Langmyhr, Dr. W. L. Griffin, and Mr. H. C. Seip from Universitetet i Oslo in carrying out the analytical work. All such help and the support and cooperation received from the Norwegian Agency for International Development (NORAD), Oslo; A/S Sulitjelma Gruber, Sulitjelma and Indian School of Mines, Dhanbad, in carrying out this study, are gratefully acknowledged.

June 1976

References

Barton, P. B. Jr. & Skinner, B. J. 1967: Sulfide mineral stabilities, p. 236–333. *In* Barnes, H. L. (ed) *Geochemistry of Hydrothermal Ore Deposits*. Holt, Rinehart and Winston, New York. 670 p.

Barton, P. B. & Toulmin, P. III 1966: Phase relations involving sphalerite in the Fe-Zn-S system. *Econ. Geol. 61*, 815–849.

Henley, K. J. 1970a: The structural and metamorphic history of the Sulitjelma region, Norway with special reference to the nappe hypothesis. *Nor. Geol. Tidsskr. 50*, 97–136.

Henley, K. J. 1970b: Application of the muscovite-paragonite geothermometer to a staurolite-grade schist from Sulitjelma, north Norway. *Mineralog. Mag. 37*, 693–704.

Kautsky, G. 1953: Der geologische Bau des Sulitjelma – Salojauregebietes in den Nordskandinavischen Kaledoniden. *Sv. Geol. Unders. Ser C. No. 528, Årbok 46(4)*.

Kullerud, G., Padget, P. & Vokes, F. M. 1955: The temperature of deposition of sphalerite-bearing ores in the Caledonides of Northern Norway. *Nor. Geol. Tidsskr. 35*, 121–127.

Langmyhr, F. J. & Paus, P. E. 1968: The analysis of inorganic siliceous materials by atomic absorption spectrophotometry and the hydrofluoric acid decomposition technique – Part I. *Anal. Chim. Acta, 43*, 397–408.

Langmyhr, F. J. 1970: The analysis of sulphide minerals – Part VIII. *Anal. Chim. Acta 43*, 397–408.

Mason, R. 1967: The field relations of the Sulitjelma gabbro. *Nor. Geol. Tidsskr. 47*, 237–248.

Nicholson, R. & Rutland, R. W. R. 1969: A section across the Norwegian Caledonides: Bodø to Sulitjelma. *Nor. Geol. Unders. 260*, 1–86.

Oftedal, I. 1940: Untersuchungen über die Nebenbestandteile von Erzmineralien Norwegischer Zinkblende führender Vorkommen. *Skr. Nor. Vidensk. Akad. i Oslo. Mat.-naturvidensk. Kl., 1940, No. 8*, 1–103.

Rai, K. L. 1972: Geology and geochemistry of Caledonian massive sulphide deposit at Sulitjelma, Nordland, Norway. Unpublished Research Contrib. Geologisk Institutt, Oslo. 50 p.

Rai, K. L. 1977: A geochemical approach to the genesis of the Caledonian sulphide mineralization at Sulitjelma, Norway. *Nor. Geol. Tidsskr. 57*.

Ramdohr, P. 1938: Antimonreiche Paragenesen von Jakobsbakken bei Sulitjelma. *Nor. Geol. Tidsskr. 18*, 275–289.

Ramdohr, P. 1969: *The Ore Minerals and Their Intergrowths*. Pergamon Press. 1174 p.

Scott, S. D. 1973: Experimental calibration of the sphalerite geobarometer. *Econ. Geol. 68*, 466–474.

Scott, S. D. & Barnes H. L. 1971: Sphalerite geothermometry and geobarometry. *Econ. Geol. 66*, 653–669.

Sjögren, H. 1900: Öfversigt at Sulitelmaområdets geologi. *Geol. Fören. Stockh. Forh. 22*, 432–462.

Smith, F. G. 1955: Structure of zinc-sulphide minerals. *Am. Min. 40*, 658–675.

Vogt, J. H. L. 1894: Über die lagerstatten von Typus Røros, Vigsnæs, Sulitjelma in Norwegen und Rammelsberg in Deutschland. *Zeitschr. prakt. Geologie, 1894*, 41–50, 117–134, 173–181.

Vogt, J. H. L. 1927: Sulitjelmafeltets Geologi og Petrografi. *Nor. Geol. Unders. 121*.

Vokes, F. M. 1962: Mineral parageneses of the massive sulphide orebodies of the Caledonides of Norway. *Econ. Geol. 57*, 890–903.

Wilson, M. R. 1973: The geological setting of the Sulitjelma orebodies, Central Norwegian Caledonides. *Econ. Geol. 68*, 307–316.

UNIVERSITY OF UTAH
RESEARCH INSTITUTE
EARTH SCIENCE LAB.

FC
625

The geochemistry of meta-igneous rocks from the amphibolite facies terrain of south Norway

ROBERT BEESON

Beeson, R.: The geochemistry of meta-igneous rocks from the amphibolite facies terrain of south Norway. *Norsk Geologisk Tidsskrift*, Vol. 58, pp. 1–16. Oslo 1978. ISSN 0029-196X.

The field relations, petrography, and geochemistry of a suite of amphibolite facies metamorphic rocks from the Bamble Sector of the Fennoscandian Shield in south Norway are described and discussed. Field and geochemical parameters suggest an igneous origin for the suite, in particular the mineralogical and chemical continuum from acid to basic members, element associations and trends, and the abundance of major constituents. The Na and K contents are consistent with calc-alkaline igneous suites.

Element diffusion trends typical of high-grade metamorphism, particularly those involving K and related elements, contrast with those observed in the meta-igneous rocks, and the metamorphism is considered to be largely isochemical. Therefore the pre-metamorphic chemical characteristics of the area, e.g. high Th concentrations, can be used to assess the metamorphic processes which have affected adjacent granulite and granitic terrains.

R. Beeson, Geological Survey, Private Bag X112, Pretoria 0001, South Africa.
Present address: Uriran Private Company, P.O. Box 11/1664, Tehran, Iran.

The Songe-Ubergsmoen area of south Norway is in the Bamble Sector of the Fennoscandian Shield. Songe is 250 km south of Oslo, and 40 km north of Arendal (Fig. 1).

The Bamble Sector in the Arendal region consists of high-grade metamorphic rocks of upper amphibolite and granulite facies (Bugge 1943, Touret 1968). The Songe-Ubergsmoen area lies in the upper amphibolite facies terrain. The grade of metamorphism increases southward towards Arendal, where the granulite facies rocks are located (Cooper 1971, Andreae 1974).

The geological history proposed by Starmer (1972) can be applied in general to the Songe-Ubergsmoen area. The main metamorphic episode seen today is the Svenconorwegian orogeny (D3 of Starmer 1972) at an approximate age of 1160–1200 m.y. (O'Nions & Baadsgaard 1971). This was followed by a major period of granitisation, which had a profound effect on the gneisses around Tvedestrand, immediately to the south of the area under discussion (Field 1969).

The Songe-Ubergsmoen has been mapped by the author at a scale of 1:15,000. Four major lithological units occur in the area: metasedimentary gneisses, typified by the presence of sillimanite and graphite (Beeson 1975); the meta-igneous rocks described here; granitic and granodioritic gneisses (Starmer 1969a); and basic rocks of three recognisable ages and varying metamorphism (Starmer 1969b, Elliott 1973). The spatial distribution of these lithologies has been previously described (Beeson 1975).

The meta-igneous rocks and to a lesser extent the metasedimentary gneisses of the Songe-Ubergsmoen area offer an excellent opportunity to study lithologies which have not been extensively affected by the movement of elements during granitisation or K-feldspathisation processes prevalent in adjacent areas. These processes have occured in the area, but detailed mapping has shown that the meta-igneous rocks are only partially affected. This has enabled the sampling of a suite of rocks which offers an indication of the primary nature of the pre-metamorphic lithologies, and the processes active in high-grade metamorphism.

The field relations, petrography and geochemistry of the meta-igneous rocks are discussed, and compared with both metamorphic and igneous rocks suites from elsewhere in the world with which they show affinities.

Field relations

The meta-igneous rocks consist typically of quartz, plagioclase, biotite, and hornblende. The hornblende is normally restricted to the in-

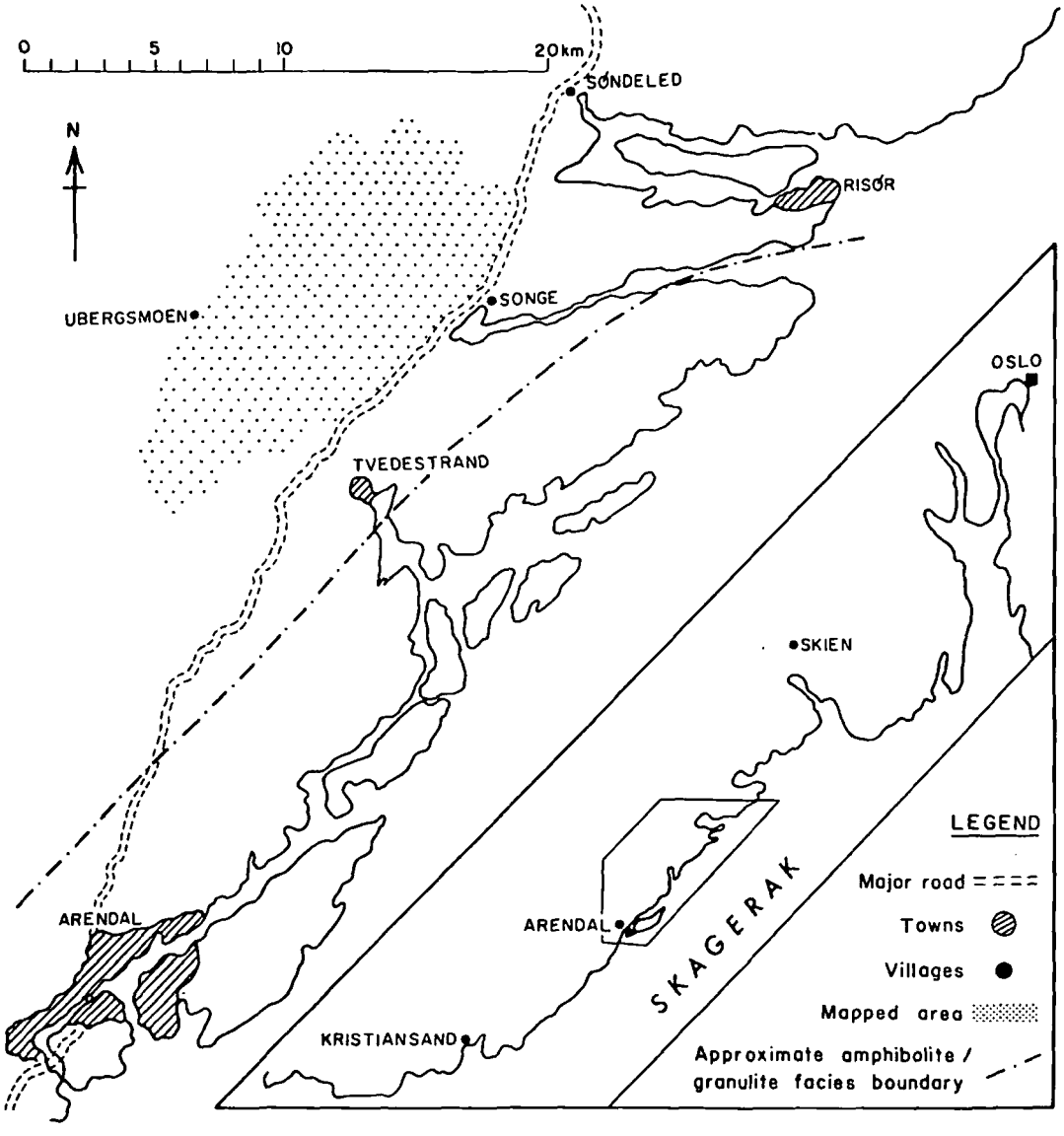

Fig. 1. Location map of the Songe-Ubergsmoen area, south Norway.

termediate and basic varieties of the rock suite. Garnet, when present, is red in colour. K-feldspar is rare in the meta-igneous rocks, but when present the field and petrographic evidence indicates that this mineral replaces plagioclase. This mineralogy contrasts with that of the metasedimentary gneisses in the area, and allows distinction between the two rock groups in the field. The metasedimentary gneisses commonly have sillimanite and graphite in the more acid varieties, and a pale pink garnet in relatively iron-rich varieties. Only rocks with a mineralogy of biotite-quartz-plagioclase are common to both the meta-igneous and metasedimentary lithologies.

The rock suite normally has a well-developed gneissic texture, but it is locally massive. It varies from leucocratic quartz-plagioclase gneisses with minor contents of biotite to amphibolites consisting of only plagioclase and hornblende. Banding of leucocratic and melanocratic layers occurs, commonly with a pre-

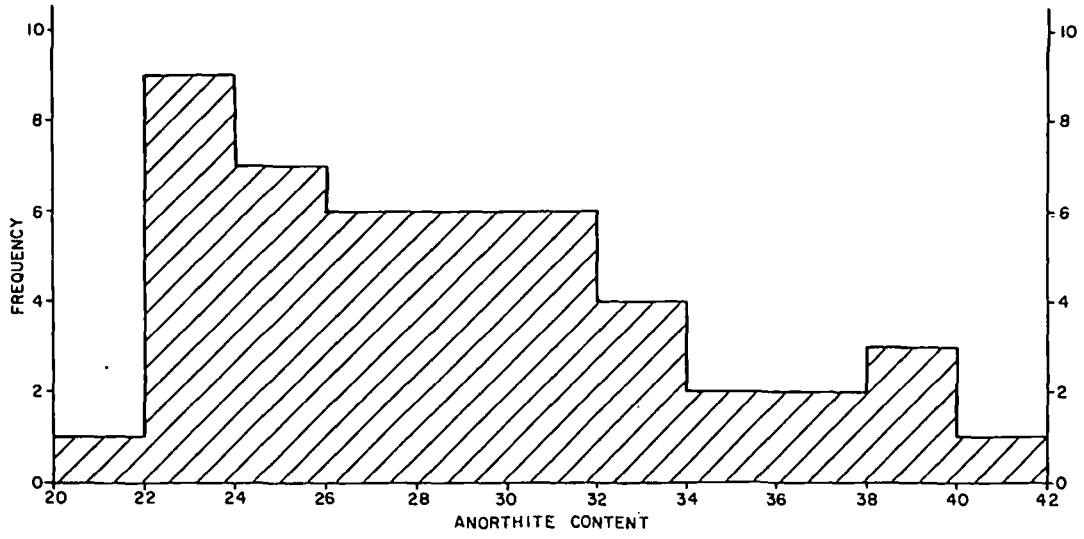

Fig. 2. Frequency distribution of the anorthite content of plagioclase in the meta-igneous rocks.

dominance of the former. The individual layers vary from 1 centimetre to several metres in width. The amphibolite horizons within the quartz-plagioclase-biotite gneisses (± hornblende) can be much wider than these banded gneisses, being tens or hundreds of metres in width. These amphibolite horizons can extend for more than a kilometre along strike.

Metasedimentary gneisses rarely occur as thin intercalations within the meta-igneous rocks, but are commonly at least 50 m in width. However, the reverse is not true, and thin intercalations of the meta-igneous rocks are not found in the metasedimentary gneisses. Units of the meta-igneous rocks can be extremely persistent, one 500 m wide unit continuing for 15 km throughout the area.

Petrography

The petrographic description tendered here is a generalised summary of the features of the meta-igneous rocks as a whole.

Two main varieties of quartz (3–59%) are present. The first occurs as sub-rounded grains (0.1–5 mm) with a non- or partially-undulose extinction and curved or lobate margins. The second variety has an irregular shape, frequently displays sutured margins, and undulose extinction. The latter may occasionally contain trains of inclusions parallel to the foliation. These are considered to have formed during two metamorphic stages, i.e. syn- and post-the main metamorphic episode (Beeson 1975).

Plagioclase (2–82 %) is normally present as equidimensional grains (≤3 mm), although slightly elongate, coarser varieties (≤7 mm) are present. The grain shape can be rounded, angular or irregular. Plagioclase composition shows a continuous increase in Ab content with silica in this rock type (Fig. 2). The plagioclase is occasionally antiperthitic. In such cases the antiperthitic types are patch, flame and rod forms.

Biotite (0–69 %) is predominantly pleochroic pale to dark brown (X, Y) or brown (Z), although pale phlogopitic micas and iron-rich medium-brown to black varieties are represented. Primary mica varies from stubby, shortened grains to thin, platelike crystals (0.5–4 mm). Mica defines the foliation plane, particularly when abundant, but the foliation can be distorted by either the growth of garnet or quartz veinlets. Biotite commonly replaces hornblende, both in the presence and absence of K-feldspar. Two replacement forms are recognised: distinct stubby or elongate laths cutting across the hornblende grains, or a felted mosaic of fine-grained mica. The biotite also replaces garnet and rarely epidote. Minerals occuring as inclusions in the biotite are zircon, apatite, and opaque minerals. The biotite alters to chlorite and prehnite.

The hornblende (0–33 %) is exclusively green in colour, commonly with X, Y pleochroic pale

Table 1. Meta-igneous rocks, Songe-Ubergsmoen area: summary statistics. Major elements in oxide percentages, trace elements in ppm (n = 50)

Element	Mean	Standard deviation	Maximum	Minimum	Crustal average
SiO_2	66.12	7.87	78.19	47.62	60.3
Al_2O_3	14.63	2.15	21.32	10.51	15.6
TiO_2	0.73	0.44	2.13	0.17	1.0
Fe_2O_3	2.50	2.02	8.20	0.29	7.2
FeO	2.67	1.85	8.97	0.43	
MgO	2.40	2.47	13.14	0.14	3.9
CaO	3.99	1.85	8.17	0.21	5.8
Na_2O	3.72	1.50	8.46	0.30	3.2
K_2O	1.83	1.19	5.62	0.14	2.5
MnO	0.07	0.07	0.20	0.01	0.10
P_2O_5	0.17	0.12	0.52	0.02	0.11
S	292	458	3011	7	260
Cl	358	318	1302	25	130
Sc	14	9	45	2	22
V	127	85	523	13	135
Cr	27	35	149	0*	100
Co	20	12	53	0*	25
Ni	17	23	86	0*	75
Cu	25	30	198	1	55
Zn	76	47	216	6	70
Ga	21	4	34	12	15
Rb	65	45	215	0*	90
Sr	254	138	587	13	375
Y	35	38	188	0*	33
Zr	294	197	1754	70	165
Sn	1	4	23	0*	2
Ba	860	335	1886	276	425
La	29	24	100	1	30
Ce	88	53	261	24	60
Pr	21	11	45	1*	8
Nd	26	15	74	7	28
Sm	11	6	28	3*	6
Pb	14	10	52	3*	13
Th	9	9	35	0*	10
U	1	1	4	0*	3

(1) From Taylor (1964)
* indicates value below the direction limit

green to medium green-brown or emerald green and Z pale to dark green-brown. Grain size is variable, and increases proportionally with the hornblende content of the rock. Commonly the hornblende is xenoblastic or elongate xenoblastic, although it is also often prismatic. Quartz, plagioclase, apatite and opaque minerals occur as inclusions in the hornblende.

The garnet (0–15 %) is present as large poikiloblastic grains (≤15 mm) which are irregular, angular, rounded or elongate in shape. Included minerals are quartz, opaques, apatite, and altered plagioclase. Elongate grains commonly form in bands parallel to the foliation or rarely as individual grains cutting across the foliation.

Other minerals occurring in the meta-igneous rocks are K-feldspar, cordierite, and epidote. Accessory minerals present include opaque minerals (magnetite and pyrite), zircon, and apatite.

Geochemistry

50 samples of the meta-igneous rocks have been analysed for 11 major and 24 trace elements. Sample collection was based on 2 principles. To establish a representative collection of the rock group, samples were taken at 100 m intervals along road traverses perpendicular to the strike of the foliation. In addition samples were collected in all parts of the mapped area to establish the regional variation.

Only the summary statistics of the data are presented here (Table 1). The individual analyses , Niggli values, cation percentages, modal analyses and katanorms have been presented elsewhere (Beeson 1972).

The majority of elements in this lithology are typified by a lognormal distribution with a positive skew (Table 1). Only SiO_2, Al_2O_3, and Ga have normal distributions. The distributions of CaO, Na_2O, Zr, and Th are irregular, which may indicate the presence of sub-populations.

Only limited data are available for amphibolite grade metamorphic rocks from other areas but there are similarities in chemistry between the meta-igneous rocks from the Songe-Ubergsmoen area and elsewhere. The major-element composition of the meta-igneous rocks can be compared with the sub-acid and intermediate rocks from Brazil (Sighinolfi 1971), and with amphibolite facies rocks from northern Norway (Heier & Thoresen 1971). However, trace-element compositions, particularly the elements associated with K, are less related to other areas.

Cluster analysis is used in this study to summarise element associations. Cluster analysis is based on all inter-element correlations, and hence identifies groups of related elements. The degree of correlation between the groups can also be identified. The results of the clustering are shown as a dendrogram, which is a simplification of the multi-dimensional correlations in two dimensional form (Fig. 3). This gives the following associations: Mg, V, Co, Cr and Ni; Fe, Ti, Mn, Sc, P and Zn; K, Rb and Ba; Zr, Y,

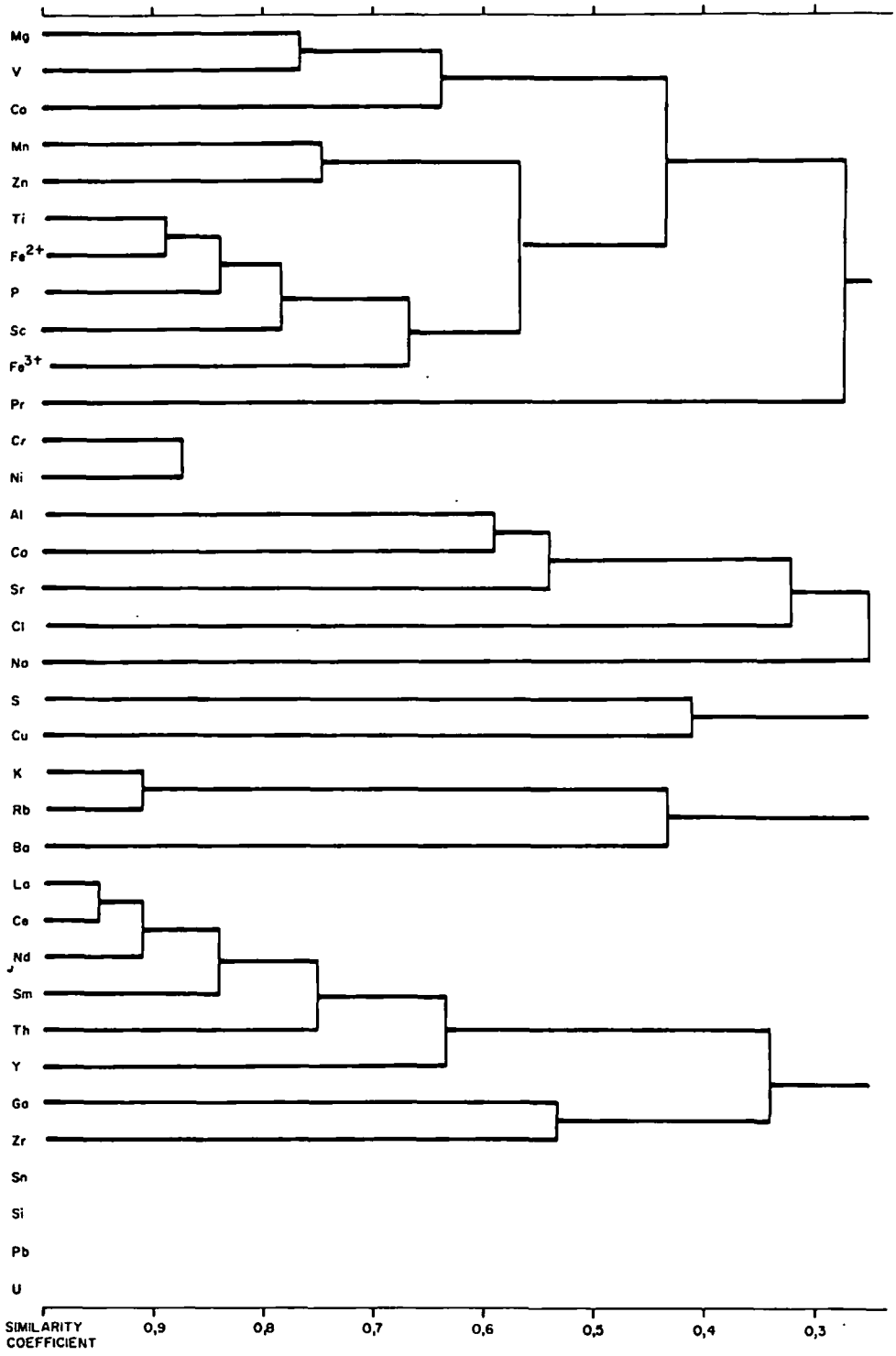

Fig. 3. The R-mode dendrogram for the cluster analysis of elements in the meta-igneous rocks. Clustering terminated at the 95 % confidence level (0.25).

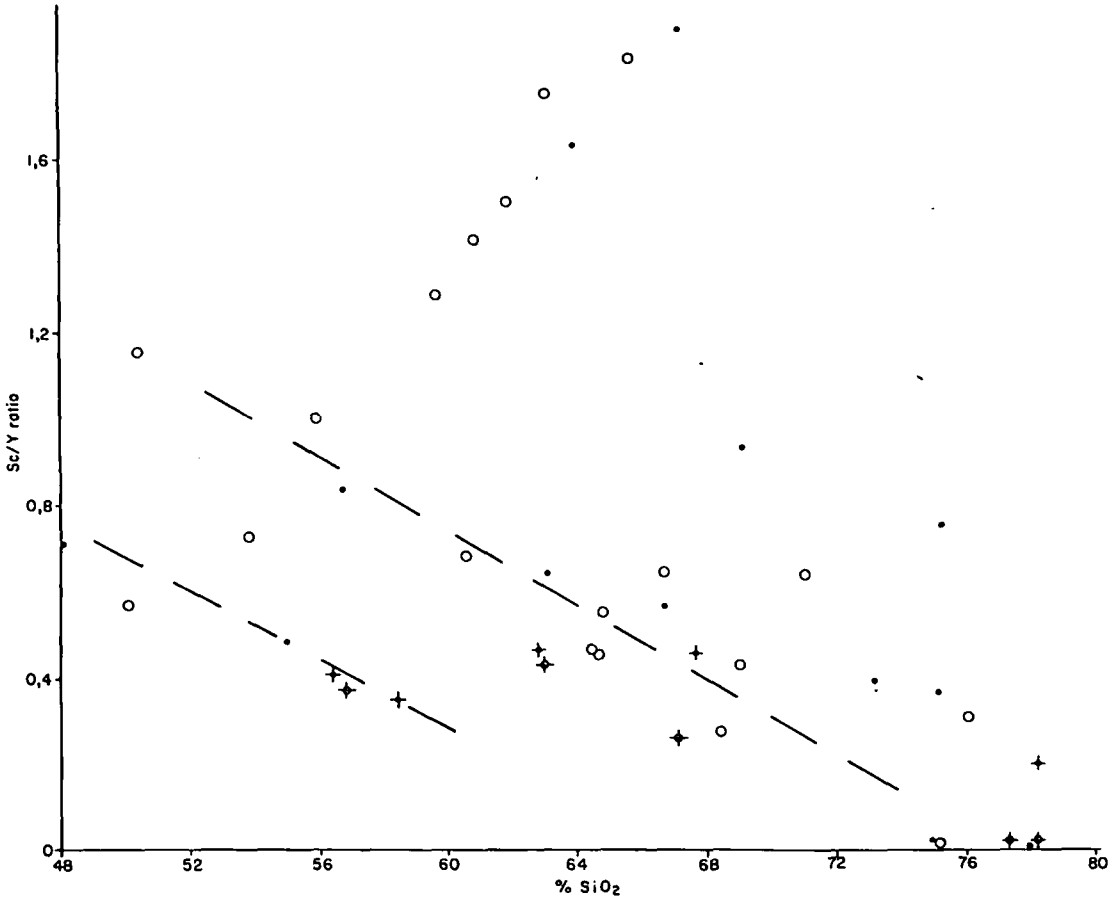

Fig. 4. The Sc/Y ratio versus percentage SiO_2 diagram for the meta-igneous rocks, divided into biotite gneisses (closed circles), biotite-hornblende gneisses (open circles), and garnet-bearing gneisses (crosses).

Ga, Th and the rare-earth elements; Ca, Na, Al, Cl and Sr; S and Cu; and the less significantly clustered elements Si, Sn, Pb, and U. The more important associations are discussed below.

Silicon has a wide range of values (47–78 %); this gives it strong negative correlations with the 15 elements which are most abundant in basic rocks because of the closed percentage system.

Zirconium group (Zr, Y, Th, and the rare-earth elements): Zr is clustered with Y, Th and the rare-earth elements in both the metasedimentary and meta-igneous rocks of the Songe-Ubergsmoen area, but a correlation with Na in the former lithology suggests that at least a proportion of these elements is located in plagioclase (Beeson 1975). In the meta-igneous rocks the elements are only correlated with Zr. Zr normally occurs in zircon in acid and intermediate rocks (Taylor 1965), and hence it is probable that the other elements of this group are present as isomorphous inclusions in the zircon structure in the meta-igneous rocks (Vlassov 1966).

All elements of this association excepting Y are positively correlated with Si, although only La, Ce, Sm, and Th are correlated at the 99 % confidence level. Y decreases with Niggli Si, and hence has positive correlations with both the mafic elements and Zr. A strong, positive correlation between Zr and Ga exists, particularly at high concentrations of both elements, but this correlation cannot be explained.

Taylor (1965) suggests that the Sc/Y ratio is a guide to igneous fractionation. The Sc/Y ratio shows two individual and distinct decreasing

trends with increasing SiO_2 (Fig. 4), excepting seven high values of the ratio. This suggests that this lithology has an igneous origin.

Fig. 4 also indicates that garnet only occurs in rocks with a Sc/Y ratio of less than 0.5. As Sc is strongly correlated with Fe^{2+} in these rocks, the high Sc/Y ratios would normally be expected in garnet-bearing rocks.

Potassium group (K, Rb and Ba): K-feldspar constitutes over 1 % of the mode in only 20 % of the meta-igneous rocks, and hence K and Rb are normally located in biotite. In K-feldspar-bearing rocks the K content is markedly increased. When present, K-feldspar replaces plagioclase in this lithology, and consequently both K and Rb show a negative correlation with Ca and Na. The negative correlation between the latter two elements and Ba is less pronounced than that of K and Rb, and hence it is considered that at least part of the Ba abundance is present in the plagioclase.

The mean K/Rb ratio (292) is higher in the meta-igneous rocks than crustal average estimates (e.g. Taylor 1965, table II). However, it has a wide range of values (138–1200), and the relatively high mean is caused by the high ratios in rocks deficient in K and Rb, where the mean is 739 for rocks with less than 0.5 % K. The median value for the meta-igneous rocks is consequently lower (238).

Comparative data in the Bamble Sector are currently only available for metabasites from the area of the granulite facies transition south of the Songe-Ubergsmoen area (Field & Clough 1976), and the charnockitic gneisses from the granulite facies (Cooper & Field 1977). Although a similar mean K/Rb ratio is obtained for the metabasites from amphibolite facies samples (378), both the granulite facies metabasites (mean 567) and particularly the charnockitic gneisses (mean 1323) show the Rb depletion typical of many high grade metamorphic terrains (e.g. Sighinolfi 1969, 1971). Consequently the linear trend exhibited by the metabasites and the field of the charnockitic gneisses are both on the K-rich side of the regression lines calculated by Shaw (1968) for igneous rock suites, and have an atypical orientation (Fig. 5). In contrast the field of the meta-igneous rocks falls well within that of examples given by Shaw, and have similar K/Rb ratios to several unmetamorphosed rock suites, e.g. the hornblende dacites from the western USA and the andesites and dacites from the Solomon Islands (Jakes & White 1970). The meta-igneous trend is also not markedly divergent from the Lewis & Spooner (1973) granulite trend, although Field & Clough (1976) indicate that this is for a composite sample and not necessarily typical of observed individual trends. Six meta-igneous rocks with below 15 ppm Rb do not conform to the regular trend of the remainder of the rock suite. These samples are deficient in K-bearing minerals, having no K-feldspar and biotite being absent or less than 1 % of the mode.

Table 2. Mean K/Rb and K/Ba ratios for the meta-igneous rocks and metamorphic rocks from elsewhere in the world.

	1	2	3	4	5	6	7	8	9	10
K/Rb	292	378	1330	240	217	258	688	232	297	539
K/Ba	19	18	20	40	28	48	13	–	–	–

1. Meta-igneous rocks, Songe-Ubergsmoen area.
2. Amphibolites, Sogne-Ubergsmoen area.
3. Charnockitic gneisses (Cooper & Field 1977).
4. Granitic gneisses, Arendal area (Cooper 1971).
5. Sub-acid gneisses, Musgrave Range, Australia (Lambert & Heier 1968).
6. Acid gneisses, Musgrave Range, Australia (Lambert & Heier 1968).
7. Basic rocks, Musgrave Range, Australia (Lambert & Heier 1968).
8. Crustal average (Taylor 1964).
9, 10. Amphibolite facies rocks, northern Norway (Heier & Thoresen 1971).

Although K/Ba ratios in the meta-igneous rocks are similar to those recorded in the amphibolite facies terrains of Australia (Lambert & Heier 1968, table II), and the adjacent granulite facies rocks (Cooper & Field 1977), the Ba values (mean 860 ppm) are considerably higher than the estimates for the average of the continental crust (e.g. Taylor 1965, 425 ppm).

Comparison of the K, Th and U concentrations of the meta-igneous rocks with a range of rock types from elsewhere in the world indicates that Th is relatively enriched (Table 3). This results in high values of the Th/U and Th/K ratios in comparison with granitic rocks (Heier & Rojers 1963). Granitic rocks from the Sogne-Ubergsmoen area are similar in respect of these elements to those reported by Killeen & Heier (1974) for gneisses from elsewhere in the Bamble Sector.

The sodium group (Na, Ca, Sr, Al and Cl): the elements of this association are variably located

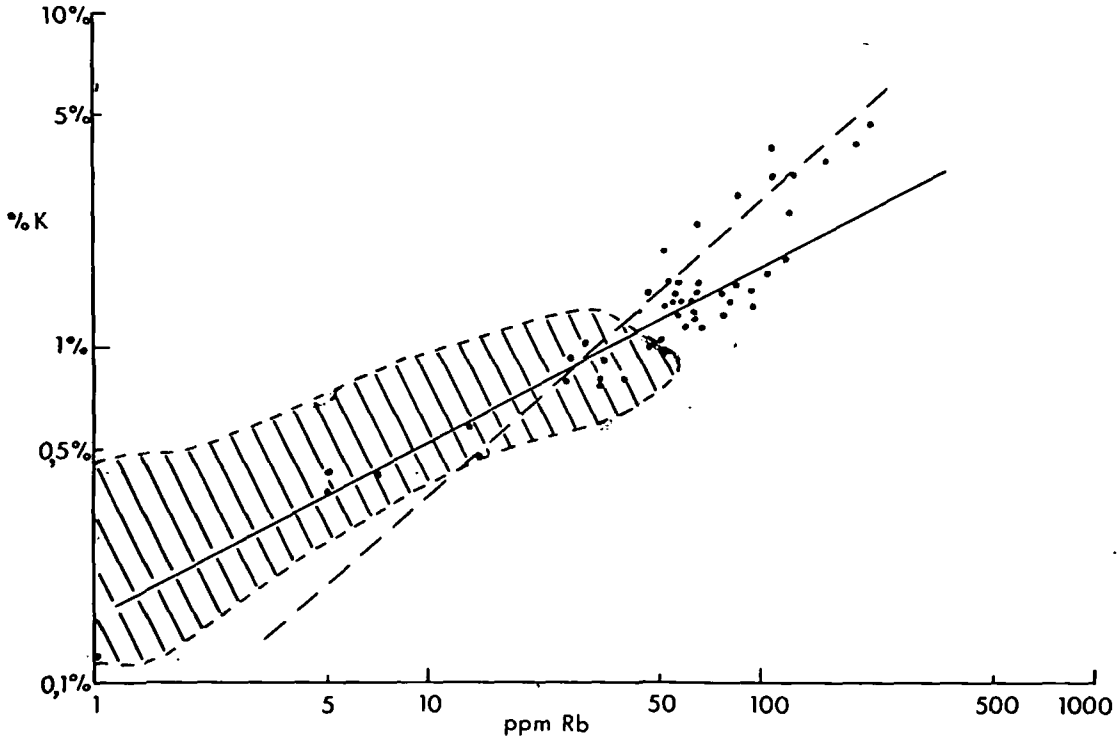

Fig. 5. K versus Rb for the meta-igneous rocks. The dashed line represents the ratio calculated by Lewis & Spooner (1973) for granulites, the continuous line the regression calculated for metabasites (Field & Clough 1976), and the hatched area is the upper part of the charnockitic gneiss field (Cooper & Field 1977).

in plagioclase and hornblende in the meta-igneous rocks. The Na is largely restricted to the former, and it displays a reasonable correlation with the plagioclase content (Fig. 6). The relatively limited range of anorthite contents of the plagioclase (Fig. 2) is not sufficient to disturb this relationship markedly. Ca is contained within both hornblende and plagioclase. The latter normally constitutes 30–65 % of the mode of these rocks, and no systematic variation between Ca and modal abundance was observed (Fig. 7a). However, it is evident that Ca concentrations above 3 % are directly related to the abundance of modal hornblende (Fig. 7b). Only two samples which contain less than 3 % Ca also contain hornblende. At the higher abundances of Ca (>9 %) and modal hornblende (>40 %), plagioclase and hornblende are the main constituents and their linear relationship noted above is disturbed.

Table 3. Mean values of Th, U, K and ratios for metamorphic and granitic rocks.

	1	2	3	4	5
Th	9	21	20	10	17
U	1	3	5	2	5
K	1.52	3.17	3.09	2.58	3.79
Th/U	5.86	9.05	5.2		3.5
Th/k (E4)	6.06	8.55	6.7		3.9
U/K (E4)	1.00	1.45	1.5	0.95	1.2

1. Meta-igneous rocks, this study
2. Granitic gneisses, this study.
3. Levang gneisses, Killeen & Heier (1974).
4. Canadian Shield, Shaw et al. (1967).
5. Granitic rocks, Heier & Rogers (1963).

Sr correlates with both CaO and Na_2O at the 99 % significance level, and shows a similar relationship as Na in respect of modal plagioclase. Hence it can be assumed that Sr substitutes for both Na and Ca in that mineral.

The association between Ca and modal hornblende causes strong positive correlations between the former and the elements of the Fe and Mg associations. Al has a similar behaviour pattern to both Ca and Na, giving correlations at

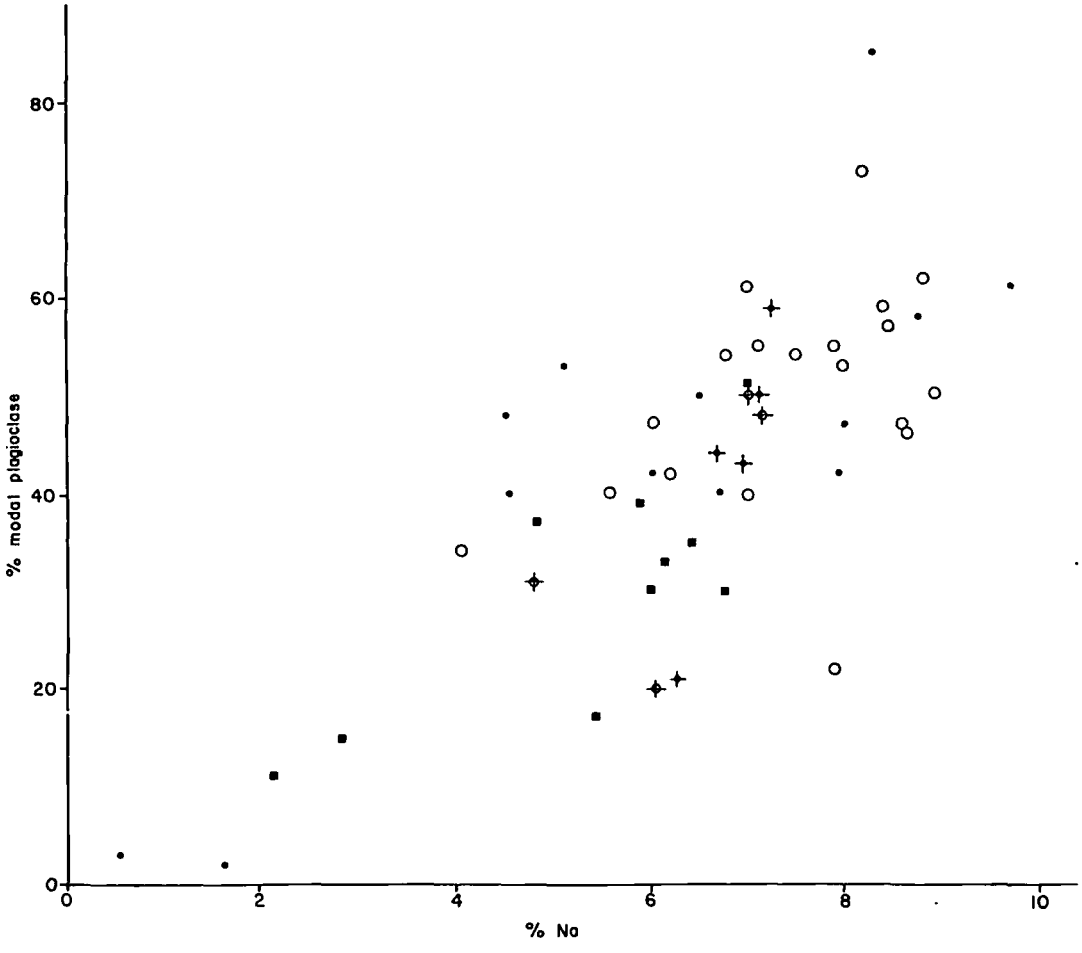

Fig. 6. Modal plagioclase versus percentage Na for the meta-igneous rocks. Key as for Fig. 4, plus amphibolites (squares).

the 99 % significance level with Ca and at the 95 % level with Na, indicating the major element association in plagioclase and hornblende. Cl would normally be expected to associate with the elements in mica, and its presence in this grouping cannot be readily explained.

Magnesium and associated elements (Mg, V, Co, Cr, Ni): the meta-igneous rocks are divided into two associations centred on Mg and Fe. Although correlations between the two groups are commonly above the 99 % significance level for individual elements, V, Cr, Co, and Ni have a more close association with Mg. Cluster analysis (Fig. 3) displays these two associations, although it shows that Cr and Ni have no direct relationship with Co and V except through Mg.

The Co/Mg and V/Mg ratios show no variation with an increase in the Niggli value Si. Cr and Ni have a sympathetic relationship with each other (Fig. 8) and with Mg except in samples with particularly high Mg values. Hornblende-bearing rocks have both high and low values of Cr and Ni (Fig. 8). The Ni/Cr ratio does not vary with increasing silica and, as stated by Taylor (1965), is not a good indicator of fractionation.

The Cr/FeO ratio splits the meta-igneous rocks into two distinct fields which are not related to any contrasts in modal abundances.

Iron and the associated elements (Ti, Mn, Sc, Zn): this forms the closest association found within the meta-igneous rocks, except that between the individual rare-earth elements. This relationship of elements has been previously noted by Sighinolfi (1971) in granulite facies

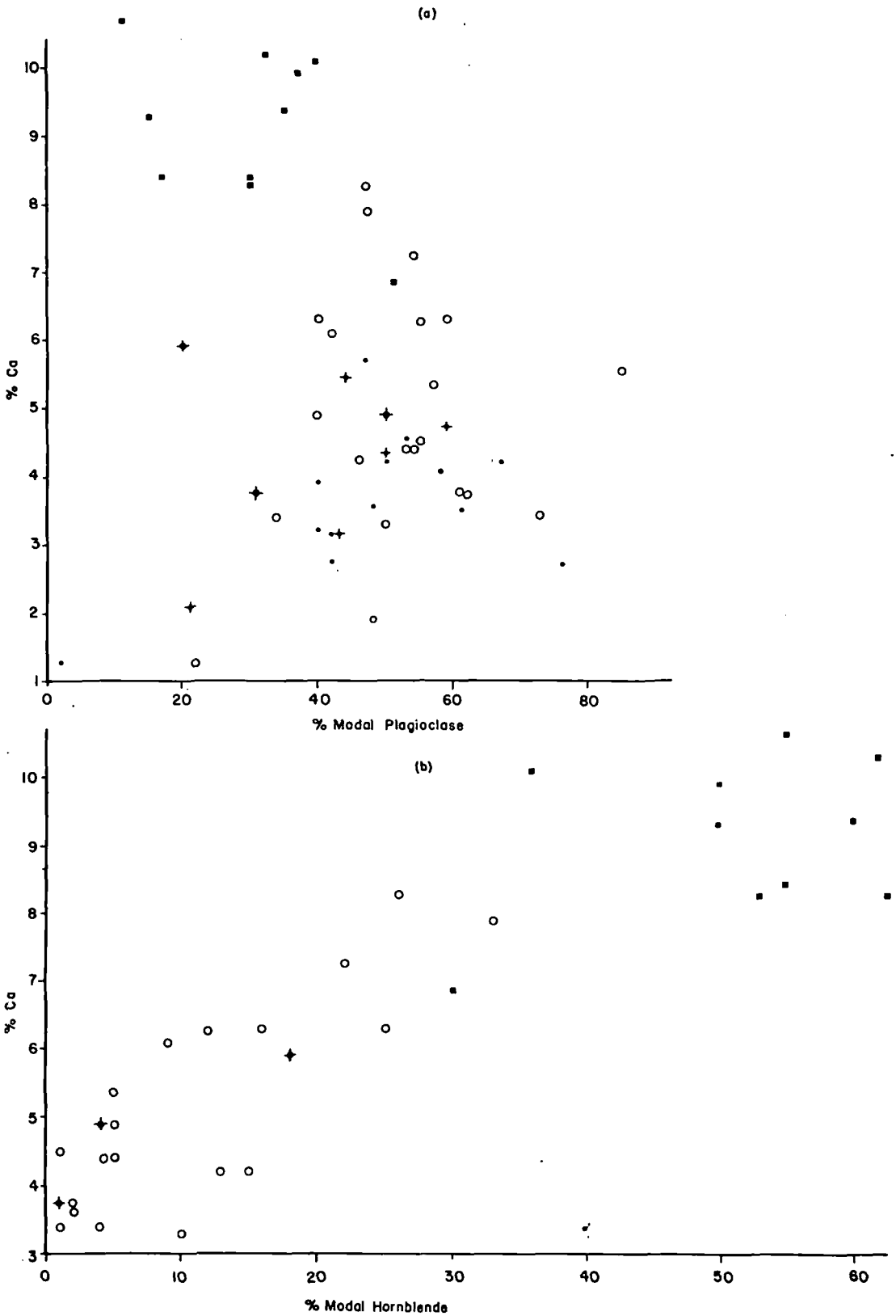

Fig. 7. Percentage Ca versus modal plagioclase (7a) and modal hornblende (7b) for the meta-igneous rocks. Key as for Fig. 4.

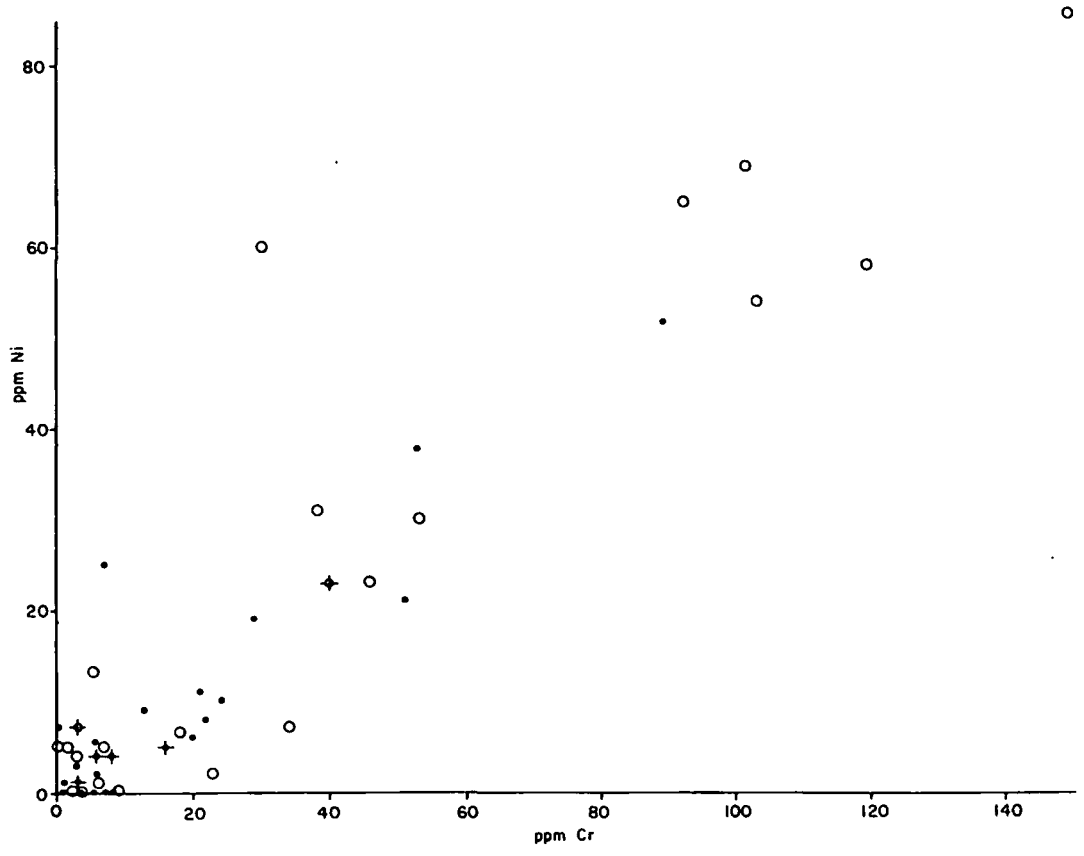

Fig. 8. Cr versus Ni for the meta-igneous rocks. Key as for Fig. 4.

metamorphic rocks in Brazil, and is common in both igneous (e.g. Gruza 1965) and sedimentary rocks (e.g. Condie 1967). Both Mn and Zn are closely correlated with Fe^{2+}, and appear to substitute for that element.

With increasing silica the ratios Mn/Fe^{2+} and Zn/Fe^{2+} exhibit no change, but the ratios Ti/Fe^{2+} and Sc/Fe^{2+} both decrease. The Mn/Fe^{2+} ratio is normally constant during igneous fractionation (e.g. Putman & Burnham 1963) and appears to remain so in the meta-igneous rocks. The Zn/Fe^{2+} ratio, however, decreases in the later stages of igneous fractionation (e.g. Papezik 1965).

Ti/Mg, Fe^{2+}/Mg, and Zn/Mg ratios show no variation with increasing silica, whereas the Sc/Mg ratio decreases. The Co/Fe^{2+} ratio decreases sharply with increasing Fe^{2+}, despite the strong correlation between the two elements. The Ti/Zr ratio, an indicator of fractionation (Taylor 1965), decreases with increasing silica content (Fig. 9).

The close association of Fe and related elements is considered to be a primary, igneous feature, particularly as there is a contrast with the element ratio behaviour in the meta-sedimentary gneisses of this area (Beeson 1975). The clear distinction of two groups of mafic elements in the meta-igneous rocks is difficult to explain for certain elements, particularly V. This element occurs chiefly as V^{3+} and should enter Fe^{3+} position in the later stages of igneous fractionation in igneous rocks, but V and Fe^{3+} are barely correlated here. This is the converse of the findings of Field & Elliott (1974), who established a complimentary increase of these two elements in the amphibolitisation of basic rocks in the southern Bamble Sector. Cr and V have similar characteristics except in their ionic radii, normally resulting in Cr fractionating in

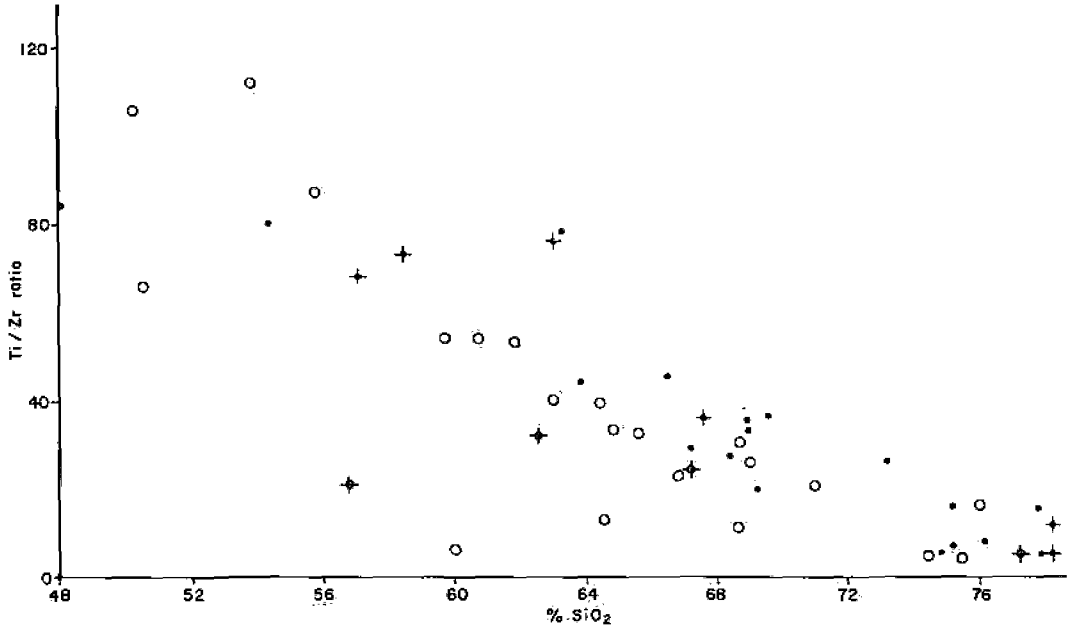

Fig. 9. The Ti/Zr ratio versus percentage SiO_2 for the meta)igneous rocks. Key as for Fig. 4.

the more basic rocks. In view of their similar distributions here, this may explain the Mg-Cr-V association in the meta-igneous rocks.

Discussion

Igneous characteristics of the meta-igneous rocks

Several features combine to justify the classification of the above described lithology as being meta-igneous. It is an individual rock suite which can be recognised in the field, and contrasted with other lithologies of previously determined origin, e.g. the metasedimentary gneisses which contain meta-graywackes, -pelites, and -quartzites (Beeson 1975). The individual members of the meta-igneous rocks have sharp contacts with other lithologies which are parallel to the foliation.

The lithology constitutes a chemical continuum from basic 'amphibolitic' rocks to rocks containing up to 78 % silica. The continuum is reflected in the observed mineralogy, in which the four essential minerals – quartz, plagioclase, biotite and hornblende – all have a wide variation in modal abundance which is controlled by the major element chemistry (see above).

The mean values of the major elements in the meta-igneous rocks are comparable with those of intermediate and acid rocks compiled by Nockolds (1954). As the meta-igneous rocks have a wide compositional range it is difficult to make direct comparisons, but dacites and quartz-diorites have similar compositions (Table 4). The $Na_2O + K_2O$ contents of meta-igneous rocks are similar in relation to SiO_2 for the majority of acid and intermediate volcanic rocks (Fig. 10).

In contrast, metasedimentary gneisses from the Songe-Ubergsmoen area have values dissimilar to igneous rocks, particularly for MgO, CaO and Na_2O (Table 4). In addition, major and trace elements show fractionation trends characteristic of known igneous models, e.g. $Na_2O + K_2O$, Sc/Y, Ti/Zr, Cr/Fe^{2+}, Ti/Fe^{2+} and Mn/Fe^{2+}.

Affinities of the meta-igneous rocks

The geochemistry of the meta-igneous rocks suggests that the element concentrations have undergone little modification during the high-grade metamorphism. Consequently comparisons can be made with modern equivalents with

some confidence. The meta-igneous rocks display close affinities with several tholeitic rock suites, e.g. the Scottish Tertiary Province (Kuno 1968) Fig. 10. Some high silica rocks do not fit directly onto the tholeitic trend, and it is suggested that these are clastic rocks of which a proportion of the material was derived from an igneous source. An example of such sedimentary lithologies has been recorded by Kuno (1968), and given in Fig. 10.

Significance of this study to the Bamble Sector

The southern Bamble Sector is an excellent region for the study of metamorphic processes. Detailed geological mapping has defined the nature of the amphibolite and granulite facies metamorphism and a transitional zone with intense K-feldspathisation. The meta-igneous rocks of the Songe-Ubergsmoen area lie adjacent to the zone of K-feldspathisation and are apparently little affected by this process. Consequently this lithology exhibits igneous characteristics which have not been substantially modified by subsequent metamorphism, and provides a reference against which the rocks of adjacent areas can be compared to determine high-grade metamorphic processes.

Of particular interest to the Bamble Sector is the marked similarity for the majority of elements between the meta-igneous rocks and the charnockitic gneisses of the adjacent granulite

Table 4. Comparison of the major-element compositions of meta-igneous rocks (1) and metasedimentary gneisses (2) of the Songe-Ubergsmoen area with charnockitic gneisses (3, Cooper & Field 1977), and averages for dacites (4) and quartz-diorites (5, Nockolds 1954).

	1	2	3	4	5
SiO_2	66.12	70.05	68.35	63.58	66.15
Al_2O_3	14.63	13.07	13.83	16.67	15.56
TiO_2	0.73	0.74	0.53	0.64	0.62
Fe_2O_3	2.50	1.37	6.01	2.24	1.36
FeO	2.67	3.61		3.00	3.42
MgO	2.40	2.72	1.90	2.12	1.94
CaO	3.99	2.44	3.64	5.53	4.65
Na_2O	3.72	2.03	4.67	3.98	3.90
K_2O	1.83	2.57	0.47	1.40	1.42
MnO	0.07	0.06	0.09	0.11	0.08
P_2O_5	0.17	0.15	0.12	0.17	0.21

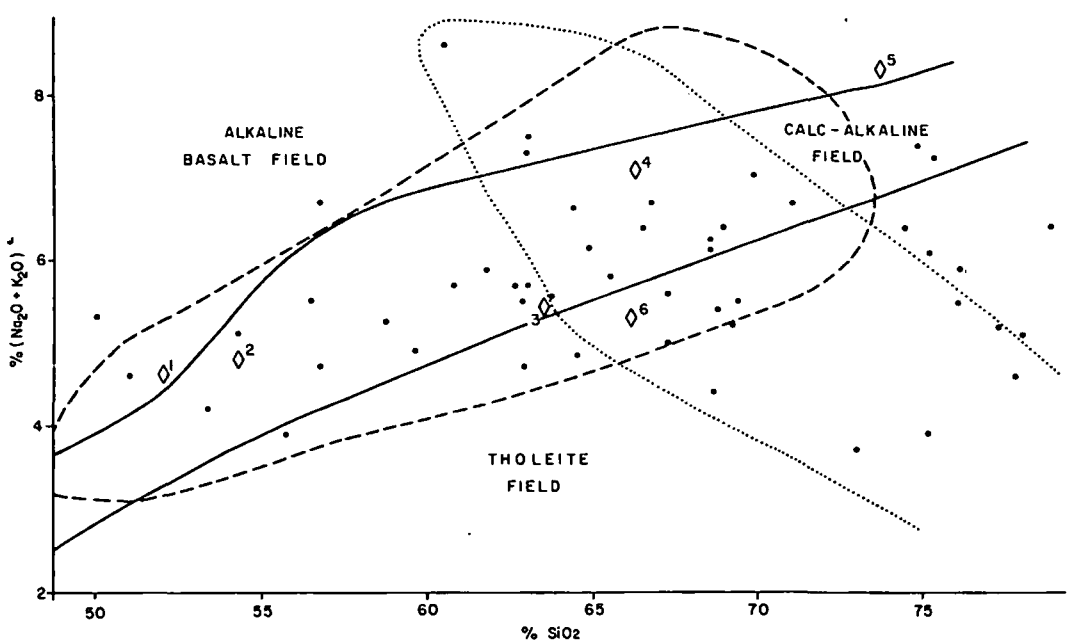

Fig. 10. Percentage ($Na_2O + K_2O$) versus SiO_2 for the meta-igneous rocks (after Kuno 1968). Represented are the fields of the tholeitic series of the Scottish Tertiary Province (dashed line) and geosynclinal deposits from Japan (dotted line). The mean values for the igneous rock types compiled by Nockolds (1954) are given as diamonds: 1 – diorite, 2 – andesite, 3 – dacite, 4 – rhyodacite, 5 – rhyolite, 6 – quartz diorite.

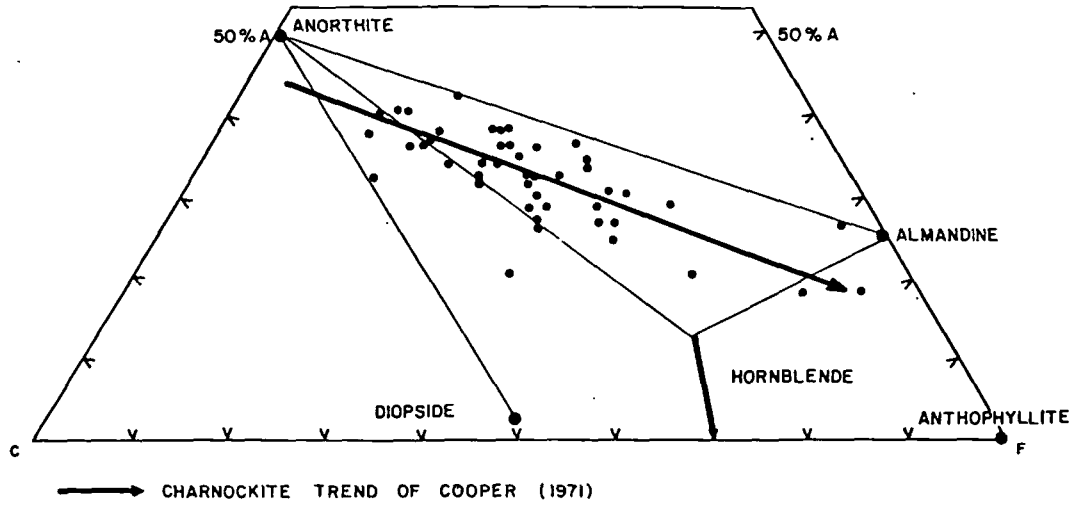

Fig. 11. ACF diagram for the amphibolite facies showing the composition of the meta-igneous rocks (after Winkler 1967).

facies. This is well illustrated by the ACF diagram (Fig. 11), in which the fields of both rocks are identical. Consequently both rock types may well have had the same parentage, and subsequent metamorphic processes have not affected the abundances of Al, Ca, Mg, Fe, and other elements.

Comparisons are drawn by Cooper & Field (1977) between the charnockitic gneisses and Fe-rich rapakivi suites of the Archaean in the northern hemisphere. However, the rapakivi intrusives are Rb-rich with relatively low K/Rb ratios, whereas the charnockitic gneisses and the meta-igneous rocks are predominantly poor in Rb. Consequently this comparison may not be valid.

Relationship to other metamorphic terrains

The evidence given above substantiates a model of isochemical metamorphism for the meta-igneous rocks, and hence the geochemical parameters are original. The majority of elements have similar concentrations to that of estimates of the earth's crust. However, Rb and U, two elements important to the study of high grade metamorphic terrains, are depleted in relation to associated elements. As both metasedimentary and meta-igneous rocks have high K/Rb ratios, it can only be concluded that this is an original characteristic of the Bamble Sector in this area.

Acknowledgements. – This work was carried out with the assistance of an NERC Studentship Award at the Department of Geology, University of Nottingham. The author thanks Professor the Lord Energlyn for allowing the use of departmental facilities and equipment, and Drs. R. B. Elliott and P. K. Harvey for supervision. The author is also indebted to the Director of the South African Geological Survey for the use of facilities in the preparation of the paper, and to Dr. C. Frick for criticising the manuscript.

June 1976
Revised November 1977

Appendix

1. *Optical determinations*

The modal analyses were made by the point counting method covering the whole of the thin section on a 0,3 × 0,6 mm grid. This totalled approximately 1500 counts per section.

Plagioclase compositions were determined using the Michel-Levy technique on random grains, making 6 determinations per thin section.

2. *Analytical methods*

Major and trace elements were determined by X-ray fluorescence spectrometry using a Philips PW 1212 spectrograph. Major-element analysis was carried out on fused glass discs according to the method described by Harvey et al (1973).

Trace-element analysis was carried out on pressed powder pellets and was based on the ratio technique. The calibration and corrections are made according to the method described by Field & Elliott (1974). The USGS standard AGV. 1 was used as a control standard on a daily basis.

References

Andreae, M. O. 1974: Chemical and stable isotope composition of high grade metamorphic rocks from the Arendal area, Southern Norway. *Contrib. Mineral. Petrol. 47*, 299–316.

Beeson, R. 1972: *The Geology of the Country between Songe and Ubergsmoen, Southern Norway*. Unpubl. Ph. D. thesis, Univ. of Nottingham.

Beeson, R. 1975: Metasedimentary gneisses from the Songe-Ubergsmoen area, South Norway. *Nor. Geol. Unders. 321*, 87–102.

Bugge, J. A. W. 1943: Geological and petrological investigations in the Kongsberg-Bamble Formation. *Nor. Geol. Unders. 160 p.*

Collerson, K. D. 1975: Contrasting patterns of K/Rb distribution in Precambrian high-grade metamorphic rocks from Central Australia. *J. Geol. Soc. Aust. 22*, 145–160.

Condie, K. C. 1967: Geochemistry of early Precambrian graywackes from Wyoming. *Geochim. Cosochim. Acta, 31*, 2135–2149.

Cooper, D. C. 1971: *The Geology of the Area around Eydehavn. South Norway*. Unpubl. Ph. D. Thesis, Univ. of Nottingham.

Cooper, D. C. & Field, D. 1977: The chemistry and origins of Proterozoic low-potash, high-iron, charnockitic gneisses from Tromøya, South Norway. *Earth Plan. Sci. Lett. 35*, 105–115.

Elliott, R. B. 1973: The chemistry of gabbro/amphibolite transitions in South Norway. *Contrib. Mineral. Petrol. 38*, 71–79.

Field, D. 1969: *The Geology of the Country around Tvedestrand, South Norway*. Unpub. Ph. D. thesis, Univ. of Nottingham.

Field, D. & Clough, P. W. L. 1976: K/Rb rations and metasomatism in metabasites from a Precambrian amphibolite-granulite transition zone. *J. Geol. 132*, 277–288.

Field, D. & Elliott, R. B. 1974: The chemistry of gabbro/amphibolite transitions in South Norway. *Contrib. Miner. Petrol. 47*, 63–76.

Gruza, V. V. 1965: An investigation of petrochemical characteristics of rocks of similar composition by the method of mathematical statistics. *Geochem. Int. 2*, 88–91.

Harvey, P. K., Taylor, D. M., Hendry, R. D. & Bancroft, F. 1973: An accurate fusion method for the analysis of rocks and chemically related materials by X-ray fluorescence spectrometry. *X-ray Spectrometry 2*, 33–44.

Heier, K. S. & Rojers, J. J. W. 1963: Radiometric determination of thorium, uranium, and potassium in basalts and in two magmatic differentiation series. *Geochem. Cosmochim. Acta, 27*, 137–154.

Heier, K. S. & Thoresen, K. 1971: Geochemistry of high-grade metamorphic rocks, Lofoten–Vesterålen, North Norway. *Geochim. Cosmochim. Acta, 35*, 89–99.

Jakes, P. & White, A. J. R. 1970: K/Rb ratios of rocks from island arcs. *Geochim. Cosmochim. Acta, 34*, 849–856.

Killeen, P. G. & Heier, K. S. 1974: Radioelement variation in the Levang granite-gneiss, Bamble region, South Norway. *Contrib. Mineral. Petrol. 48*, 171–177.

Kuno, H. 1968: Differentiation in basalt magmas. *In* Hess H. H. & Poldervaart A. (Eds.), *Basalts*. Wiley, New York.

Lambert, I. B. & Heier, K. S. 1968: Geochemical investigations of deep-seated rocks in the Australian Shield. *Lithos, 1*, 30–53.

Lewis, J. D. & Spooner, C. M. 1973: K/Rb ratios in Precambrian granulite terranes. *Geochim. Cosmochim. Acta, 37*, 1111–1118.

Nockolds, S. R. 1954: Average chemical composition of some igneous rocks. *Bull. Geol. Soc. Amer. 65*, 1007–1032.

Onions, R. K. & Baadsgaard, H. 1971: A radiometric study of polymetamorphism in the Bamble region, Norway. *Contrib. Mineral. Petrol. 34*, 1–21.

Papezik, V. Z. 1965: Geochemistry of some Canadian anorthosites. *Geochim. Cosmochim. Acta 29*, 673–709.

Shaw, D. M. 1968: A review of K/Rb fractionation trends by covariance analysis. *Geochim. Cosmochim. Acta. 32*, 573–601.

Shaw, D. M., Reilly, G. A., Maysson, J. R., Pattenden, G. E. & Campbell, F. E. 1967: The chemical composition of the Canadian Precambrian shield. *Can. J. Earth. Sci. 4*, 829–853.

Sighinolfi, G. P. 1969: K-Rb rations in high-grade metamorphism: A conformation of the hypothesis of a continual crustal evolution. *Contrib. Mineral. Petrol. 21*, 346–356.

Sighinolfi, G. P. 1971: Investigations into deep crustal levels: fractionating effects and geochemical trends related to high grade metamorphism. *Geochim. Cosmochim. Acta 35*, 1005–1021.

Starmer, I. C. 1969a: The migmatite complex of the Risør area, Aust-Agder, Norway. *Nor. Geol. Tidsskr. 49*, 33–56.

Starmer, I. C. 1969b: Basic plutonic intrusions of the Risør-Søndeled area, South Norway: the original lithologies and their metamorphism. *Nor. Geol. Tidsskr. 49*, 403–431.

Starmer, I. C. 1972: Polyphase metamorphism in the granulite facis terrain of the Risør area, southern Norway. *Nor. Geol. Tidsskr. 53*, 43–71.

Taylor, S. R. 1964: Abundance of chemical elements in the continental crust: A new table. *Geochim. Cosmochim. Acta, 28*, 1273–1285.

Taylor, S. R. 1965: The application of trace element data to problems in petrology. *Phys. Chem. Earth, 6*, 133–123.

Touret, J. 1968: The Precambrian metamorphic rocks around Lake Vegar. *Nor. Geol. Unders. 257*.

Vlassov, K. A. (ed.) 1966: *Geochemistry of Rare Elements*. Vol. 1, Oldbourne Press.

Winkler, A. G. F. 1967: *Petrogenesis of Metamorphic Rocks*. 2nd edition. Springer Verlag, Berlin.

UNIVERSITY OF UTAH
RESEARCH INSTITUTE
EARTH SCIENCE LAB.

Geochimica et Cosmochimica Acta, 1975, Vol. 39, pp. 1515 to 1524. Pergamon Press. Printed in Great Britain

A uranium and thorium enriched province of the Fennoscandian shield in southern Norway*

P. G. KILLEEN† and K. S. HEIER
Mineralogisk-geologisk Museum, University of Oslo, Sars gate 1, Oslo 5, Norway

(*Received* 30 *December* 1974; *accepted in revised form* 18 *April* 1975)

Abstract—The Precambrian Flå, Iddefjord, and Bohus granites lie along a line striking roughly northwest which crosses the Permian Oslo Province to the southwest of Oslo. Radioelement investigations in the three bodies show they all contain abnormally high thorium and uranium concentrations relative to the published literature on average radioelement contents of granitic rocks. Trend surface analysis of the radioelement distribution in the Iddefjord granite suggests there was relative movement of uranium to the east with respect to thorium, possibly as the result of Permian activity in the adjacent rocks. Geological considerations, radiometric evidence and published gravimetric data suggest that the 3 granites represent a continuous belt enriched in thorium and uranium during the Sveconorwegian orogeny. A portion of the belt was later involved in the Permian igneous activity which produced the igneous Oslo Province. There is some evidence that the Permian Drammen and Finnemarka granites represent that part of the belt which was modified in Permian time.

INTRODUCTION

TWO LARGE Precambrian granites, the Flå and Iddefjord, located in southeast Norway were investigated to determine their Th, U, and K concentrations by gamma-ray spectrometry. The Flå granite, situated to the northwest of the Oslo region, is a large elliptical body covering approximately 700 km^2. Geological studies and gravity investigations of the Flå granite have been discussed in detail by SMITHSON (1963). The Iddefjord granite, located to the southeast of the Oslo region, covers an area of about 900 km^2. The geology of the Iddefjord granite has been briefly described in HOLTEDAHL (1960). Gravity interpretations have been made by RAMBERG and SMITHSON (1971). In addition to the 186 samples analyzed from these 2 granites, 5 specimens were analyzed from the northern area of the Bohus granite, a large elongate granite which stretches southward down the Swedish coast, covering an area of 1500 km^2. The Bohus granite is generally conceded to represent the same granite body as the Iddefjord, separated only by a thin band of gneissic country rock near the Norwegian–Swedish border. The geology of the Bohus granite has been described in MAGNUSSON *et al.* (1960), and gravity interpretations have been given by LIND (1967). The geological environment of these 3 granites is shown in Fig. 1. The 3 granites lie on a line which strikes roughly northwest, crossing the Permian rocks of the Oslo region, through the large Drammen granite (area, approximately 600 km^2) and the Finnemarka granite of about 150 km^2. The length of this zone from the northern tip of the Flå granite where it appears from

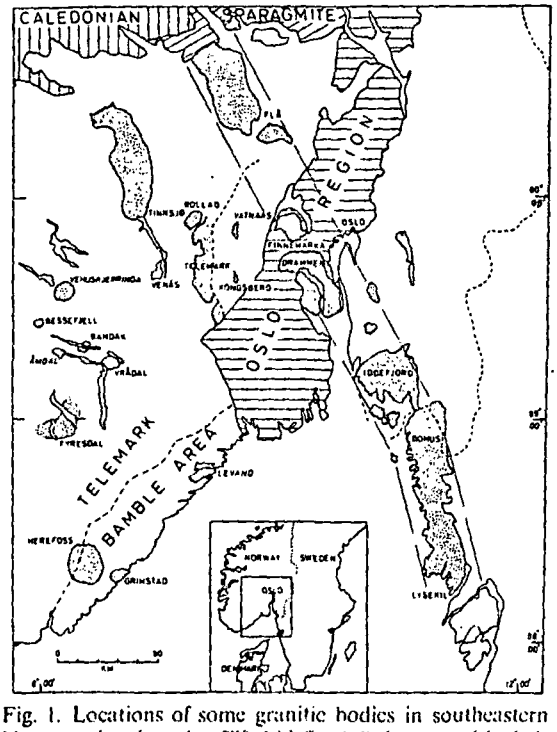

Fig. 1. Locations of some granitic bodies in southeastern Norway showing the Flå–Iddefjord–Bohus granitic belt cutting across the plutonic rocks of the Oslo region.

* Contribution no. 105 in the Norwegian geotraverse project.

† Present address: Geological Survey of Canada, Ottawa, Ontario, Canada.

beneath Paleozoic rocks to the southern border of the Iddefjord granite is 210 km with an additional 90 km being added by the Bohus granite which stretches southwards to the town of Lysekil in Sweden. The possibility of the existence of a semi-continuous belt of cogenetic rocks which includes all 3 of these granites is indicated by the radiometric results and other evidence. There is also some evidence that the two above-mentioned large Permian granites of the Oslo region may represent a complete remelting of a portion of this belt, with consequent dilution of Th and U by material of lower Th and U content arising from the Upper Mantle or lower crust. This belt is enriched in Th and U relative to average granitic rocks and may represent a Th and U province analogous to the Rum Jungle complex in Australia (HEIER and RHODES, 1966).

Analytical technique—gamma-ray spectrometry

The analysis of Th, U and K concentrations was done by gamma-ray spectrometry, a standard technique which has been described by ADAMS and GASPARINI (1970) with respect to analysis of rocks. The laboratory apparatus consisted of a 400 channel gamma-ray spectrometer with a 5 × 5 in. NaI(Tl) detector. Samples averaged over 700 g in weight, and counting times were adjusted to maintain results within the following limits of accuracy: ± 5% for U, ± 3% for Th, and ± 1% for K. More details on the laboratory equipment, its calibration, and the analytical precision have been given by RAADE (1973) and by KILLEEN and HEIER (in press).

The Flå granite

The geology and gravimetric work on the Flå granite by SMITHSON (1963) is briefly summarized here. The granite is composed of a large northern body referred to as the Hedal granite, and a smaller adjacent body called the Adal granite. The granite is primarily porphyric with a fine-grained centre in the Hedal granite. The composition of the granite falls within the range of quartz monzonites. The granite is generally concordant with gradational contacts with the gneissic country rocks. Gravity data indicates it is a thin plate with a thickness of from 1·7 to a maximum of 2·5 km with a possible extension plunging southeast under the gneisses. A combined anatectic origin, modified by metasomatism, appears to be indicated. The neighbouring gneisses and the mineral assemblages in the granite are middle amphibolite facies.

Rb/Sr *whole rock age determinations*

Reconnaissance Rb/Sr whole rock isochron ages obtained on the Flå and Iddefjord granites showed them to be of identical age and initial $^{87}Sr/^{86}Sr$ ratios. The analytical data are given in Table 1. The ages ($\lambda = 1{\cdot}39 \times 10^{-11}yr^{-1}$) and initial ratios obtained were 913 ± 28 m.y.(2σ), Ri = 0·7093 for the Flå granite and 900 ± 35(2σ), Ri = 0·7098 for the Iddefjord granite.

Th, U *and* K *distribution in the Flå granite*

The arithmetic means and standard deviations for the results of the analysis of 52 samples of the Flå granite are presented in Table 2. Histograms showing the range in concentration and element ratios are illustrated in Fig. 2. The results, map coordinates and other statistics for individual samples which contribute to mean values discussed in this paper can be obtained from tables listed in KILLEEN and HEIER (in press). Unusually high thorium concentrations are found in the Flå granite. For comparison, Table 3 lists some granitic and upper crustal average radioelement contents. The mean Th content is more than

Table 1. Rb/Sr data for the Flå and Iddefjord granites

Sample no. Flå granite	Rb/Sr	$^{87}Sr/^{86}Sr$
F33	1·06	0·74922
F16	1·34	0·75903
F15	1·63	0·76954
F12	1·34	0·75797
F1	1·57	0·76894
Age = 913 ± 28 m.y.		
Ri = 0·70933		
Iddefjord		
117	1·80	0·77408
137	3·05	0·82511
139	4·49	0·87606
1106	3·35	0·83167
1132	1·51	0·76618
Age = 900 ± 35 m.y.		
Ri = 0·7098		

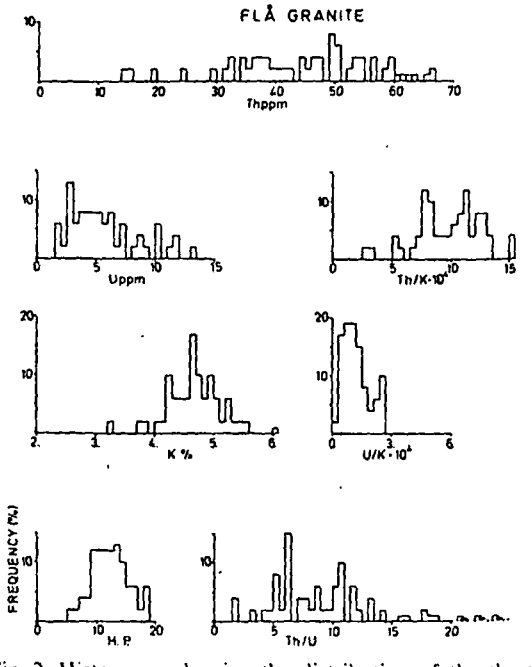

Fig. 2. Histograms showing the distribution of the three radioelements, their ratios, and heat production for 52 samples from the Flå granite.

double the mean Th gi
(1963) and by CLARK *et al*
The mean U content is
the granite averages give
histograms of Fig. 2 illus
the mean, but that the
The mean K concentrat
the range of alkali gran
The surprisingly high m
the wide spread shown in
possibility that oxidatio
migration of U at some
to the increase in K by
SMITHSON (1963). Some
because when U is plotte
line through the points ha
a slight decrease in U a
Th/U ratio against K sh
the Th against K plot h
tion. The mean Th/K ra
HEIER and ROGERS (196
mean U/K ratio, howeve
granite given by these au
ation of both U and K e
granites, yet maintaining
a super-enrichment of T
abnormally high Th/U a
not appear to be any pa
radiometric results and t
center of the Hedal grani
High and low values
throughout the Flå gra
produced the existing v
and their ratios for the
the Iddefjord and Bohus
these are discussed belo

The Iddefjord granite

To the authors' knowled
detailed geological investig
Iddefjord granite. SMITHSO
granite resembles the Id
appearance, shape, and c
fjord granite was mentione
(1963) as being medium-g
SiO_2. They pointed out tha

Table 2. Arithmetic means

Granite	Th (ppm)
Flå	45·7
Iddefjord	50·2
Bohus	63·5

double the mean Th given by HEIER and ROGERS (1963) and by CLARK *et al.* (1966) for average granites. The mean U content is more than 20% greater than the granite averages given by the above authors. The histograms of Fig. 2 illustrate the wide spread about the mean, but that the mean is close to the median. The mean K concentration puts the Flå granite in the range of alkali granites of CLARK *et al.* (1966). The surprisingly high mean Th/U ratio coupled with the wide spread shown in the histogram indicates the possibility that oxidation of U has occurred with migration of U at some time. This may be related to the increase in K by metasomatism invoked by SMITHSON (1963). Some evidence for this exists because when U is plotted against K, the least squares line through the points has a negative slope indicating a slight decrease in U as K increases. A plot of the Th/U ratio against K shows a positive relation since the Th against K plot has the normal positive relation. The mean Th/K ratio is double that given by HEIER and ROGERS (1963) for average granites. The mean U/K ratio, however, is the same as for average granite given by these authors. Thus we have the situation of both U and K enrichment relative to average granites, yet maintaining the average U/K ratio, while a super-enrichment of Th has taken place producing abnormally high Th/U and Th/K ratios. There does not appear to be any particular correlation between radiometric results and the fine-grained granite at the center of the Hedal granite, or with the Adal granite. High and low values are randomly distributed throughout the Flå granite. Some clues as to what produced the existing values for the radioelements and their ratios for the Flå granite are found when the Iddefjord and Bohus granites are investigated, and these are discussed below.

The Iddefjord granite

To the authors' knowledge, at present there is no single detailed geological investigation published concerning the Iddefjord granite. SMITHSON (1963, p. 177) stated "The Flå granite resembles the Iddefjord granite in megascopic appearance, shape, and contact phenomena". The Iddefjord granite was mentioned briefly by BARTH and REITAN (1963) as being medium-grained and containing 71–75% SiO_2. They pointed out that it is considered as equivalent to the Bohus granite in Sweden which has been discussed in greater detail. Gravity interpretation by RAMBERG and SMITHSON (1971) indicated it is a "floored platelike body emplaced in a dome". They showed it can be "represented by a slab 3–5 km. thick that thickens to the east and plunges under the gneisses there". It is also suggested that the granite plunges under the gneisses to the north and reappears in small domes. Formation by anatexis is indicated.

Th, U *and* K *distribution in the Iddefjord granite*

The Iddefjord granite contains Th and U concentrations (Table 2) which are more than double the average granite values (Table 3). The histograms of the radioelements and their ratios (Fig. 3) indicates the wide spread in values but with the mean close to the mode, similar to the Flå granite. The mean K content is in the range of alkali granites given by CLARK *et al.* (1966), and only slightly lower than the mean K content of the Flå granite.

The most significant difference between the Flå and Iddefjord granites is the relatively higher mean U content of the Iddefjord granite. The mean Th/U ratio is then slightly less than the Flå granite, and the U/K ratio is slightly higher. The Th/K ratio is still very high similar to the Flå granite.

Thus it appears that both the Flå and Iddefjord granites are exceptionally high in Th, yet the Flå granite has only a 20% U enrichment rather than the 100% U enrichment over average granites shown by the Iddefjord granite. Why does the Iddefjord granite contain a greater amount of uranium? Some evidence as to the behaviour of Th and U within the large Iddefjord granite can be seen in the following trend surface analyses.

Trend surface analysis—Iddefjord granite

Before presenting the results of trend surface analysis, a brief discussion of the technique and method of selection of best trend surface will be given.

Trend surface analysis is simply a mathematical technique for determining trends in a set of spatially distributed data. For example, in one application here a number of thorium concentrations have been determined for samples with known coordinates x and y. A polynomial equation can be fitted by a least

Table 2. Arithmetic means of radiometric results for 52 samples of Flå granite, 134 samples of Iddefjord granite and 5 samples of Bohus granite

Granite	Th (ppm)	U (ppm)	K (%)	Th/U	Th/K $\times 10^4$	U/K $\times 10^4$	Heat production (cal/cm^3 sec $\times 10^{-13}$)
Flå	45·7	5·7	4·70	10·2	9·8	1·2	12·4
Iddefjord	50·2	9·9	4·52	6·9	11·2	2·2	15·7
Bohus	63·5	5·5	5·14	12·7	12·1	1·1	15·4

Table 3. Average Th, U and K contents of continental crust and granitic rocks

	Th ppm	U ppm	K%	H.P.*	
Continental	11·4	3·0	—	—	ADAMS *et al.* (1959)
Crust (surface)	10·0	2·8	2·6	4·04	HEIER and ROGERS (1963)
	9·6	2·7	2·09	3·78	TAYLOR (1964)
Canadian	10·3	2·45	2·58	3·86	SHAW (1967)
Shield	13·0	2·1	2·68	4·13	EADE and FAHRIG (1971)
Archaean shield crust	4·5	0·7	1·5		LAMBERT and HEIER (1968)
Paleozoic crust	7	1·3	1·7		LAMBERT and HEIER (1968)
Granitic	—	4·75	3·79	6·76	HEIER and ROGERS (1963)
Rocks	17·36	—	3·47	6·69	HEIER and ROGERS (1963)
Granodiorite	9·3	2·6	2·55	3·78	CLARK *et al.* (1966)
Silicic	20·0	4·7	4·26	7·29	CLARK *et al.* (1966)
Igneous Rocks				(alkali granite)	
Granitic	Th/K × 10^4 ratio = 4:9				HEIER and ROGERS (1963)
Rocks	U/K × 10^4 ratio = 1:2				HEIER and ROGERS (1963)
Canadian Shield	U/K × 10^4 ratio = 0:95				SHAW (1967)

* H.P. (Heat production) in units of 10^{-13} cal/cm^3/sec (assuming specific gravity = 2·67 g/cm^3). All values computed from given Th, U. K values using: H.P. = 0·62 U ppm + 0·17 Th ppm + 0·23 K%.

squares technique to all of the available data and its coefficients determined. Then this polynomial is the equation of a surface through the data, and it can be used to compute thorium concentrations between and around the measured data points. Thus a contour map can be constructed which hopefully illustrates the trend shown by the data. This trend surface may or may not be a faithful representation of the true trends in the thorium concentration, depending on the complexity of the trend, and the degree of the polynomial used for the trend surface. The trend surface is called a linear, quadratic, cubic, etc., surface depending on whether it has linear terms, quadratic terms, cubic terms, etc., in the equation. As higher degree terms are added to the polynomial, the closer the trend surface will fit the data since the surface is able to twist and turn to meet the measured data points. The linear trend surface is simply a plane fitted through the data. This does not mean that the highest degree trend surface is the best, unfortunately, since in fact the closer it fits the data, the more it hides the trends. On the other hand, the linear surface may not be the best to use since the trend surface could be convex (or concave) with a central maximum (or minimum), or some other more complex shape. Determining which surface is the best is partially a subjective decision, made by comparing the data to the trend surface contours. In an effort to help make the decision more objective, the coefficient of determination (hereafter referred to as c.d.) was developed. Its meaning and usage has been described by ALLEN and KRUMBEIN (1962). The c.d. is simply the fraction of the total variation in the data which can be explained by the variation in the trend surface. When the c.d. equals 1·0 it is a perfect fit and, as mentioned above, there is no trend left. HOWARTH (1967) attempted to determine what would be considered a 'good' value for the c.d. by computing trend surfaces for random data. Since it was random data theoretically it contained no 'trend' and therefore the c.d. for each surface should be the lowest possible value. His work suggested that if the c.d. were below 0·06, 0·12, and 0·162 for linear, quadratic, and cubic surfaces, respectively, the data distribution could be considered close to not being significantly different from random. But these values still cannot be considered as proof that there is no trend. He also pointed out that the mean value of the dependent variable in the data will affect the value of the c.d. As SINCLAIR (1967) has indicated, where there is a tendency for data to have a large standard deviation, there will be a tendency "for calculated trend surfaces to have a wide scatter of true values and a poor statistical fit even where a definite trend exists". Thus the subjective approach may have to be used. One indication that a trend surface is statistically significant is given when several related variables show similar trends, even though the c.d. is low. It is unlikely that similar trends could be generated from completely random distributions.

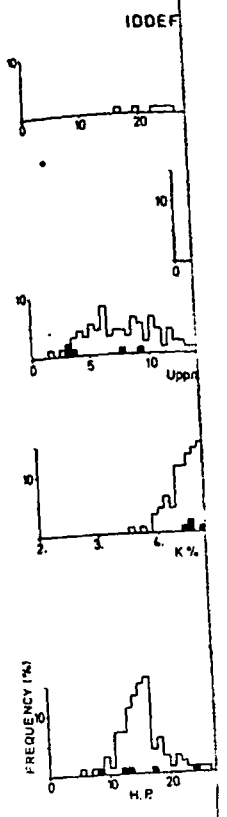

Fig. 3. Histograms sh
radioelements, their r
samples from the Idd
from the northern

All trend surface a
carried out using a
program by O'LEARY
tion was a logarithi
Linear to sixth deg
all variables, and by
above, the fourth de
representing the tren
spread in radioeleme
fjord granite (large
easily seen in the his
c.d. for the trend su
and the similarity be
cate the trends are d
bution of the 134 s
basis of the trend s
4. The fourth degr
potassium is given
spread in K values
However, there is a
centrations (4·2–4·4

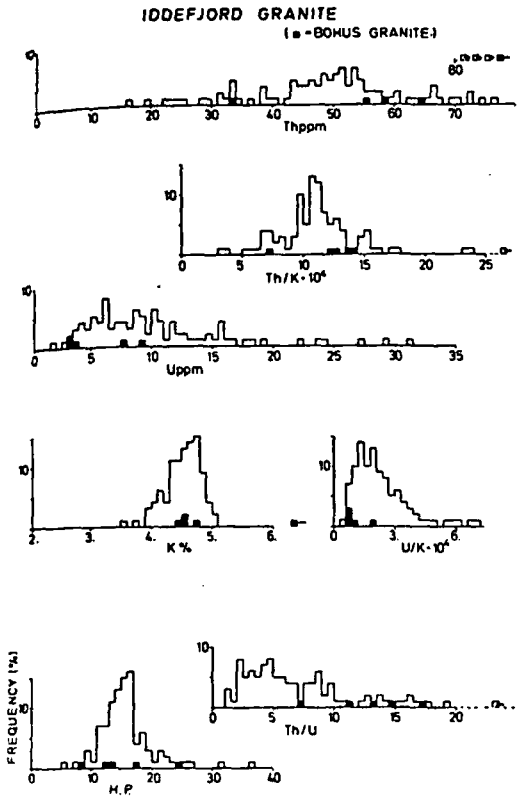

Fig. 3. Histograms showing the distribution of the three radioelements, their ratios, and heat production for 134 samples from the Iddefjord granite (white) and 5 samples from the northern part of the Bohus granite (black).

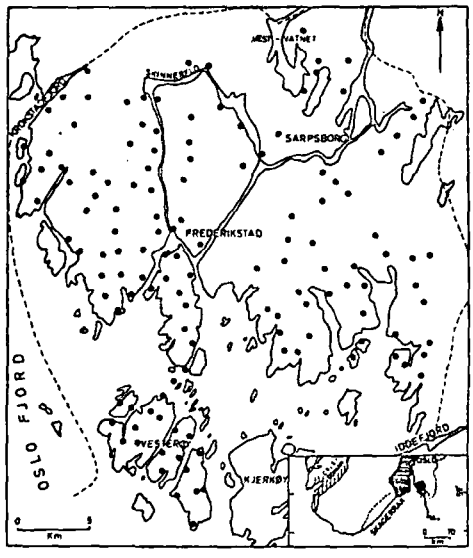

Fig. 4. Sample localities within the Iddefjord granite used as a basis for the trend surface analysis of the radioelement distribution.

All trend surface analyses in this investigation were carried out using a modified version of a computer program by O'LEARY *et al.* (1966). The main modification was a logarithmic transformation of the data. Linear to sixth degree surfaces were computed for all variables, and based upon the factors discussed above, the fourth degree surface was chosen as best representing the trends in the distribution. The wide spread in radioelement values measured in the Iddefjord granite (large standard deviation) which are easily seen in the histograms of Fig. 3 produce a low c.d. for the trend surfaces. Geological considerations and the similarity between related trend surfaces indicate the trends are definite and significant. The distribution of the 134 sample locations which were the basis of the trend surface analysis are given in Fig. 4. The fourth degree trend surface (c.d. = 0·17) for potassium is given in Fig. 5. The relatively uniform spread in K values about the mean of 4·5% is evident. However, there is a slight tendency for the lower concentrations (4·2–4·4% K) to be located on the east side of the body, and values greater than 4·6% to be located on the southwest or northwest sides of the body. The trend surface (c.d. = 0·12) of uranium distribution in Fig. 6 shows a strong increasing trend from west to east, with a tendency for some high U values in the northwest corner of the body. Thus the slightly negative relation between U and K found for the Flå granite is also indicated here. The lower K contents of the east side of the body are associated

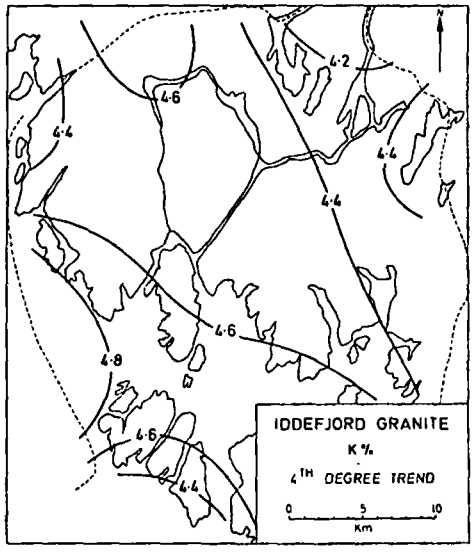

Fig. 5. Fourth degree trend surface of K(%) for the Iddefjord granite.

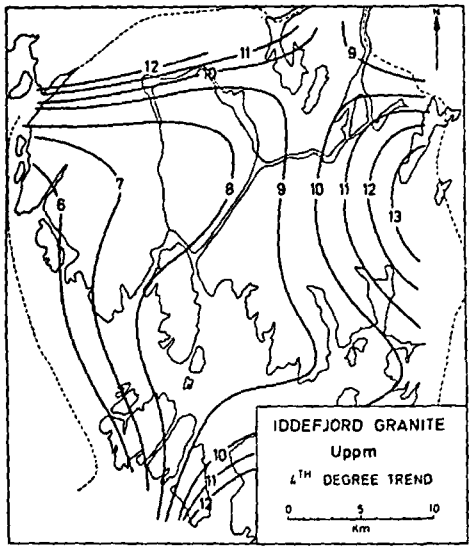

Fig. 6. Fourth degree trend surface of U (ppm) for the Iddefjord granite.

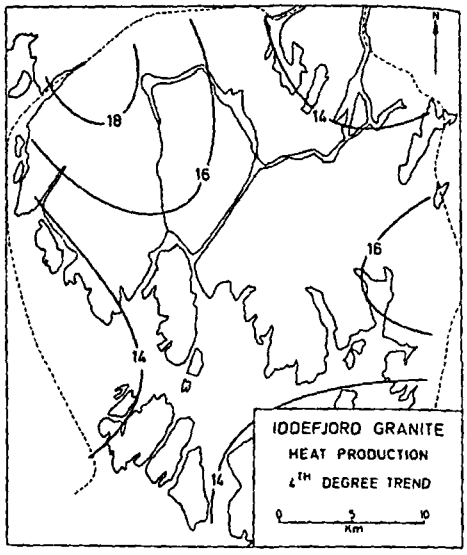

Fig. 8. Fourth degree trend surface of heat production (cal/cm^3/sec × 10^{-13}) for the Iddefjord granite.

with the higher U contents and vice versa for the west, although it is not a strong relation.

The thorium trend surface (c.d. = 0·29) in Fig. 7 shows the rather interesting result of high values in the west and lowest values to the east, exactly the opposite trend shown by uranium. This obviously points to relative movement of uranium and thorium.

The trend surface for Th/U ratios (not shown) is almost identical in shape to the uranium trend surface, with Th/U ratios of greater than 7 in the west grading to less than 4 in the east.

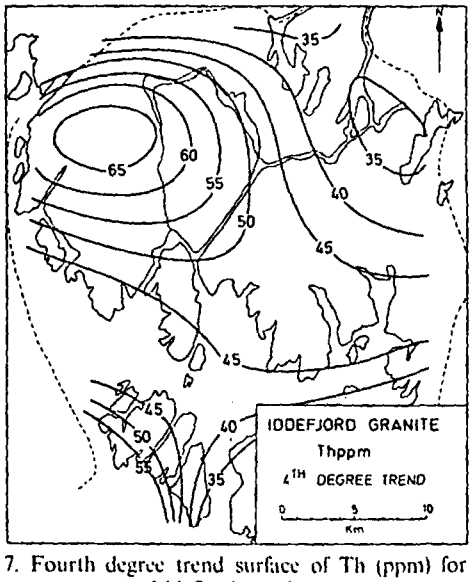

Fig. 7. Fourth degree trend surface of Th (ppm) for the Iddefjord granite.

The trend surfaces for the Th/K × 10^4 ratio were also computed and they resemble the Th trend surface with values ranging from a western high of 13 and greater to an eastern low of 9 or less.

The U/K × 10^4 trend surface resembles the U trend surface and ranges from 1·6 and less on the west to 2·6 or greater on the east.

The trend surface for heat production (c.d. = 0·08) which is a combination of the effect of all 3 radioelements, is given in Fig. 8. The greater part of the body lies between 14 and 16 h.p.u. (1 h.p.u. = 10^{-13}cal/cm^3/sec) with a tendency to increase to 18 h.p.u. to the northwest. Thus the west side of the Iddefjord granite resembles the Flå granite to a greater extent than the east side. The west side of the Iddefjord granite has similar Th, U, and K contents and Th/U, Th/K, and U/K ratios to the Flå granite. It appears that either the west side of the Iddefjord granite and the Flå granite were depleted in U, or that the east side of the Iddefjord granite was enriched in U by some process. It is interesting to note here that the Flå granite is relatively thin, and that the Iddefjord granite is thinnest in the west, and thickens to the east as it plunges under the gneisses (RAMBERG and SMITHSON, 1971). Before coming to any final conclusions the results for the Bohus granite will be discussed.

The Bohus granite

The geology of the Bohus granite has been described by ASKLUND (1947), and a summary by GEIJER (1963) indicates it is a flat lacolith. MAGNUSSON (1960) reported K–Ar ages of 920 m.y. and 1010 m.y. for 2 samples of Bohus

...rate north of Lyseki1. Gravity measurements by LIND ... indicate a similar thickness and plate-like shape ...ging under the gneisses that is indicated by RAMBERG ... SMITHSON (1971) for the Iddefjord granite. He also ...ulates a feeder stalk beneath the body.

U and K results for the Bohus granite

The mean radioelement concentrations and their ...ios for the Bohus granite are given in Table 2. The extremely high mean Th is remarkable, being ...ver 3 times the average granite values of Table 3. The mean U is about equal to the mean U measured ...or the Flå granite. The mean K content is slightly higher than for either the Flå or Iddefjord granites but closest to the K content of the Flå granite. The mean Th/U ratio is very high, again similar to the Flå granite. The mean Th/K ratio is also only slightly higher than for either the Flå or Iddefjord granites. The mean U/K ratio is similar to the Flå granite value and the values found on the west side of the Iddefjord granite. It must be remembered that these are the means of only 5 samples, and it is only meant to be a quick check on the radioelement contents of the Bohus granite to confirm the present belief that the Bohus and Iddefjord granites are one body. The standard error of the mean is fairly high but our purpose was accomplished.

DISCUSSION

The overall picture of the radioelement contents of the 3 granites is the following:

(1) all 3 granites are enriched in thorium relative to granitic averages by at least a factor of two. The thorium concentration increases southward from the Flå, to Iddefjord to Bohus granite.

(2) All 3 granites are enriched in uranium relative to granitic averages, but only the Iddefjord granite is enriched by as much as a factor of two.

(3) A close study by trend surface analysis of the distribution of uranium in the Iddefjord granite shows that the enrichment is on the east side of the body, and the west side resembles the Flå and Bohus granites in uranium contents.

(4) All 3 granites are high in potassium (alkali granites), with the concentrations being slightly higher in the Flå and Bohus granites than in the Iddefjord granite. If the slight enrichment in potassium on the west side of the Iddefjord (relative to east side) granite is considered, the pattern is increasing potassium from 4·7% in the Flå granite to 5·1% in the Bohus granite.

Thus the picture is one of a belt of granitic rocks about 300 km long with similarly high thorium and potassium contents increasing from northwest to southeast. Uranium, however, is approximately constant from the Flå granite to the west side of the Iddefjord granite to the Bohus granite. The displaced high U content (which produces the mean of twice granitic averages for Iddefjord) must be related to some event which could cause oxidation and relative movement of U with respect to the Th high. The fact that the west side which is depleted in U is in contact with the Permian igneous rocks of the Oslo region, and is also the thinnest side seems to indicate that Permian volcanism may have heated the Iddefjord granite on the west side causing oxidation and migration of U. The Bohus granite lies fairly close to the southern extension of the Oslo region into the Skagerrak. The Flå granite lies at about the same distance as the Bohus granite from the Permian Oslo region. It is possible that sufficient heating occurred to cause U migration. This can be done without resetting of the Rb–Sr radiometric clocks as in the case of the Levang granite gneiss dome in south Norway (KILLEEN and HEIER, 1975).

Thus it is proposed that the entire belt had its U content modified by the Permian Oslo event, but otherwise the belt is unchanged. The migration of U is incomplete in the Iddefjord granite possible due to its greater thickness towards the east and perhaps its greater width, than the other two granites.

The other alternative is that the belt, though obviously enriched in Th is only enriched in U to about 20% above granite averages, and the Iddefjord granite is a specially enriched part of the belt. Yet why this enrichment is on the east side of the Iddefjord granite nearest the gneisses is unknown. This, and other radioelement investigations by the authors appears to indicate that a $U/K \times 10^4$ ratio of about 1·2 is a stable ratio and any increase in U which increases this ratio represents U which is easily lost and contained in a substantially different mode in the rock than the stable U. It is likely that there are a limited number of vacancies for U, and these are filled when $U/K \times 10^4 = 1{\cdot}2$, and any additional U is held very loosely. This could explain the observed concentrations in the 3 granites, the observed distribution in the Iddefjord granite, and in addition the ease with which the Permian Oslo region's igneous activity could have induced migration of the excess U in all 3 granites.

Previously reported K/Ar dates ranged as low as 776 m.y. for the Iddefjord granite (BROCH, 1964). When this is compared with the data in Table 1, and the K/Ar data on the Bohus granite reported above it could indicate loss of argon which possibly occurred as a result of heating by adjacent Permian

igneous activity, as is suggested here for the uranium movement.

The Flå, Iddefjord and Bohus granites as a Th–U *province*

The similar geology, ages, initial Sr^{87}/Sr^{86} ratios, and gravitationally determined shape, indicate the granites belong to one continuous or semi-continuous belt of rocks 300 km long, and about 25 km wide (area approximately 7500 km^2 = 3000 square miles) originating in a structurally favorable zone. The similarly high radioelement concentrations which differ considerably from most other Norwegian granites (KILLEEN and HEIER, in press) also tend to confirm the fact that they have a related genesis.

The mean Th contents of this belt are similar to the concentrations reported by HEIER and RHODES (1966) for the granites of the Rum Jungle Complex of Australia. The Rum Jungle granites have mean Th and U contents of 45·7 and 10·3 ppm, respectively. They designated the Rum Jungle Complex and surrounding area a thorium–uranium province because of this enrichment above crustal averages. TREMBLAY (1972) reported average uranium contents of 5·4 ppm in granites in the Beaverlodge area of Saskatchewan, Canada, and EADE and FAHRIG (1971) reported mean Th and U contents of 35·7 and 8·1 ppm, respectively, for the Bear Province of Canada represented by 92 granite samples collected in the Hardisty Lake area (approximately 3750 km^2). Both of these areas are uranium mining areas (LANG *et al.*, 1962) and as such can be considered U and Th provinces analogous to the Rum Jungle Complex. PHAIR and GOTTFRIED (1964) described the Colorado Front Range (area approximately 18,000 km^2) as a uranium and thorium province with mean U and Th contents of 4·6 and 22·7 ppm, respectively. In the Canadian Shield three radioactive belts outlined by airborne gamma-ray spectrometry contain mean U and Th contents of 6 and 33·4 ppm, respectively (DARNLEY *et al.*, 1971, 1972; RICHARDSON *et al.*, in press). The belts are approximately 240–280 km long and 70–80 km wide. The Th and U concentrations represent more than twice the average for the Canadian Shield given in Table 3 (SHAW, 1967; EADE and FAHRIG, 1971).

The Flå–Iddefjord–Bohus granitic belt is of comparable dimensions to these areas with mean radioelement concentrations which equal or exceed the above concentrations, and as such could be considered a uranium and thorium province.

ROSCOE (1966) has indicated that most of the world's low cost uranium is derived from non-marine sedimentary rocks. Areas favorable for uranium exploration would be sedimentary geologic settings in the vicinity of crystalline provenance rocks which are enriched in the radioelements. The Th–U provinces could provide such enriched source rocks for sedimentary-type uranium deposits.

The Drammen granite and Finnemarka granite as a Permian portion of the Th–U *province*

The radioelement concentrations of the Permian rocks of the Oslo province have been studied in detail by RAADE (1973) and the mean values for 109 samples of the Drammen granite, and 22 samples of the Finnemarka granite shown in Fig. 1 are reproduced in Table 4.

Also included in Table 4 are the mean values for the entire Oslo region compiled by RAADE (1973). He was able to subdivide the plutonic rocks of the Oslo province into two main groups on the basis of their Th/U ratios. His group 1 has relatively constant Th/U ratios with low mean values (Th/U = 3·5–4·5) while Group 2 has high mean values (Th/U = 4·5–6·5) which are very variable (i.e. have high standard deviations). He suggests "this clear division of the plutonic rocks undoubtedly reflects a profound difference in origin and/or differentiation history of the 2 main groups". Group 2 comprises the Nordmarkite, Ekerite and biotite granites.

RAADE (1973) accounts for the group with variable ratios by postulating a process of contamination from overlying Precambrian rocks. He also suggests that selective loss of U by oxidation due to higher oxygen fugacity in the upper crust could explain the highly variable Th/U ratios.

The Precambrian rocks which were part of the postulated contamination could very likely include that portion of the Flå–Iddefjord belt which is missing

Table 4. Arithmetic means of radiometric results for two Permian granites and means for the entire igneous Oslo Province (taken from RAADE, 1973)

Granite	Th (ppm)	U (ppm)	K (%)	Th/U	Th/K $\times 10^4$	U/K $\times 10^4$	Heat production (cal/cm^3 sec $\times 10^{-13}$)
Drammen	27·1	4·7	4·26	6·19	6·43	1·10	8·48
Finnemarka	21·1	4·6	3·86	5·13	5·48	1·20	7·36
Oslo Province	19·1	4·3	4·0	—	—	—	6·88

now where it is cut by t
nian Oslo region.

It is interesting to not
of granitic rocks is par
southwest of a belt of gra
sions. This other belt str
Sweden) in the southeast
way in the northwest wh
Paleozoic rocks, as does

The granitic rocks of
dated by PRIEM *et al.* (19
(in press). It appears to b
my. The radioelement c
LEEN and HEIER (in press
have mean Th and U co
average granites.

It is too early to spe
between the two belts suf
cient information reg
centrations in the easte
region between them.

Acknowledgements—We w
RAADE for his assistance wit
fruitful discussions, and all
published data for the radi
of the Permian plutonic
Rb/Sr age determinations'
Recherches Petrographiqu
(CRPG), and we wish to th
for inviting us to use their
much assistance in the labo
One of us, (P.G.K.), wish
lesen Foundation for a pos
stay in Norway.
The field work and most
covered by grant no. D.
Research Council for Scien

REFE

ADAMS J. A. S., OSMOND J.
The geochemistry of tho
and Chemistry of the Ear
mon Press.
ADAMS J. A. S. and GASPA
trometry of Rocks. 295 p
ALLEN P. and KRUMBEIN
components in the top
history. *J. Geol.* 70, 507
ASKLUND B. (1947) Sven
Sver. Geol. Undersoka,
BARTH T. F. W. and RETTA
of Norway. In *The Ge*
cambrian. (editor K. Ra
BROCH O. A. (1964) Ag
minerals up to March
228, 84–113.

...ow where it is cut by the igneous rocks of the Per-...an Oslo region.

It is interesting to note that the Flå–Iddefjord belt ...f granitic rocks is parallel to and about 150 km ...outhwest of a belt of granitic rocks of similar dimen...sions. This other belt stretches from Lake Vanern (in ...weden) in the southeast to the Trysil district in Nor...way in the northwest where it disappears beneath the Paleozoic rocks, as does the Flå–Iddefjord belt.

The granitic rocks of the Trysil area have been dated by PRIEM *et al.* (1970) and KILLEEN and HEIER (in press). It appears to be in the range of 1500–1600 m.y. The radioelement contents determined by KILLEEN and HEIER (in press) shows the Trysil granite to have mean Th and U concentrations lower than for average granites.

It is too early to speculate on any relationship between the two belts since there is at present insufficient information regarding radioelement concentrations in the easternmost belt, and the gneiss region between them.

Acknowledgements—We wish to thank cand. real. G. RAADE for his assistance with the analytical work, for many fruitful discussions, and allowing us to use his so far unpublished data for the radioactive element concentrations of the Permian plutonic rocks of the Oslo region. The Rb/Sr age determinations were done at the Centre de Recherches Petrographiques et Geochimiques, Nancy (CRPG), and we wish to thank Professor H. DE LA ROCHE for inviting us to use their facilities, and Mr. SONNET for much assistance in the laboratory.

One of us, (P.G.K.), wishes to thank the G. Unger Vetlesen Foundation for a post-doctoral fellowship during his stay in Norway.

The field work and most of the laboratory expenses were covered by grant no. D.48.91–2 from the Norwegian Research Council for Science and the Humanities.

REFERENCES

ADAMS J. A. S., OSMOND J. K. and ROGERS J. J. W. (1959) The geochemistry of thorium and uranium. In *Physics and Chemistry of the Earth*, Vol. 3, pp. 298–348. Pergamon Press.

ADAMS J. A. S. and GASPARINI P. (1970) *Gamma-ray Spectrometry of Rocks*, 295 pp. Elsevier.

ALLEN P. and KRUMBEIN W. C. (1962) Secondary trend components in the top Ashdown Pebble Bed: a case history. *J. Geol.* 70, 507–538.

ASKLUND B. (1947) Svenska Stenindustriområden I–II. *Sver. Geol. Undersökn. Ser.* C, No. 479. (in Swedish).

BARTH T. F. W. and REITAN P. H. (1963) The Precambrian of Norway. In *The Geologic Systems*, Vol. 1, *The Precambrian*, (editor K. Rankama). Interscience.

BROCH O. A. (1964) Age determination of Norwegian minerals up to March 1964. *Norg. Geol. Undersokelse* 228, 84–113.

CLARK S. P., JR., PETERMAN Z. E. and HEIER K. S. (1966) Abundances of uranium, thorium and potassium. *Geol. Soc. Amer. Mem.* 97.

DARNLEY A. G., GRASTY R. L. and CHARBONNEAU B. W. (1971) A radiometric profile across part of the Canadian Shiels. *Geol. Surv. Can. Paper* 70–46, 42 pp.

DARNLEY A. G., GRASTY R. L. and RICHARDSON K. A. (1972) Regional variation in radioelement content within the Canadian Shield (abstract). *24th Int. Geol. Congr. Montreal*, Section 9, Exploration Geophysics, p. 14.

EADE K. E. and FAHRIG W. F. (1971) Geochemical evolutionary trends of continental plates—a preliminary study of the Canadian Shield. *Geol. Surv. Can. Bull.* 179, 51 pp.

GEIJER P. (1963) The Precambrian of Sweden. In *The Geologic Systems*, Vol. 1, *The Precambrian*, (editor K. Rankama). Interscience.

HEIER K. S. and RHODES J. M. (1966) Thorium, uranium and potassium concentrations in granites and gneisses of the Rum Jungle Complex, Northern Territory, Australia. *Econ. Geol.* 61, 563–571.

HEIER K. S. and ROGERS J. J. W. (1963) Radiometric determinations of thorium, uranium and potassium in basalts and in two magmatic differentiation series. *Geochim. Cosmochim. Acta* 27, 137–154.

HOLTEDAHL O., Editor (1960) Geology of Norway. *Norges Geol. Undersokelse* 208, 540 pp.

HOWARTH R. J. (1967) Trend surface fitting to random data—an experimental test. *Amer. J. Sci.* 265, 619–625.

KILLEEN P. G. and HEIER (in press) Radioelement distribution and heat production in Precambrian granitic rocks, southern Norway. *Skr. Norske Videnskaps-Akad. Oslo, Mat. Naturv. Kl.*

KILLEEN P. G. and HEIER K. S. (1975) Radioelement variation in the Levang granite-gneiss, Bamble region, south Norway. *Contrib. Mineral. Petrol.* 48, 171–177.

LAMBERT I. B. and HEIER K. S. (1968) Estimates of the crustal abundances of thorium, uranium and potassium. *Chem. Geol.* 3, 233–238.

LANG A. H., GRIFFIN J. W. and STEACY H. R. (1962) Canadian deposits of uranium and thorium. *Geol. Surv. Can. Econ. Geol.* series No. 16, (second edition), 324 pp.

LIND G. (1967) Gravity measurements over the Bohus granite in Sweden. *Geol. Foren. Stockholm Forh.* 88, 542–548.

MAGNUSSON N. H. (1960) Age determinations of Swedish Precambrian rocks. *Geol. Foren. Stockholm Forh.* 82, 407–432.

MAGNUSSON N. H. THORSLUND P., BROTZEN F., ASKLUND B. and KULLING O. (1960) Description to accompany the map of prequaternary rocks of Sweden. *Sveriges Geol. Undersökn. Ser.* Ba, No. 16, 177 pp.

O'LEARY M., LIPPERT R. H. and SPITZ O. T. (1966) Fortran IV program for computation and plotting of trend surfaces for degrees 1 through 6, 48 pp. Kansas Geol. Survey.

PHAIR G. and GOTTFRIED D. (1964) The Colorado Front Range, Colorado, U.S.A. as a uranium and thorium province. In *The Natural Radiation Environment*, (editors J. A. S. Adams and W. M. Lowder), pp. 7–38. University of Chicago Press.

PRIEM H. N. A., VERSCHURE R. H., VERDURMEN E. A. TH., HEBEDA E. H. and BOELRIJK N. A. I. M. (1970) Isotopic evidence on the age of the Trysil porphyries and granites of eastern Hedmark, Norway. *Norsk Geol. Undersokelse* 266, 263–276.

RAADE G. (1973) Distribution of radioactive elements in the plutonic rocks of the Oslo region, 162 pp. Unpublished cand. real. thesis. University of Oslo.

RAMBERG I. B. and SMITHSON S. B. (1971) Gravity interpretation of the southern Oslo graben and adjacent Precambrian rocks, Norway. *Tectonophysics* **11**, 419–431.

RICHARDSON K. A., DARNLEY A. G. and CHARBONNEAU B. W. (in press) Airborne gamma-ray measurements over the Canadian Shield. In *Proc. 2nd Natural Radiation Environment Symposium*, Houston, 1972.

ROSCOE S. M. (1966) Unexplored uranium and thorium resources of Canada. *Geol. Surv. Can. Paper* 66–12.

SHAW D. M. (1967) Uranium, thorium and potassium in the Canadian Precambrian shield and possible mantle compositions. *Geochim. Cosmochim. Acta* **31**, 1111–1115.

SINCLAIR A. J. (1967) Trend surface analysis of minor elements in sulfides of the Slocan mining camp, British Columbia, Canada. *Econ. Geol.* **62**, 1095–1101.

SMITHSON S. B. (1963) Granite studies II: the Precambrian Flå granite, a geological and geophysical investigation. *Norsk Geol. Undersokelse* **219**, 212 pp.

TAYLOR S. R. (1964) Abundance of chemical elements in the continental crust: a new table. *Geochim. Cosmochim. Acta* **28**, 1273–1285.

TREMBLAY L. P. (1972) Geology of the Beaverlodge mining area, Saskatchewan. *Geol. Surv. Can. Mem.* **367**, 265 pp.

...ochimica et Cosmochimica Acta, 197...

A...

Inorganic Chemistry Laborat...

(Re...

Abstract—A theoreti... in silicate melts. Th... states of altervalent... expression for the e...

INTRO...

IT IS usually assumed in ... of trace elements betwee... co-existing melts, that ... centrations, trace elemen... ideal solutions (e.g. P... 1970). In a recent paper, ... have shown using an e.p... that in silicate melts, th... with increasing basicity ... This is the opposite of ... the simple equation:

$$4\,Eu^{3+} + 2\,O...$$

To account for this ... duced solvent coeffici... changes in chemical p... a completely dissociat... state in which the comp... cate melt (MORRIS and ... $(\mu_i^* - \mu_i^0)/RT$ where μ_i^* ... gas and dissolved stan... ing the mean solvent ... oxide as $\Gamma_{\pm}^{(\nu_+ + \nu_-)} = \Gamma...$

$$K'(O^{2-})^2 \frac{(\Gamma...}{(...}$$

where $K' = Kg/p_{O_2}$ an... for (1) when the speci... gases. The ratio $(\Gamma_3...$ ... decrease faster than ... explain the observed ... This led to the impor... $4\,O^{2-}$ is more solu... melt with a higher ... melt with a lower va... p. 1443).

UNIVERSITY OF UTAH
RESEARCH INSTITUTE
EARTH SCIENCE LAB.

MINERALOGICAL AND GEOCHEMICAL STUDIES OF LOWER PALAEOZOIC ROCKS FROM THE TRONDHEIM AND OSLO REGIONS, NORWAY

HENNING DYPVIK

Dypvik, H.: Mineralogical and geochemical studies of Lower Palaeozoic rocks from the Trondheim and Oslo Regions, Norway. *Norsk Geologisk Tidsskrift*, Vol. 57, pp. 205–241. Oslo 1977.

84 samples of Lower Palaeozoic sediments and volcanics were analysed geochemically and mineralogically.

In the eugeosynclinal sections in the SW Trondheim Region the composition of the sediments reflects local erosion of volcanic rocks. Sediments derived from basic, tholeiitic volcanic rocks in this part of the Trondheim Region are enriched in the minerals chlorite, albite, and trace elements Sc, Co, and V. While the Trondheim Region sediments show geochemical variations characteristic of immature, fast deposited sediments, those from the Oslo Region seem to reflect conditions where slow sedimentation of fine-grained material predominated. High concentrations of chlorite, Sc, and Co in the epicontinental sediments of Middle Ordovician age from the Oslo Region indicate enrichments of basic volcanic debris in these beds.

Henning Dypvik, Institutt for geologi, Universitetet i Oslo, Blindern, Oslo 3, Norway.

The present study was designed to provide information on the mineralogy and geochemistry of time-equivalent rocks representing two different sedimentary environments: shallow epicontinental seas on the platform (Oslo Region) and a part of an eugeosynclinal area in the Trondheim Region. The present work is a part of a broad mineralogical and geochemical study of the Lower Palaeozoic sediments from the Oslo and Trondheim Regions, Fig. 1 (Bjørlykke 1974 a, b, Bjørlykke & Dypvik 1975, Dypvik & Brunfelt 1976).

Geochemical analyses were carried out using X-ray fluorescence (Si, Ti, Al, Fe, Mg, Mn, Ca, K, P, Ni, Rb, Ba, Sr, Zn) and instrumental neutron activation analyses (Na, Cr, Sc, Th, Co, La, Sm, Ce, Eu). Mineralogical analyses were performed using X-ray diffraction and thin-section studies.

Geology

It is now assumed that the typical eugeosynclinal rocks of the Trondheim Region occur in allochthonous position and have been derived from the west (Strand 1961, Wolff 1967). The Cambro-Silurian sediments in the Oslo Re-

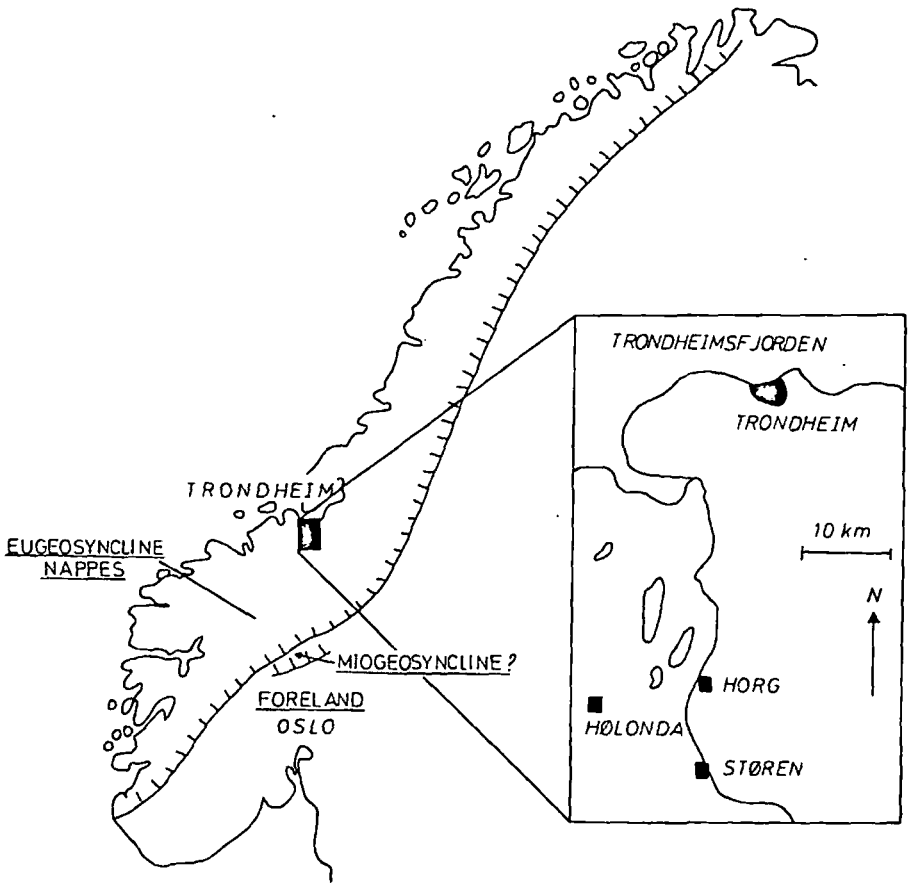

Fig. 1. Simplified map showing the extension of the Scandinavian Caledonides.

gion (Fig. 1) represent epicontinental foreland sediments (Størmer 1967). Fig. 2 is a stratigraphical correlation column for the sediments from the two regions (Dypvik 1974).

Trondheim Region

The stratigraphical division applied in the Hølonda-Horg area (Fig. 1) of the Trondheim Region (Fig. 2) was established by Th. Vogt (1945). The sequence is typical of eugeosynclinal deposition, and consists mainly of shales, graywackes, and limestones which are locally richly fossiliferous. Volcanic rocks are present in several horizons in the investigated area.

The Gula Group, which consists of pelitic to semipelitic sediments often with black phyllite horizons, forms the basal stratigraphic unit in the studied area. Occurrences of *Dictyonema flabelliforme* in some of the younger layers to the east in the Trondheim Region point to a Lower Ordovician (Tremadocian) age (J. H. L. Vogt 1888, Th. Vogt 1940). South of Støren (Fig. 1) serpentinitic bodies are often found in the group (I. Rui, pers. comm. 1974).

The Støren Group, comprising a thick sequence of spilitic greenstones, mainly pillow lavas, is considered to lie stratigraphically above the Gula Group. In the Støren Group intercalated jasper layers are often found.

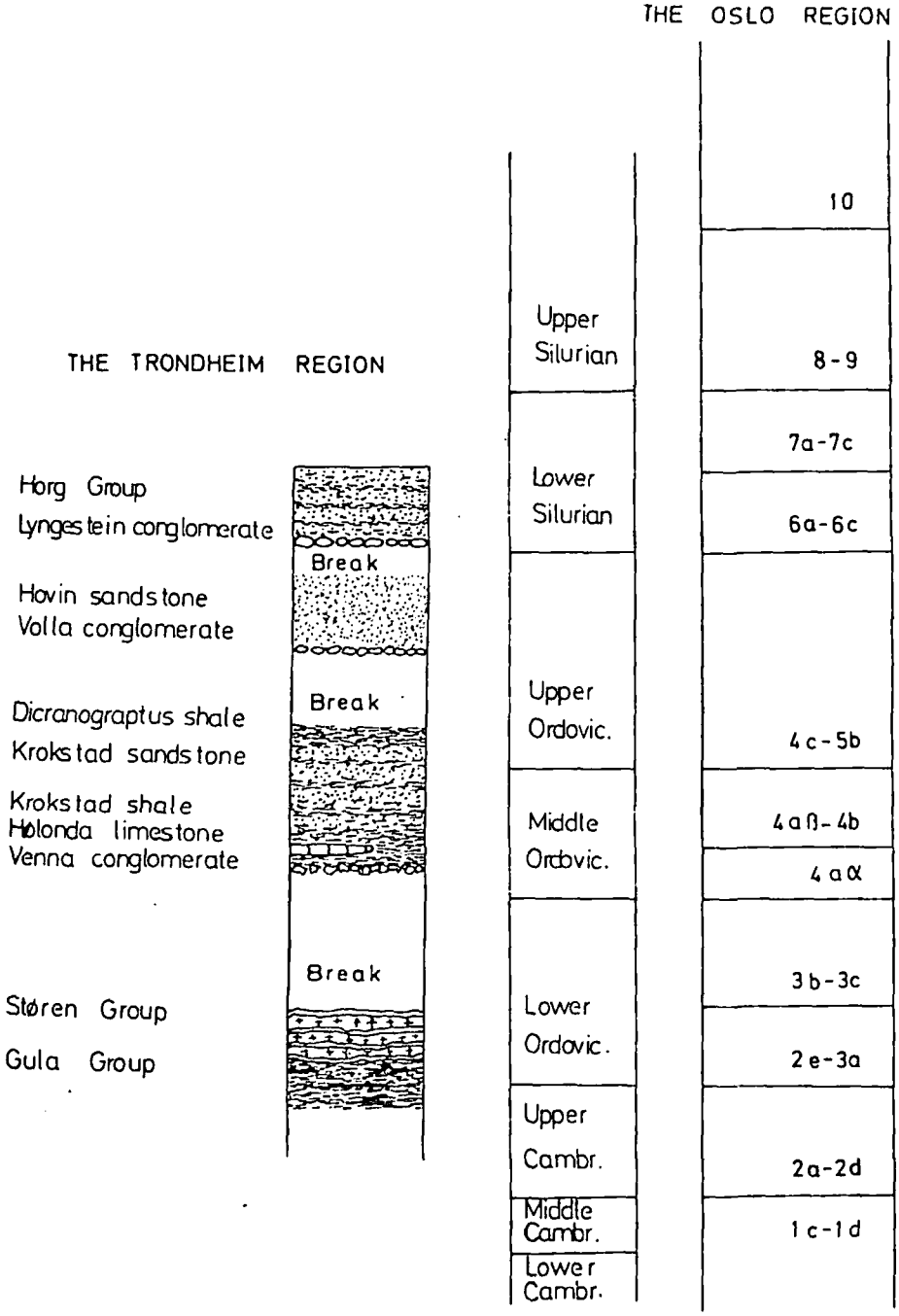

Fig. 2. Stratigraphy of Lower Palaeozoic sediments in the Hølonda – Horg area of the Trondheim Region and in the Oslo Region. The stratigraphy of the Oslo Region is subdivided into stages (etasjer).

A polymictic poorly sorted conglomerate, the Venna conglomerate, lies directly above the Støren Group. It is made up of angular fragments of greenstone, limestone, and jasper. Available stratigraphic evidence suggests a break in sedimentation in Lower Ordovician times (Holtedahl 1920, Bjørlykke 1974 b). The Venna conglomerate forms the base of the Lower Hovin Group, which dominantly consists of graywackes, shales, and limestones. In the graywackes from the Hølonda area, graded bedding and slumping structures have been observed (Chadwick et al. 1962), and they are probably formed by turbidity currents. Fossils from the Hølonda limestone, a limestone unit in this group, indicate a late Arenig to early Llanvirn age (Neumann & Bruton 1974). The Dicranograptus shale, a dark shale in the uppermost part of the Lower Hovin Group, is also of Middle Ordovician age (Hadding 1932). In the Lower Hovin Group volcanic rocks are also found; the Hølonda andesite, of about Krokstad shale age, and the Hareklett rhyolitic tuff, which is situated between Krokstad sandstone and Dicranograptus shale.

At the base of the Upper Hovin Group lies the polymictic Volla conglomerate. The remainder of the Upper Hovin Group consists of a dark grey sandstone, the Hovin sandstone, which is interlayered with thin shale horizons.

After a new break in sedimentation, the Lyngestein quartzite conglomerate was deposited. Above this conglomerate lies the Horg Group, consisting of alternating shales and graywackes.

The stratigraphy published by Chaloupský (1962, 1969) differs from that of Vogt (1945) mainly in the stratigraphical positions of the Horg Group and the Hovin sandstone. Chaloupský considered the Hovin sandstone to be of Lower Silurian age, while the Horg Group was supposed to have been formed in Upper Ordovician time. In this work I have followed the stratigraphical usage of Vogt (1945).

Most of the rocks investigated from the Hølonda-Horg area have suffered lower greenschist facies metamorphism.

Oslo Region

The sedimentology and mineralogy of the Lower Palaeozoic epicontinental sediments from the Oslo Region have recently been described by Bjørlykke (1974 a, b).

Rocks of Middle Cambrian age (stage 1c–1d) are the oldest from the Oslo Region described in this paper. They consist predominantly of black shales with some carbonate beds. Stratigraphically above these beds follow the dark carbon- and sulphide-rich Alum shales (stage 2a–2e) of Upper Cambrian to Lower Ordovician age. At this time, large parts of the Baltic Shield were covered by a shallow sea (Holtedahl 1920) and the sedimentation rates dropped to about 1mm/1000 years. The younger Ordovician sediments consist of alternating shale and limestone beds, showing a successive increase in sedimentation rates (Bjørlykke 1974a).

The Silurian of the Oslo Region is predominantly made up of micritic limestones and calcareous shales. In the upper part of the main sequence (stage 9) a major development of estuarine shales and fresh water deltaic sandstones succeed the younger marine beds (Bjørlykke 1974a).

Sampling and analytical techniques

35 samples from the Hølonda-Horg area were collected from road sections by the author and Prof. Chr. Oftedahl. Oftedahl collected also the 23 samples from a tunnel section by the river Lundesokna (Horg area), 39 samples from the Oslo Region were collected by Prof. K. Bjørlykke.

All the samples looked fresh and unaltered. They are grouped together in relatively well defined units (Fig. 2). The samples from the Oslo Region are divided into shales and limestones, those containing more than 10 % CaO called limestones, while those containing less than 10 % CaO are called shales. Other data and descriptions of the samples analysed in this work are presented in Bjørlykke (1974a,b), Bjørlykke & Dypvik (1975), and Dypvik & Brunfelt (1976).

Each sample was crushed to rock powder in a steel disc mill before being analysed.

The major elements Si, Ti, Al, Fe, Mg, Ca, K, P, and Mn were determined by X-ray fluorescence (XRF) as oxides on diluted, melted pellets according to the method of Müller (1967) and Skaar (1972). The same instrument was used for determinations of Ni, Rb, Ba, Sr, Zn, and V, but these analyses were performed on undiluted, pressed pellets.

USGS, ZGI, and Nancy standards were used for the calibration of major element determinations. Especially made additional standards were used in the trace-element analyses.

Th, Na, Co, Sc, and Cr contents were determined by instrumental neutron activation analyses (INAA). A Ge(Li)-detector system comprising an Ortec 24 cm^3 Ge(Li)-detector with a resolution of 3.8 KeV (FWHM) for the 1331 KeV peak of 60 Co, a Hewlett Packard 200 MHz ADC, and a NORD-1 computer were used. Rock samples of about 100 mgs were wrapped in small polyethylene bags for irradiation. The samples were irradiated for 1 hour at a neutron flux of about 1.5×10^{13} n/cm^2 sec in a JEEP-II reactor at Kjeller, Norway. γ-spectrometric measurements were carried out 3 and 20 days after irradiation.

USGS standards BCR-1 and G-2 were used for calibration with values from Gordon et al. (1968), Brunfelt & Steinnes (1971), and Flanagan (1973).

U and Th were determined on 35 samples from the Horg profile by γ-spectrometry. The equipment consists of a NaI (Tl) scintillation detector and a pulse high analysator with 400 channels. Coarse crushed rock samples of about 600 g were used. The method is described by Adams & Gasparini (1970) and Raade (1972).

Table 1. Mineralogical analyses of Lower Palaeozoic sediments and volcanics from the Trondheim Region.
Data as relative percentages from X-ray diffractograms.

	Stratigraphical unit	No. of analyses	Chlorite 7 Å	Illite 10 Å	Albite 3.19 Å	Quartz 4.26 Å	Calcite 3.03 Å	Dolomite 2.88 Å	Actinolite 8.42 Å	Potash Feldspar 3.24 Å
	The Lundesokna profile									
Silurian	Horg Group	4	15.6	11.5	31.8	17.8	22.3	1.0	–	–
	Lyngestein conglomerate	1	18.9	8.5	10.2	18.0	27.7	16.7	–	–
Ordovician	Hovin sandstone	2	16.3	6.7	14.9	19.0	25.6	17.5	–	–
	Dicranograptus shale	3	21.8	5.0	43.9	21.2	8.1	–	–	–
	Krokstad sandstone	4	27.6	5.2	45.8	17.1	4.3	–	–	–
	Krokstad shale	4	37.4	14.0	27.8	15.4	5.4	–	–	–
	Venna conglomerate	2	27.8	9.9	38.7	17.3	6.3	–	–	–
	Støren greenstone	1	34.1	2.0	48.5	0.7	–	–	14.7	–
Cambrian	Gula Group	2	24.7	10.0	21.7	26.8	11.8	–	–	5.0
	The Horg profile									
Silurian	Horg Group	4	22.8	12.3	45.6	13.2	4.4	1.7	–	–
	Lyngestein conglomerate	1	14.3	4.2	8.2	12.7	60.6	–	–	–
Ordovician	Hovin sandstone	3	18.5	10.2	11.9	17.0	21.8	20.6	–	–
	Dicranograptus shale	3	20.5	5.4	30.6	14.1	29.4	–	–	–
	Krokstad sandstone	3	34.4	8.3	37.4	15.6	4.3	–	–	–
	Krokstad shale	2	38.7	10.1	36.4	14.8	–	–	–	–
	Venna conglomerate	1	18.8	14.2	18.2	18.6	30.2	–	–	–
	Støren greenstone	4	26.9	1.1	41.5	2.9	11.8	–	15.8	–
Cambrian	Gula Group	3	29.7	16.5	25.2	18.8	5.8	4.0	–	–
	Hølonda andesite	1	11.0	6.8	69.2	7.8	2.7	–	2.5	–
	Hareklett rhyolitic tuff	1	5.3	11.7	30.1	20.1	32.8	–	–	–

Hareklett rhyolitic tuff

Table 2. Mineralogical analyses of Lower Palaeozoic shales and limestones from the Oslo Region. Data as relative precentages from X-ray diffractograms. Shale < 10 % CaO, Limestone > 10 % CaO.

Stratigraphical unit			No. of analyses	Chlorite 7 Å	Illite 10 Å	Albite 3.19 Å	Potash Feldspar 3.21 Å	Quartz 4.26 Å	Calcite 3.03 Å	Dolomite 2.88 Å
	10	shale	1	11.7	5.4	32.0	–	45.7	5.2	–
	8–9	shale	2	25.7	17.7	14.9	–	17.9	17.0	6.8
Silurian		limestone	1	0.6	1.2	0.8	–	2.2	93.1	2.1
	7a–7c	limestone	2	4.7	3.5	2.1	1.4	5.6	80.9	1.8
	6a–6c	shale	2	15.3	10.7	8.7	4.9	32.3	27.7	0.4
	4c–5b	shale	2	6.6	19.9	15.0	1.7	24.8	17.8	14.2
		limestone	5	2.8	1.2	2.9	3.1	16.8	73.2	–
	4aβ–4b	shale	2	17.9	23.8	10.3	1.0	12.2	25.8	9.0
		limestone	1	7.6	2.8	3.7	–	5.4	80.5	–
Ordovician	4aα	shale	2	29.7	24.7	10.4	–	15.5	14.0	5.7
	3b–3c	shale	3	9.2	19.9	23.0	17.3	22.9	–	7.7
		limestone	2	1.9	4.6	1.8	–	5.0	76.9	9.8
	2e–3a	shale	4	–	38.4	13.9	15.9	27.0	–	4.8
	2a–2d	shale	4	–	46.7	11.3	15.7	22.0	–	– FeS_2 4.3
		limestone	2	–	1.1	–	–	2.6	93.4	2.9
Cambrian	1c–1d	shale	2	6.5	51.3	9.5	6.2	23.0	2.3	–
		limestone	2	–	–	–	–	2.0	98.0	1.2

Table 3. Major element analyses of Lower Palaeozoic sediments and volcanics from the Trondheim Region.
All concentrations in percent. Ign. loss = ignition loss.

	Stratigraphical unit	No. of analyses	SiO_2 %	TiO_2 %	Al_2O_3 %	Fe_2O_3 %	MnO %	MgO %	CaO %	Na_2O %	K_2O %	P_2O_5 %	Ign. loss %	Total %
	The Lundesokna profile													
	Horg Group	4	58.4	0.61	16.7	4.1	0.06	2.60	6.60	2.11	3.31	0.12	5.81	100.42
Silurian	Lyngestein conglomerate	1	56.3	0.58	10.6	4.6	0.06	5.02	9.51	1.12	2.51	0.11	11.00	101.41
	Hovin sandstone	2	55.8	0.50	10.2	3.9	0.05	5.50	9.93	1.28	2.07	0.14	12.09	101.46
	Dicranograptus shale	3	65.1	0.69	14.3	6.1	0.07	2.83	2.66	3.12	1.86	0.10	3.61	100.44
Ordovician	Krokstad sandstone	4	62.3	0.96	14.6	8.6	0.08	4.11	2.96	3.00	1.53	0.15	3.29	101.58
	Krokstad shale	4	55.2	1.03	16.4	8.9	0.10	4.39	2.40	2.36	3.09	0.21	4.87	98.95
	Venna conglomerate	2	62.7	0.91	13.8	8.1	0.09	3.50	2.49	2.83	2.18	0.18	3.52	100.30
	Støren greenstone	1	45.4	1.40	16.7	10.9	0.15	8.80	10.79	2.49	0.61	0.12	3.41	100.77
Cambrian	Gula Group	2	65.9	0.96	10.9	7.1	0.10	3.25	3.12	1.58	2.71	0.15	4.35	100.11
	The Horg profile													
Silurian	Horg Group	4	58.1	0.74	17.5	6.2	0.09	3.52	4.77	2.81	2.86	0.13	4.37	101.09
	Lyngestein conglomerate	1	60.2	0.52	10.6	4.2	0.06	4.09	9.77	1.27	1.45	0.12	9.21	101.49
	Hovin sandstone	3	61.1	0.59	11.0	4.3	0.05	4.60	7.28	1.06	2.12	0.11	9.15	101.36
	Dicranograptus shale	3	51.3	0.66	12.0	6.4	0.14	3.52	12.58	1.98	1.18	0.16	10.78	100.70
Ordovician	Krokstad sandstone	3	58.3	0.91	16.1	8.8	0.10	4.28	3.03	2.50	2.09	0.18	3.78	100.07
	Krokstad shale	2	57.2	0.99	16.0	8.9	0.11	4.72	3.45	2.61	1.92	0.22	4.04	100.16
	Venna conglomerate	1	56.5	0.51	12.8	7.0	0.09	2.32	9.09	1.40	1.38	0.08	9.66	100.83
	Støren greenstone	4	46.7	1.57	15.6	10.0	0.15	6.92	12.45	2.52	0.28	0.19	4.33	100.71
Cambrian	Gula Group	3	58.3	0.88	15.7	7.0	0.06	4.36	2.82	1.67	2.33	0.13	5.08	98.33
	Hølonda andesite	1	56.3	0.93	18.0	6.4	0.09	2.22	6.31	3.34	3.01	0.34	2.63	99.57
	Hareklett rhyolitic tuff	1	58.9	0.52	14.7	2.4	0.08	1.26	8.64	1.73	3.03	0.09	6.13	97.48

Table 4. Major element analyses of Lower Palaeozoic shales and limestones from the Oslo Region. All concentrations in percentages. Shale < 10 % CaO, Limestone > 10 % CaO. Data from Bjørlykke (1974a). Ign. loss = Ignition loss.

	Stratigraphical unit		No. of analyses	SiO_2 %	TiO_2 %	Al_2O_3 %	Fe_2O_3 %	MnO %	MgO %	CaO %	Na_2O %	K_2O %	P_2O_5 %	Ign. Loss %	Total %
	10	shale	1	79.6	0.40	8.4	2.7	0.04	1.56	1.99	1.95	1.49	0.12	2.68	100.93
	8–9	shale	2	53.7	0.75	14.6	6.6	0.09	4.66	5.97	1.43	3.35	0.15	8.89	100.19
Silurian		limestone	1	11.1	0.16	3.1	1.7	0.05	2.03	43.63	0.27	0.98	0.01	35.81	98.84
	7a–7c	limestone	2	24.1	0.34	6.6	2.9	0.12	2.00	33.50	0.45	1.63	0.04	27.60	99.28
	6a–6c	shale	2	65.1	0.58	10.3	4.7	0.07	2.96	5.93	0.76	2.43	0.07	7.32	100.22
	4c–5b	shale	2	61.7	0.72	12.1	4.7	0.06	2.43	6.32	1.00	3.16	0.15	7.06	99.40
		limestone	5	33.3	0.20	3.5	1.5	0.05	1.67	31.38	0.54	1.04	0.01	25.68	98.87
	4aβ–4b	shale	2	49.6	0.67	16.2	6.8	0.06	5.01	7.49	0.91	3.38	0.09	10.47	100.68
		limestone	1	25.9	0.32	7.4	4.0	0.29	2.74	30.32	0.61	1.57	0.18	25.81	99.14
Ordovician	4aα	shale	2	51.4	0.77	18.2	8.4	0.08	4.03	4.21	1.00	3.92	0.12	7.81	99.94
	3b–3c	shale	3	57.4	0.92	17.3	4.1	0.03	2.22	2.71	0.97	4.48	0.20	5.62	95.95
		limestone	2	19.6	0.28	5.1	2.8	0.13	1.93	36.25	0.25	1.40	0.26	31.31	99.31
	2e–3a	shale	4	59.3	1.00	18.8	3.6	0.01	1.42	0.55	0.88	5.45	0.14	6.20	97.35
	2a–2d	shale	4	55.5	0.89	16.4	4.0	0.01	1.10	0.18	0.72	4.64	0.07	16.56	100.07
		limestone	2	7.8	0.07	1.5	1.2	0.09	2.39	47.69	0.08	0.25	0.39	37.82	99.28
Cambrian	1c–1d	shale	2	59.9	1.05	19.1	4.8	0.04	1.73	0.33	0.16	5.37	0.07	6.45	99.00
		limestone	2	5.9	0.06	1.5	0.6	0.15	1.34	50.66	0.04	0.15	0.21	39.33	99.94

Precisions of the chemical analyses are given as standard deviation in Table 8.

Mineral determinations were carried out by thin-section studies and X-ray diffraction analyses. For semi-quantitative X-ray determinations, slides with rock powder mounted on glass with vaseline were used. Oriented samples were made by the pipette-on-glass slide technique (Gibbs 1965). The analyses were executed on a Siemens X-ray diffractometer with an Omega goniometer.

It is assumed that peak height multiplied by the width at half height will be an expression of the peak area and therefore of the relative content of each mineral (Norrish & Taylor 1962). The relative amount of each mineral is calculated as the percentages of the sum of the intensities to the characteristic peaks of these minerals.

Gravimetric carbon determinations were made using a Leco Induction furnace. Twelve standard parallels gave a precision as per cent deviation from the mean of $\pm$ 1.5 %.

Trondheim Region

LITHOLOGICAL DESCRIPTIONS

The mineralogical analyses presented here were carried out by X-ray diffraction and thin section analyses. All the percentages given for the different minerals are relative percentages from diffractograms (Tables 1 and 2). Figs. 3 and 4 summarize the mineralogy in the samples from the two regions.

The Gula Group

The samples from the Gula Group are fine-grained phyllites and schists, some rich in organic carbon. They consist of quartz- and mica-rich layers, quartz often with undulating extinction. Samples of higher metamorphic grade consist very often of biotite. Chromite, tremolite, and garnet are found in some samples after mineral separation. The garnet is probably an Mn-rich variety of the almandine-spessertine series, since a garnet-rich sample contains ten times as much MnO as the other samples from the group.

The Venna conglomerate

The samples from the matrix of this horizon consist of much albite, chlorite and some illite, quartz, and calcite. The analysed samples are from the matrix of the conglomerate which often contains 1–2 mm angular greenstone fragments. Fragments of jasper are also found.

The Krokstad shale

In the Krokstad shale, a group made up of shales and greywackes, chlorite and albite, and smaller amounts of illite and quartz were found by X-ray diffraction. In some of the samples finer and coarser layers alternate, with

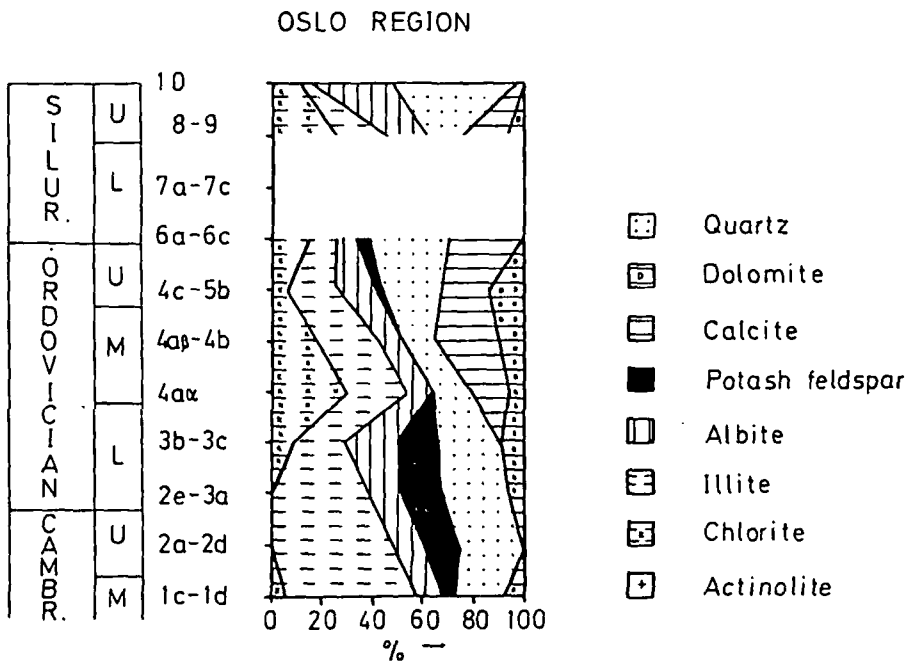

Fig. 3. Stratigraphical variation in mineralogical composition of whole rock samples of shales from the Oslo Region, calculated as relative percentage from X-ray diffractometer analyses. Samples of shales from stages 7a–7c have not been analysed.

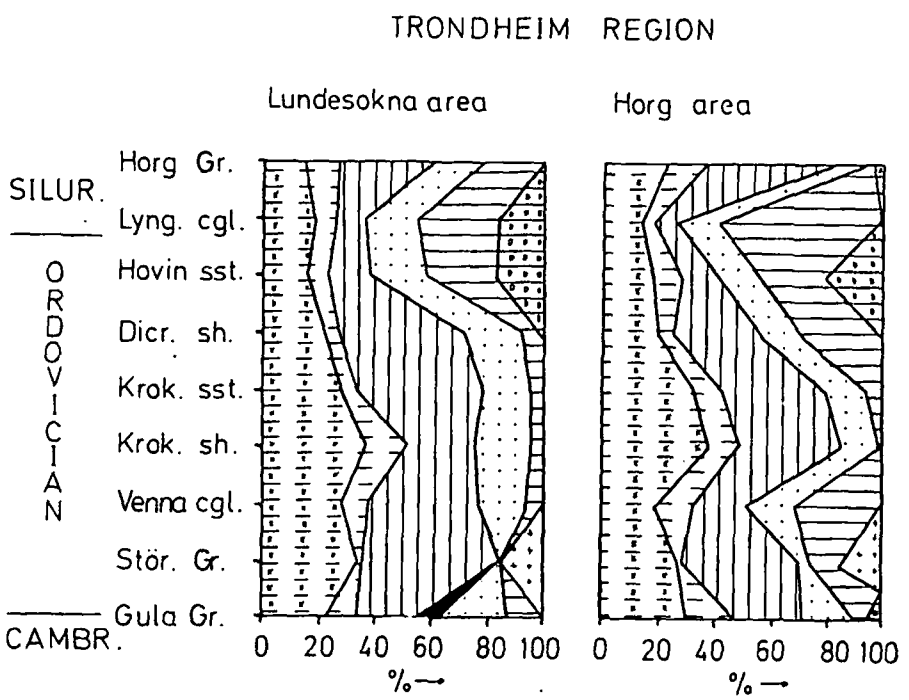

Fig. 4. Stratigraphical variation in mineralogical composition of whole rock samples from Lundesokna and Horg areas in the SW Trondheim Region, calculated as relative percentage from X-ray diffractometer analyses. Legend in Fig. 3.

Table 5. Trace element analyses of Lower Palaeozoic sediments and volcanics from the Trondheim Region. All concentrations in ppm, except for organic carbon which is given in percent. Not determined = n. d.

	Stratigraphical unit	No. of analyses	Ba ppm	Rb ppm	Sr ppm	V ppm	Ni ppm	Zn ppm	Sc ppm	Cr ppm	Co ppm	Th ppm	U ppm	$C_{org.}$ %
	The Lundesokna profile													
Silurian	Horg Group	4	675	150	433	69	22	75	13.9	29	13	14.1	n. d.	n. d.
	Lyngestein conglomerate	1	435	100	255	54	43	76	9.5	63	11	8.7	n. d.	n. d.
	Hovin sandstone	2	379	93	209	52	50	65	9.1	65	12	7.9	n. d.	n. d.
	Dicranograptus shale	3	1068	63	251	121	71	260	20.5	68	16	5.1	n. d.	n. d.
Ordovician	Krokstad sandstone	4	564	72	191	127	97	83	22.1	112	28	6.9	n. d.	n. d.
	Krokstad shale	4	538	125	143	143	98	107	22.9	82	25	13.2	n. d.	n. d.
	Venna conglomerate	2	445	72	92	124	88	137	18.7	98	20	5.8	n. d.	n. d.
	Støren greenstone	1	63	2	116	181	167	62	38.1	166	51	0	n. d.	n. d.
Cambrian	Gula Group	2	420	80	189	106	121	78	13.2	228	19	8.0	n. d.	n. d.
	The Horg profile													
Silurian	Horg Group	4	748	144	388	92	26	80	16.2	61	19	11.6	3.6	0.75
	Lyngestein conglomerate	1	335	75	231	59	24	58	9.7	147	11	8.5	2.3	0.67
	Hovin sandstone	3	424	107	187	66	54	60	10.7	164	14	10.4	2.4	0.83
	Dicranograptus shale	3	475	49	275	99	52	89	18.3	96	22	6.1	2.4	0.99
Ordovician	Krokstad sandstone	3	529	95	203	136	91	104	23.1	125	26	9.8	2.7	0.63
	Krokstad shale	2	458	90	258	147	83	109	22.3	128	26	8.6	2.7	0.63
	Venna conglomerate	1	395	53	431	105	34	66	16.8	101	18	3.1	1.0	0.63
	Støren greenstone	4	64	3	238	201	168	77	35.3	178	44	0.4	0.3	0.55
Cambrian	Gula Group	3	590	122	137	121	93	96	19.7	120	26	9.2	2.4	1.07
	Hølonda andesite	1	941	131	802	81	0	73	10.8	24	9	22.7	5.7	1.02
	Hareklett rhyolitic tuff	1	519	179	725	47	28	35	7.6	157	15	12.7	4.4	0.66

"	Hølonda andesite	1	941	131	802	81	0	73	10.8	24	9	22.7	5.7	1.02
	Hareklett rhyolitic tuff	1	519	179	725	47	28	35	7.6	157	15	12.7	4.4	0.66

Table 6. Trace element analyses of Lower Palaeozoic shales and limestones from the Oslo Region. All values in ppm. Ba, Rb, V, Ni, and Zn values from Bjørlykke (1974a). Sc, Cr, Co, and Th have been determined by the author. Shale < 10 % CaO, Limestone > 10 % CaO.

	Stratigraphical unit		No. of analyses	Ba ppm	Rb ppm	Sr ppm	V ppm	Ni ppm	Zn ppm	Sc ppm	Cr ppm	Co ppm	Th ppm
	10	shale	1	319	61	142	98	68	28	5.4	50	6	5.7
	8–9	shale	2	448	153	148	182	110	127	14.5	82	20	7.7
Silurian		limestone	1	314	31	951	36	35	40	3.1	10	5	3.1
	7a–7c	limestone	2	253	84	585	72	44	53	7.1	27	9	6.2
	6a–6c	shale	2	786	181	279	232	119	61	9.4	421	13	6.8
	4c–5b	shale	2	1310	126	133	175	96	111	11.2	664	18	11.3
		limestone	5	140	47	1410	49	82	42	4.1	154	7	2.5
	4aβ–4b	shale	2	835	154	289	213	242	120	19.0	409	29	9.2
		limestone	1	759	61	627	108	96	69	8.4	144	20	3.5
Ordovician	4aα	shale	2	991	146	264	249	112	142	24.2	179	33	9.3
	3b–3c	shale	3	33227	130	350	180	60	107	15.1	76	11	15.3
		limestone	2	324	90	700	100	37	54	5.7	15	7	5.4
	2e–3a	shale	4	25775	168	163	589	62	89	14.4	88	6	15.1
	2a–2d	shale	4	2457	159	73	775	114	65	10.9	56	10	9.0
		limestone	2	337	25	677	41	42	161	13.3	11	4	1.6
Cambrian	1c–1d	shale	2	1024	234	25	393	67	151	15.9	72	13	14.3
		limestone	2	69	28	210	21	36	39	1.9	8	4	2.2

UNIVERSITY OF UTAH LIBRARIES

graded bedding often seen in thin section. The coarser layers often consist of angular quartz- and rock fragments with 0.5 mm as a mean diameter.

The Krokstad sandstone

This group also consists of shales and greywackes. Chlorite and albite are the most common minerals in this group, but illite, quartz, and calcite are also present. In thin sections layers of finer and coarser grained beds are seen. 3–4 mm, angular rock fragments are also often found in thin section.

The Dicranograptus shale

The shaly samples from this horizon consist of albite, chlorite, quartz, and calcite. Thin-section examinations show that some of these samples are dense, and rich in organic carbon and pyrite without any lamination. Coarser layers with 2–3 mm sized particles are also usual.

The Hovin sandstone

These samples of shales and fine-grained sandstone are generally calcareous. They also consist of chlorite, illite, quartz, and small amounts of albite. Some rounded quartz- and rock fragments of about 0.5 mm in diameter are usually found in thin section. Dolomite has been detected in X-ray diffractograms, and also as rombs, typical of late diagenetic dolomitization, in thin section.

The Lyngestein conglomerate

In these samples from the matrix of the conglomerate, dolomite was found by X-ray diffraction analyses, and dolomite rhombs have been seen in thin section, suggesting a late diagenetic dolomitization. In addition to dolomite, these samples consist of calcite, chlorite, illite, albite and quartz.

The Horg Group

The samples from this group are made up of much albite and some chlorite, illite, quartz, and calcite. Dolomite is also found in the X-ray diffractograms, and dolomite rhombs have been seen in thin sections. The samples are shales and fine- to medium-grained sandstones, often with graded bedding.

Discussion

A major part of the chlorite content in the sediments is probably derived from the basaltic rocks of the Støren Group or basalts akin to these (Table 1). The decreasing chlorite content from the Krokstad shale to sediments of the Horg Group (Fig. 4) may indicate a decreasing influx of basaltic material. A peak value in the chlorite content in the Krokstad shale, which is situated just above the lavas, also indicates that the chlorite was derived from the basalts. Fig. 5 shows a plot of the stratigraphical variation in chlorite/illite ratio expressed by the 7Å/10Å ratio. The decreasing ratio (Fig. 5) means a

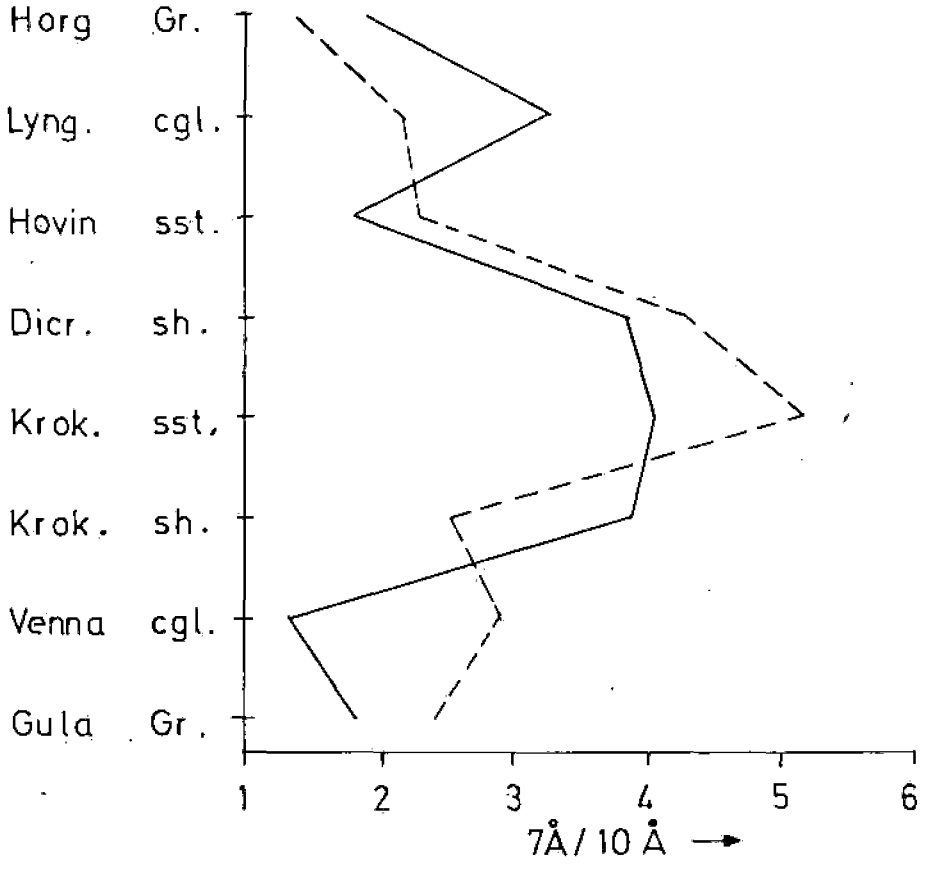

Fig. 5. Stratigraphical variation in the 7 Å/10 Å ratio in the Trondheim Region. Values from X-ray diffractometer analyses. Solid line Horg profile. Broken line – Lundesokna profile.

decreasing chlorite content relative to illite, which also confirms the above conclusion.

The 7Å/14Å ratios are always greater than two in the samples from the Trondheim Region. This means that the chlorite is relatively rich in iron (Grim 1968). Samples from the Oslo Region show about the same ratios. This result confirms the conclusion of Bjørlykke (1974b) that the chlorite found in samples from the Oslo Region is probably derived from eugeosynclinal rocks similar to those in the Trondheim Region.

Decreasing chlorite content towards the top of the profiles in the Trondheim Region (Fig. 4) can be caused by the increased influx of material derived from more acid rocks or a decreased influx of basaltic debris. Albite, a major component of the Støren greenstones (Fig. 4), has a distribution akin to that of chlorite. This indicates that much of the albite also has a clastic origin. In the Horg Group the albite content increases, which may be due to authigenic albite formation, calcite dilution effects in the Hovin sandstone, and Lyngestein conglomerate or renewed influx of basaltic debris.

Table 7. Average geochemical composition of Lower Palaeozoic sediments from the Oslo Region and of Lower Palaeozoic sediments and volcanics from the Trondheim Region. Main element data and data for Ba, Rb, Sr, V, Ni, Zn and organic carbon ($C_{org.}$) for the Oslo Region sediments from Bjørlykke (1974a). Not determined = n. d.

		Oslo Region	Trondheim Region	Gula Group gr. A	Gula Group gr. B	Støren greenst.	Alum shale
SiO_2	%	41.4	57.0	61.6	53.1	45.7	57.0
TiO_2	%	0.55	0.82	0.91	0.85	1.47	0.94
Al_2O_3	%	10.7	14.2	13.7	15.0	15.8	17.3
Fe_2O_3	%	3.5	7.4	7.0	11.4	10.1	4.3
MnO	%	0.06	0.10	0.07	0.22	0.15	0.02
MgO	%	2.16	4.16	3.92	6.71	7.17	1.31
CaO	%	18.58	6.40	2.94	3.04	13.05	0.23
Na_2O	%	0.63	2.08	1.64	0.78	2.74	0.53
K_2O	%	2.77	2.21	2.48	4.39	0.25	4.88
P_2O_5	%	0.12	0.16	0.14	0.31	0.17	0.07
Ign. loss	%	18.66	5.87	4.79	3.75	4.16	13.19
Ba	ppm	583	527	522	842	37	1979
Rb	ppm	113	93	105	140	2	184
Sr	ppm	466	250	158	68	229	57
V	ppm	248	117	115	232	190	648
Ni	ppm	83	93	104	345	187	98
Zn	ppm	83	103	89	256	60	94
Sc	ppm	10.7	18.9	17.1	19.8	35.6	12.6
Cr	ppm	140	121	163	327	187	61
Co	ppm	11	23	23	38	47	11
Th	ppm	8.0	8.6	8.7	9.1	0.3	10.8
U	ppm	n. d.	2.5	2.4	5.7	n. d.	n. d.
$C_{org.}$	%	n. d.	n. d.	1.07	1.72	0.36	7.6
Number of samples		39	42	5	4	5	8

GEOCHEMISTRY

The Gula Group

The samples from the Gula Group are schists, which can be subdivided into two groups: Group A – consisting of weakly metamorphic samples, and Group B – consisting of samples of a higher metamorphic grade. The samples in group A represent lower greenschist facies, while those in group B the upper part of this facies. Table 7 shows the geochemical composition of the two groups compared to the Alum shales from the Oslo Region.

Fig. 6 is a comparison diagram for groups A and B. All samples are normalized to the mean of group A. The area between the dotted lines represents the variation area of the samples from group A, while the drawn, solid line shows the mean variation of the samples from group B. The horizontal line through 1.0 is the mean of group A. In Fig. 6 it is clearly seen that the samples from group B are enriched in Fe_2O_3, MnO, MgO, K_2O, P_2O_5, V, Ni, Zn, Co, U and $C_{org.}$, depleted in Na_2O and Sr, and have a lower ignition loss (ign. loss) than those from group A. See also Table 7.

By supposing similar diagenesis, the variations in the diagram probably

Table 8. Standard deviation based on six parallels.

SiO_2, TiO_2, Al_2O_3, Fe_2O_3, MnO, CaO, K_2O, Rb, Sr, V & Ba	± 1 %
MgO, P_2O_5	± 3 %
Ni, Zn	± 4 %
Th	± 5 %
Co	±10 %
Na, Cr, Sc	± 2 %

show differences in primary composition or chemical variations due to metamorphic reactions. The $C_{org.}$, V, and U enrichments in group B are probably due to primary composition variations, and show that some of the samples are formed in an environment with higher organic production than others. The enrichments of P_2O_5 may underline this.

Variations in Cr, Ni, and Co content may be the result of different heavy mineral content. In sample H-36, chromite was found after mineral separation and X-ray diffraction analyses. This chromite content is the most probable source to the enrichments of the above-mentioned elements. The chromite is probably derived from serpentinitic layers in the Gula Group.

The positive MnO anomaly in group B is probably a product of reactions connected with the metamorphism. Sample H-37, which contains 0.59 % MnO, also contains garnet. This agrees well with the X-ray diffraction results, which point to a garnet from the almandine-spessertine series.

In the slightly higher grade metamorphic samples, biotite is common and only small amounts of muscovite are found. The occurrence of biotite is the

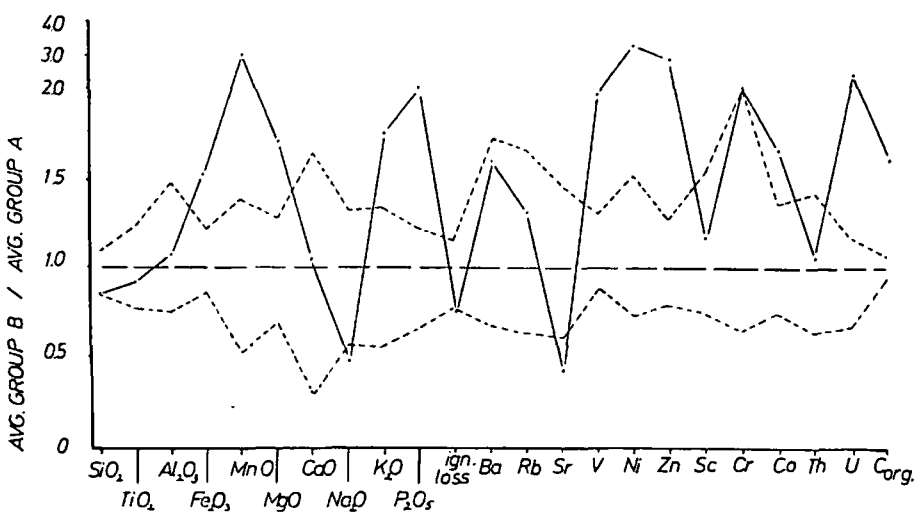

Fig. 6. A comparison plot for the analysed elements in samples from group A and B in the Gula Group. The average of group B is normalized to the average of group A by dividing element by element. Horizontal, broken line through 1.0 represents the average of group A, while the dotted lines on both sides represents the variation interval for samples of group A. The solid line is the average of group B normalized to the average of group A.

most probable reason why the samples have high concentrations of Fe_2O_3 and MgO.

The high amount of K_2O in group B is due to the large amount of mica in these samples. Based on these variations, it is supposed that during metamorphism a K-fixation took place. The metamorphic samples are enriched in Zn. These samples also contain large amounts of biotite. De Vore (1955a, b) found biotites with up to 900 ppm Zn. The formation of biotite during metamorphism may therefore have led to higher Zn concentrations. 1550 ppm Zn was, however, found in chromite from serpentinites by Pearre & Heul (1960). Large amounts of Zn may therefore also be the result of greater concentrations of heavy minerals such as chromite.

The samples from group B are depleted in Sr, and have lower $\frac{Sr.\ 10^3}{Ca}$ ratios than group A, probably a result of metamorphic reactions. By recrystallisation of calcite, Sr will disappear from the structure (Turekian 1964). A recrystallisation connected with the metamorphism will therefore lead to Sr losses.

Low ignition loss for the metamorphic samples is most probably due to the higher P-T conditions that existed during metamorphism. During such conditions water would have been expelled from several minerals. Denser minerals with less water may be the product of such reactions.

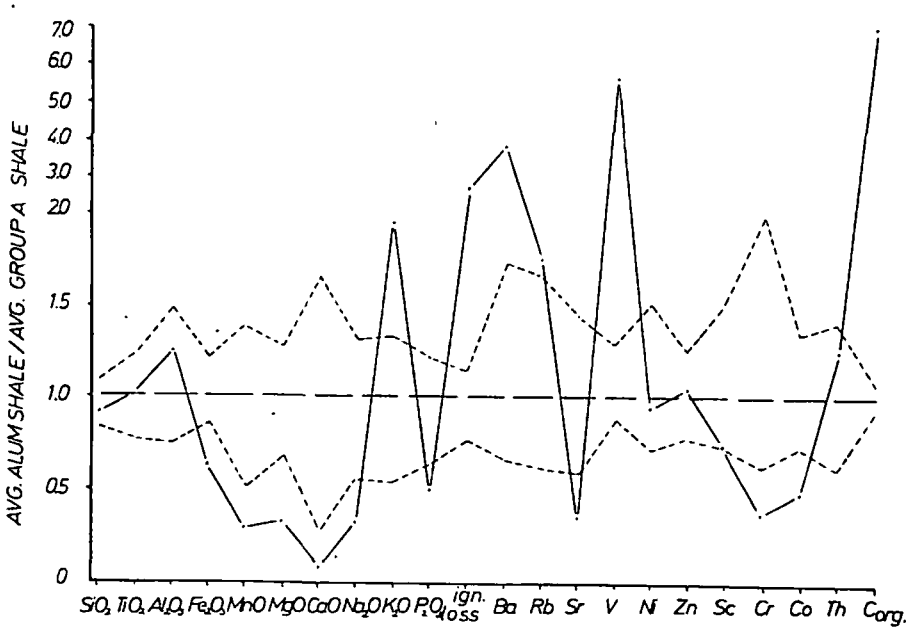

Fig. 7. A comparison plot for the average Alum shale from the Oslo Region and the average shale from the Gula Group in the Trondheim Region. The samples have been normalized to the group A average, by dividing element by element. Horizontal broken line through 1.0 represents the average of group A, while the dotted lines on both sides represent the variation interval for samples of group A. The solid line represents the average Alum shale normalized to the average of group A.

A transition from an An-poor plagioclase to more An-rich variety will lead to a loss in Na_2O. This reaction may explain why the samples from group B contain less Na_2O than the samples from group A.

Fig. 7 shows the Cambrian Alum shales from the Oslo Region plotted in a similar comparison diagram. In this case the average Alum shale is compared to the average of group A.

The solid drawn line shows the mean Alum shale composition. In Fig. 7 K_2O, Ign. loss, Ba, Rb, V, and $C_{org.}$ enrichments and Fe_2O_3, MnO, MgO, CaO, Na_2O, P_2O_5, Sr, Cr and Co depletions are clearly seen in the Alum shales.

A lower chlorite content in the Alum shales explains the relatively smaller amounts of Fe_2O_3, MgO, Sc, Cr, and Co in these beds. The Alum shales contain less calcite and more organic carbon than group A. Such mineralogical distributions result in lower CaO, P_2O_5, and Sr, and higher V concentrations in the Alum shales than in the Gula schists. Relatively small amounts of albite in the Alum shales may explain why these shales contain less Na_2O than Gula schists from group A. Large amounts of illite in the same Alum shales probably explain the higher K_2O, Ba, and Rb contents and higher ignition loss than group A samples. The Th/U ratio of samples H-36 and H-38 are 0.63 and 0.58. Similar ratios are found in the Alum shales (Bjørlykke 1974a). Following Adams & Weaver (1958), these values are typical of black marine shales. Sample H-38 contains in addition great amounts of V and Zn, which are also characteristic of black shales. The other analysed samples from the Gula Group have Th/U ratios typical for grey and green shales (Adams & Weaver 1958).

Volcanic rocks from the Horg area, SW Trondheim Region

The samples from the Støren Group are from the Horg area, where the sequence consists primarily of spilitic pillow lavas, with tuffaceous layers and thin jasper beds of probably Lower Ordovician age, equivalent to 2e-3a time in the Oslo Region (Blake 1962, Chaloupský 1969). The five samples represent lower greenschists facies. In the Lower Hovin Group the somewhat younger Hølonda andesite and Hareklett rhyolitic tuff are found. The mineralogy of the samples is shown in Table 1.

Dewey (1969) maintained that the Støren greenstone is part of an ophiolitic belt and, like Wilson (1966), he attempted to give a tectonic model of the Caledonian Orogeny by using new global tectonics.

Mineralogical and geochemical studies of modern basalts have shown that their composition varies in relation to plate tectonic position, with alkali basalts on the continent side and tholeiites on the ocean side of island arcs (Kuno 1960, Hart 1969, Hart et al. 1970, Jakěs & Gill 1970).

Island arc tholeiites (low potassium tholeiites) are situated on the trench side of island arcs, while oceanic tholeiites form parts of the ocean floor outside the trench (Jahn et al. 1974).

Several authors have noted that seawater alterations, lower degrees of

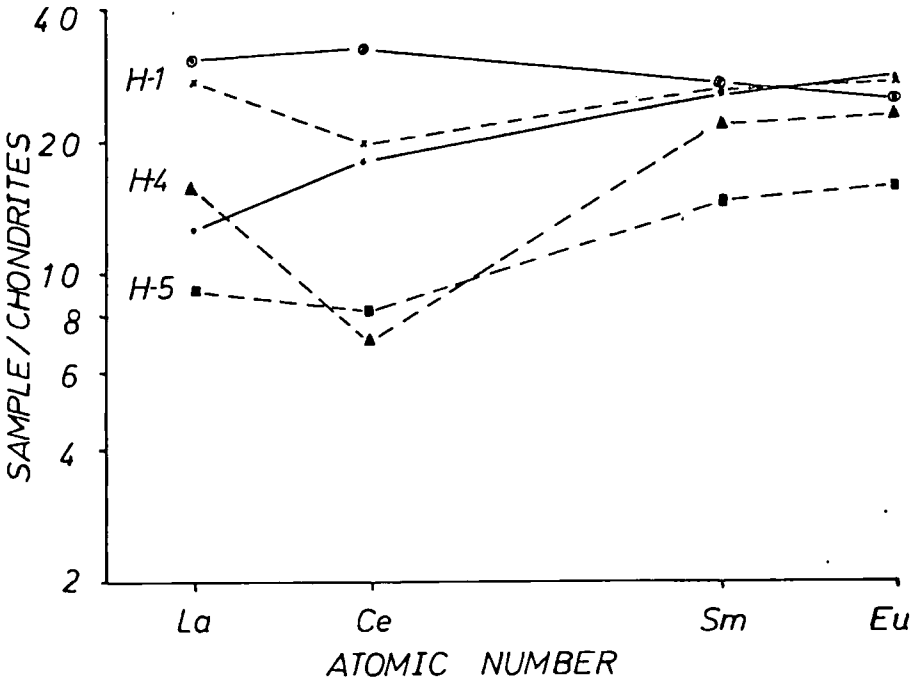

Fig. 8. Comparison plot for the La, Ce, Sm, Eu content in sample H-1 (×), H-4 (▲), H-5 (■), ocean floor tholeiite (· and solid line), and island-arc tholeiite (⊙ and solid line). All the samples are normalized after Coryell et al. (1963) to chondrites with values from Haskin et al. (1968). Values for the tholeiites from Schmitt et al. (1963), Frey & Haskin (1964), and Frey et al. (1968).

metamorphism, and spilitisation processes do not seem to alter simple geochemical parameters (Philpotts et al. 1969, Hart et al. 1970, Herrmann & Wedepohl 1970, Herrmann et al. 1974). Geochemical studies of basalts may therefore assist in the reconstruction of Lower Palaeozoic palaeoenvironments. Basalts from the Støren Group have, for this purpose, been sampled and analysed by Gale & Roberts (1972, 1974), who found mainly oceanic tholeiites in the group.

Geochemistry. – The total content of REE and the enrichment of the lighter rare-earth elements increase from oceanic tholeiites to alkali basalts (Schilling & Winchester 1969). In this way the different types of basalts obtain their own, special rare-earth element patterns. Dypvik (1974) and Dypvik & Brunfelt (1976) analysed the REE concentrations in some of the samples from the Støren greenstones. The samples were found to possess typical tholeiitic patterns, but it appeared difficult using such studies to differentiate between island-arc tholeiites and oceanic tholeiites. In Fig. 8 the REE patterns for sample H-1, H-4 and H-5 are shown. The samples are normalised to chondrites after a method described by Coryell et al. (1963). Values for H-1, H-4, and H-5 are taken from Dypvik (1974) and Dypvik & Brunfelt (1976). Values for the tholeiites are taken from Schmitt et al. (1963), Frey

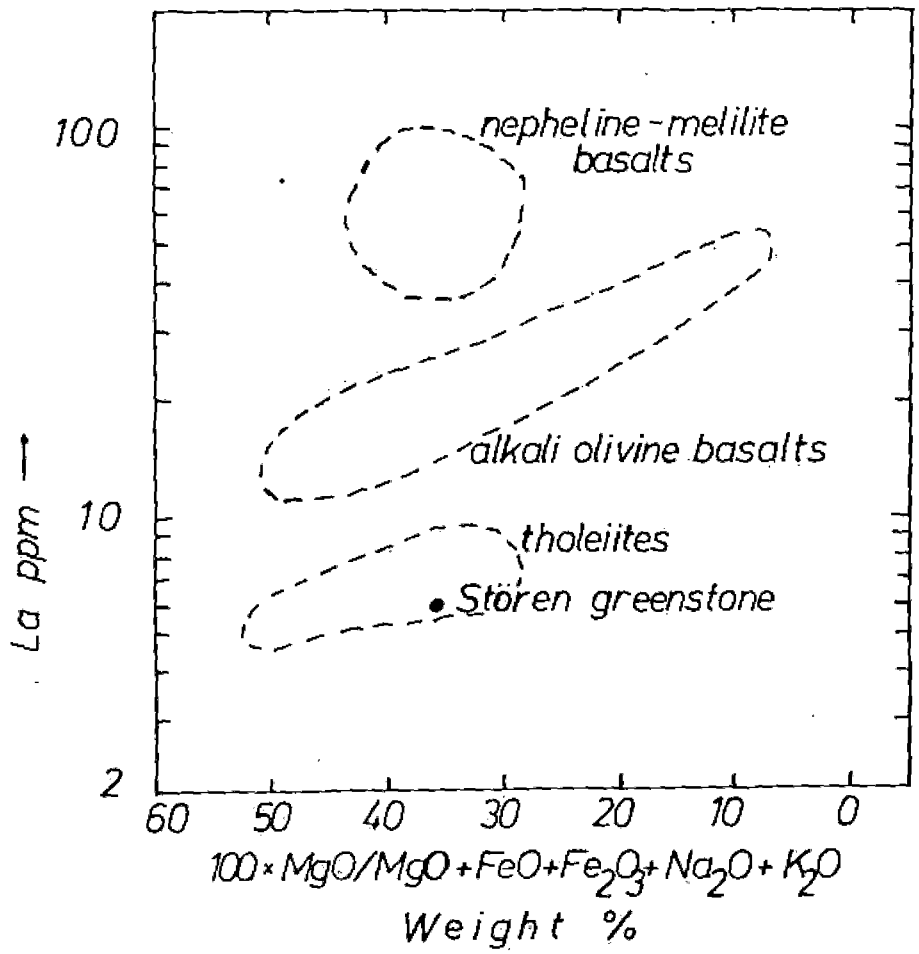

Fig. 9. The La content plotted against the fractionation index 100x MgO/MgO + FeO + Fe_2O_3 + Na_2O + K_2O, after Schilling & Winchester (1969). The average Støren greenstone is plotted in the figure.

& Haskin (1964) and Frey et al. (1968). Sample H-1 displays an island arc tholeiitic pattern, while H-4 and H-5 seem to be more akin to ocean-floor tholeiites.

Schilling & Winchester (1969) used different fractionation indexes plotted against the La content to classify basalts. Fig. 9 shows analysis of the average Støren greenstone plotted on one of their diagrams, and this indicates a clear tholeiitic affinity.

Pearce et al. (1975) published a $TiO_2 - K_2O - P_2O_5$ diagram which could discriminate between oceanic and non-oceanic basalts. This diagram is shown in Fig. 10, where the analysed samples from the Støren greenstone are plotted. They all plot in the field of oceanic basalts.

In a more refined classification by Jahn et al. (1974) the La/Sm ratios were used. In their figures, island-arc tholeiites and oceanic tholeiites define their own trends. The spilites from the Støren group have been plotted in

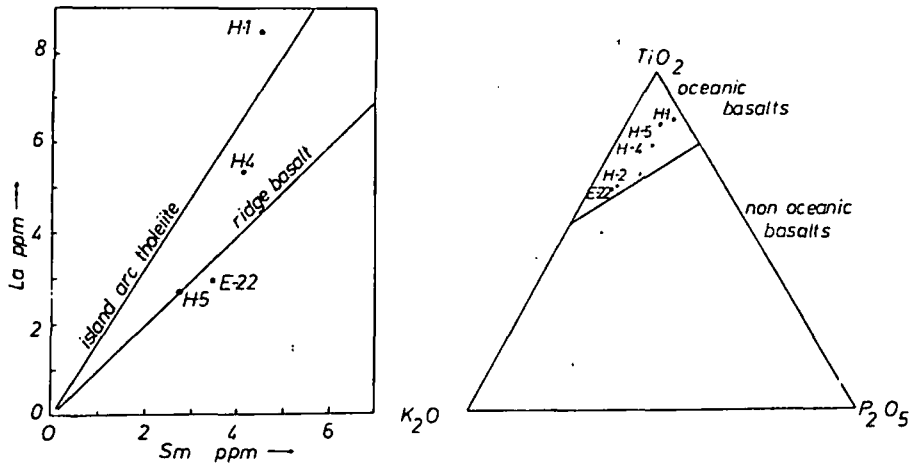

Fig. 10. The left figure is a correlation plot between La and Sm, after Jahn et al. (1974). Samples H-1, H-4, H-5, and E-22 from the Støren greenstones are plotted in the figure. The right figure is a TiO_2-K_2O-P_2O_5 diagram, after Pearce et al. (1975). The samples H-1, H-2, H-4, H-5 and E-22 are plotted in the figure.

one of these figures (Jahn et al. 1974), as shown in Fig. 10 (REE values from Dypvik & Brunfelt 1976). H-1 have a ratio typical for island-arc tholeiites, H-5 and E-22 have oceanic tholeiitic ratios, and H-4 display an intermediate affinity.

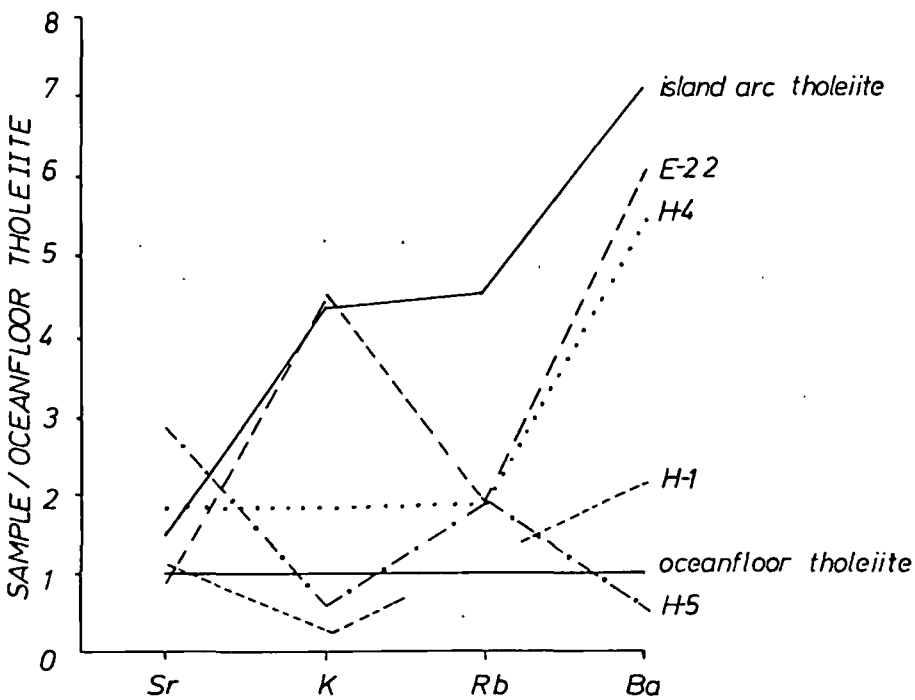

Fig. 11. Comparison plot after Jahn et al. (1974). Each sample is normalized to ocean-floor tholeiite. Values for the tholeiites from Jahn et al. (1974). E-22, H-1, H-4, and H-5 are samples from the Støren greenstones.

Seawater alteration does lead to changes in the concentrations of the incompatible elements (Hart 1969, Philpotts et al. 1969). An increasing potassium content and a decreasing K/Rb ratio have been found to be the result of such a process in young basalts (Hart 1969, Philpotts et al. 1969). Philpotts et al. (1969) also found that the Ba content could be changed in both positive and negative direction. No variations were found concerning Sr.

Hekinian (1971) showed that spilitisation may give textural, mineralogical, and chemical variations over short distances. By spilitic degradations of a tholeiitic basalt, Vallance (1974) discovered variation in the concentrations of several elements. Hart et al. (1970) claimed that rocks of low metamorphic grade could be regarded as closed systems.

By supposing that the lavas have undergone little seawater alteration, that an isochemical metamorphism has occurred, and that samples are large enough (about 500 g) so that eventual spilitisation alterations are negligible, it is possible to use K, Rb, Ba, and Sr in classification.

Hart et al. (1970) and Jahn et al. (1974) used Sr, K, Rb, and Ba, in order to produce a subdivision of basalts. Fig. 11 is from Jahn et al. (1974) and shows the different trends for various kinds of tholeiites. The samples are normalized to oceanic thoeliite. In Fig. 11 the following rocks are plotted: Oceanic tholeiite, island-arc tholeiite, E-22, H-1, H-4, and H-5. Values for the tholeiites are from Hart et al. (1970) and Jakěs & White (1972).

The low Rb values obtained for the Støren greenstones are uncertain. By ignoring these values, it is seen in Fig. 11 that E-22 will be classified as an island-arc tholeiite and H-1 and H-5 as oceanic tholeiites. Sample H-4 has a distribution akin to low potassium tholeiites (island-arc tholeiites, Jahn et al. 1974).

In Table 9 the Ni and Cr content for island-arc tholeiites and oceanic tholeiites is compared with the Ni and Cr concentrations determined in the greenstones. The Støren greenstones have Ni and Cr values similar to those in the oceanic tholeiites.

Hølonda andesite and Hareklett rhyolitic tuff are enriched in Ba, Rb, Sr, Th, U and REE, while they are depleted in V, Ni, Sc, Cr, and Co relative to the Støren greenstones (Table 5 and Dypvik & Brunfelt 1976).

Table 9. The Ni and Cr content in different tholeiites and samples from the Støren greenstone. Values for the tholeiites from Hart et al. (1970) and Jakěs & White (1972).

SAMPLE	Ni	Cr
Island arc tholeiite	0–30 ppm	0–50 ppm
Oceanic tholeiite	30–200 ppm	200–400 ppm
E–22	167 ppm	166 ppm
H–1	85 ppm	145 ppm
H–4	85 ppm	139 ppm
H–5	412 ppm	299 ppm

Discussion. – The different methods of classification used classify the lavas from the Støren Groups as tholeiites. A further subdivision, however, appears to give divergent results.

REE pattern comparisons classify H-1 as island-arc tholeiite and H-4 and H-5 are grouped together with oceanic tholeiites.

La/Sm ratios classify H-1 as an island-arc tholeiite, E-22 and H-5 as oceanic tholeiites, and H-4 somewhere in between.

Sr, K, Rb, and Ba classification fix E-22 and H-4 as island-arc tholeiites, while H-1 and H-5 have concentrations more akin to oceanic tholeiites.

All the samples from the Støren Group have Ni and Cr contents of the same order as oceanic tholeiites.

Based on the few executed analyses and the classifications used here, it seems very difficult to decide whether the basalts in the Støren Group represent island-arc tholeiites or oceanic tholeiites. This can be due to chemical seawater alterations, metamorphism, or spilitisation. The classification problem may also be connected with the extension of the principle of actuality on which these classifications are based.

Gale & Roberts (1972, 1974) presented several trace-element analyses of Lower Ordovician basaltic rocks from different areas in the Norwegian Caledonides. Based on Y, Ti, and Zr determinations they classified the basalts using a method presented by Pearce & Cann (1971, 1973). The lavas were mainly classified as oceanic tholeiites, but low potassium tholeiites were found in the Løkken and Grong areas. In 1974, Hart et al. showed that seawater alteration may lead to some changes in TiO_2 and Zr content and that the Y concentrations were not changed. The process of spilitisation has been shown to lead to notable changes in the TiO_2, Zr, and Y contents (Vallance 1974). Combining these results with the geochemical data presented above, it seems doubtful if the tholeiites can be classified and interpreted to the extent done by Gale & Roberts (1974).

Sediments overlying the Støren greenstone

Vanadium, scandium, nickel, cobalt, manganese, and titanium (V, Sc, Ni, Co, MnO and TiO_2). – As mentoned earlier, TiO_2, MnO, V, Sc, Ni, and Co are enriched in the Støren greenstones, while the younger more acidic volcanics, the Hølonda andesite, and the Hareklett rhyolite contain smaller quantities of these elements (Tables 3 and 5, Fig. 12).

In the sediments also the TiO_2, MnO, V, Sc, Ni, and Co concentrations decrease from peak values in Krokstad shale and sandstone towards the youngest layers (Fig. 12, Tables 3 and 5). Such similarities between the volcanics and sediments in the Trondheim Region indicate a relationship between these deposits.

Fig. 12. Stratigraphical distributions of TiO_2 (the upper figure), Ba (the middle figure), and Sr (the lower figure) in sediments and volcanics from the Trondheim Region. Solid line the Horg profile, dotted line the Lundesokna profile, and broken line volcanic rocks.

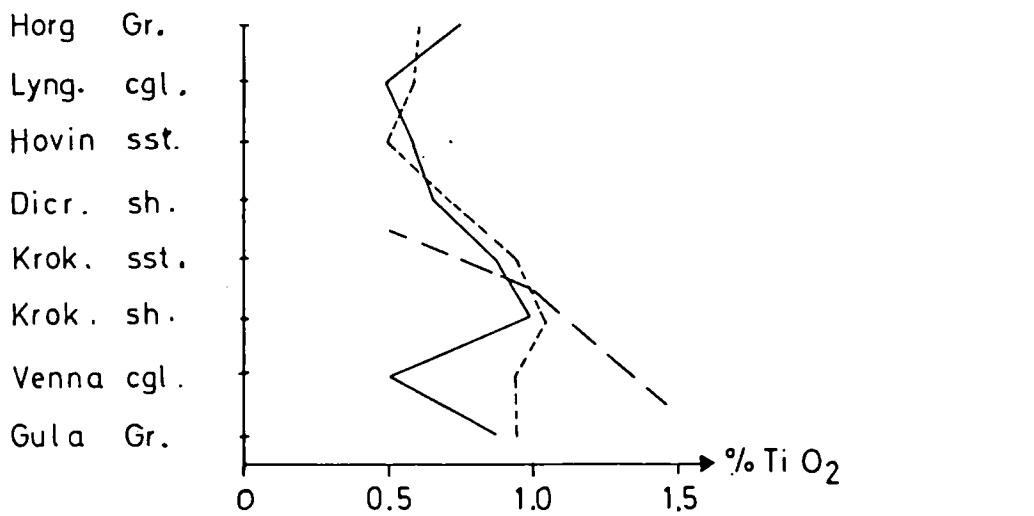
Horg Gr.
Lyng. cgl.
Hovin sst.
Dicr. sh.
Krok. sst.
Krok. sh.
Venna cgl.
Gula Gr.
% Ti O2
0
0.5
1.0
1.5

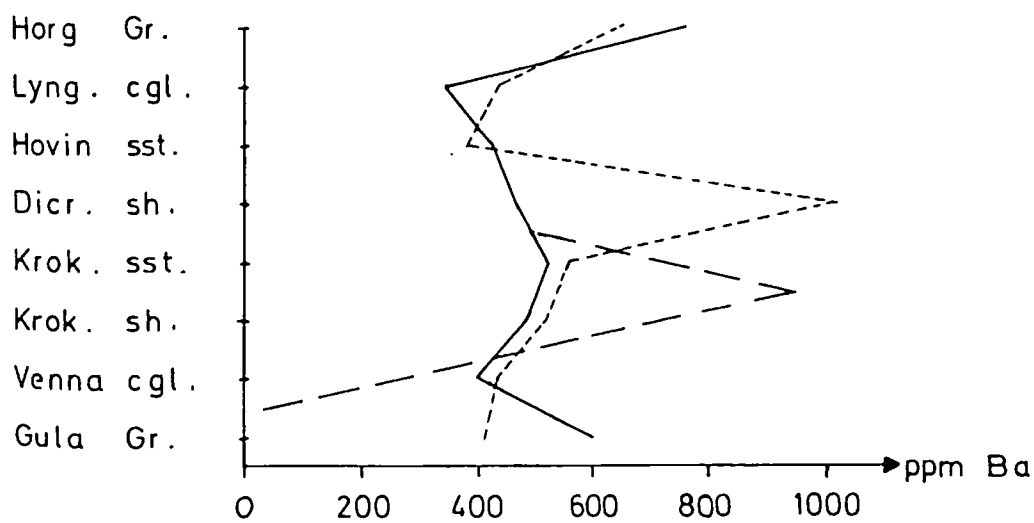
Horg Gr.
Lyng. cgl.
Hovin sst.
Dicr. sh.
Krok. sst.
Krok. sh.
Venna cgl.
Gula Gr.
ppm Ba
0
200
400
600
800
1000

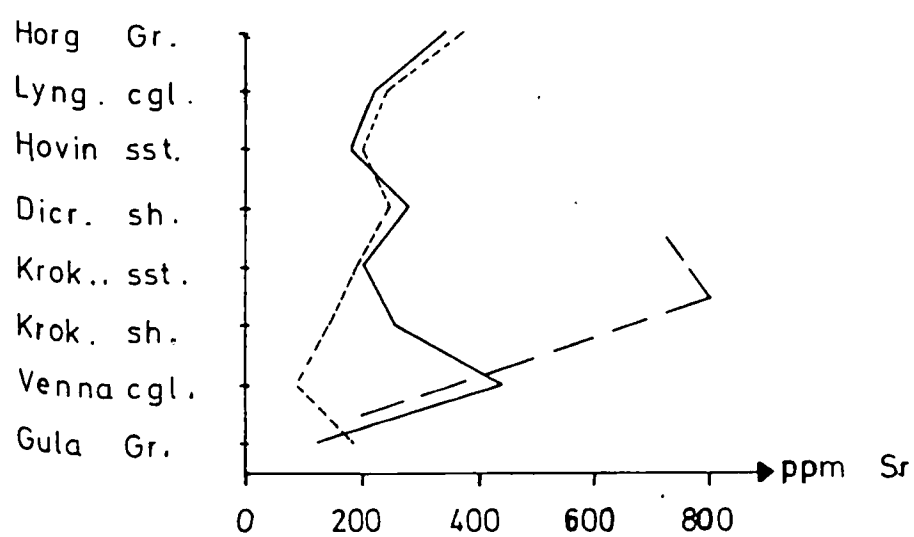
Horg Gr.
Lyng. cgl.
Hovin sst.
Dicr. sh.
Krok.. sst.
Krok. sh.
Venna cgl.
Gula Gr.
ppm Sr
0
200
400
600
800

There exists positive correlation between TiO_2 and minerals enriched in the Støren greenstones such as: TiO_2–Chlorite (0.55) and TiO_2–Albite (0.47). Co and Ni are also well correlated with MgO, 0.79 and 0.76 respectively. Sc correlates well with Mg (0.77), TiO_2 (0.79), and Co (0.90). Good correlation also exists between V and TiO_2 (0.93), V and Zn (0.85), V and Sc (0.95), and V and Co (0.90). These results, combined with poor correlation between $C_{org.}$ and V for samples from the Horg profile, indicate that minor amounts of V are enriched with organic material, and that TiO_2, MnO, V, Sc, Ni, and Co are mainly found in clastic greenstone debris. It is reasonable to suppose that after eruption, chloritization and elevation of the greenstone took place. Later these rocks were eroded and the products of erosion were deposited as the Krokstad shale and sandstone.

By supposing that the Krokstad shale is a mixture of an average shale and the Støren greenstone it is possible to estimate the minimum content of volcanic Støren greenstone debris in these samples. Such estimates, based on the Sc, V, Co, and Ni contents, indicate that at least 30–40 % of the Krokstad shale samples are made up of debris from such volcanic rocks.

Barium (Ba). – In the Trondheim Region Ba does not display any specific trend, Fig. 12. The concentrations are similar in the two profiles, except in the Dicranograptus shale where the samples from Lundesokna contain 2–3 times as much Ba as those from the other profile. Correlation beween Ba and Al_2O_3 (0.54) and K_2O (0.70) suggests that Ba is found in the clay fraction. Ba enrichment in the Dicranograptus shale from Lundesokna is probably due to the great content of organic carbon in these samples. A high content of organic carbon is clearly seen in thin section. In modern sediments it is usual to find joint enrichments of organic material and Ba (Boström et al. 1973). The mean content of Ba in the Trondheim sediments is 527 ppm, while average values for shale are 546 ppm (Puchelt 1969).

Strontium (Sr). – The Sr variations in the two profiles from the Trondheim Region are rather similar, except in the Venna conglomerate and the Krokstad shale, where the Horg samples are more enriched than those from Lundesokna (Fig. 12).

The high values in the Venna conglomerate are probably due to higher calcite contents in the samples from the Horg profile. The difference in the Krokstad shale indicates that this group from the Lundesokna profile ($\frac{Sr \cdot 10^3}{Ca} = 8.3$) has lost more Sr by recrystallization or contains more basaltic debris than the one from the Horg area ($\frac{Sr \cdot 10^3}{Ca} = 10.5$). A higher albite content in the Horg layers may also explain Sr enrichments. The correlation coefficient between Sr and CaO, 0.46, may suggest that the calcite has lost Sr during recrystallization. Sr present in albite will also lead to low Sr–CaO correlation.

The samples from the Trondheim Region consist of 250 ppm Sr as an average, while the average for shale is 300 ppm (Taylor 1965).

Zinc (Zn). – The Zn variations in the two profiles display analogous stratigraphical distributions, except in the Venna conglomerate and Dicranograptus shale, where samples from the Lundesokna profile have higher Zn concentrations than those from the Horg profile (Fig. 13).

From the Krokstad shale to the top of the profile there is a decrease in the Zn concentration. The volcanics display a similar trend. Some correlation between Zn and Fe_2O_3, P_2O_5, Ba, V indicates that some of the Zn is found in chlorite. Chlorites found in other parts of the world are reported to be enriched in Zn (Lee et al. 1966), because Zn may substitute for Mg and/or Fe in the octahedral layers.

The samples from the Dicranograptus shale in the Lundesokna area contain much organic carbon, as described earlier. Zn enrichments in this horizon may be a result of reducing environments and organic activity. Zn may be concentrated in sulphides and organic material (Vine & Tourtelot 1970).

Much Zn is also detected in magnetites and chromites from other areas (Dissanayake & Vincent 1972, Pearre & Heul 1960). Variations in these minerals would therefore create Zn variations.

The sediments contain 100 ppm Zn as an arithmetic mean, and the same concentration is found in the average shale (Taylor 1965).

Uranium, thorium, and organic carbon (U, Th and $C_{org.}$). – U and Th display a stratigraphical distribution which is akin to those of the volcanic rocks, with enrichments in the youngest layers (Fig. 13), while $C_{org.}$ in the Horg profile does not display any specific pattern except for peak values in the Gula Group and in the Dicranograptus shale (Table 5).

Good correlations between U and Th (0.91), U and K_2O (0.85), and Th and K_2O (0.88) probably mean that U and Th are associated with the clay fraction, either with heavy minerals of this size or with the clay minerals themselves. The correlation may surely also be an expression for variations in the source material.

The samples from the Trondheim Region are on the average made up of 8.6 ppm Th and 2.5 ppm U. These values are smaller than those for average shale which consists of 12 ppm Th and 4 ppm U, and indicates that much of the Trondheim sediments are made up of U and Th poor greenstone debris.

All of the analyzed samples have Th/U values between 2 and 5 (Fig. 14), which is typical of partly weathered and leached rock material (Adams & Weaver 1958).

Increasing Th/U ratios up-succession from the Venna conglomerate to the Krokstad sandstone may show that the sediments are becoming more mature or that the concentration of basaltic debris in the samples is decreasing. The low ratios in the Dicranograptus shale may be explained by

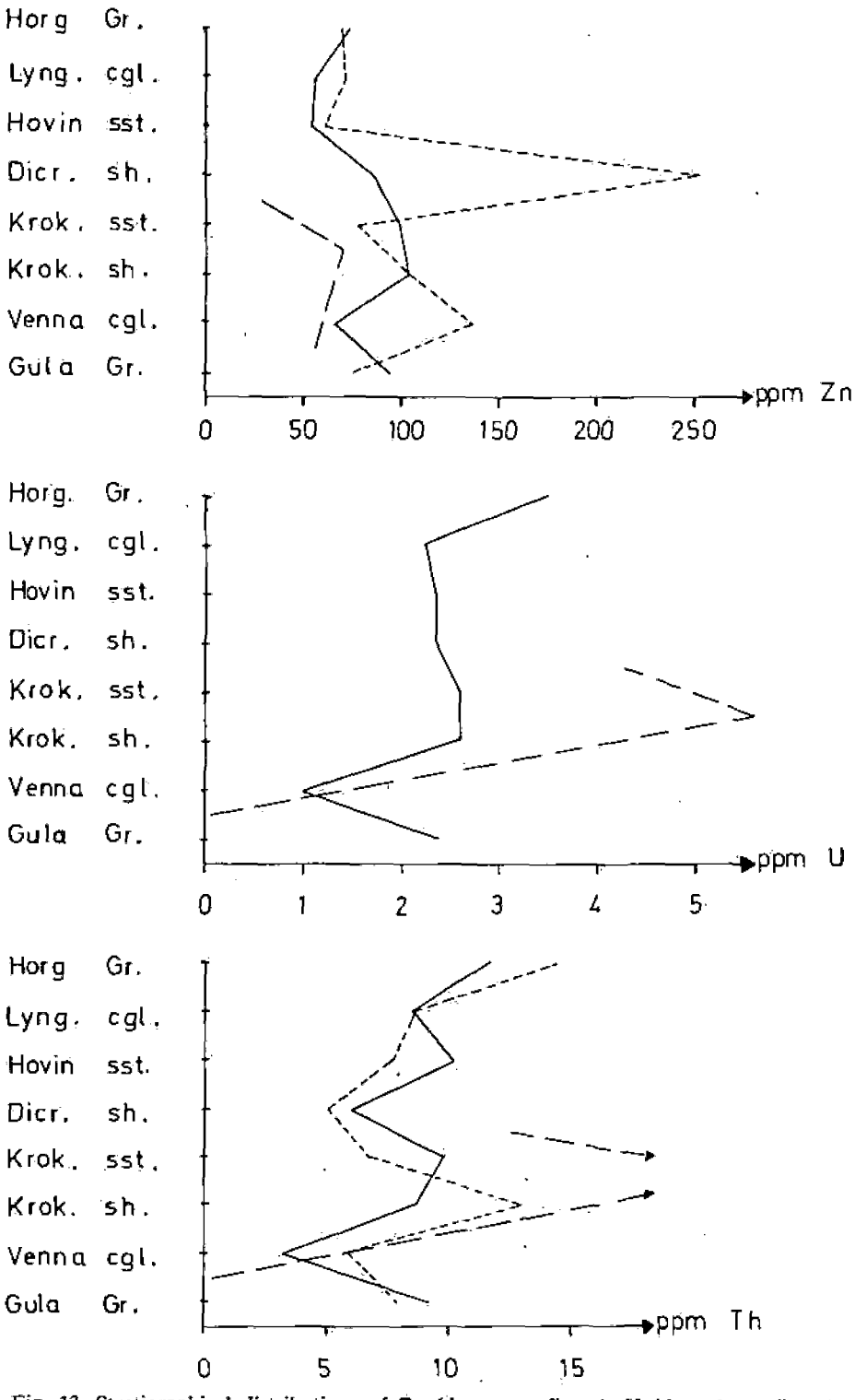

Fig. 13. Stratigraphical distributions of Zn (the upper figure), U (the middle figure), and Th (the lower figure) in sediments and volcanics from the Trondheim Region. Solid line the Horg profile, dotted line the Lundesokna profile, and broken line volcanic rocks.

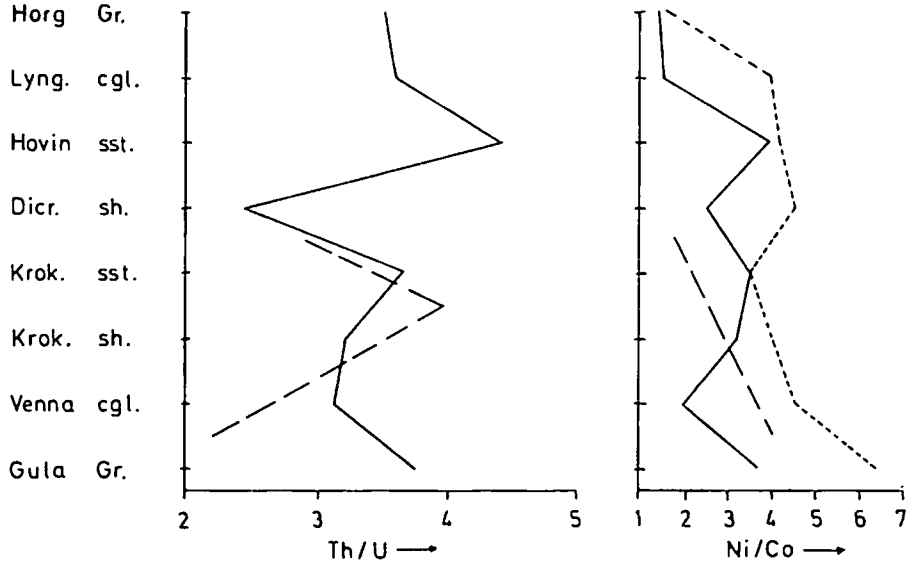

Fig. 14. Stratigraphical distribution of the Th/U ratio (left) and the Ni/Co ratio (right) in sediments and volcanics from the Trondheim Region. Solid line the Horg profile, dotted line the Lundesokna profile, and broken line volcanic rocks.

the $C_{org.}$ enrichment in this bed. In a reducing environment like this it is possible to get a U fixation, which will lead to a decrease in the Th/U. The Hovin sandstone has the highest Th/U ratios in the Trondheim Region. Following Adams & Weaver (1958), this should mean that these layers represent the most mature sediments in the Horg area. It may also be the result of a minor amount of greenstone debris in these beds.

Geochemical comparison of the two profiles from the SW Trondheim Region. – A closer study of the MnO, Cr, K/Rb, and Ni/Co distributions indicates differens between the depositional environments represented by the two profiles from the Trondheim Region.

The samples from the Horg profile consist always of the same amount or even more MnO than those from the Lundesokna area (Table 3). This MnO enrichment may be due to precipitation of MnO_2 in more oxidizing environments, or be a result of greater amounts of basaltic greenstone debris in these samples.

The variations in the Ni/Co ratios (Fig. 14), however, show something different. The stratigraphical Ni/Co variations are in both profiles similar to the magmatic rocks; decreasing concentrations in the younger layers. The samples from the Lundesokna profile have, however, generally higher Ni/Co ratios than samples from the Horg profile. According to Carvajal & Landergren (1969), this suggests that the Horg profile represents the most oxidizing environment, or is the poorest in basaltic greenstone debris of the two profiles.

If this result is combined with that of the MnO distribution, it seems reasonable to conclude that the sediments from the Horg profile were deposited during more oxidizing environments than the sediments from Lundesokna.

In modern oceanic sediments, and also in older rocks, the Cr distributions are controlled to a great extent by detritic material and not so much by the physical-chemical characteristics of the depositional environment (Turekian & Imbrie 1966, Cronan 1969, Chester et al. 1970, Curtis 1969, Bjørlykke 1974b). Minor enrichments of heavy minerals, especially chromite and magnetite, in the samples from the Horg profile, are a possible explanation for the Cr enrichments in these layers. This indicates that these samples are richer in ultrabasic debris or represent more winnowed deposits than those from the Lundesokna profile.

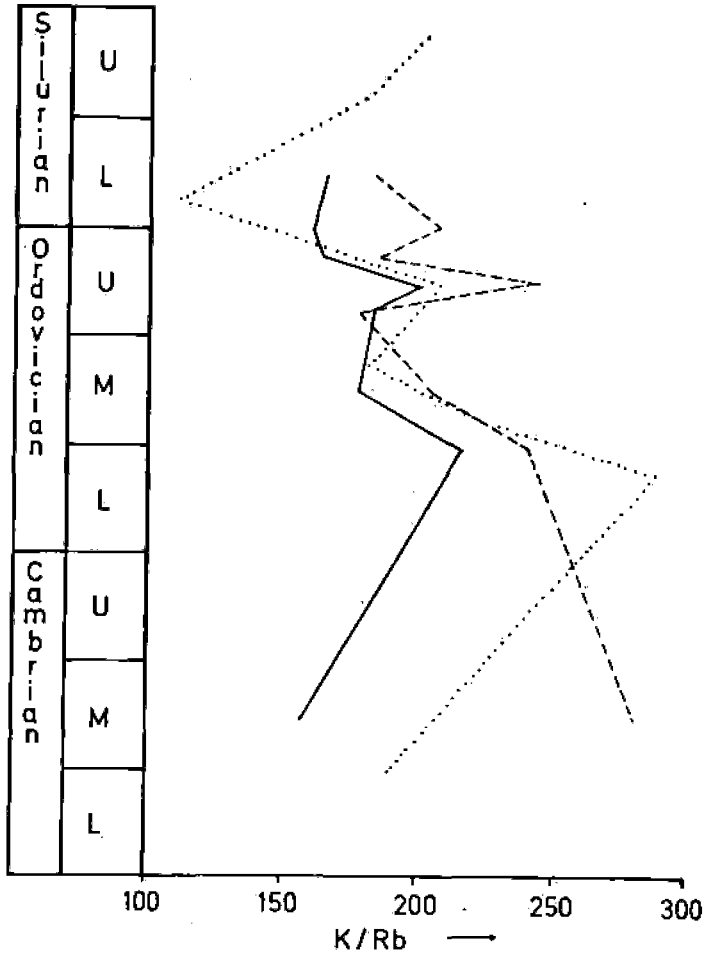

Fig. 15. Stratigraphical variation of the K/Rb ratio in sediments from the Trondheim Region and shales from the Oslo Region. Solid line the Horg profile, broken line the Lundesokna profile, and dotted line shales from the Oslo Region.

The K/Rb ratios in the samples from the Trondheim Region show a decrease upwards in both profiles, and this probably reflects the 'magmatic development from basaltic to rhyolitic and andesitic rocks' (Fig. 15). The samples from Lundesokna have the highest K/Rb ratios in all horizons, except in the Krokstad sandstone. This indicates that the sediments from the Lundesokna profile consist of less leached, more immature material or contain more basaltic debris than those from the Horg profile.

Summary of Trondheim Region geochemistry

The Middle Ordovician-Lower Silurian sediments from the SW Trondheim Region contain much basaltic greenstone debris. The Krokstad shale is estimated to be made up of at least 30–40 % of such debris, the real amount probably about 50–60 %. After eruption and erosion of the different types of volcanic rocks, their denudation products were transported to the basin. The geochemical characteristics of the different volcanics are found in the somewhat younger sediments. The geochemical distributions clearly indicate a decreasing influx of TiO_2, MnO, V, Sc, Ni and Co rich and U, Th, Rb & K poor greenstone debris, similar to the Støren greenstone, towards the younger layers.

Compared with the samples from the Lundesokna profile, those from Horg seem to reflect more oxidizing environments where more winnowed and leached material was deposited.

Oslo Region

Cobalt and the nickel/cobalt ratio (Co, Ni/Co). – The Co distribution in the Oslo Region shows two peak values; one in the interval stage 4aβ–4b and one in the interval stage 8–9 (Fig. 16). The sulphide-rich beds from 1c to 3c possess small amounts of Co, which indicates that only small amounts of Co are found in sulphides. The peak values in Fig. 16 match, however, peak values in the chlorite distribution, Fig. 3. This indicates that much Co is found in chlorite and that variations in Co concentrations may correspond to fluctuations in the chlorite content. The assumptions are further confirmed by the correlation established between Co and Fe (0.87) and Co and MgO (0.60). The correlation coefficient between Co and Ni, 0.75, indicates a common occurrence.

Bjørlykke (1974a) reported Ni enrichments in sulphuric Cambrian beds, and noted that Ni is found both in the silicate and sulphide face. Low Ni/Co values are found in Middle Cambrian (1c–1d), Middle Ordovician (4aα), Upper Ordovician (4c–5b), and Upper Silurian (8–9), while higher ratios pointing towards more reducing conditions are found in 2a–3a, 4aβ–4b, 6a–6c and 10, Fig. 16. As seen in the beds 4aβ–4b and 4c–5b the limestones have a shale-inverse behaviour. These differences may be expressions for Eh variations in the sedimentary basin.

The Ni/Co ratios are higher in the Oslo Region than in the SW Trondheim

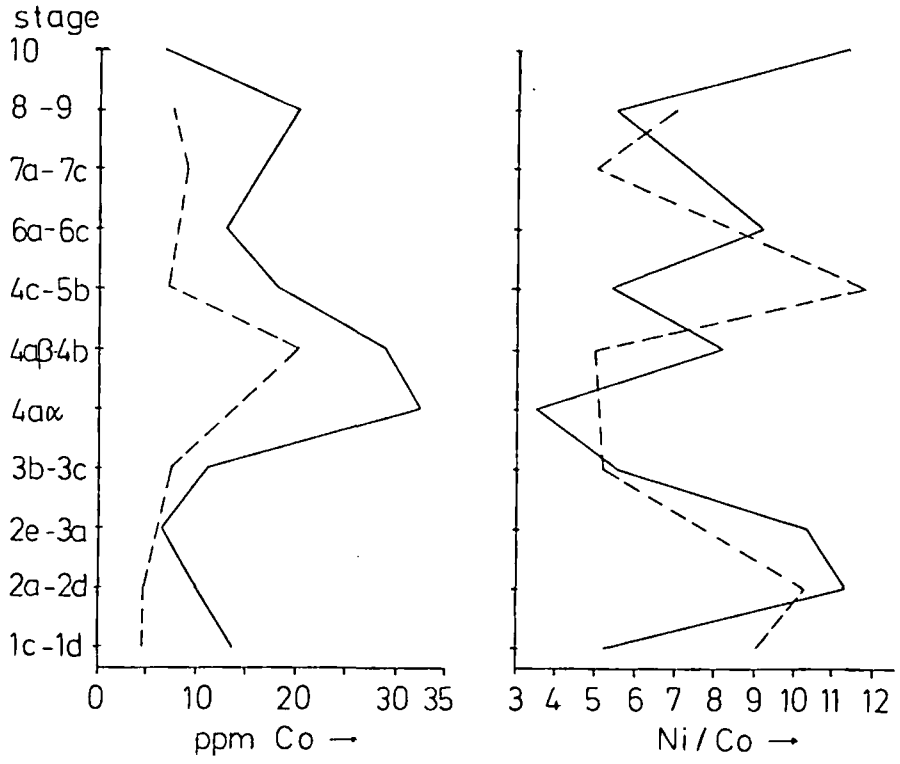

Fig. 16. Stratigraphical distribution of Co (left) and stratigraphical variation in the Ni/Co ratio (right) in shales and limestones from the Oslo Region. Solid line shales and broken line limestones.

Region, and this reflects the more stagnant conditions that dominated the epicontinental foreland, compared with the quicker sedimentation of coarser, less altered material in the Trondheim Region. In both areas Co and Ni are probably bound in chlorite, but in the Oslo Region some Ni is also found in the sulphides.

The shales from the Oslo Region consist on the average of 11 ppm Co.

Scandium (Sc). – Also in the sediments from the Oslo Region the Sc variations are believed to reflect variations in the source material, Fig. 17. Stages 4aα and 8–9 are rich in Sc; these beds were earlier shown to possess peak values of chlorite and Co. This, together with the fact that Sc is correlated with TiO_2, Al_2O_3, Fe_2O_3 and MgO makes it reasonable to assume that most of the Sc is probably bound in chlorite.

Sc seems to be rather immobile in the two different sedimentation environments represented by the Trondheim Region sediments and those from the Oslo Region. Changes in source material are the main factor controlling the stratigraphical Sc distribution both in the eugeosynclinal and the epicontinental basins.

The shales from the Oslo Region consist on the average of 10.7 ppm Sc.

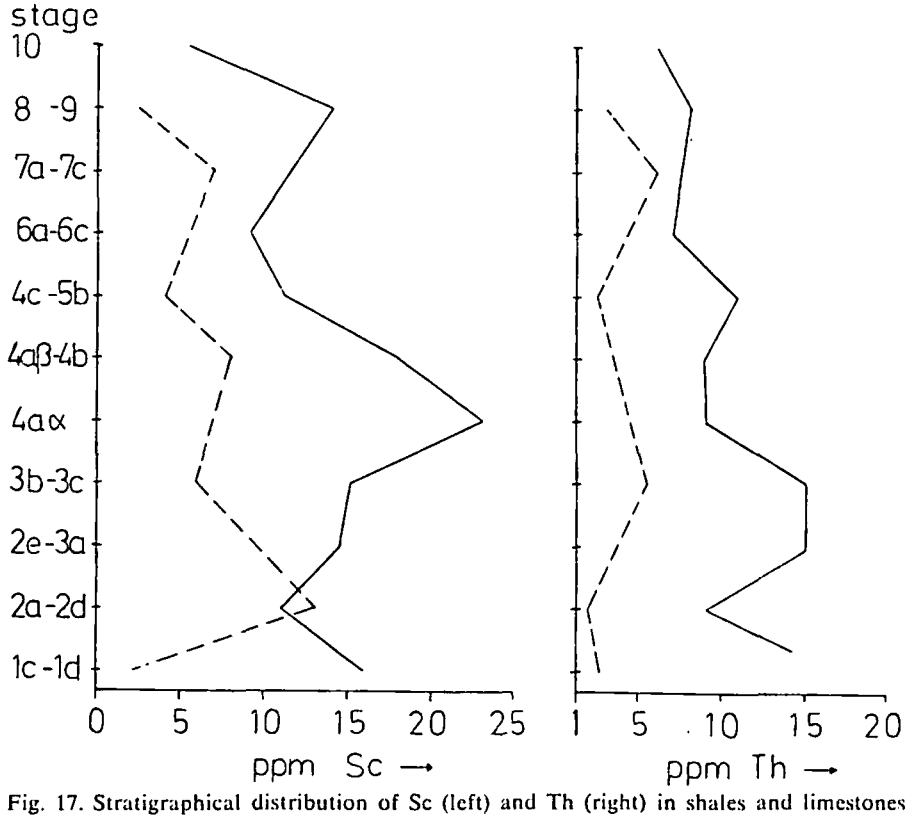

Fig. 17. Stratigraphical distribution of Sc (left) and Th (right) in shales and limestones from the Oslo Region. Solid line shales and broken line limestones.

Thorium (Th). – Some Th and U analyses have been carried out on samples from the Oslo Region by Bjørlykke (1974a). In the present work, however, only Th determinations have been made. The stratigraphical distribution of Th in the Oslo Region, Fig. 17, shows an upward decreasing trend. Th is well correlated with K_2O, 0.87, which means that Th, in this region too, is found in the clay fraction.

Th-enrichments in stage 2e–3c and 4c–5b, Fig. 17, may be related to the stratigraphical unconformities in the Oslo Region, Bjørlykke (1974a, Fig. 13). It is possible that there has been an increased reworking of sediments in connection with the shallowing of the water at these times.

The samples from the Oslo Region consist on the average of 8.0 ppm Th.

Conclusions

In the Hølonda-Horg area of the Trondheim Region both the chlorite and albite distributions in the sediments display a similar trend as in the volcanics. This suggests that the mineral composition of the sediments is strongly influenced by volcanic rock debris. The maximum chlorite and albite concentrations in the Krokstad shale correspond to a phase of uplift and ero-

sion. In the younger sediments the chlorite and albite content decrease, indicating a decreasing influx of basaltic debris in the basin.

Rates of sedimentation in the basin were high because of the influence of turbidity currents. In such environments also the trace elements and the geochemical variations will follow mineralogical variations and reflect erosion of local source rocks. The analyzed elements and geochemical parameters discussed do show close connection between sediments and volcanics. The element distributions in the sediments indicate a decreasing influx of basaltic material or an increasing influx of more acidic debris up-succession. This close relationship between sediments and volcanics is also indicated by calculations of the content of basaltic debris in the Krokstad shale. These estimates show that at least 20–40 % of these beds are made up of greenstone debris.

In a southwestern part of the Trondheim Region, samples from two different sections were analyzed, one from the Horg area and one from Lundesokna. Comparison of geochemical variations, like those of the Ni/Co- and K/Rb-ratios and of Cr and MnO, in the two sections, show that the Horg section contains more mature sediments, which were deposited during more ventilated conditions than those at the Lundesokna section.

While the composition of the sediments from the Trondheim Region can be a direct response to the local erosion of volcanic rocks, the sediments deposited in the epicontinental environments in the Oslo Region may also show some basic volcanic debris affinity. The appearance of chlorite together with an increased sodium content in the Oslo Region has been interpreted by Bjørlykke (1974) as due to derivation of sediment debris from a basic volcanic source in the northwest. Sc and Co enrichments in samples from stage 4aα and stage 8–9, also indicate the influx of probable greenstone derived material at that time, reflecting orogenic movements in the eugeosynclinal area in the north-west. Except for these variations the samples from the Oslo Region seem to be more mature and with chemical variations more influenced by the physical-chemical conditions prevailing during deposition, than those from the SW Trondheim area. The higher Ni/Co-ratios and Cr-concentrations in the Oslo Region samples indicate that they represent more reworked sediments, deposited during quiet, more stagnant conditions than those in the SW Trondheim area.

Some depositional similarities existed also for the Alum shales and Gula shales, being the oldest rocks studied in this work. In both regions there have been found shales with typical black shale characteristics. Those from the Gula Group, which contain more 'ultrabasic elements' as Fe, Mg, Cr, and Co, have been studied in some detail in this paper. It is concluded that some of the samples may consist of some serpentinitic debris and that the later metamorphism to the upper part of greenschist facies was not an isochemical one.

It is of great importance to classify the basalts of the Støren Group when trying to decide the tectonic environments more exactly. The classifications

do, however, lead to uncertain results, but in all classification systems used, the basalts display a tholeiitic affinity. The tholeiitic affinity of the Støren basalts, and the occurrence of andesite and rhyolite and of thick, immature sediments deposited by turbidity currents higher up in the succession, suggest that the sediments were deposited in a back-arc environment and thus confirm the conclusion of Gale & Roberts (1974) for this part of their Trondheim Supergroup.

Acknowledgements. – The present investigation is part of a thesis submitted for the cand. real. degree at Universitetet i Oslo in 1974. I wish to thank Professors K. Bjørlykke, K. S. Heier, and Chr. Oftedahl for valuable discussions and for making sample collections avaiable, and Drs. D. Bruton, B. Bue, and P. Jørgensen for their comments on the manuscript.

April 1976

REFERENCES

Adams, J. J. A. & Weaver, C. E. 1958: Th-to-U ratios as indicators of sedimentary process – an example of geochemical facies. *Am. Assoc. Petrol. Geol. Bull. 42,* 387–430.

Adams, J. S & Gasparini, P. 1970: Gamma-ray spectrometry of rocks. *Methods in Geochem. Geophys. 10,* Elsevier Publ. Comp., Amsterdam. 295 p.

Bjørlykke, K. 1974a: Depositional history and geochemical composition of Lower Palaeozoic epicontinental sediments from the Oslo Region. *Nor. Geol. Unders. 305,* 1–81.

Bjørlykke, K. 1974b: Geochemical and mineralogical influence of Ordovician Island Arcs on epicontinental clastic sedimentation. A study of Lower Palaeozoic sedimentation in the Oslo Region, Norway. *Sedimentology 21,* 251–272.

Bjørlykke, K. & Dypvik, H. 1975: Geochemical and mineralogical response to the evolution of the Caledonian geosyncline in eugeosynclinal and epicontinental sediments in Norway. *Proceeding IX Internat. Sed. Congr. Nice, Theme 4,* 21–26.

Blake, D. H. 1962: A new Lower Ordovician Gaptolite Fauna from the Trondheim Region. *Nor. Geol. Tidsskr. 42,* 223–237.

Bostrøm, K., Joensuu, O., Moore, C., Bostrøm, B., Dalziel, M. & Horowitz, A. 1973: Geochemistry of barium in pelagic sediments. *Lithos 6,* 159–174.

Brunfelt, A. O. & Steinnes, E. 1971: Determination of rare earths in silicate rocks by epithermal neutron activation and a simple group separation. *J. Radioanal. Chem. 13,* 11–20.

Carvajal, M. C. & Landergren, S. 1969: Marine sedimentation process. The interrelationships of manganese, cobalt and nickel. *Stockh. Contr. Geol. 18,* 99–122.

Chadwick, B., Blake, D. H., Beswick, A. E. & Rowting, J. W. 1962: The Geology of the Fjeldheim-Gåsbakken Area, Sør-Trøndelag. *Nor. Geol. Unders. 223,* 41–60.

Chaloupský, J. 1962: Notes on the geology of an area west of Støren. *Nor. Geol. Unders. 223,* 61–66.

Chaloupský, J. 1969: Geology of the Hølonda-Hjulsjøen Area. Trondheim region. *Nor. Geol. Unders. 266,* 277–304.

Chester, R. & Messiha-Hanna, R. G. 1970: Trace element partition patterns in North Atlantic deep-sea sediments. *Geochim. Cosmochim. Acta 34,* 1121–1128.

Coryell, A. D., Chase, J. W. & Winchester, J. W. 1963: A procedure for geochemical interpretation of terrestrial rare-earth abundance patterns. *J. Geophys. Res. 68,* 559–566.

Cronan, D. S. 1969: Inter-element associations in some pelagic deposits. *Chem. Geol. 5,* 99–106.

Curtis, C. D. 1969: Trace element distribution in some British Carboniferous sediments. *Geochim. Cosmochim. Acta 33,* 519–523.

De Vore, G. 1955a: The role of absorption in the fractionation and distribution of elements. *Journ. Geol. 63,* 159–190.

De Vore, G. 1956b: Crystal growth and the distribution of elements. *J. Geol. 63,* 471–494.

Dewey, J. F. 1969: Evolution of the Appalachian/Caledonian orogen. *Nature 222*, 124–129.

Dissanayake, C. B. & Vincent, E. A. 1972: Zinc in rocks and minerals from the Skaergaard intrusion, East Greenland. *Chem. Geol. 9*, 285–297.

Dypvik, H. 1974: Geokjemiske studier av bergarter fra Trondheimsfeltet og Oslofeltet. Unpublished cand. real. thesis, Universitetet i Oslo. 184 p.

Dypvik, H. & Brunfelt, A. O. 1976: Rare-earth elements in Lower Palaeozoic epicontinental and eugeosynclinal sediments from the Oslo and Trondheim regions. *Sedimentology 23*, 363–378.

Flanagan, F. J. 1973: 1972 values for international geochemical reference samples. *Geochim. Cosmochim. Acta 37*, 1189–1200.

Frey, F. A. & Haskin, L. A. 1964: Rare earths in oceanic basalts. *J. Geophys. Res. 69*, 775–780.

Frey, F. A., Haskin, M. A., Poetz, J. A. & Haskin, L. A. 1968: RE abundances in some basic rocks. *J. Geophys. Res. 73*, 6085–6098.

Gale, G. H. & Roberts, D. 1972: Palaeogeographical implications of greenstone petrochemistry in the southern Norwegian Caledonies. *Nature Phys. Sci. 238*, 60–61.

Gale, G. H. & Roberts, D. 1974: Trace element geochemistry of Norwegian Lower Palaeozoic basic volcanics and its tectonic implications. *Earth Planet. Sci. Lett. 22*, 380–390.

Gibbs, R. J. 1965: Error due to segregation in quantitative clay mineral X-ray diffraction mounting techniques. *Am. Miner 50, 741–751.*

Gordon, G. E., Randle, K., Goles, G. G., Corliss, J. B., Beeson, M. H. & Oxley, S. S. 1968: Instrumental activation analysis of standard rocks with high-resolution of X-ray detectous. *Geochim. Cosmochim. Acta 32*, 369–396.

Grim, R. E. 1968: *Clay Mineralogy*. 2nd ed. McGraw-Hill, New York. 384 pp.

Hadding, A. 1932: The Graptolites from Gauldalen. Skr. Norske Vidensk.-Akad. i Oslo, Mat.-naturv. kl., 1937, no 4, 97 p.

Hart, S. R. 1969: K, Rb, Cs contents and K/Rb, K/Cs ratios of fresh and altered submarine basalts. *Earth Planet. Sci. Lett. 6*, 295–303.

Hart, S. R., Brooks, C., Krogh, T. E., Davis, G. L. & Nava, D. 1970: Ancient and modern volcanic rocks: a trace element model. *Earth Planet. Sci. Lett. 10*, 17–28.

Hart, S. R., Erlank, A. J. & Kable, E. J. O. 1974: Sea floor basalt alteration. Some chemical and Sr isotopic effects. *Contr. Min. Pet. 44*, 219–230.

Haskin, L. A., Wildeman, T. R. & Haskin, M. A. 1968: A procedure for the determination of the rare earths by neutron activation. *J. Radioanal. Chem. 1*, 337–348.

Hekinian, R. 1971: Petrological and geochemical study of spilites and associated rocks from St. John, U. S. Virgin Islands. *Geol. Soc. Am. Bull. 82*, 659–682.

Herrman, A. G. & Wedepohl, K.H. 1970: Untersuchungen an spilitischen Gesteinen der variskischen Geosynkline in Nordwestdeutschland. *Contr. Min. Pet. 29*, 255–274.

Herrman, A. G., Potts, M. J. & Krake, D. 1974: Geochemistry of the rare earth elements in spilites from the oceanic and continental crust. *Contr. Min. Pet. 44*, 1–16.

Holtedahl, O. 1920: Tørkesprekker i den øvre del av den marine Silur i Bærum. *Nor. Geol. Tidsskr. 5*, 105–108.

Jahn, B. M., Shih, C. Y. & Murthy, V. R. 1974: Trace element geochemistry of Archean volcanic rocks. *Geochim. Cosmochim. Acta 38*, 611–627.

Jakěs, P. & Gill, J. 1970: Rare earth elements and the island arc tholeiitic series. *Earth Planet. Sci. Lett. 9*, 17–28.

Jakěs, P. & White, A. J. R. 1972: Major and trace element abundances in volcanic rocks of orogenic areas. *Geol. Soc. Am. Bull. 83*, 29–40.

Kuno, H. 1960: High-alumina basalt. *J. Petrol. 1*, 121–145.

Lee, D. E., Coleman, R. S., Bastron, H. & Smith, V. C. 1966: A two-amphibole glaucophane schist in the Franciscan formation, Cazadero area, Souoma Country, California. *U. S. Geol. Surv. Profess. Pap. 550c.* 148.

Müller, R. O. 1967: *Spektrochemische Analysen mit Röntgen fluoreszenz*. R. Oldenbourg, München-Wien. 315 p.

Neumann, B. R. & Bruton, D. L. 1974: Early middle Ordovician fossils from the Hølonda area, Trondheim Region, Norway. *Nor. Geol. Tidsskr. 54*, 60–115.

Norrish, K. & Taylor, R. M. 1962: Quantitative analyses by X-ray diffraction. *Clay Min. Bull 5*, 98–104.
Pearce, J. A. & Cann, J. R. 1971: Ophiolite origin investigated by discriminant analyses using Ti, Zr and Y. *Earth Planet. Sci. Lett. 12*, 339–349.
Pearce, J. A. & Cann, J. R. 1973: Tectonic setting of basic volcanic rocks determined using trace element analyses. *Earth Planet. Sci. Lett. 19*, 290–300.
Pearce, T. H., Gorman, B. E. & Birkett, T. C. 1975: The TiO_2–K_2O–P_2O_5 diagram: A method of discriminating between oceanic and non-volcanic basalts. *Earth Planet. Sci. Lett. 24*, 419–426.
Pearre, N. C. & Heul, A. V. 1960: Chromite and other mineral deposits in serpentine rocks of the Piedmont Upland, Maryland, Pennsylvania and Delaware. *U. S. Geol. Surv. Bull. 1082 K*, 707–833.
Philpotts, J. A., Schnetzler, C. C. & Hart, S. R. 1969: Submarine basalts: Some K, Rb, Sr, Ba, RE, H_2O, and CO_2 data bearing on their alteration, modification by plagioclase, and possible source materials. *Earth Planet. Sci. Lett. 7*, 293–299.
Puckett, H. 1969: Ba. In Wedepohl, K. H. (Ed.) *Handbook of Geochemistry, II–3*, 5601–5602. Springer-Verlag, Berlin.
Raade, G. 1972: Distribution of radioactive elements in the plutonic rocks of the Oslo Region. Unpubl. cand. real. thesis, Universitetet i Oslo.
Schilling, J. G. & Winchester, J. W. 1969: Rare earth contribution to the origin of Hawaiian lavas. *Contr. Min. Pet. 23*, 27–37.
Schmitt, R. A., Lasch, J. E., Mosen, A. W., Olehy, D. A. & Vasilevskis, J. 1963: Abundances of the fourteen rare earth elements, Sc, and Y in meteoric and terrestrial matter. *Geochim. Cosmochim. Acta 27*, 577–622.
Skaar, F. E. 1972: Orthocerkalksteinen (etasje 3c) i Oslofeltet. En undersøkelse av den mineralogiske og kjemiske sammensetning regionalt og stratigrafisk. Unpubl. cand. real. thesis, Universitetet i Oslo.
Strand, T. 1961: The Scandinavian Caledonides; a review. *Am. J. Sci. 259*, 161–172.
Størmer, L. 1967: Some aspects of the Caledonian geosyncline and foreland west of the Baltic Shield. *Quart. J. Geol. Soc. Lond. 123*, 183–214.
Taylor, S. R. 1965: The application of trace element data to problems in petrology. 133–214. *In* Ahrens, L. A., Press, F., Runcorn, S. K. & Urey, C. (Eds.) *Physics and Chemistry of the Earth 6*, Pergamon Press, Oxford.
Turekian, K. K. 1964: The marine geochemistry of strontium. *Geochim. Cosmochim. Acta 28*, 1479–1496.
Turekian, K. K. & Imbrie, J. 1966: The distribution of trace elements in deep-sea sediments of the Atlantic Ocean. *Earth Planet. Sci. Lett.* 1, 161–168.
Vallance, T. G. 1974: Spilitic degradation of a tholeiitic basalt. *J. Petrol. 15*, 79–96.
Vine, J. O. & Tourtelot, E. B. 1970: Geochemistry of black shale deposits – A summary report. *Econ. Geol. 65*, 253–272.
Vogt, J. H. L. 1888: Funn av Dictyonema ved Hjulsøen, Holtålen. Vidensk. Selsk. Christiania (Oslo) Forh. Oversikt over Videnskabsselskabets Møder i 1888.
Vogt, Th. 1940: Geological notes on the Dictyonema locality and the upper Gauldal districts in the Trondheim area. *Nor. Geol. Tidsskr. 20*, 171–192.
Vogt, Th. 1945: The geology of part of the Hølonda-Horg district, a type area in the Trondheim Region. *Nor. Geol. Tidsskr. 25*, 449–528.
Wilson, J. T. 1966: Did the Atlantic close and then re-open? *Nature 211*, 676–681.
Wolff, F. Chr. 1967: Geology of the Meråker area as a key to the eastern part of the Trondheim region. *Nor. Geol. Unders. 245*, 123–146.

PROGRAM REVIEW
for
DIVISION OF GEOTHERMAL ENERGY
U.S. Department of Energy

29 March 1979
Earth Science Laboratory
420 Chipeta Way
Salt Lake City, Utah

by

DEPARTMENT OF GEOLOGY & GEOPHYSICS
University of Utah

and

EARTH SCIENCE LABORATORY
University of Utah Research Institute
Salt Lake City, Utah

sulphide mineralizations in Scandinavian Caledonides in general. Contributions made so far in the field of ore geology relating to this deposit seem to be surprisingly few. As stated in his monograph on the geology of Sulit-

UNIVERSITY OF UTAH LIBRARIES

jelma region, Th. Vogt (1927) had planned to write another monograph dealing with the ore geology of the Sulitjelma deposit, but this was unfortunately never done owing to his sad and untimely demise. Ramdohr (1938) described the antimony-rich paragenesis from the Jakobsbakken ore body of the deposit. J. H. L. Vogt (1894), Th. Vogt (1927), and Kautsky (1953) presented their views regarding the geological setting of this famous deposit, as parts of their respective studies on the geology of the region. Recently, Wilson (1973) reviewed the present state of knowledge in this connection and gave his own assessment of the setting in the light of his detailed structural studies in the area. However, systematic and detailed studies covering many other aspects of the mineralization, particularly the geochemical studies, have been long awaited.

It has been the author's contention that, in view of the highly complex geologic history of this deposit, the only way to throw light on the primary mode of sulphide genesis in this region is to undertake an exhaustive chemical and geochemical study of its ores and the associated geologic environment. The present contribution represents but a test case of such a contention. Accordingly, greater stress has been laid in this paper on the genetic evaluation and other implications of the geochemical study of the deposit, while the methods, procedures, and results thereof have only been summarized briefly.

Geology of the deposit

The metasedimentary environment of the ore deposit belongs to the lower part of the Caledonian (Ordovician) succession of eugeosynclinal rocks and comprises a varied sequence of calcareous and aluminous pelitic-schists, quartzites, amphibolites etc. All these rocks are intruded by a huge gabbroic

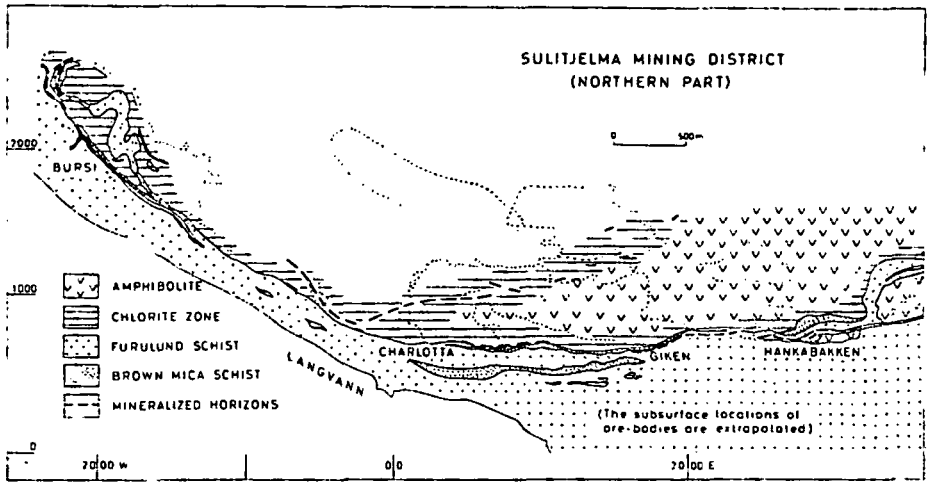

Fig. 1. Geological map of Sulitjelma mining district (northern part), Nordland, Norway. (Modified after Fr. Carlson, 1926–30).

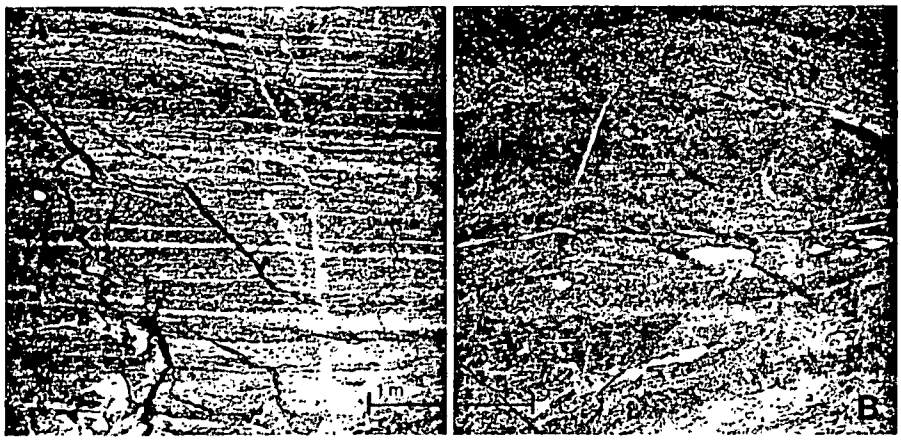

Fig. 3 (A). Typical disseminated pyritic ore exhibiting layered structure. Hankabakken ore body, Level 361 west.
Fig. 3 (B). Layers and bands of massive pyritic ore interstratified within Furulund mica schist, Giken ore body, Level-61 west.

mineralogic types of ores: the massive-pyritic ore, disseminated ore, and the pyrrhotite-chalcopyrite ore. The three ore types tend to be assimilated or intermixed in widely variable proportions in the different ore bodies. Figs. 3 and 4 exhibit some of the commonly observed physical and morphological characteristics of these ores in their subsurface expositions or in a representative hand specimen.

The mineralogy of the ores is, in general, remarkably simple. Varying proportions of pyrite, pyrrhotite, chalcopyrite, and sphalerite constitute the bulk of the different ore types. A number of minor and rare minerals,

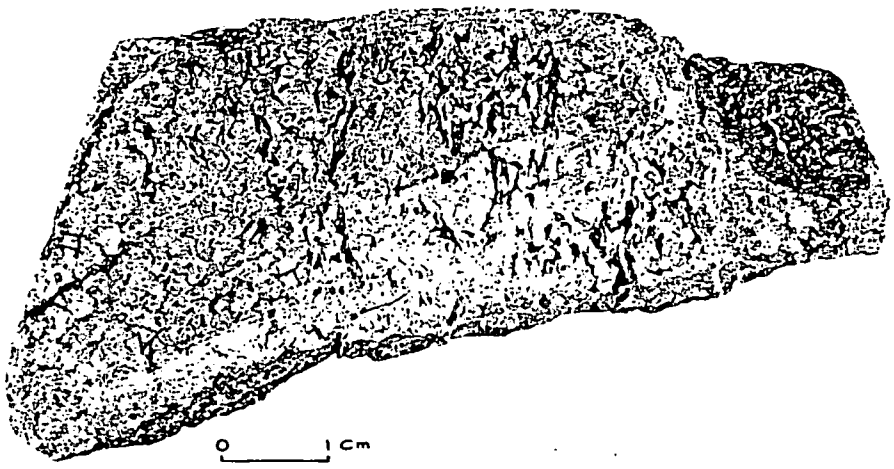

Fig. 4. Specimen photograph of typical coarse-grained massive pyritic ore from Giken ore body. Several lenticles of sericite-schist may be seen interstratified within the ore.

UNIVERSITY OF UTAH LIBRARIES

constituting hardly 2–3 % of the ore mass, are observed sparsely distributed in the ores; these include galena, arsenopyrite, tetrahedrite, molybdenite, mackinawite, bournonite, and many other sulpho-salts. The occurrence of a multitude of Cu-, Pb-, Ag-, As-, and Sb-sulphides and sulphosalts, and silver, gold, and antimony as native metals, was reported by Ramdohr (1938) from an antimony-rich paragenesis in Jakobsbakken ore body. The observed textures and structures in ores show that they have generally undergone varied effects of high-grade regional metamorphism.

Method of study

The geochemical investigation was carried out on the selected samples of ores and their constituent monomineralic sulphide-mineral fractions. The samples for the study were collected according to definite sampling schemes from four of the principal ore bodies of the deposit, namely Giken, Hankabakken, Charlotta, and Bursi. The ores from Jakobsbakken ore body lying in the now-abandoned southern part of the mining district have been studied only to a limited scale.

Analytical work on major, minor, and trace elements in the ores/ore minerals and host rocks was accomplished principally by the atomic absorption spectrophotometric method following well-tested techniques of Langmyhr & Paus (1968, 1970) in their own laboratory at Kjemisk institutt, Universitetet i Oslo; Norway. A high degree of accuracy of results was ensured from numerous replicate analyses of selected samples and available international standards.

Sulphur isotopic analyses were kindly undertaken by Prof. M. L. Jensen at Laboratory of Isotope Geology, University of Utah. A precision of ± 0.2 permil in the analytical results was obtained.

Results

In the major-elemental composition of ores, it is principally the analytical results of copper and zinc and their varying ratios that seem to have significant genetic implications. These are presented in Figs. 5 & 6.

The abundance of several minor and trace elements was determined in about 350 samples of different sulphide minerals from ores representing various ore types and ore bodies of the deposit.

The elements that were looked for in the various typomorphic minerals of ores and were determined quantitatively included Co, Ni, Mn, Mo, Cr, Ti, V, Ga, Cd, Ag, and Pb. A few others, such as Zn, Cu & Fe, were determined in selected major mineral fractions as a final check on the purity of analysed samples. As, Sb, Bi, Sn, and Se were determined semi-quantitatively. The results of all these analyses have already been presented earlier in detail (Rai 1971, 1972). Only a few critical results having significant genetic implications are presented in this paper. Fig. 7 depicts the distribu-

tion of cobalt and nickel in the pyrite and pyrrhotite fractions of ores from Charlotta and Bursi ore bodies, while Figs. 8A and 8B bring out the patterns of cobalt-nickel relations in different ore types and ore bodies of the deposit. The abundance of different elements in pyrites from different ore types/ore bodies are summarized in Table 1, while Table 2 summarizes the distribution-ratios of selected trace-elements among the typomorphic sulphide phases of various ore-types from different ore-bodies. Figs. 9 and 10 depict the patterns of partition-distribution of various trace-elements in different mineral pairs of the ores.

The results of sulphur-isotopic study of the deposit are shown in Figs. 11 and 12.

Discussion

Major element composition of the ores

The Sulitjelma ore, in general, represents a rich massive concentration of iron sulphides with subsidiary amounts of copper and zinc. All the other metals, notably lead, arsenic, antimony, tin, gold, silver, etc., tend to occur in minor to trace amounts.

Marked differences are observed in the base-metal composition of ores from different ore bodies of the deposit. The relevant results in this connection, as depicted in triangular diagram in Fig. 5A, show that a wide range of zinc-rich to zinc-poor ore bodies is represented in this deposit. No systematic trend in the spatial distribution of such ores or ore bodies is, however, discernible. Observed wide variations in base-metal composition of ores in different ore bodies of the deposit that are located so close to each other in the same geologic environment appear difficult to explain by observations made in the field. The distribution pattern of copper and zinc in the deposit (Fig. 5A) indicates some sort of progressive metal differentiation in the ore-forming fluids following different paths, most probably prior to the deposition of the ores itself. The observed pattern compares remarkably well with that reported for the basic rocks (Fig. 5B) by Sandell & Goldich (1943). Following Wilson & Anderson (1959), such an observation may be suggestive of primarily basic igneous parentage of the ore-forming fluids referred to above.

The various ore types show minor, yet distinctive, differences in their major metal values. The pyrrhotitic ores appear to be generally richer in base metals, particularly in copper, as compared to the massive-pyritic ores. The massive and disseminated pyritic ores, although differing markedly in their absolute content of copper and zinc, exhibit remarkably similar trends in their frequency distribution of Cu/(Cu+Zn) ratios (Fig. 6). This observation seems to be in significant contrast to that noted by Wilson & Anderson (1959) at Geco mine deposit of Canada, where the trends of Cu : Zn ratios for massive and disseminated ores are distinctly opposed to each other and are attributed to different pulses of ore-forming fluids. The two

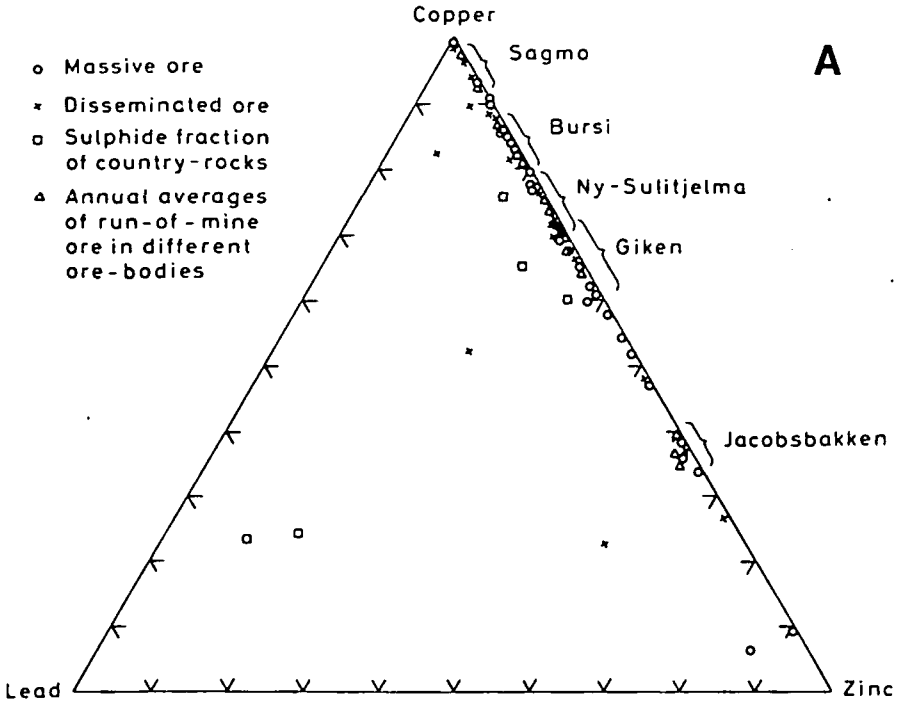

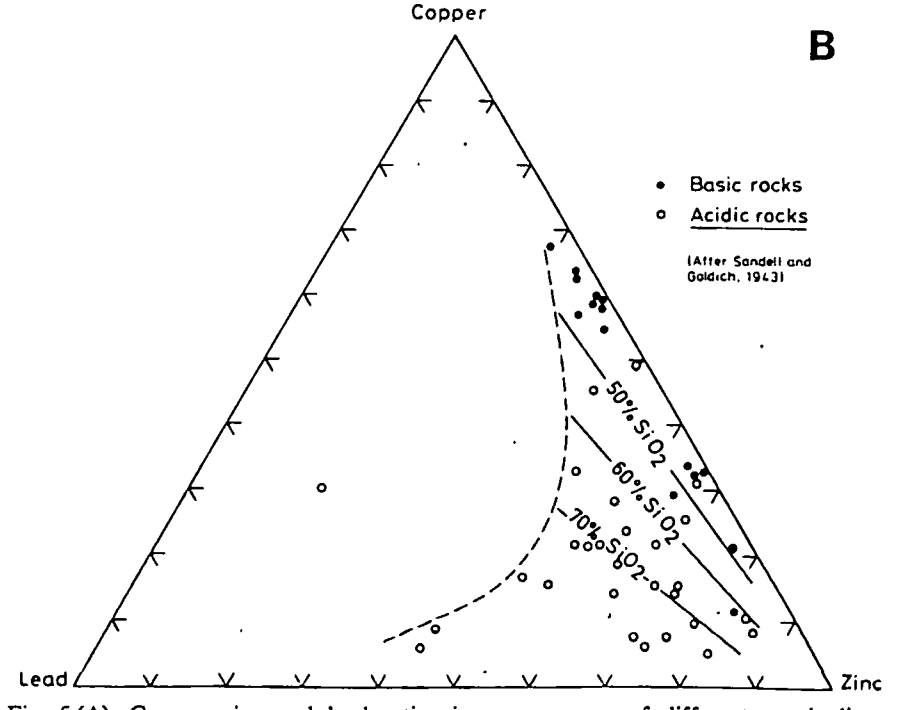

Fig. 5 (A). Copper, zinc and lead ratios in average ores of different ore bodies of Sulitjelma deposit.
Fig. 5 (B). Copper, zinc, and lead ratios in some igneous rocks. (After Sandell & Goldich 1943).

UNIVERSITY OF UTAH LIBRARIES

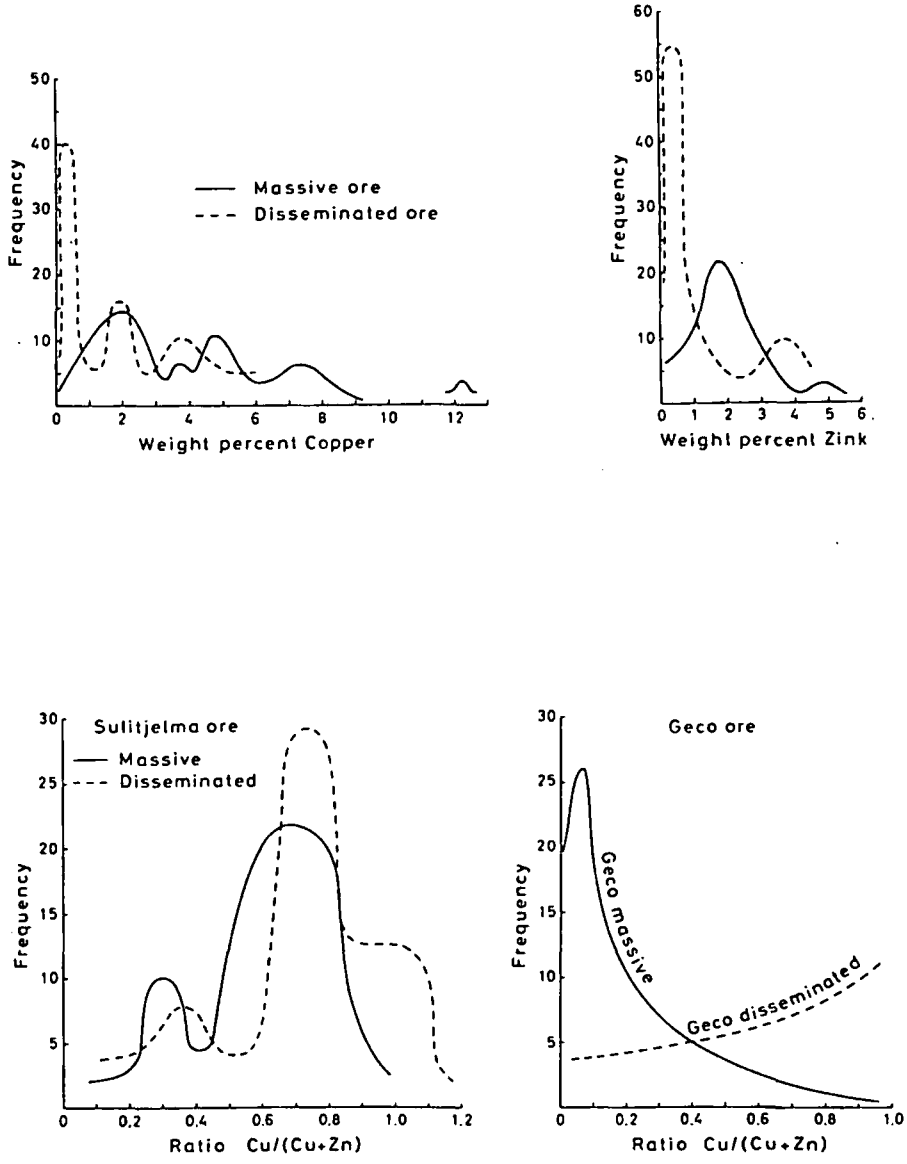

Fig. 6. Frequency distribution of copper: zinc ratios in the massive and disseminated ores of Sulitjelma deposit compared with that in Geco deposit, Canada.

ore types at Sulitjelma, by comparison, appear to be closely related to each other belonging, by and large, to the same pulse of ore-forming fluids.

Minor and trace-element composition of the ores

Abundances and patterns of distribution of various minor and trace elements in the ores and their typomorphic sulphide minerals representing various ore types and ore bodies have been described and discussed earlier in detail

Table 1. Trace-elements in pyrite from different ore types and ore bodies of Sulitjelma deposit. All values given below are in parts per million (ppm). Ore-type A corresponds to massive pyritic-ore, B to disseminated ore and C to pyrrhotitic-chalcopyrite ore.

Orebody	Ore-type	No. of samples	Co	Ni	Co:Ni	Mn	Mo	Ga	Ag
GIKEN	A	28	302	104	2.9	16	23	17	4.5
	B	16	449	101	4.5	14	20	16	4.3
	C	19	943	90	10.5	14	27	17	6.0
GIKEN	average	63	533	99	5.6	15	23	17	5.0
CHARLOTTA	A	7	1271	123	10.3	12	19	16	6.4
	B	15	1318	134	9.8	11	10	16	5.2
	C	12	1397	119	11.7	10	15	15	4.7
CHARLOTTA	average	34	1332	127	10.5	11	15	16	5.2
HANKABAKKEN	average B	11	711	117	6.1	13	17	17	5.6
STURRE	B	2	592	115	5.2	22	7	14	5.0
BURSI	average B	11	1589	89	17.8	9	26	14	5.4
JAKOBSBAKKEN	C-I	1	1875	60	31.2	87	5	15	8.5
	C-II	1	4000	90	44.5	38	8	20	6.0

(Rai 1971, 1972). Only the generalized observations of this study are presented here.

In general, the various types of ores exhibit much the same suite of minor and trace elements throughout their occurrence in the deposit. The abundance of a minor or trace element in a particular typomorphic mineral generally displays almost regular and uniform pattern on the broad scale of the deposit. Elements like Ni, Mn, Ga, Ag, As, and Sb exhibit fairly

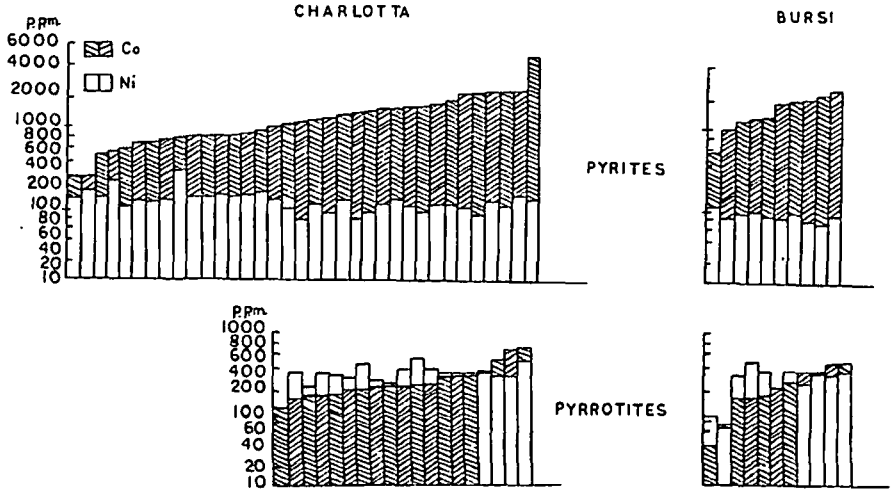

Fig. 7. Distribution of cobalt and nickel in pyrites and pyrrhotites from Charlotta and Bursi ore bodies.

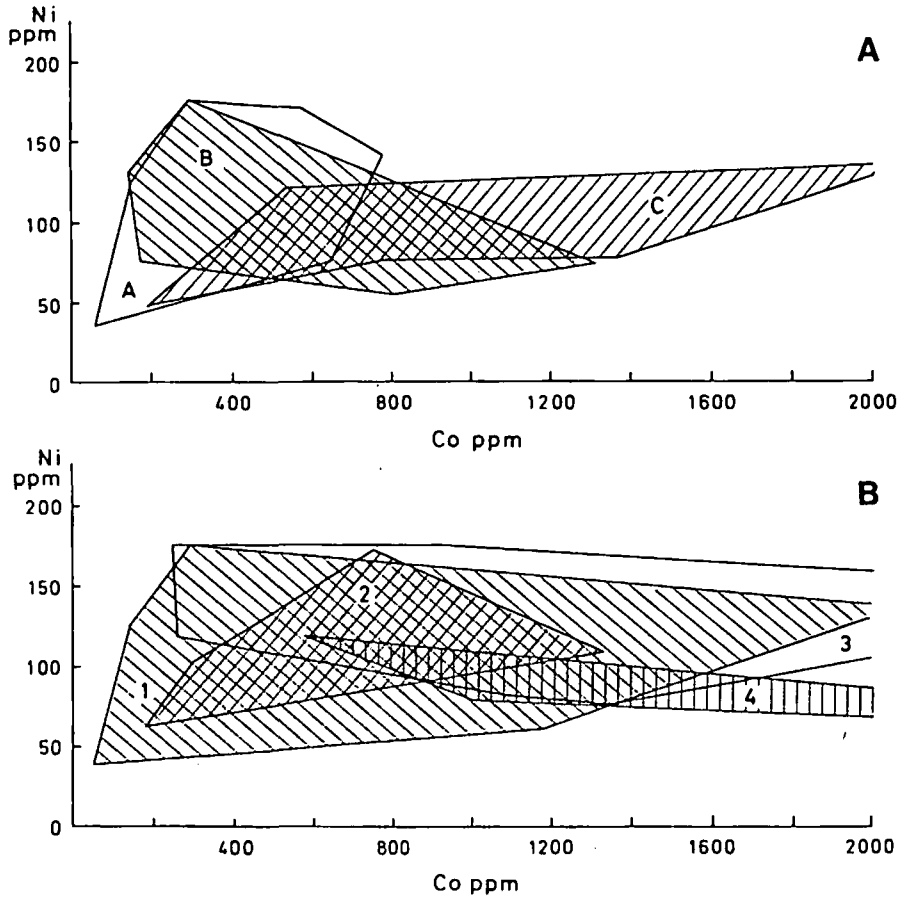

Fig. 8 (A). Fields demarcating cobalt-nickel relations in pyrites belonging to various ore types of Giken ore body, Sulitjelma deposit. (A stands for massive pyritic, B for disseminated and C for pyrrhotitic ore types).
Fig. 8 (B). Fields demarcating cobalt-nickel relations in pyrites belonging to the various ore bodies of Sulitjelma deposit. 1. Giken, 2. Hankabakken, 3. Charlotta, and 4. Bursi.

consistent behaviour (Table 1). The erratic behaviour of elements like cobalt may be attributed to its extraordinary sensitivity to post-depositional events such as metamorphism, recrystallization, and remobilization of the ores. General consistency of element concentration in a particular mineral phase is better pronounced on the scale of an individual ore body, and is further refined considering a particular ore type belonging to it (Table 1, Fig. 7). Extensive geochemical studies on the sulphide deposits of different modes of origin from the Western and Little Carpathians and other parts of the world by Cambel & Jarkovsky (1967, 1968) have shown that the geochemical regularities of the type noted as above are generally diagnostic of primarily the sedimentary or volcanic-exhalative type of sulphide genesis. They are in distinct contrast to the abundance pattern of minor and trace elements in the typomorphic minerals of magmatic and hydrothermal deposits. The geo-

chemical picture of the later type of deposits, according to them, is generally variable and irregular, the visible variance being caused by influences of wall-rocks, temperature of ore solutions, periodicity of mineralization, and several other factors.

While the geochemical regularities, in a relatively broader sense, characterize the Sulitjelma deposit in general, certain minor, yet appreciably characteristic differences among its different ore types and ore bodies appear noteworthy. Such differences, magnified to different scales by different elements, are best represented by elements like cobalt and nickel. The geochemical data presented in Table 1 and Fig. 8 show this clearly. Other typomorphic minerals – namely pyrrhotite, chalcopyrite and sphalerite – show exactly similar behaviour regarding their elemental abundances. It seems very significant to note that a particular ore type generally exhibits slightly, yet characteristically different levels of concentration of an element in a particular mineral in different ore bodies of the deposit, while exhibiting remarkable consistency in the abundance of that element in the mineral on the scale of an ore body. Such definite and consistent differences in the minor and trace element composition of ores in different ore bodies of the deposit, coupled with the kind of observed differences in their base metal composition (Fig. 5A), seemingly reflect primary differences in the overall composition of ores in different ore bodies of the deposit and are possibly explained by relatively small changes of genetic, thermodynamic, and other conditions of ore deposition in different ore bodies.

It has been further observed that a particular ore type exhibits closer and rather interdependent geochemical relations with other ore types associated with it in the same ore body rather than with the same ore type in other ore bodies of the deposit. As evident from the data of Tables 1 and 2, this relationship is best displayed by massive pyritic and pyrrhotitic ore types and indicates an intimate genetic relation between them. The interdependence of the abundance patterns of different elements and of their distribution-ratios in typomorphic minerals in these ore-types offers strong support to the idea of palingenetic mode of origin of pyrrhotitic ores as proposed earlier by several leading Scandinavian workers (Bugge 1948, 1954, Kautsky 1958, Vokes 1962) for the Caledonian pyrrhotitic ores in general.

Statistical studies on the distribution of different trace-elements among the various sulphide-mineral phases of the ores bring out fairly regular and meaningful patterns, particularly for Co, Ni, Mn, and Ag. Average distribution ratios of these elements in pyrite, pyrrhotite, and chalcopyrite from the various ore types and ore bodies of the deposit are given in Table 2, while the patterns of distribution of various elements in different mineral pairs are shown by distribution diagrams in Figs. 9 and 10. On the whole, a good measure of regularity or uniformity seems discernible in the partitioning of an element among the three typomorphic sulphide minerals of ores on the scale of an ore body as well as on the deposit scale. This is borne out also by the definite trends towards linearity of distribution curves

Table 2. Distribution of elements in pyrite, pyrrhotite, and chalcopyrite of Sulitjelma ores.

Element	Ore-type	No. of samples averaged	Giken	Charlotta	Bursi
			Pyritic ore (10)* Pyrrhotitic ore (6)	Pyritic ore (10)* Pyrrhotitic ore (7)	Pyritic ore (8)* Pyrrhotitic ore (4)
COBALT	Pyritic ore	Py.	491	1229	1662
		Po.	107	285	213
		Cpy.	97	111	189
		D.Ratio	4.6:1:0.90	4.3:1:0.4	7.8:0:0.89
	Pyrrhotitic ore	Py.	798	1435	1596
		Po.	149	272	288
		Cpy.	98	121	178
		D.Ratio	5.3:1:0.65	5.3:1:0.44	5.5:1:0.62
NICKEL	Pyritic ore	Py.	117	127	84
		Po.	185	350	288
		Cpy.	42	40	41
		D.Ratio	0.63:1:0.23	0.36:1:0.12	0.30:1:0.14
	Pyrrhotitic ore	Py.	91	115	101
		Po.	186	438	280
		Cpy.	70	81	40
		D.Ratio	0.49:1:0.37	0.39:1:0.18	0.36:1:0.14
MANGANESE	Pyritic ore	Py.	15	9	7
		Po.	93	134	116
		Cpy.	72	43	64
		D.Ratio	0.16:1:0.77	0.07:1:0.33	0.06:1:0.55
	Pyrrhotitic ore	Py.	15	10	9
		Po.	109	112	168
		Cpy.	80	50	71
		D.Ratio	0.14:1:0.74	0.11:1:0.44	0.05:1:0.42
SILVER	Pyritic ore	Py.	3.8	5.9	5.1
		Po.	55	40	28
		Cpy.	131	49	55
		D.Ratio	0.07:1:2.38	0.15:1:1.21	0.18:1:1.94
	Pyrrhotitic ore	Py.	3.0	3.7	5.7
		Po.	53	42	84
		Cpy.	128	50	66
		D.Ratio	0.06:1:2.40	0.09:1:1.19	0.07:1:0.78

* Numericals in the parentheses refer to the No. of samples averaged.

in most of the distribution diagrams pertaining to both massive pyritic and pyrrhotitic ores. A detailed geochemical study on sphalerites belonging to these two prominent mineral parageneses in this deposit (Rai 1977) also brings out a comparable regularity or uniformity of minor and trace-element partitioning between sphalerite and other associated minerals. However, it appears difficult to surmise the implications of these observations in the

UNIVERSITY OF UTAH LIBRARIES

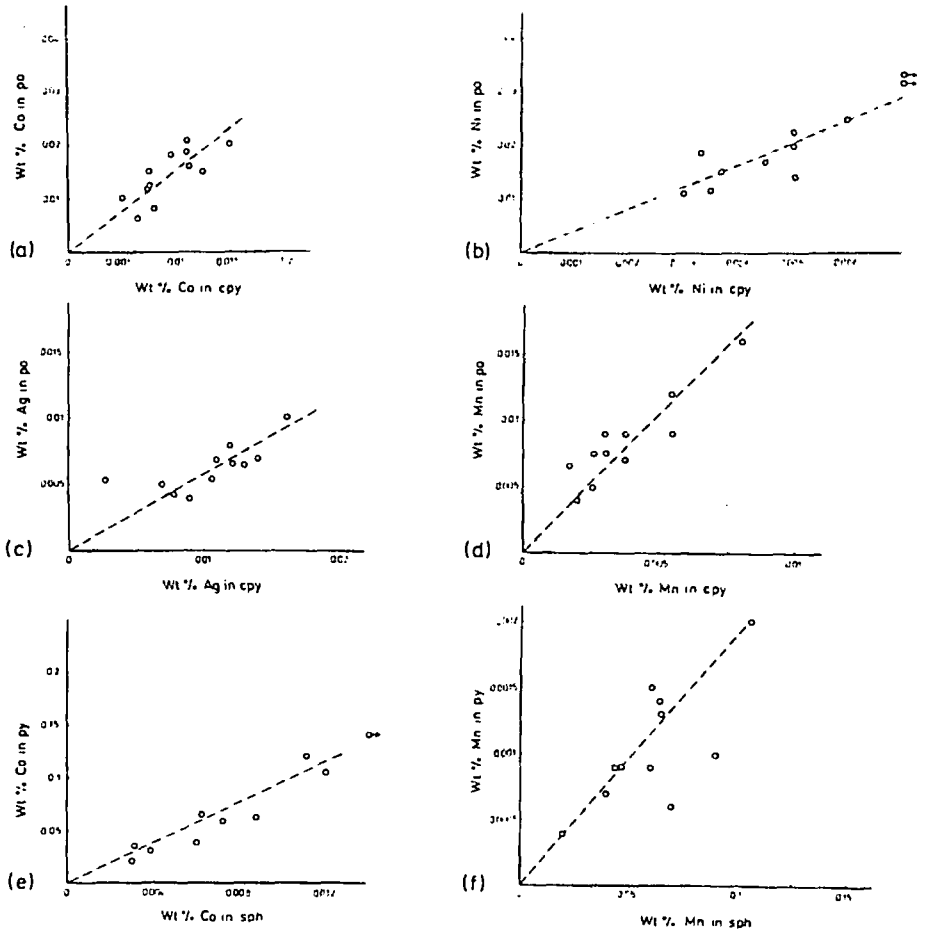

Fig. 9 (a)–(d). Distribution of Co, Ni, Ag, and Mn between co-existing pyrite and pyrrhotite in pyritic ore.
(e)–(f). Distribution of cobalt and manganese between co-existing pyrite and pyrrhotite in pyrrhotite-chalcopyrite ore.

evaluation of equilibrium or disequilibrium of primary depositional conditions in view of the known involvement of the ores in high-grade regional metamorphism.

Isotopic composition of sulphur

The isotopic analyses of sulphur in pyrite fractions of different types of ores from the deposit exhibit an overall spread of 8.55 per mill of δS^{34} values in the range of -0.1 permil to $+8.44$ permil with an average value of $+3.57$ permil (Fig. 11). Within this general range, it seems highly significant to find the massive ores (including both pyritic- and pyrrhotitic-types) displaying a much narrower spread of only about 3.5 permil in $+1$ to $+4.5$ permil range. δS^{34} values outside this sub-range seem to correspond exclusively to the disseminated-pyritic ores.

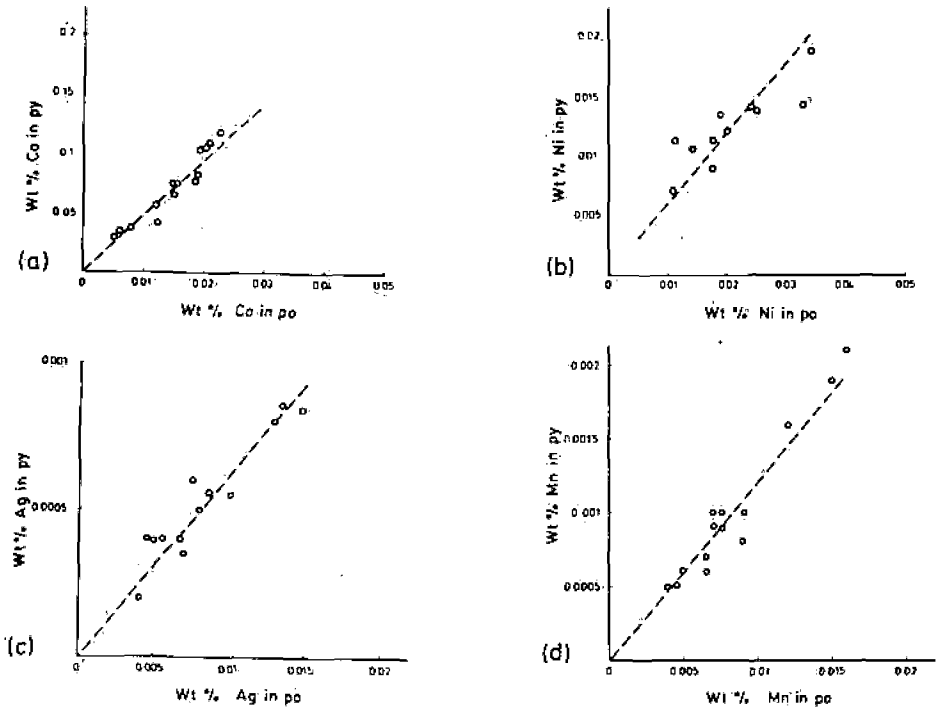

Fig. 10 (a)–(d). Distribution of Co, Ni, Ag, and Mn between co-existing pyrrhotite and chalcopyrite in massive ores.

Notwithstanding these differences in patterns corresponding to different ore types, the overall spread of δS^{34} values seems to be rather narrow and close enough to the value of the meteorite standard. A general enrichment tendency of the heavier stable isotope (S^{34}) is clearly discernible. These observations seem to be meaningful and characteristic enough to suggest essentially a single, almost uncomplex primary genetic process in which the ore fluids might have been derived basically from an independent and fairly homogeneous deep-seated magmatic source. Observed close similarities of the distribution pattern and spread of δS^{34} values in Sulitjelma deposit with those in some of the type deposits of geosynclinal volcanic type – e.g. the Tertiary volcanic ores of Japan (Tatsumi 1965) and the Cambrian ores of Mt. Lyell, Tasmania (Solomon, Rafter & Jensen 1969) – seem to be strongly suggestive of an analogous mode of origin of the deposit.

Synthesis

The overall geochemical picture of the deposit emerging from the present study seems to be appreciably uniform with well-defined and meaningful geochemical characteristics of the ores. In detail, however, minor yet systematic and consistent differences characterize the geochemistry of various ore types in different ore bodies of the deposit.

UNIVERSITY OF UTAH LIBRARIES

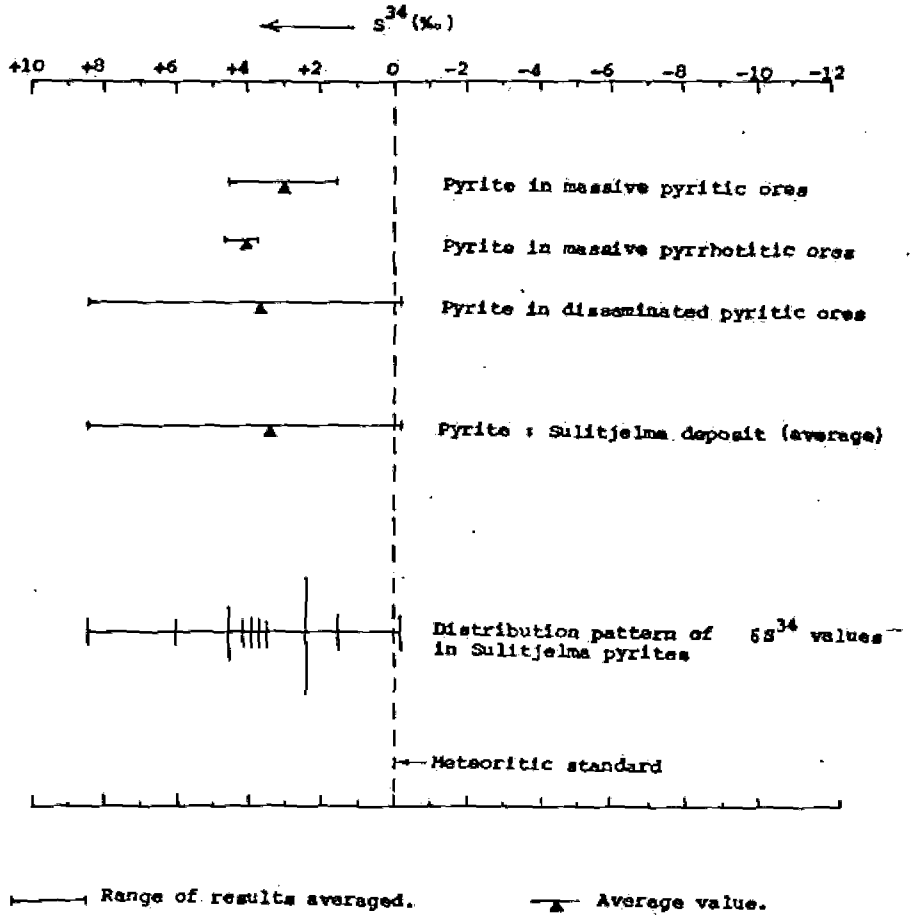

Fig. 11. Pattern of sulphur-isotopic fractionation in pyrites from Sulitjelma.

Studies on the distribution of major metals, particularly copper and zinc, in various ore types and ore bodies of the deposit, bring out certain important aspects of metallogeny in the region. They suggest primarily a basic igneous parentage of the ores and indicate close genetic linkage between massive pyritic and disseminated type of ores, both of them belonging possibly to the same pulse of ore-forming fluids. Some sort of base-metal differentiation in the ore fluids supplying ores to the different ore bodies appears to have taken place.

Detailed studies on the minor and trace elements in various typomorphic minerals of the ores bring out notable geochemical regularities on the scale of the deposit in general and that of individual ore bodies in particular. The palingenetic mode of origin of pyrrhotitic ores, presumably during regional metamorphism of the deposit, is supported by the study. Interpretation of the observed results of minor and trace element study in terms of primary genetic and depositional conditions is circumscribed by the unknown effects of metamorphism on the primary geochemistry of the ores. Minor, yet

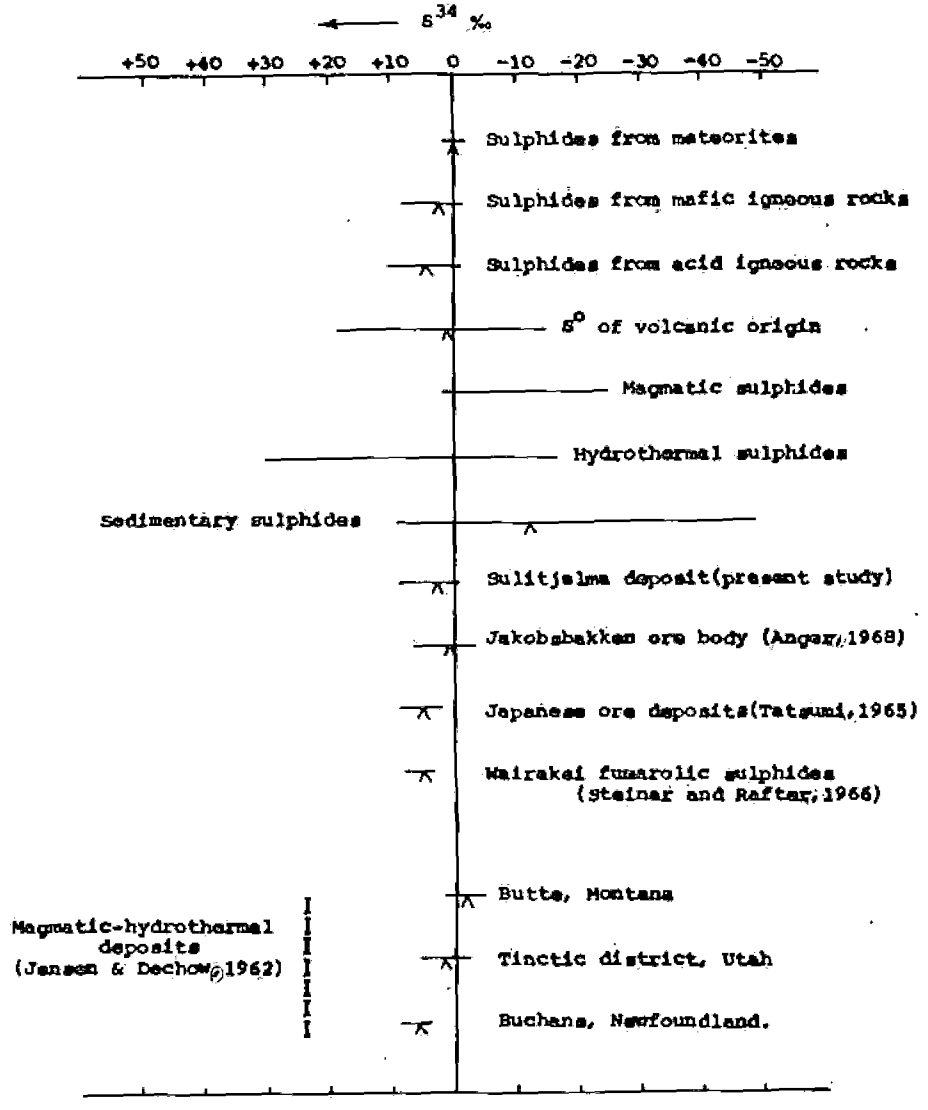

Fig. 12. Sulphur-isotope distribution in Sulitjelma ores compared with that in some typical deposits reported in the literature.

definite and consistent differences in the composition of ores in different ore bodies of the deposit, however, seem to be basically a primary feature of the deposit, which seems difficult to explain by a simple sedimentary or hydrothermal concept of ore-genesis. Although derived primarily from a common source, the ore-forming fluids seem to have undergone some differentiation of their metallic content before the final deposition of ores in different ore bodies. The possibility of existence of small time-lags in the deposition of ores corresponding to the different ore bodies, as may be implied in distinct, though slight differences in their relative positions in

UNIVERSITY OF UTAH LIBRARIES

the mineralized zone, cannot be ruled out. The overall observations may be best explained by the volcanic-exhalative mode of ore deposition in the region.

Observations from the study on isotopic fractionation of sulphur in the deposit are characteristic and meaningful enough to suggest essentially a single, almost uncomplex primary genetic process in which the ore fluids were derived basically from an independent, deep-seated magmatic source. Such a source of ore material is compatible with the proposed volcanic-exhalative mode of ore-deposition, which is favoured also by the comparison of the observed pattern of sulphur-isotopic fractionation in the deposit with that exhibited by typical massive sulphide deposits reported in the literature.

Acknowledgements. – Thanks are due to Prof. J. A. W. Bugge for his encouragement and guidance during the work and for critical reading of the manuscript; to Dr. F. J. Langmyhr of Kjemisk institutt, Universitetet i Oslo, for his unfailing help in atomic absorption spectrophotometric work; and to Prof. M. L. Jensen, University of Utah, for kindly undertaking the sulphur-isotopic analytical work in his laboratory. Financial assistance received from NORAD and the help and cooperation received from A/S Sulitjelma Gruber, Norway and the Indian School of Mines, Dhanbad, are gratefully acknowledged.

REFERENCES

Bugge, C. 1948: Kisene i Fjellkjeden. *Nor. Geol. Tidsskr. 27*, 97–102.

Bugge, C. 1954: Den Kaledonske fjellkjede i Norge. *Nor. Geol. Unders. 189*, 1–79.

Brøgger, W. C. 1901: Om dannelsen av de norske Kisforekomster av typen Røros-Sulitjelma. *Krist. Vidensk. Akad. Forh. 1901.*

Cambel, B. & Jarkovsky, J. 1967: Geochemie der Pyrite einiger Lagerstatten der Tschechslowakei. *Vydavatelstvo Slovenskej Akademie vied Bratislava.*

Cambel, B. & Jarkovsky, J. 1968: Geochemistry of nickel and cobalt in pyrrhotites of different genetic types. *XXIII Int. Geol. Cong. 6*, 169–183.

Carstens, C. W. 1935: Zur Genesese des Kiesvorkommen des Trondhjem-Gebietes. *Skr. Kg. nor. Vidensk. selsk. 11.*

Henley, K. J. 1968: The Sulitjelma metamorphic complex. *Unpublished Ph.D. thesis*, Univ. of London.

Henley, K. J. 1970: The structural and metamorphic history of the Sulitjelma region, Norway, with special reference to the nappe hypothesis. *Nor. Geol. Tidsskr. 50*, 97–136.

Kautsky, G. 1953: Der geologische Bau des Sulitjelma-Salojauregebietes in den Nordskandinavischen Kaledoniden. *Sver. Geol. Unders. Ser. C. 528*, 1–232.

Kautsky, G. 1958: The theory of exhalative sedimentary ores, proposed by Chr. Oftedahl: A criticism. *Geol. For Sth. Forh. 492, 80*, 283–287.

Krause, H. 1956: Zur Kenntnis der metamorphen Kieslagerstätte von Sulitjelma (Norwegen). *Neues Jb. Mineral. Abh. 89*, 137–148.

Langmyhr, F. J. & Paus, P. E. 1968: The analysis of inorganic siliceous materials by atomic absorption spectrophotometry and the hydrofluoric acid decomposition technique. Part I. *Anal. Chim. Acta. 43*, 397–408.

Langmyhr, F. J. & Paus, P. E. 1970: The analysis of sulphide minerals – Part VIII. *Anal. Chim. Acta 43*, 515–516.

Middendorf, K. von. 1914: Sulitjelma-VII. *Der Freiberger Geol. Gesell.*

Oftedahl, Chr. 1958: A theory of exhalative-sedimentary ores. *Geol. For. Sth. Forh. 80*, 1–19.

Rai, K. L. 1971: On the genetic implications of trace-element abundance study of pyrites from the stratiform sulphide deposit at Sulitjelma, Norway. *VIII International Sed. Congress, Heidelberg. Section 5 'Ores in Sedimentary rocks' Abst. Vol.*, 80–81.

Rai, K. L. 1972: Geology and geochemistry of Caledonian massive sulphide deposit at Sulitjelma, Nordland, Norway. *NORAD Res. Contrib. Inst. Geol. Oslo*, 50 pp.
Ramdohr, P. 1938: Antimonreiche Paragenesen von Jakobsbakken bei Sulitjelma. *Nor. Geol. Tidsskr. 18*, 275–289.
Sandell, E. B. & Goldich, S. B. 1943: The rarer metallic constituents of some American Igneous Rocks. *J. Geol. 51*, 99–115 and 167–189.
Sjøgren, Hj. 1894: Om Sulitjelmakisenes geologi. *Geol. For. Sth. Forh. 16*, 394–437.
Solomon, M., T. A. Rafter & M. L. Jensen 1969: Isotope studies on the Rosebery. Mount Farrell and Mount Lyell Ores, Tasmania. *Min. Depos. 4*, 172–199.
Stelzner, A. W. 1891: Die Sulitjelma. *Gruben im nördlichen Norwegen*. Frib. im. Sachen.
Stutzer, O. 1906: Alte und neue geologische Beobachtungen an den Kisslagerstätten Sulitjelma-Roros-Klingenthal. *Oster. Zt. für Berge- und Hurtenwesen, 54*.
Tatsumi, T. 1965: Sulphur-isotope fractionation between coexisting sulphide minerals from some Japanese ore deposits. *Econ. Geol. 60*, 1645–1659.
Vogt, J. H. L. 1894: Über die Kieslagerstätten vom types Røros. Vigsnos, Sulitjelma in Norwegen und Rammelsberg in Deutschland. *Zt. für prakt. Geol.*
Vogt, Th. 1927: Sulitjelma feltets geologi og petrografi. *Nor. Geol. Unders. 121*, 1–560.
Vokes, F. M. 1962: Mineral parageneses of the massive sulfide ore bodies of the Caledonides of Norway. *Econ. Geol. 57*, 890–903.
Wilson, H. D. B. & Anderson, D. T. 1959: The composition of Canadian sulphide ore-deposits. *Can. Inst. Min. Met. Bull. 52*, 619–631.
Wilson, M. R. 1973: The geological setting of the Sulitjelma orebodies, Central Norwegian Caledonides. *Econ. Geol. 68*, 307–316.

UNIVERSITY OF UTAH LIBRARIES